DISSERTATION

submitted to the
Combined Faculties for the Natural Sciences and for Mathematics
of the Ruperto-Carola University of Heidelberg, Germany
for the degree of
Doctor of Natural Sciences

presented by
M. Sc. (Technical Biology) Valentino De Leo
born in Ludwigsburg, Germany

Date of oral examination: May 21st, 2019

Cancer-testis antigen specific chimeric antigen receptor T cells for cancer immunotherapy

Examiners:

Prof. Dr. Hans-Reimer Rodewald

Prof. Dr. Juergen Krauss

Abstract

Adoptive chimeric antigen receptor (CAR) T cell therapy has shown promising results in early phase clinical trials, in particular when treating hematological malignancies. In this novel immunotherapeutic approach, isolated autologous T cells are *ex vivo* engineered to express a CAR, expanded to obtain sufficient cell numbers and finally infused back to the patient.

Such CAR T cells are redirected to a predefined target antigen by an antibody derived binding domain and have been shown to substantially reduce the tumor burden as long as the cancer cells present the target antigen. However, solid tumors do not express exclusive target antigens, thereby hampering therapeutic safety due to potential on-target/off-tumor toxicity.

In this project, we developed CARs that contain phage display selected fully human antibody binding domains specific for the tumor associated antigens AKAP4, SP17 and SPAG9. In healthy tissues, the expression of these so called cancer-testis antigens is restricted to spermatocytes, however, it has been shown that their expression can be upregulated in certain tumor entities most probably due to deregulated epigenetic events. We successfully selected AKAP4, SP17 and SPAG9 antibody fragments (scFvs) from human B cell repertoires that were further characterized as soluble scFv-hFc fusion proteins. We demonstrated antigen specificity by ELISA and SPR spectroscopy as well as surface binding to several tumor cell lines representing colorectal, ovarian, plasma cell and B cell cancers.

Importantly, we also observed binding of the scFv-hFc fusion proteins to primary plasma cells isolated from multiple myeloma patients, but neither to plasma cells from two 2 out of 3 patients showing unremarkable bone marrow morphology, nor to peripheral blood mononuclear cells derived from healthy donors. SP17 and SPAG9 specific scFv lead candidates were fused as antigen binding domain to five different CAR backbones that contained either CD8α or hFc extracellular spacer domains and intracellular second or third generation stimulatory domains. The second generation CAR constructs showed superior characteristics compared to the third generation CARs as indicated by higher transduction efficiencies of the T cells and a higher surface expression of the CAR molecule. In addition, T cells expressing the second generation CARs showed less signs of T cell exhaustion, preferentially differentiated toward the central memory phenotype and showed specific cytotoxicity towards ovarian cancer and multiple myeloma cell lines.

We here provide the basis for a novel cellular therapy by redirecting CAR T cells to tumor specific cancer-testis antigens to safely treat various cancer entities.

Zusammenfassung

Adoptive Therapie mit chimären Antigenrezeptor- (CAR-) T-Zellen zeigte in frühen klinischen Studien hohe Wirksamkeit, vor allem bei hämatologischen Krebserkrankungen. Bei diesem neuartigen immuntherapeutischen Ansatz werden isolierte autologe T-Zellen *ex vivo* modifiziert, zu einer ausreichenden Zellmenge expandiert und dem Patienten per Infusion zurückgeführt.

Diese CAR-T-Zellen werden durch eine von Antikörpern abgeleitete Bindedomäne aktiv zu einem definierten Zielantigen gelenkt. In einigen Studien wurde eine maßgebliche Reduktion der Tumorlast gezeigt, solange die Krebszellen das Zielantigen präsentierten. Solide Tumore exprimieren jedoch keine exklusiven Zielantigene, wodurch die therapeutische Sicherheit aufgrund potentieller tumorunspezifischer Toxizität beeinträchtigt wird.

In diesem Projekt entwickelten wir chimäre Antigenrezeptoren, die vollhumane Antikörperbindedomänen aus Phagen-Display-Selektionen enthalten und gegen die tumorspezifischen Antigene AKAP4, SP17 und SPAG9 gerichtet sind. Die Expression dieser sogenannten Tumor-Hoden-Antigene ist in gesunden Geweben auf Spermatozyten limitiert, wird jedoch bei einigen Tumorentitäten hochreguliert, vermutlich aufgrund deregulierter epigenetischer Ereignisse. Wir selektierten erfolgreich AKAP4-, SP17- und SPAG9-spezifische Antikörperfragmente (scFvs) aus humanen B-Zell-Repertoires und charakterisierten diese als lösliche scFv-hFc-Fusionsproteine. Wir zeigten Antigenspezifität mittels ELISA, Oberflächenplasmonenresonanzspektroskopie und Oberflächenbindung an Tumorzelllinien, die Kolon-, Ovarial-, Plasmazell- und B-Zell-Tumoren repräsentierten.

Wir beobachteten Bindung der scFv-hFc-Fusionsproteine an primäre Plasmazellen von Patienten mit Multiplem Myelom, jedoch weder an Plasmazellen aus 2 von 3 getesteten unauffälligen Knochenmarksproben, noch an mononukleäre Zellen des peripheren Blutes gesunder Spender. SP17- und SPAG9-spezifische scFvs wurden als Bindedomäne in fünf verschiedene CAR-Konstrukte integriert, die einen CD8α- oder hFc-Spacer und stimulatorische Domänen der zweiten oder dritten Generation enthielten. Die CAR-Konstrukte der zweiten Generation verliehen den T-Zellen im Vergleich zu denjenigen der dritten Generation verbesserte Eigenschaften, darunter höhere CAR-Expression, geringere Anzeichen von T-Zell-Erschöpfung und die bevorzugte Differenzierung zu zentralen Gedächtnis-T-Zellen. T-Zellen, die einen CAR der zweiten Generation exprimierten, zeigten spezifische Zytotoxizität gegenüber Zelllinien des Ovarialkarzinoms und Multiplen Myeloms.

Mit dieser Arbeit schaffen wir die Basis für eine neuartige Zelltherapie, in der CAR-T-Zellen gegen tumorspezifische Tumor-Hoden-Antigene gerichtet werden, um diverse Tumorentitäten sicher zu behandeln.

Table of content

Abbreviations

2^{nd}	second
3^{rd}	third
°C	degree Celsius
α	anti
A	adenine
aa	amino acid
Abs	absorbance
ACT	adoptive cell therapy
AKAP4	A-kinase anchor protein 4
APC	allophycocyanin
APS	ammonium peroxidsulfate
AU	absorption unit
BCR	B cell receptor
bio-	biotinylated
bp	base pair
BSA	bovine serum albumin
BV	Brilliant Violet
C	cytosine
CAIX	carbonic anhydrase 9
cAMP	cyclic adenosine monophosphate
CAR	chimeric antigen receptor
CD	cluster of differentiation
CDR	complementarity determining region
CFSE	carboxyfluorescein succinimidyl ester
C_H	heavy chain constant domain
C_L	light chain constant domain
CMV	cytomegalovirus
c-myc	myelocytomatosis oncogene
CO_2	carbon dioxide
cPPT	central polypurine tract
CTA	cancer-testis antigen
D	diversity gene segment
Da	Dalton
ddH_2O	double distilled water
DMEM	Dulbecco's Modified Eagle's Medium
DMSO	dimethyl sulfoxide

DNA	deoxyribonucleic acid
dNTP	deoxynucleoside triphosphate
DTT	dithiothreitol
ECL	enhanced chemiluminescence
E. coli	*Escherichia coli*
EDTA	ethylenediaminetetraacetic acid
ELISA	enzyme linked immunosorbent assay
env	envelope
ERBB2	erythroblastic oncogene B
Fab	antigen binding fragment
FCS	fetal calf serum
Fc	fragment crystallizable
FcR	fragment crystallizable receptor
FITC	fluorescein isothiocyanate
FPLC	fast protein liquid chromatography
Fv	variable fragment
fw	forward primer (sense)
g	Gravitational constant
G	Guanine
GD2	disialoganglioside
h	hour
HAL9/10	human antibody libraries 9/10
HD	healthy donor
hFc	human fragment crystallizable
HRP	horseradish peroxidase
IFNγ	interferon gamma
Ig	immunoglobulin
IGHV	heavy chain V gene segment
IL	interleukin
IPTG	isopropyl β-D-1-thiogalactopyranoside
IRES	internal ribosomal entry site
J	Joining gene segment
L	liter
LAG-3	lymphocyte activation gene 3
LB medium/agar	lysogeny broth medium / agar
LB-A/-K medium/ agar	LB medium / agar with ampicillin or kanamycin
Lck	lymphocyte specific tyrosine kinase

LDH	lactate dehydrogenase
LTR	long terminal repeat
LYNDAL	LYmph Node Derived Antibody Libraries
M	Molar (mol/L)
mAb	monoclonal antibody
MAGE-A3	melanoma antigen A3
mFc	murine fragment crystallizable
MFI	median fluorescence intensity
MHC	major histocompatibility complex
min	minute
MM	multiple myeloma
MOI	multiplicity of infection
MPBS	milk phosphate buffered saline
NY-ESO-1	New York esophageal squamous cell carcinoma-1
OD_{600}	optical density at 600 nm wavelength
ori	origin of replication
pA	polyadenylation signal
PAGE	polyacrylamide gel electrophoresis
PBMC	peripheral blood mononuclear cell
PBS(T)	phosphate buffered saline (with Tween 20)
PCR	polymerase chain reaction
PD-1	programmed cell death protein 1
PE	phycoerythrin
PEG	polyethylene gylcol
PEI	polyethylenimine
pen/strep	penicillin/streptomycin
pH	*potentia Hydrogenii*
PUBM	patient showing unremarkable bone marrow morphology
RNA	ribonucleic acid
rpm	revolutions per minute
RPMI-1640	Roswell Park Memorial Institute 1640 medium
RRE	rev response element
RT	room temperature
RU	response unit
rv	reverse primer (antisense)
scFv	single chain variable fragment
SDS	sodium dodecyl sulfate
SEC	size exclusion chromatography

SOC	super optimal broth supplemented with glucose
SP17	Sperm protein 17
SPAG9	Sperm associated antigen 9
SPR	Surface plasmon resonance
strep	streptavidin
SV	simian virus
T	thymine
TAE	tris acetate EDTA buffer
Tcm	central memory T cell
TCR	T cell receptor
Teff	effector T cell
Tem	effector memory T cell
TEMED	tetramethylethylenedamine
TIL	tumor infiltrating lymphocyte
TIM-3	T cell immunoglobulin and mucin domain containing 3
Tm	melting temperature
TMB	tetramethylbenzidine
Tn	naïve T cell
Treg	regulatory T cell
Tris	tris(hydroxymethyl)aminomethane
Tryptone N1	TN1
Tscm	stem cell memory T cell
U	enzyme unit
UV	ultraviolet
V	variable gene segment
V_H	heavy chain variable domain
V_L	light chain variable domain
v/v	volume per volume
w/v	weight per volume
WPRE	woodchuck hepatitis virus posttranscriptional regulatory element
YT medium	yeast tryptone medium
YT-A medium	yeast tryptone medium with ampicillin
YT-AK medium	yeast tryptone medium with ampicillin and kanamycin
YT-GA medium/ agar	yeast tryptone medium / agar with glucose and ampicillin
YT-K agar	yeast tryptone agar with kanamycin

1 Introduction

1.1 The innate and adaptive immune system

Although being continuously exposed to pathogenic microorganisms, we rarely develop a disease. Our immune system identifies these pathogens and generates immediate responses to disrupt the infection, as well as protective responses to prevent reinfection with the same pathogen. Besides pathogen clearing, immune cells are able to distinguish normal somatic cells from cancerous cells that aberrantly express certain cellular proteins. To rapidly and specifically eliminate pathogens, the immune system comprises two lines of defense: the innate and the adaptive immunity [1,2].

For the identification of microorganisms, immune cells need to distinguish “non-self” from “self” to avoid autoreactivity [3]. When initially encountering a foreign pathogen, the innate immune system triggers a powerful response within hours. The response includes phagocytic activity by macrophages, dendritic cells and granulocytes, as well as cytotoxic natural killer cells and also non-cellular components such as the complement system, a complex of soluble proteins that flags the pathogen for other immune cells and attacks microbial membranes. Almost every cell type presents its intracellular protein status via the class I major histocompatibility complex (MHC), which transports fragments of degraded proteins (peptides) to the cell surface. Innate immune cells recognize pathogens either by the absence of cell surface MHC molecules or by pattern recognition receptors that possess inherited specificity. Upon ingestion of pathogens, phagocytic cells display fragments thereof via class II MHC molecules and thereby activate the second line of defense, the adaptive immune system [4-6].

If the innate immune response is not sufficient for pathogen clearance, cells from the adaptive immune system get involved – the T and B lymphocytes (or T and B cells). In contrast to the limited repertoire of pattern recognition receptors, the antigen receptors of the adaptive immune cells can generate a much broader diversity and consequently create a fine specificity for a theoretically unlimited number of antigens [7]. Both, the B cell receptor (BCR) and the T cell receptor (TCR) acquire their diversity through the process of V(D)J recombination. The germline DNA encoding these receptors is organized as clusters of distinct V (variable), D (diversity) and J (joining) gene segments. The mechanism of V(D)J recombination selects one of each gene segment for rearrangement (inclusion of D only in variable domain of BCR heavy chain and TCR β chain, see below), and causes additions or deletions of nucleotides at the joining sites that further increase the diversity of the recombined antigen receptors [8,9]. Somatic hypermutation is another process that contributes to the genetic receptor diversity by introducing a vast number of point mutations

within the antigen binding regions, leading to receptor affinity maturation toward its cognate antigen during an immune response. Although somatic hypermutation was thought to exclusively occur for BCRs, there are indications that it might also be involved in TCR diversification [10,11]. The assembled V(D)J segments form the variable domains of the BCR and TCR which contain six hypervariable loops – the complementarity determining regions (CDRs) – three provided by each chain. CDRs are flanked by less variable framework regions and protrude into the antigen binding site, thereby conferring the antigen specificity. BCRs consist of two identical heavy and light chains (two types exist for the latter, κ and λ) that result in a combined diversity. The variable domains are referred to as V_H (heavy chain) and V_L (light chain). Similarly, TCRs are composed of α and β chains. Apart from the variable domains, BCRs and TCRs possess constant domains and transmembrane regions which anchor them to the plasma membrane [1,12].

While the BCR recognizes extracellular antigens in their native conformation, the TCR recognizes antigen fragments presented by MHC. When B and T lymphocytes bind the cognate antigen via their antigen receptor, they become activated and expand clonally. This is further triggered by interactions between B cells and T cells, mainly via co-receptors and cytokines. This intensive communication among immune cells is essential to ensure a balanced immune response [1,13-15].

Until the adaptive immune response is fully induced to develop high antigen specificity and affinity, it takes up to seven days. Some of the activated lymphocytes generate a protective long-term immunity by differentiating into memory B or T cells. This immunological memory is rapidly reactivated upon following encounters with the identical antigen and initiates a fast and specific response [16].

1.2 Antibodies, derived formats and therapeutic application

In contrast to T cells, activated B cells are able to secrete a soluble variant of their BCR known as immunoglobulin (Ig) or antibody. Antibodies that are bound to their cognate antigen not only have a neutralizing effect on the pathogen, but also tag it for other immune cells by exposing their fragment crystallizable (Fc) region and thus possess effector function. Antibody Fc regions are recognized by innate immune effector cells that express Fc receptors (FcRs). FcR binding to antibody-antigen complexes induces signal transduction and leads to activation of these cells [1,17]. Antibodies possess almost the identical structure as their BCR counterparts, but lack a transmembrane region due to alternative splicing events. In humans, five major classes of Igs exist that are defined by distinct C_H domains –

IgA, IgD, IgE, IgG and IgM – with IgG being the most abundant class in blood plasma [1,12]. The default configuration of the Ig in naïve B cells is IgM and IgD. When naïve B cells are activated by antigen and T cell help, they participate in germinal center reactions through which they modify antigen binding affinities by somatic hypermutations and switch the isotype to IgG, IgA or IgE by class switch recombination [1,18].

Antibody engineering allows to generate recombinant antibodies as well as various formats derived thereof (*Figure 1*), and to introduce modifications to manipulate effector functions for therapeutic purposes. The formats differ in their pharmacokinetical properties and effector functions, which enables their usage according to the therapeutic need. For instance, a full-length antibody has a high serum half-life and confers effector functions by its Fc, but lacks efficient tissue penetration due to its large molecular size. In contrast, a single chain variable fragment (scFv, V_H and V_L domain connected by a flexible linker, *Figure 1*) has a low serum half-life due to its small molecular size, is incapable of mediating effector functions, but efficiently penetrates tissue [19,20]. Furthermore, antibody sequences can be modified to modulate certain antibody mediated functions. For instance, Armour *et al.* demonstrated that the replacements of the PELLG and ISR motifs within the C_H2 domain of an IgG1 antibody with corresponding residues of an IgG2 antibody, prevented binding of the mutated antibody to FcγR expressing monocytes and their activation [21].

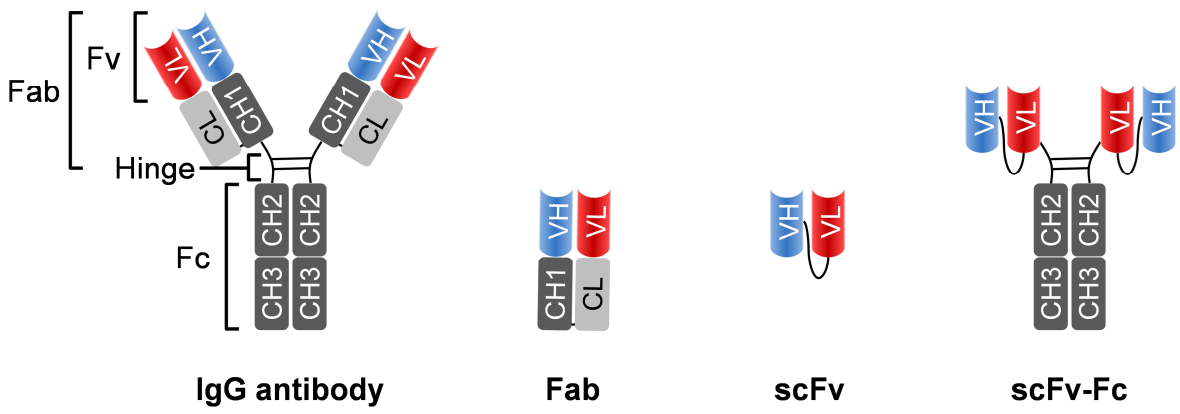

Figure 1. Schematic representation of an IgG antibody and derived formats. Antibody fragments with antigen binding activity such as the variable (Fv) and antigen binding (Fab) fragment can be used to generate self-contained antibody derived formats. While Fab is naturally linked by a disulfide bond in the constant regions, V_H and V_L domains from Fv need to be connected with a flexible synthetic linker, resulting in a single chain variable fragment (scFv). Fusion of scFv to Fc yields the antibody like scFv-Fc format. Red: variable region of the light chain (V_L), blue: variable region of the heavy chain (V_H), dark grey: constant region of the heavy chain (C_H), light grey: constant region of the light chain (C_L). Image based on Frenzel *et al.* [19].

Since Koehler and Milstein developed the hybridoma technology in 1975 that allowed the production of monoclonal antibodies (mAbs), the field of antibody engineering was further accelerated by newly emerging antibody *in vitro* selection technologies such as phage display, which was invented by Smith and Winter [22,23]. Both platforms were regarded as milestones in the field that was further outlined by the inventors being awarded with the Nobel Prize in 1984 (Koehler and Milstein) and, only recently, in 2018 (Smith and Winter) [24]. These and other technological advances led to the development of a plethora of antibodies aimed to be applied for immunotherapy. As of December 2018, over 80 therapeutic mAbs were approved since 1986 by either the U.S. Food and Drug Administration or the European Commission [25-27].

MAbs were developed for targeted immunotherapy to treat inflammatory diseases (e.g. anti-TNFα, Adalimumab), neurodegenerative disorders (e.g. anti-β-amyloid, Aducanumab), cancer (e.g. anti-CD20, Rituximab) and many other diseases [28-30]. Apart from directly targeting tumor cells with mAbs, they are also used to modulate immune cells by binding to so called immune checkpoints. These checkpoints play an important role in self-tolerance as checkpoint receptors mediate inhibitory signals to prevent immune cells from inappropriate activation. However, cancer cells are able to exploit this mechanism by expressing inhibitory receptors and thereby restrain immune cells that directly attack them. Blockade of such checkpoint receptors expressed on immune cells by mAbs can restore the immune cell function [31,32]. In this regard, Ipilimumab (anti-CTLA-4) and Nivolumab (anti-PD-1) proved to enhance the antitumor immune response and in combination even showed synergistic activity in melanoma patients [33,34]. These examples demonstrate how mAbs are applied for immunotherapy with different strategies.

1.3 Cellular immunotherapy to treat cancer

According to estimations of the World Health Organization, 18.1 million new cases of cancer were diagnosed and 9.6 million cancer deaths were registered worldwide in 2018. The top three diagnosed tumor types were lung (11.6%), breast (11.6%) and colorectal (10.2%) cancer. It is expected that cancer burden will further increase in the future due to population growth and ageing [35].

Conventional tumor therapies like chemotherapy or radiation therapy can counteract tumor growth, but fail to spare healthy tissues and thus induce severe toxicities. In contrast, targeted immunotherapy with recombinant mAbs or derived formats showed major advantages over conventional therapies regarding tumor specificity and adverse effects.

However, depending on the antibody format, the therapeutic efficacy may not be optimal due to unfavorable pharmacokinetical properties such as short half-lives, or inefficient tumor tissue penetration and retention [36,37].

Further comprehension of how immune cells interact with cancer cells led to a new wave of immunotherapeutical approaches – the cellular immunotherapies. One option involves the adoptive cell therapy (ACT). The aim of ACT is to isolate immune cells, either directly from the tumor site or from the peripheral blood of patients, to select for antitumor specificities and to expand them *ex vivo*. After expansion, the cells are infused back to the patient and ideally act as “living drugs” to eliminate the tumor. Beside highly increased tumor specificity, ACT reduces graft-versus-host-disease due to autologous administration and the immune cells have the potential to develop a long-term memory which might prevent the patient from tumor recurrence. To date, the most advanced ACT uses T cells for tumor recognition [38-40].

1.3.1 ACT with tumor infiltrating lymphocytes

Tumor infiltrating lymphocytes (TILs) are B and T cells localized at the tumor site that possess certain antitumor reactivity. T cells can be isolated from tumor biopsies, specifically activated with anti-CD3/anti-CD28 antibodies and expanded in the presence of cytokines such as interleukin (IL-) 2 before being retransferred to the patient [41-44].

In a phase I/II clinical trial, Rosenberg *et al*. showed that adoptive transfer of autologous TILs could entirely eradicate the tumor in metastatic melanoma patients, as they observed complete remission in 22% of these patients [45]. An earlier study using autologous TILs already demonstrated that more than 70% of all peripheral blood lymphocytes consisted of one single TIL clone in two responding melanoma patients and long-term persistence over four months was shown for this clone [46]. Previous lymphodepletion by chemotherapy increased the therapeutic efficacy due to promotion of innate immune cells, elimination of immunosuppressive regulatory T cells (Tregs) and TILs not having to compete with host T cells over cytokines that support T cell homeostasis [47,48].

The *ex vivo* expansion of TILs for therapeutic purposes is challenging and the preparation process is complex. Another drawback is the unknown tumor specificity of TILs which might have caused off-target reactions in some treated patients [46,49]. To reduce uncontrollable therapeutic factors, T cells with predefined specificity are desirable.

1.3.2 ACT with TCR engineered T cells

Naturally, the N-terminal variable domains of the α and β chains define the antigen specificity of the TCR. The TCR can be genetically engineered to generate a predefined specificity and then be transferred into T cells from peripheral blood, for instance via viral vectors, leading to surface expression of the recombinant TCR. This modification allows the active redirection of TCR engineered T cells to cancer cells for an enhanced tumor killing in a MHC dependent manner [50,51].

June and colleagues developed a high affinity TCR that recognized a peptide from the tumor associated antigen NY-ESO-1 in complex with a human leukocyte antigen (human MHC). They reported that *ex vivo* expanded T cells modified with this TCR were well tolerated, trafficked to the diseased bone marrow and elicited durable antitumor responses in a phase I/II clinical trial treating multiple myeloma patients. 70% of the treated multiple myeloma patients experienced complete remissions [52].

As tumors can downregulate MHC expression or dysregulate the antigen processing and MHC peptide loading machinery to escape immune cell recognition, the therapeutic efficacy of TCR engineered T cells highly depends on the escape mechanisms developed by the tumor cells [53]. In addition, only processed intracellular proteins that contain tumor specific mutations might be recognized in the context of MHC, but not presented non-mutated peptides or unprocessed antigens expressed on the tumor cell surface [54]. These limitations would be overcome by targeting extracellular tumor associated antigens.

1.3.3 ACT with chimeric antigen receptor T cells

In the late 1980s, Eshhar and colleagues presented a revolutionary work: they replaced variable TCR α and β domains with immunoglobulin V_H and V_L domains and called these constructs “T-bodies”. They demonstrated that murine T cells armed with an antibody based chimeric receptor were successfully redirected to the cell surface bound the hapten trinitrophenyl in a MHC independent fashion. The T cells were efficiently activated upon antigen encounter [55]. In a later study, they fused a scFv to a TCR activation domain derived from CD3ζ, resulting in a chimeric antigen receptor (CAR) that showed improved antitumor effects [56,57]. This CAR was remarkably similar to CARs that are used nowadays, but such modified T cells still lacked efficient antitumor responses in mice xenografted with human tumors. Since these first reports of CAR T cells, further progress was achieved in this field culminating in successful clinical translation (*Figure 2*) of the first CAR products in recent years [58,59].

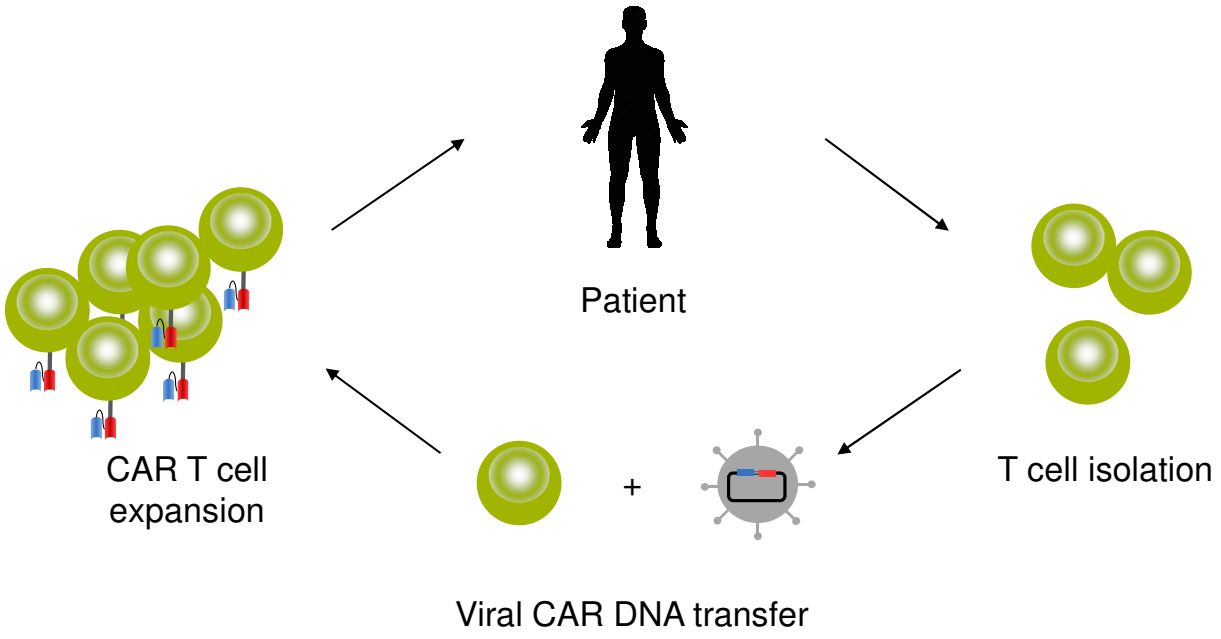

Figure 2. Adoptive CAR T cell therapy. Autologous T cells are isolated from patient blood and receive a CAR gene via viral transfer (transduction). After *ex vivo* expansion, CAR T cells are infused back to the lymphodepleted patient. The expressed CAR redirects CAR T cells to a predefined target by its targeting domain. The variability of the CAR targeting domain and the exchangeable CAR design allow for individualized treatments.

1.4 Chimeric antigen receptors

1.4.1 CAR design and mode of action

Basically, a CAR consists of an extracellular antigen targeting domain – in most cases a scFv – a spacer domain, a transmembrane region and one or more intracellular signaling domains which modulate CAR T cell activation and cytotoxicity [60].

In the first CAR design, the scFv was fused to the transmembrane and intracellular parts of the ζ chain derived from the CD3 TCR complex [56]. Because such CAR T cells showed only poor expansion capacities, later CAR designs incorporated costimulatory domains such as CD28 [61,62], OX40 [63] and 4-1BB [64] in addition to the CD3ζ activation domain to enable a more powerful signaling for full T cell activation [60]. These CAR constructs were termed as first, second and third generation according to the number of costimulatory domains (*Figure 3*) [65].

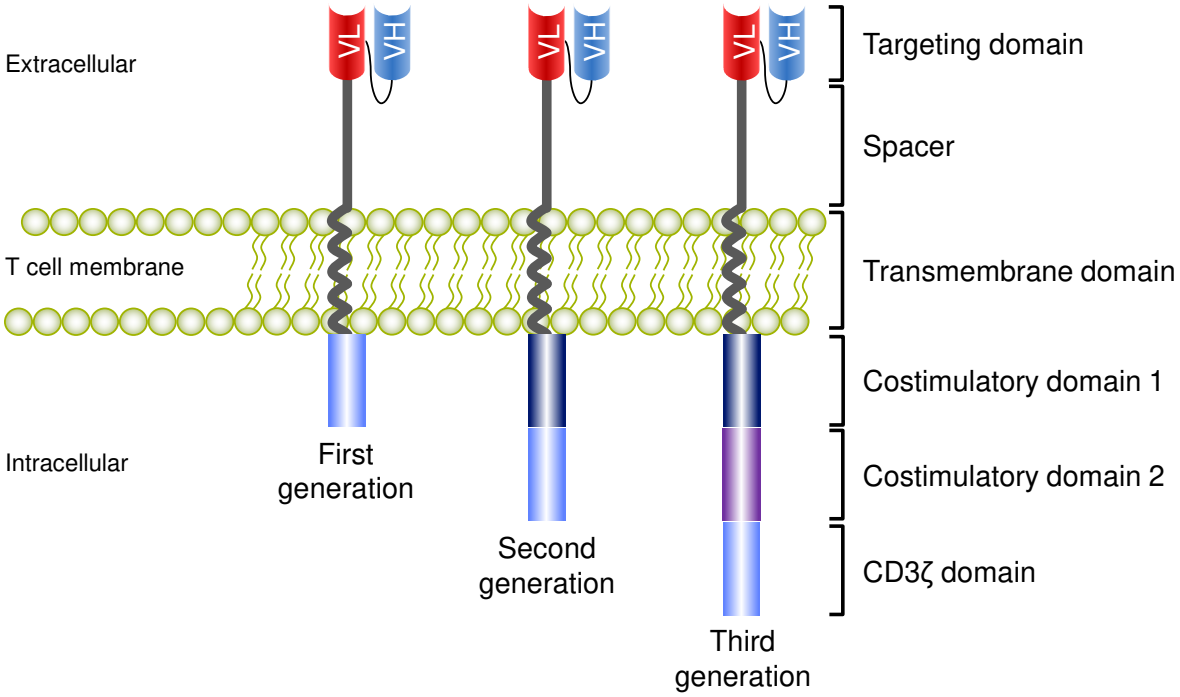

Figure 3. Structural representation of first, second and third generation CARs. CARs consist of an extracellular targeting domain (here: scFv, illustrated by a V_H domain linked to a V_L domain) possessing a specificity of interest and a spacer to enable membrane distance. A transmembrane domain connects the extracellular units to the intracellular CD3ζ signaling domain (first generation) which can be extended with one (second generation) or two (third generation) costimulatory domains.

Each unit in the modular setup of the CAR impacts the CAR T cell's mode of action. The CAR can affect T cell activation by its affinity to the cognate antigen. In general, high affinity (nanomolar range) CARs correlate with enhanced cytolytic T cell activity. However, it has been shown that when a particular affinity threshold is reached, the antitumor activity is not further improved because CAR T cells only hardly dissociate from a bound target cell. In contrast, lower CAR affinities (micromolar range) may reduce CAR T cell trapping at the bound target cell and thereby enhance the overall antitumor response. Furthermore, CARs with moderate affinities allow a certain tolerance toward healthy tissues with low cell surface density of the targeted tumor associated antigen, while still inducing a cytolytic response against tumor cells with high antigen density [66-68]. The spacer is usually composed of an extracellular CD8α hinge, a CD28 hinge, an IgG1 or IgG4 Fc, which differ in flexibility and length. It has been reported that efficient CAR T cell activation depends on the intercellular space at the immunological synapse between CAR T cell and tumor cell. This space is influenced by the position of the epitope within the targeted antigen and the length of the CAR spacer. Thus, CAR spacer length needs to be adjusted accordingly to identify the optimal CAR configuration [67,69,70].

When the CAR T cell recognizes its cognate antigen presented by the tumor cell, the clustering of CAR molecules on the T cell surface induces cytoplasmic signaling events that trigger T cell activation (*Figure 4*) [71,72]. The activation signaling component is the CD3ζ chain derived from the TCR – which is sufficient to induce cytotoxic activity. However, CD3ζ signaling in the absence of costimulation drives the T cells into a state called anergy, which is defined as functional unresponsiveness to antigenic stimulation, thereby impairing serial killing and long-term expansion [73-75].

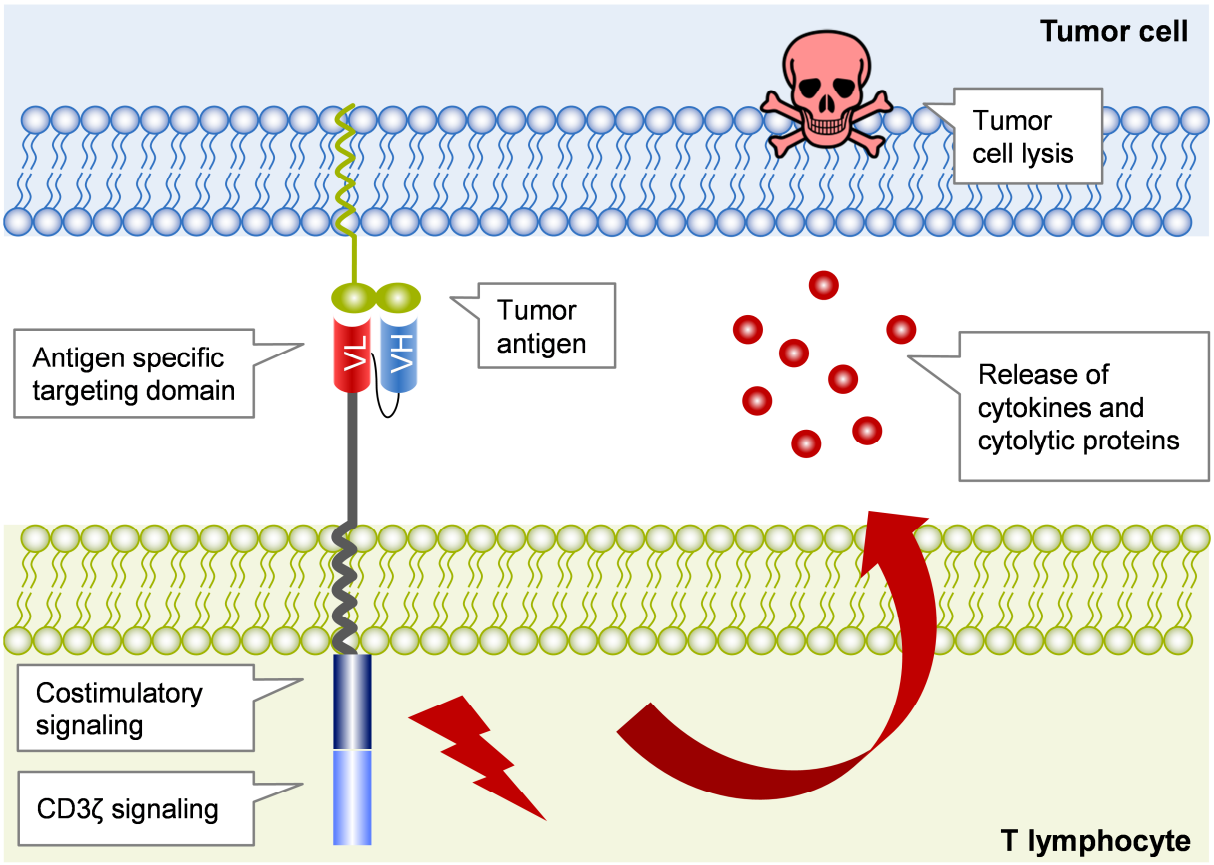

Figure 4. CAR T cell mode of action. The CAR targeting domain recognizes a specific tumor antigen. The CAR T cell binds to antigen positive tumor cells and antigen induced CAR clustering enables downstream signaling by the costimulatory domain(s) and the CD3ζ domain. The activated CAR T cell kills the tumor cell via secretion of cytokines (e.g. IFNγ, TNFα) and other cytolytic proteins (e.g. perforin) in a MHC independent manner.

Commonly used costimulatory domains are derived from CD28 and/or CD137 (4-1BB), both of which affect the CAR T cell metabolism and phenotype in very different ways. CD28 signaling drives anabolic glucose uptake, thereby supporting effector cell differentiation and cytolytic activity at the expense of long-term expansion. In contrast, 4-1BB enhances catabolic activity, thereby supporting memory cell differentiation and long-term

persistence *in vivo* [74,76]. Both costimulatory domains promote IFNγ release, but only CD28 additionally enhances IL-2 secretion, which may be disadvantageous as IL-2 potentially promotes Treg formation at the tumor site and thereby inhibition of CAR T cell responses [77]. To circumvent IL-2 dependent Treg formation at the tumor site, a report described that specific mutations within the CD28 signaling tail impaired binding of the lymphocyte specific tyrosine kinase (Lck) to the CD28 costimulatory domain of the CAR, which counteracted CAR T cell induced IL-2 release. The concomitant reduction in Treg numbers was shown to enhance the CAR T cell antitumor activity [78]. After years of testing various second generation CARs that either contained a CD28 or 4-1BB costimulatory domain, the latter was found to possess some advantages over CD28. These included improved T cell expansion, persistence *in vivo* and ameliorating effects on T cell exhaustion [79,80]. Physiologically, T cell exhaustion is a protective mechanism to prevent excessive T cell activation due to persisting antigen exposure as occurs during chronic infections. Otherwise, the lasting secretion of proinflammatory proteins by activated T cells would cause tissue damage [81,82]. In terms of CAR T cells, it was reported that exhaustion can result from antigen independent constitutive CAR signaling due to clustering of the CAR molecules on the T cell surface driven by aggregation tendencies of the scFv moieties. Exhausted CAR T cells show reduced antitumor effects, only poor expansion capacities *in vitro* and *in vivo*, and are characterized by the expression of the inhibitory receptors PD-1, TIM-3 and LAG-3 [80,83,84].

In general, no “gold standard” CAR configuration has been described, as the CAR mechanistically interacts with the tumor cell in a highly antigen – and even epitope – dependent way. Thus, the optimal CAR configuration needs to be determined empirically for each individual epitope.

1.4.2 Role of T cell populations in adoptive CAR T cell therapy

Among T cells, different subpopulations exist with distinct functions. Roughly, T cells can be divided into $CD4^+$ and $CD8^+$ T cells. In general, $CD4^+$ T cells organize the immune response, induce humoral immune responses and influence the killing activity of $CD8^+$ T cells via cytokines [1]. Interestingly, Hombach and Abken showed that a certain subset of $CD4^+$ CAR T cells ($CD4^+/CD25^-$) also possessed the ability to directly lyse target cells with the same potency as $CD8^+$ T cells. In contrast, CAR expressing Tregs ($CD4^+/CD25^+$) were incapable of target cell killing, but had a strong inhibitory influence on surrounding lymphocytes [85]. Researchers took advantage of these characteristics and developed CAR Tregs to treat chronic inflammatory diseases by downmodulation of inappropriate responses in

autoimmune settings [86,87].

When first encountering an antigen, naïve T (Tn) cells progressively differentiate into memory T cell subsets with specific phenotypes that further differentiate into effector T (Teff) cells. However, the process might be partly reversible in that Teff cells dedifferentiate into memory T cells to develop a long-term memory [88,89]. T cell subsets can be distinguished phenotypically by the distinct expression of surface markers such as CD27, CD28, CD45RA, CD45RO, CD62L, CD95 and CCR7 (CD197) [90]. CD45RA and CD45RO are splice variants from the CD45 gene and were initially used to separate naïve ($CD45RA^+/CD45RO^-$) from memory ($CD45RA^-/CD45RO^+$) T cells [91,92]. The chemokine receptor CCR7 was later found to further separate memory T cells into two individual subsets. $CCR7^+$ memory T cells are attracted to lymphoid organs and release low levels of effector cytokines, such as interferon gamma (IFNγ), but at the same time have a high proliferation potential due to increased IL-2 secretion, thus being termed central memory T (Tcm) cells. In contrast, $CCR7^-$ memory T cells behave vice versa, release high levels of IFNγ and possess premature cytotoxic granules. Being equipped with these preliminary effector functions, they were classified as effector memory T (Tem) cells [93,94]. By studying the expression of the death receptor CD95 in Tn cells, another subset was identified. Apart from being $CCR7^+$, Tn cells do not express CD95 prior to antigen encounter, but antigen mediated activation does induce the expression of CD95. The resulting subset ($CD45RO^-/CCR7^+/CD95^+$) was termed stem cell memory (Tscm) as it is a multipotent precursor of other memory T cell subsets, but with the ability to self-renew and higher persistence. It was shown for retrovirus infected macaques that Tscm cells persisted tenfold longer than Tcm cells upon loss of the cognate viral antigen [90,95,96].

In summary, progressing differentiation reduces the proliferative capacity, enhances effector functions and promotes peripheral presence of T cells (*Figure 5*). In terms of CAR T cell therapy, only a lasting and stable antitumor response ensures effective tumor clearance. Furthermore, CAR T cells need to develop an immunological memory to prevent tumor reappearance. Considering the short lifespan of effector (memory) T cells and that they are prone to activation induced cell death, the less differentiated Tscm and Tcm subsets are favored for CAR T cell therapy to fulfill the requirements listed above. Importantly, Tscm and Tcm subsets still possess the capacity to generate effector functions for potent tumor killing through differentiation [40,97,98]. Early clinical trials confirmed that prolonged persistence correlated with therapeutic efficacy. In this regard, especially the 4-1BB costimulatory domain contributed to outgrowth of long-lived $CD8^+$ CAR Tcm cells [76,99,100]. These results outline the CAR design and the T cell subset as important key factors to be considered when developing CAR T cell therapies.

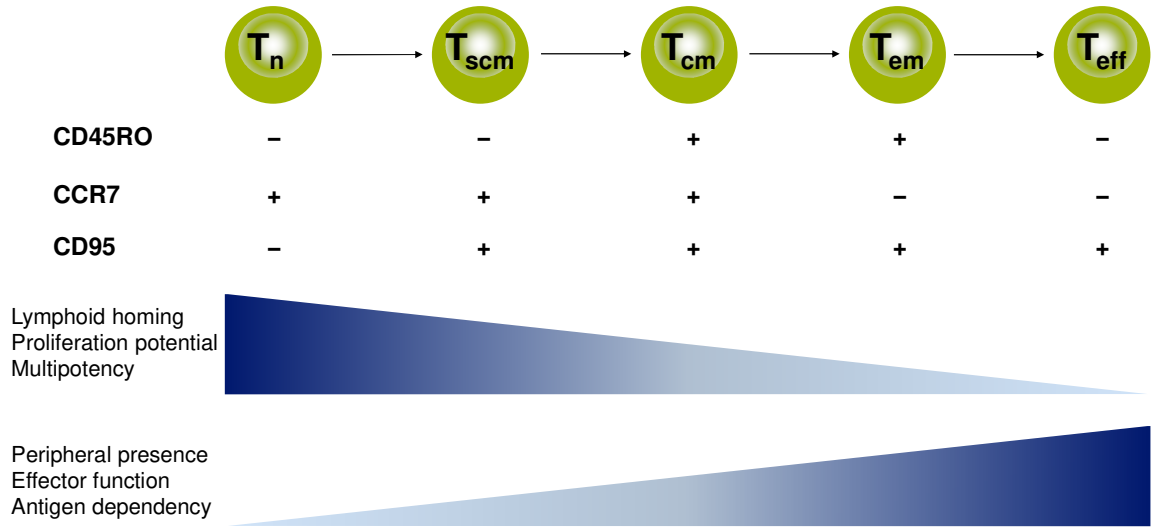

Figure 5. T cell subset identification and characteristics. According to the surface markers CD45RO, CCR7 and CD95, specific T cell subsets can be identified. Naïve T cells (Tn) have the highest multipotency and proliferation potential. Progressive differentiation from stem cell memory (Tscm) to central memory (Tcm), effector memory (Tem) and effector (Teff) T cells is driven by antigen dependent activation. The more differentiated T cell subsets have a higher presence in the periphery and possess distinct effector functions compared with the less differentiated subsets. Image based on Mahnke *et al.* [90].

1.4.3 CAR T cell therapies in the clinic

Initial phase I trials using T cells with first generation CARs for ACT failed to elicit a robust and consistent antitumor response [101,102]. Only when costimulatory domains were included in CARs, the full potential of CAR T cell therapy was revealed: long-term T cell persistence combined with a much more effective antitumor activity [60,103]. Treatment of hematological malignancies with CAR T cells was most successful among several studied cancers [104,105].

To date, two CD19 targeting CAR T cell therapies named Kymriah® and Yescarta® are approved by the U.S. Food and Drug Administration [106] and the European Commission [107,108]. Both products use second generation CARs containing either the 4-1BB (Kymriah®) or the CD28 (Yescarta®) costimulatory domain [109]. Out of 30 patients suffering from relapsed or refractory acute lymphoblastic leukemia, 27 patients (90%) experienced complete remission within one month after treatment with Kymriah®. Follow-up investigation revealed sustained remission in 19 of these patients accompanied by the persistence of the CD19 CAR T cells [110]. Complete remissions were also observed in 6 out of 14 patients

(43%) with diffuse large B cell lymphoma and in 10 out of 14 patients (71%) with follicular lymphoma when treated with Kymriah®. Both groups showed high rates (86-89%) of durable remissions over a period of about 28 months [111]. Therapy of diffuse large B cell lymphoma patients with Yescarta® led to complete remissions in 55 of 101 patients (54%), out of which 40% retained complete remission within the follow-up period of 15 months [112].

During the treatment with CD19 specific CAR T cells, most patients experienced common adverse effects such as B cell aplasia, cytokine release syndrome and neurotoxicity. B cell aplasia resulted from the eradication of healthy CD19 positive B cells by the CD19 targeting CAR T cells, but the consequent lack of blood immunoglobulins could be compensated by immunoglobulin replacement therapy. Almost all patients showed the cytokine release syndrome, a systemic inflammatory response due to intense CAR T cell activation, which could be reversed with anti-inflammatory medication. Some patients with initial complete remission relapsed, due to either lack of CAR T cell persistence, emergence of malignant CD19 negative escape variants or redifferentiation of the malignant B cells to CD19 negative myeloid cells. These CD19 negative cases of leukemia and lymphoma need to be treated with alternative options such as targeting of other B cell markers [104,110,113].

While leukemias and lymphomas represent only 8% of all cancers, solid tumors account for over 90% [114]. However, CAR T cell therapy against solid tumors is challenging as they form an immunosuppressive microenvironment that inhibits antitumor responses. Moreover, the tumor associated stroma secretes pro-tumorigenic factors and mechanically blocks CAR T cell penetration. Solid tumors are highly heterogeneous and often lack the expression of tumor exclusive antigens, thus bearing the risk of on-target/off-tumor toxicities during CAR T cell therapy [65,115]. The severity of such toxic cross-reactions with healthy tissues was shown in 2010 when a fatal case was reported. Only minutes upon infusion of ERBB2 specific CAR T cells into a patient with metastatic lung and liver cancer, the patient showed respiratory distress and died five days post treatment despite medical intervention. After autopsy, metastatic tissues from lung and liver were confirmed to overexpress ERBB2, but also normal lung and liver tissue were found to express ERBB2 in low levels. The clinicians concluded that the death was caused by CAR T cells additionally recognizing ERBB2 on these healthy tissues, followed by their rapid release of inflammatory cytokines in high amounts, eventually leading to multi-organ failure [116]. In a phase I clinical trial using CEA specific CAR T cells, 7 out of 10 patients with refractory colorectal carcinoma showed stable disease and partial tumor shrinkage. Although high doses of CAR T cells were well tolerated, no complete remissions were achieved due to low CAR T cell persistence *in vivo* [117]. Poor efficacy was also observed in another clinical study, in which no clinical responses were obtained for 12 patients with metastatic renal cell carcinoma treated with CAIX recognizing CAR T cells. 4 out of 12 patients experienced liver toxicities due to basal

CAIX expression on bile duct epithelial cells. These patients were subsequently pretreated with a CAIX specific mAb before CAR T cell infusion and the previously observed liver toxicities could be efficiently prevented. It was concluded that blocking of antigenic sites in healthy tissues with mAbs might allow higher CAR T cell dosage for treatment of solid tumors [118].

These studies demonstrate that although severe cytokine release syndromes were rather rarely observed when treating solid cancers with CAR T cells, on-target/off-tumor toxicity as well as physical and environmental tumor barriers mainly limit the clinical efficacy. Consequently, three requirements for successful CAR therapy against solid cancers were defined: choice of a safe target, effective tumor infiltration and overcoming immune suppression [65,119].

1.5 Cancer-testis antigens as tumor targets

The identification of highly tumor specific surface structures is the essential requirement for targeted immunotherapy with CAR T cells as healthy tissues need to be prevented from damage. Cancer-testis antigens (CTAs) represent a particular class of tumor markers: their expression is restricted to male germ cells and placenta, but aberrantly reactivated in a broad spectrum of different cancer types [120,121].

CTAs were classified according to their expression profile as testis restricted (testis only), testis selective (testis and additional tissues) or testis/brain restricted (testis and central nervous system) [122]. Demethylation was suggested to be the primary driver of CTA gene reactivation in cancers [123,124]. The function of CTAs in cancers is not fully understood yet, however, their expression correlates with tumor grade, poor clinical prognosis and metastasis [125,126,127]. Simultaneous expression of multiple CTAs was found in many cancers. Shared characteristics between germ cells and cancer cells including proliferation, motility and survival signaling were discussed to promote tumorigenesis [128,129].

Testes are immune privileged and germ cells lack MHC class I molecules making them invisible for the immune system. As a consequence, CTAs are highly immunogenic and were suggested as targets for cancer immunotherapy [128,130,131]. The potential of CTAs to induce spontaneous cellular and humoral responses was shown when CTAs were discovered in 1991 and in later studies [132-134]. Notably, mRNA encoding for some CTAs was reported to be also expressed in medullary thymic epithelial cells, indicating that CTAs may not be excluded from central T cell tolerance [135].

To date, only TCR engineered T cells targeting the well characterized CTAs MAGE-A3 and NY-ESO-1 were tested in clinical trials, but no approach using CAR engineered T cells was tested yet [136,52]. While some cancer researchers encourage the use of CTAs for CAR T cell therapy, others point out their mostly intracellular localization, thus being only targetable in combination with MHC [137,138]. However, analysis of CTA surface expression was insufficiently conducted in previous studies. So far, CTA expression was found on acute myeloid leukemia cells and on several tumor cell lines, allowing for direct targeting [139-141]. For our study, we chose three CTAs with indicated surface expression in the literature.

1.5.1 A-Kinase Anchor Protein 4 (AKAP4)

A-kinase anchor protein 4 (AKAP4) is the most common protein found in the fibrous sheath of the sperm tail and highly conserved within the mammalian species. The fibrous sheath is a specialized cytoskeletal structure that enables sperm motility. AKAP4 has a precursor form, pro-AKAP4, which contains 854 amino acids (aa) and is proteolytically cleaved to a 665 aa mature form upon transport into the fibrous sheath [142-145].

It has been shown that AKAP4 is involved in signaling transduction as an intracellular adaptor protein. It contains binding motifs that interact with cyclic adenosine monophosphate (cAMP) dependent protein kinases and recruits further proteins that regulate cAMP dependent signaling [146-148].

AKAP4 is a testis restricted CTA with reported expression in ovarian cancer [149,150], multiple myeloma [151], prostate cancer [152], colorectal cancer [153], breast cancer [140], non-small cell lung cancer [154] and cervical cancer [155], while being absent in matched healthy tissues. In these tumors, AKAP4 regulates proliferation, migration, invasion and survival by interacting with extracellular signal regulated kinases and other signaling pathways [147,148]. In particular its testis exclusive expression and surface localization on several cancer cell lines outline AKAP4 as a highly interesting target for CAR T cell therapy.

1.5.2 Sperm Protein 17 (SP17)

DNA sequencing by Lea *et al*. in 1996 revealed sperm protein 17 (SP17) as a 151 aa protein [156]. It binds to the oocyte zona pellucida by a sulfated carbohydrate binding domain and thus plays an important role in sperm-egg interaction during fertilization. Moreover, SP17 possesses an intracellular regulatory subunit that binds to AKAPs and a calmodulin binding domain which mediates calcium dependent sperm functions such as motility and the acrosome reaction. Equipped with these three domains, SP17 is further involved in cell-cell

adhesion and signal transduction. Its polyfunctional nature might also explain the benefit of SP17 upregulation in tumors [157-160].

SP17 expression was found in many cancer entities such as ovarian cancer [161,162], multiple myeloma [163,164], breast cancer [165], non-small cell lung cancer [154], head and neck squamous cell carcinoma [166], esophageal cancer [167] and hepatocellular carcinoma [168]. SP17 is considered as testis selective CTA due to expression in healthy ciliated epithelial cells [169,170]. An adoptive immunotherapeutic approach with SP17 specific monoclonal cytotoxic T lymphocytes showed complete tumor eradication in an ovarian cancer mouse model [171]. A clinical trial with one multiple myeloma patient and two ovarian cancer patients (patient tumors were diagnosed SP17 positive) treated with SP17 pulsed dendritic cells showed antitumor responses without major toxicity. Importantly, none of the patients experienced pulmonary symptoms despite SP17 expression on ciliated epithelial cells [172]. As a consequence, several cancer researchers suggested SP17 as a safe target for cancer immunotherapy [154,170].

1.5.3 Sperm Associated Antigen 9 (SPAG9)

When sperm associated antigen 9 (SPAG9) was cloned from a human testis cDNA library in 1998, structural analysis revealed a 766 aa protein possessing a leuzine zipper motif and three putative antigenic regions (predicted to be coiled coil domains) within the extracellular section (*Figure 6*) [173,174].

Figure 6. Schematic representation of the SPAG9 protein. SPAG9 contains a leuzine zipper (LZ) and three putative antigenic regions (A1, A2, A3) within the extracellular section. N = NH_2 terminus, C = COOH terminus, TM = transmembrane section. Image based on Shankar *et al*. [173].

SPAG9 is a member of the c-Jun N-terminal kinase interacting protein family and is involved in spermatozoa-egg interaction. It is localized on the spermatozoa acrosomal membrane and a cell line transfected with a transmembrane deleted SPAG9 variant was shown to lose SPAG9 surface expression *in vitro*, supporting the hypothesis of a plasma membrane anchored protein [174]. SPAG9 was classified as testis selective due to its mRNA expression

in healthy tissues, but protein expression has been reported to be significantly higher in cancer tissues compared with adjacent normal tissues [122,175,176]. A broad range of tumors express SPAG9 including ovarian cancer [177,178], multiple myeloma [179], lung cancer [180], colorectal cancer [176], renal cell carcinoma [181], breast cancer [182], leukemia [183,184] and prostate cancer [175]. Many cancer patient sera were found to be positive for SPAG9 specific circulating antibodies, highlighting the immunogenic potential of SPAG9 to induce humoral responses. The circulating antibodies were discussed as biomarkers for the early detection of tumors [184,185].

SPAG9 is also involved in mitogen activated protein kinase signaling, thereby driving tumor growth, invasion, survival and drug resistance. To date, SPAG9 was not exploited as target for an adoptive T cell therapy, but was highly recommended to be further explored for use in immunotherapeutic strategies [181,186,187].

1.6 Aim of the project

Adoptive CAR T cell therapy has shown highly promising results in early clinical trials treating hematological malignancies. However, for the treatment of solid tumors major hurdles need to be solved, including the co-expression of tumor associated antigens on healthy tissues that can cause lethal toxicities during the immunotherapeutic intervention. Thus, the selection of truly tumor restricted targets is key for the development of novel immunotherapeutic approaches to ensure therapeutic safety.

This project aims at evaluating the CTAs AKAP4, SP17 and SPAG9 as tumor surface markers and to develop a specific CAR T cell therapy. By applying these CTAs for antibody fragment selection from phage display antibody libraries that contained immune or naïve repertoires, we obtained AKAP4, SP17 and SPAG9 specific scFvs. We fused the scFvs to a human IgG1 Fc backbone to be expressed as a soluble scFv-hFc fusion protein in mammalian cells. We analyzed antigen specificity by ELISA and SPR spectroscopy using purified antigens and investigated scFv-hFc binding to various tumor cell lines, primary bone marrow cells isolated from multiple myeloma patients and to peripheral blood mononuclear cells derived from healthy donors.

The scFv lead candidates with the best binding profiles toward target tumor cell lines were incorporated into five different CAR backbones with varying spacer length (CD8α vs. hFc) and signaling domain composition (second vs. third generation CARs). After lentiviral CAR gene transfer into human T cells, we analyzed CAR expression, CAR T cell expansion, CAR T cell phenotype and target cell killing *in vitro*.

2 Materials and methods

2.1 Materials

2.1.1 Laboratory equipment

Table 1. List of utilized laboratory equipment

Instrument	Type	Supplier
Absorbance and fluorescence plate reader	Infinite F200Pro	Tecan
Agarose gel station	Mini Sub-Cell GT	Bio-Rad Laboratories
	Sub-Cell GT	Bio-Rad Laboratories
Automatic dispenser pipette	Multipette Stream	Eppendorf
Automatic multichannel pipette	Xplorer	Eppendorf
Bacteriological incubator	BE 2000 32l	Memmert
	Heraeus B6	Thermo Fisher Scientific
Balance	AJ-2200CE Vibra	Shinko Denshi
Cell culture shaker	Minitron	Infors HT
	Multitron Pro	Infors HT
Centrifuge	5424 R	Eppendorf
	C5-6R	Beckmann
	Heraeus Megafuge 40R	Thermo Fisher Scientific
	Megafuge 1.0	Heraeus
	Mikro 200R	Hettich
	Multifuge 4KR	Thermo Fisher Scientific
	Sorvall RC 6+	Thermo Fisher Scientific
Centrifuge mini	3-1810	neoLab
Chemiluminescence visualization system	INTAS Advanced Fluorescence Imager	Intas Science Imaging
CO_2 incubator	Heracell 150	Thermo Fisher Scientific
	NU-5510E	Ibs Tecnorama
Electroblotting system	Trans Blot Semi-Dry Transfer Cell	Bio-Rad Laboratories
ELISA washer	Elx405	BIO-TEK
Flow cytometer	BD FACS Celesta	BD Biosciences

	BD FACS Verse	BD Biosciences
FPLC system	AEKTAFPLC system AEKTApure FPLC system	Amersham Bioscience GE Healthcare
Gel visualization system	Gel Jet Imager	Intas Science Imaging
Heating block	HBT-2 131 TH 21	HLC Biotech HLC Biotech
Hemocytometer	Neubauer improved	Karl Hecht
Inverted microscope	CKX41	Olympus
Magnetic stirrer	MR2000 2mag Mix 1 XL	Heidolph Instruments 2mag AG
Magnetic tray	DynaMag-2 Magnet	Thermo Fisher Scientific
Multichannel pipette	Pipetman neo P200	Gilson
Orbital plate shaker	DRS-12	neoLab
PCR thermocycler	peqSTAR 96 Universal Gradient	peqLab
pH meter	PB-11	Sartorius
Photometer	NanoDrop ND-1000	Thermo Fisher Scientific
Pipette controller	Pipetus	Hirschmann
Pipettes	Pipetman neo P1000, P200, P20, P10	Gilson
Power supply	PowerPac Basic PowerPac HC peqPower	Bio-Rad Laboratories Bio-Rad Laboratories peqLab
Precision balance	CPA22D-OCE	Sartorius
Real time cell analyzer	xCELLigence RTCA SP	ACEA Biosciences
Rocking plate shaker	DSG 304|M4	Heidolph Instruments
Scanner	Perfection V750 Pro	Epson
SDS gel station	Novex Mini-Cell	Invitrogen
Sterile bench	SAFE2020 HERAsafe KSP 12	Thermo Fisher Scientific Thermo Fisher Scientific
Surface plasmon resonance based instrument	Biacore 2000	GE Healthcare
Tube roller	RMS-30V CAT	neoLab
Vortex	L46	GLW

	D-6012	neoLab
Water bath	T100	Labortechnik Medingen

2.1.2 Chemicals, reagents and commercial media

Table 2. List of utilized chemicals, reagents and commercial media

Product	Supplier (Cat. No.)
10x Cut Smart buffer	New England Biolabs (B7204S)
10x T4 DNA ligase buffer	Thermo Fisher Scientific (B69)
6x Loading dye	New England Biolabs (B70245)
Acetic acid	Carl Roth (7332.1)
Agar	Sigma-Aldrich (05039)
Agarose, universal	VWR Chemicals (35-1020)
Ammonium peroxidsulfate (APS)	Carl Roth (9592.2)
Ampicillin sodium salt	Carl Roth (K029)
Aqua ad iniectabilia	Braun (2351744)
Bromphenol blue	AppliChem (7K005159)
Buffer solution pH 10	Carl Roth (P716.2)
Buffer solution pH 4	Carl Roth (P712.3)
Buffer solution pH 7	Carl Roth (A518.1)
Citric acid	Carl Roth (X863.2)
Coomassie Brillant Blue R 250	Carl Roth (3862.1)
D(+)-Glucose	Carl Roth (X997.2)
D(+)-Sucrose	Carl Roth (4621.2)
Dimethyl sulfoxide (DMSO)	Serva (20385.01)
Disodium hydrogen phosphate (Na_2HPO_4)	Carl Roth (P030.2)
Dithiothreitol (DTT)	Carl Roth (6908.3)
Dulbecco's Modified Eagle Medium (DMEM)	Sigma-Aldrich (RNBG3787)
Dulbecco's Modified Eagle Medium (DMEM), without phenol red	Sigma-Aldrich (21063029)
Dulbecco's Phosphate Buffered Saline (DPBS)	Sigma-Aldrich (D8537)
Ethanol	Carl Roth (5054.4)
Ethylenediaminetetraacetic acid disodium salt dihydrate (EDTA)	Carl Roth (8043.2)
FACS clean	BD Biosciences (340345)

FACS flow	BD Biosciences (342003)
FcR blocking reagent, human	Miltenyi (130-059-901)
Fetal calf serum (FCS)	Sigma-Aldrich (F0804)
Ficoll Paque PLUS	GE Healthcare (17-1440-03)
Freestyle F17 Medium	Life technologies (A13835)
GeneRuler 1 kb DNA Ladder	Thermo Fisher Scientific (SM0311)
Geneticin disulfate (G418)	Carl Roth (CP11.3)
Glycerol	Carl Roth (7530.4)
Glycine	Carl Roth (3908.2)
Hydrochloric acid, 2N (HCl)	Carl Roth (T134.1)
Hydrochloric acid, 37% (HCl)	Carl Roth (9277.1)
Isopropyl β-D-1-thiogalactopyranoside (IPTG)	Carl Roth (2316.1)
Isopropanol	Carl Roth (9866.2)
Kanamycin sulfate	Carl Roth (T832.2)
Kolliphor P188	Sigma-Aldrich (K4894)
L-Glutamine	Sigma-Aldrich (G7513)
Magnesium sulfate ($MgSO_4$)	Carl Roth (0261.2)
Methanol	Carl Roth (8388.2)
Penicillin Streptomycin Solution (pen/strep)	Sigma-Aldrich (P0781)
PeqGREEN DNA/RNA Dye	peqLab (37-5000)
Polybrene hexadimethrine bromide	Sigma (107689)
Polyethylene glycol 2 (PEG_2)	Novabiochem (8.51031.8500)
Polyethylene glycol 6000 (PEG_{6000})	Carl Roth (0158.1)
Polyethylenimine (PEI)	Polysciences (23966)
Potassium chloride (KCl)	Carl Roth (6781.1)
Potassium dihydrogen phosphate (KH_2PO_4)	Carl Roth (P018.1)
Powdered milk	Carl Roth (T145.2)
Rotiphorese 10x SDS PAGE	Carl Roth (3060.2)
Rotiphorese Gel A	Carl Roth (3037.1)
Rotiphorese Gel B	Carl Roth (3039.2)
Roswell Park Memorial Institute 1640 medium (RPMI-1640)	Sigma-Aldrich (RNBG6386)
Sodium acetate	Carl Roth (6773.1)
Sodium dihydrogen phosphate (NaH_2PO_4)	Carl Roth (K300.3)
Sodium dodecyl sulfate (SDS)	Carl Roth (2326.1)

Sodium azide ($NaN3_)$	Sigma-Aldrich (52002)
Sodium chloride (NaCl)	Carl Roth (9265.2)
Sodium hydroxide (NaOH)	Carl Roth (6771.1)
Spectra BR Multicolor Broad Range Protein Ladder	Thermo Fisher Scientific (26634)
Sulfuric acid (H_2SO_4)	Carl Roth (X873.1)
SYTOX Blue Dead Cell Stain	Invitrogen (S34857)
Tetramethylethylenedamine (TEMED)	Fluka (87689)
Triethylamine	Carl Roth (X875.2)
Tris Base	Calbiochem (648510)
Tris hydrochloride	Carl Roth (9090.3)
Tris Pufferan	Carl Roth (4855.2)
Trypan blue	Life Technologies (15250-061)
Trypsin/EDTA	Life technologies (25300)
Tryptone N1 (TN1)	Organotechnic SAS (19553)
Tryptone/Peptone from casein	Carl Roth (8952.2)
Tween 20	Carl Roth (9127.1)
X-VIVO15	Lonza (BE02-060F)
Yeast extract	Carl Roth (2363.2)

2.1.3 Consumables

Table 3. List of utilized consumables

Consumable	Supplier
1.5 mm SDS PAGE casette	Invitrogen
24-well plate polystyrene non-treated cell culture plate	Corning
96-deep-well polystrene microtiter plate	Sigma
96-well E-plate	ACEA Biosciences
96-well half area microtiter plate	Nunc
96-well Maxisorp microtiter plate	Nunc
96-well U-bottom polystyrene microtiter plate	Greiner Bio-One
AeraSeal breathable sealing film	Excel Scientific
Bacterial culture tube (12 mL)	Greiner Bio-One
Bottle top filter 50 mm	Thermo Fisher Scientific
Cell culture flask for adherent cells (T25, T75, T175)	Greiner Bio-One

Cell culture flask for suspension cells (T75, T175)	Greiner Bio-One
Centricon Plus-70	Merk Millipore
CM5 sensor chip	GE Healthcare
Cryogenic vial with screw cap (2.0 mL)	Greiner Bio-One
Dialysis membrane ZelluTrans	Carl Roth
Dynabeads M-280 Streptavidin	Invitrogen
Erlenmeyer cell culture flask with filter cap (500 mL)	BD Biosciences
Erlenmeyer cell culture flask with filter cap (125 mL)	Corning
Extra thick blot paper / Mini blot size	BioRad
Flow cytometry round-bottom tubes	Falcon
Nitrocellulose western blot membrane	neoLab
PCR tube strip with 8 tubes (0.2 mL)	neoLab
PCR tubes, flat cap (0.2 mL)	AHN Biotechnology
Petri dish 100 mm	Greiner Bio-One
Pipette filter tip (10, 20, 200, 1000 µL)	Greiner Bio-One
Plastic syringe (20 mL, 50 mL)	BD Biosciences
Plastic vials, 11 mm	GE Healthcare
Polypropylene conical tube (15 mL, 50 mL)	Falcon
Polystyrene round bottom tube (5 mL)	Falcon
Reaction tubes (1.5 mL, 2.0 mL)	neoLab
Reagent reservoir (50 mL)	Corning
Rubber caps, type 2	GE Healthcare
Rubber caps, type 5	GE Healthcare
Serological pipette (1, 2, 5, 10, 20 and 50 mL)	Corning
Shell vial, 4 mL, PP	Wheaton
Square dish 12 x 12 x 17 mm	Greiner Bio-One
Syringe filter 0.22 µm	Merk Millipore
Tissue culture dish with 20 mm grid	Corning

2.1.4 Chromatography columns

Table 4. List of used chromatography columns

Column	Supplier (Cat. No.)
HiLoad 16/600 Superdex 200 pg (120 mL)	GE Healthcare (28989335)
HiTrap rProtein A FF (1 mL)	GE Healthcare (17507901)
Superdex 200 Increase 10/300 GL column (20 mL)	GE Healthcare (28990944)

2.1.5 Kits

Table 5. List of applied kits

Kit	Supplier (Cat. No.)
Amine Coupling Kit	GE Healthcare (BR100050)
CFSE Cell Division Tracker Kit	BioLegend (423801)
EndoFree Plasmid Maxi Kit	QIAGEN (12362)
EndoFree Plasmid Midi Kit	QIAGEN (12362)
KAPA HiFi PCR Kit	Roche (KK2101)
Human IFNγ ELISA Set	Becton Dickinson (555142)
LDH-Glo Cytotoxicity Assay Kit	Promega (J2380)
Minute Single Cell Isolation Kit	Biocat (SC-012)
Pierce ECL Western Blotting Substrate	Thermo Fisher Scientific (32106)
Pierce TMB Substrate Kit	Thermo Fisher Scientific (34021)
Plasmid Midi Kit	QIAGEN (12143)
QIAprep Spin Minprep Kit	QIAGEN (27106)
QIAquick Gel Extraction Kit	QIAGEN (28706)
QIAquick PCR purification Kit	QIAGEN (28106)
T Cell TransAct, human	Miltenyi (130-111-160)
Zenon APC Human IgG Labeling Kit	Thermo Fisher Scientific (Z-25451)
Zenon APC Mouse IgG2a Labeling Kit	Thermo Fisher Scientific (Z-25151)

2.1.6 Buffers, solutions and media

Table 6. List of utilized buffers, solutions and media

Buffer / Solution / Medium	Components
2x YT medium	1% (w/v) tryptone, 1% (w/v) yeast extract, 0.05% (w/v) NaCl in ddH_2O
2x YT-A/-AK medium	0.1% (v/v) ampicillin stock (-A) or 0.1% (v/v) ampicillin stock and 0.1% (v/v) kanamycin stock (-AK) in 2x YT medium
2x YT-GA medium	2% (w/v) glucose, 0.1% (v/v) ampicillin stock in 2x YT medium
2x YT-GA agar	1.5% (w/v) agar in 2x YT-GA medium
2x YT-K agar	1.5% (w/v) agar, 0.1% (v/v) kanamycin stock solution in 2x YT medium
5x Laemmli buffer	250 mM Tris-HCl, 10% (w/v) SDS, 30% (v/v) glycerol, 0.05% (w/v) bromphenol blue in ddH_2O
10x HBS-EP	0.1 M HEPES, 1.5 M NaCl, 30 mM EDTA, 0.5% (v/v) Tween 20% in ddH_2O, pH 7.4
10x PBS	1.4 mM NaCl, 27 mM KCl, 101 mM Na_2HPO_4, 18 mM KH_2PO_4 in ddH_2O
Ampicillin stock solution	100 mg/mL ampicillin sodium salt in ddH_2O
Coomassie staining solution	0.06% Coomassie Brilliant Blue G-250, 35 mM HCl in ddH_2O
Flow cytometry buffer	2% (v/v) FCS, 1% (w/v) NaN_3 in PBS
Freezing medium	10% DMSO (v/v) in FCS
Kanamycin stock solution	100 mg/mL kanamycin sulfate in ddH_2O
LB-A/-K agar	1.5% (w/v) agar in LB medium, 0.1% (v/v) ampicillin (-A) or kanamycin (-K) stock solution
LB-A/-K medium	1% (w/v) tryptone, 0.5% (w/v) yeast extract, 1% (w/v) NaCl in ddH_2O, 0.1% (v/v) ampicillin (-A) or kanamycin (-K) stock solution
M9 salt solution	27.1 mM Na_2HPO_4, 22.0 mM KH_2PO_4, 8.55 mM NaCl, 9.35 mM NH_4Cl in ddH_2O, adjust to pH7.2
Minimal agar	1.5% (w/v) agar in ddH_2O 2% (w/v) glucose, 1 mM $MgSO_4$, 0.2% (w/v)

	thiamine, 10% (v/v) M9 salt solution
MPBS	2-4% (w/v) milk powder in 1x PBS
MPBST	MPBS, 0.05% (v/v) Tween 20
PBST	0.05% (v/v) Tween 20 in 1x PBS
PEI transfection reagent	0.1% (w/v) PEI dissolved at pH 2.0 in ddH_2O, adjust pH to 7.0
Periplasmic preparation buffer	30 mM Tris-HCl, 1 mM EDTA, 20% (w/v) sucrose in ddH_2O, adjust to pH 8.0 add 5% (w/v) fresh lysozyme before use
Phage elution buffer (acidic)	100 mM glycine-HCl in ddH_2O, adjust pH to 3.0
Phage elution buffer (basic)	100 mM triethylamine in ddH_2O, adjust pH to 12.0
Phage neutralization buffer	1 M Tris in ddH_2O, adjust pH to 7.4
Phage precipitation buffer	2.5 M NaCl, 20% (w/v) PEG_{6000} in ddH_2O
Protein A binding buffer	100 mM NaH_2PO_4, 100 mM NaCl, 10 mM EDTA in ddH_2O, adjust to pH 7.0
Protein A elution buffer	0.1 M citric acid in ddH_2O, adjust to pH 3.0
Protein A neutralization buffer	1 M Tris Pufferan in ddH_2O, adjust to pH 9.0
Semi-dry blot buffer	48 mM Tris Pufferan, 39 mM glycine, 1.3 mM SDS, 20% (v/v) ethanol in ddH_2O, adjust pH to 9.0-9.4
Separating gel buffer	1 M Tris Pufferan in ddH_2O, adjust to pH 8.8
SOC medium	2% (w/v) tryptone, 0.5% (w/v) yeast extract, 2.5 mM KCl, 10 mM NaCl, 20 mM $MgSO_4$, 20 mM glucose in ddH_2O
SPR regeneration buffer	10 mM glycine in ddH_2O, pH 1.7
Stacking gel buffer	650 mM Tris Pufferan in ddH_2O, adjust to pH 6.8
Supplemented DMEM medium	10% (v/v) FCS, 1% (v/v) pen/strep in DMEM medium
Supplemented F17 medium (+ G418)	4 mM L-glutamine, 0.1% (w/v) Kolliphor P188, (+ 0.05% (v/v) Geneticin)
Supplemented RPMI-1640 medium	10% (v/v) FCS, 1% (v/v) pen/strep in RPMI-1640 medium
TAE buffer	2.4% (w/v) Tris, 10% (v/v) EDTA, 5.7% acetic acid in ddH_2O

TN1 feeding medium	20% (w/v) TN1 in supplemented F17 medium w/o G418
Transfection medium	Supplemented F17 medium without G418

2.1.7 Cell lines, bacterial strains and primary cells

Table 7. List of used cell lines, bacterial strains and primary cells

Bacterial strain / Cell line	Organism	Description	Supplier (Cat. No.)
TG1	*Escherichia coli*	Bacterial strain for phage display applications	Agilent Technologies (200123)
XL-1 Blue	*Escherichia coli*	Bacterial strain for transformation and DNA amplification	Stratagene (200228)
Colo205	*Homo sapiens*	Adherent growing cell line established from colorectal adenocarcinoma	Kind gift from Prof. Dr. Roland Kontermann, University of Stuttgart
Granta-519	*Homo sapiens*	Suspension cell line established from mantle cell lymphoma	Kind gift from Dr. Dr. Klaus Podar, NCT Heidelberg
H929	*Homo sapiens*	Suspension cell line established from plasma cell myeloma	Kind gift from Dr. Dr. Klaus Podar, NCT Heidelberg
HEK293-6E	*Homo sapiens*	Suspension cell line established from embryonic kidney cells	National Research Council Canada
HEK293T	*Homo sapiens*	Adherent growing cell line established from embryonic kidney cells, expressing the SV40 large T antigen	American Type Culture Collection (CRL-3216)
MM1.S	*Homo sapiens*	Suspension cell line established from plasma cell myeloma	Kind gift from Dr. Dr. Klaus Podar, NCT Heidelberg
NALM-6	*Homo sapiens*	Suspension cell line established from B cell precursors of acute lymphoblastic leukemia	Deutsche Sammlung von Mikroorganismen und Zellkulturen GmbH (ACC-128)
Peripheral blood mononuclear cells (PBMC)	*Homo sapiens*	Isolated from fresh blood or buffy coats from donors without known diseases	NCT Heidelberg (fresh blood), Deutsches Rotes Kreuz Mannheim (buffy coats)

SKOV-3	*Homo sapiens*	Adherent growing cell line established from ovarian adenocarcinoma	American Type Culture Collection (HTB-77)
U266	*Homo sapiens*	Suspension cell line established from plasma cell myeloma	Kind gift from Dr. Dr. Klaus Podar, NCT Heidelberg

2.1.8 Bacteriophages

Table 8. List of used bacteriophages

Phage	Description	Supplier (Cat. No.)
VCSM13 (K07ΔpIII)	Kanamycin resistant helper phage capable high single-stranded phagemid yields, derivative of M13KO7	Agilent Technologies (200251)
LYNDAL library phages	Immune repertoire derived from lymph nodes of head and neck cancer patients, diversity approx. $5x10^9$ clones	Internal, AG Krauss (NCT Heidelberg)

2.1.9 Vectors

Table 9 shows used plasmids and a short description. See *Appendix* (*6.2*) for the corresponding maps.

Table 9. List of used vectors

Vector	Description
pHENIS	Phagemid vector encoding for scFv fused to the bacteriophage pIII coating protein to enable surface presentation (phage display)
pYD5	Optimized for transient expression in mammalian cells, used for the generation of recombinant SP17 antigen
pCMX2.5-hIgG1-Fc	Optimized for transient expression in mammalian cells, used for the generation of scFv-hFc fusion proteins
pENTR1a	Gateway entry vector containing recombination sites attL1 and 2
pRRL	Gateway destination vector with lentiviral backbone, used for stable expression of lentiviral vectors in mammalian cells
Lentiviral helper plasmid #1	Lentiviral envelope plasmid, used for lentiviral vector production
Lentiviral helper plasmid #2	Lentiviral packaging plasmid, used for lentiviral vector production

2.1.10 Oligonucleotides

Oligonucleotides were purchased from Thermo Fisher Scientific.

Table 10. List of used primers for cloning, mutagenesis and sequencing

ID	Name	Sequence 5'→3'	Description
User	M13-RP	CAGGAAACAGCTATGACC	Sequencing of scFv encoded in pHENIS
User	NRC_pTT_fw	TGATATTCACCTGGCCCGATCTG	Sequencing of NRC vector inserts
User	NRC_pTT_rv	TGTCCTTCCGAGTGAGAG	Sequencing of NRC vector inserts
User	SP17_BamHI_fw	TATAGGATCCTCCAACACCCACTAC	Amplification of SP17 gene and BamHI insertion
M14	SP17_EcoRV_rv	TATAGATATCTCACTTGTTTTCCTC	Amplification of SP17 gene and EcoRV insertion
NB1	prehFc_rv	GGTCCGGGAGATCATGAG	Sequencing of pCMX2.5-hIgG1-Fc inserted scFv
NB2	posthFc_rv	GGACAGTGGGAGTGGCAC	Sequencing of pCMX2.5-hIgG1-Fc inserted scFv
P101	LMB3long_fw	CAGGAAACAGCTATGACCATGATTAC	Colony PCR of scFv encoded in pHENIS
P102	Fdseqlong_rv	GTAAAACGACGGCCAGTGAATTC	Colony PCR of scFv encoded in pHENIS
RU8	CD3z-XbaI_rv	TAATCTAGATTAGCGAGGGGGCAG	CAR backbone cloning with XbaI insertion
RU32	pENTR_sense3	CATAAACTGCCAGGCATCAAACTAAG	Sequencing and cloning of CAR N-terminal sequences
RU33	pENTR_anti	GATTTTGAGACACGGGCCAGA	Sequencing and cloning of CAR C-terminal sequences
RU62	4-1BB_rv	GCAGAAAGAAGCTCCTGTATATATTCA	Sequencing upstream the 4-1BB domain
V1	murineFc_NarI_fw	TATAGGCGCCCCCAGAGGGCCCACAATC	Amplification of the murine Fc gene with NarI insertion
V2	murineFc_BmtI_rv	TATAGCTAGCTTTACCCGGAGTCCGGGAG	Amplification of the murine Fc gene with BmtI insertion
V3	post-mFc_seq_fw	ATCACCACACGACTAAGAGC	Sequencing downstream to murine Fc
V21	YU138-C01_STOP39Q_fw	TGCACTGGGTGCGACAGGCCCCTGGACAAGG	Amber stop codon mutation into glutamine
V22	NS20_rv_long	CTGACGGTCCCCCCAGGAGTTCAGGTGCTG	Amber stop codon mutation into glutamine
V23	CM2for_long	CGCAAATGGGCGGTAGGCGTGTACGGTGGG	Amber stop codon mutation into glutamine
V24	YU138-C01	CCTTGTCCAGGGGCCT	Amber stop codon mutation

	_STOP39Q_rv	GTCGCACCCAGTGCA	into glutamine
V25	YU138-D01 _STOP3Q_fw	CCATGGCCCAGGTGCA GCTGGTGCAGTCTGG	Amber stop codon mutation into glutamine
V26	YU138-D01 _STOP3Q_rv	CCAGACTGCACCAGCT GCACCTGGGCCATGG	Amber stop codon mutation into glutamine
V29	IgG VH Leader_fw	GCCACCATGGGATGGT CA	Amplification of IgG V_H leader and downstream scFv
V30	VD1.E6* scFv-CD8_Overhang_ rv	CAGGAAGACCGGCAC GAAACGTTTGATGTCC ACTTT	Overlap extension PCR to link CAR elements without restriction site insertion
V31	CD8-VD1.E6* scFv_Overhang_ fw	AAAGTGGACATCAAAC GTTTCGTGCCGGTCTT CCTG	Overlap extension PCR to link CAR elements without restriction site insertion
V32	YU106-F02* scFv-CD8_ Overhang_rv	CAGGAAGACCGGCAC GAAAGAGGAGGGTGG GAACAG	Overlap extension PCR to link CAR elements without restriction site insertion
V33	CD8-YU106*-F02 scFv_Overhang_ fw	CTGTTCCCACCCTCCT CTTTCGTGCCGGTCTT CCTG	Overlap extension PCR to link CAR elements without restriction site insertion
V34	YU138-D01* scFv-CD8_ Overhang_rv	CAGGAAGACCGGCAC GAAGACAGATGGTGCA GCCAC	Overlap extension PCR to link CAR elements without restriction site insertion
V35	CD8-YU138-D01* scFv_Overhang_ fw	GTGGCTGCACCATCTG TCTTCGTGCCGGTCTT CCTG	Overlap extension PCR to link CAR elements without restriction site insertion
V38	YU138-D01* scFv-hFc _Overhang_rv	GTCAGGAGATTTGGGC TCGACAGATGGTGCAG CCAC	Overlap extension PCR to link CAR elements without restriction site insertion
V39	hFc-YU138-D01* scFv_Overhang_ fw	GTGGCTGCACCATCTG TCGAGCCCAAATCTCC TGAC	Overlap extension PCR to link CAR elements without restriction site insertion
V40	YU106-F02* scFv-hFc_ Overhang_rv	GTCAGGAGATTTGGGC TCAGAGGAGGGTGGG AACAG	Overlap extension PCR to link CAR elements without restriction site insertion
V41	hFc-YU106-F02* scFv_Overhang_ fw	CTGTTCCCACCCTCCT CTGAGCCCAAATCTCC TGAC	Overlap extension PCR to link CAR elements without restriction site insertion
V42	VD1.E6* scFv-hFc_Overhang_ rv	GTCAGGAGATTTGGGC TCACGTTTGATGTCCA CTTT	Overlap extension PCR to link CAR elements without restriction site insertion
V43	hFc-VD1.E6* scFv_Overhang_ fw	AAAGTGGACATCAAAC GTGAGCCCAAATCTCC TGAC	Overlap extension PCR to link CAR elements without restriction site insertion
V44	IgG VH Leader	GCCACCATGGGATGGT	Amplification of IgG V_H

	long_fw	CATGTATCATCC	leader and downstream scFv
V45	CD28LckSDM_fw	CCAGGCCTATGCCGCA GCACGCGACTTCGCAG	Mutation of CD28 via site directed mutagenesis PCR
V46	CD28LckSDM_rv	GTGCTGCGGCATAGGC CTGGTAATGCTTGCGG	Mutation of CD28 via site directed mutagenesis PCR
V51	$(G_4S)_3$ Linker Seq_fw	GGTGGAGGCGGTTCA GGCGGAGGTG	Sequencing downstream to $(G_4S)_3$ linker
V52	cPPT Seq_fw	GTAGACATAATAGCAA CAGACATAC	Sequencing downstream to cPPT element

2.1.11 Sequencing

Plasmids and corresponding primers were sent in to Eurofins Scientific for sequencing.

2.1.12 Antibodies and antibody conjugates

Table 11. List of used antibodies and antibody conjugates

Target structure, clone/clonality	Host	Target	Conjugate	Supplier (Cat. No.)
AKAP4, polyclonal	rabbit	human		Proteintech (24986-1-AP)
AKAP4, YU138-C01-hFc with Yol linker, monoclonal	human (recombinant)	human		Yumab GmbH, Valentino De Leo (NCT Heidelberg)
AKAP4, YU138-D01-hFc with Yol linker, monoclonal	human (recombinant)	human		Yumab GmbH, Valentino De Leo (NCT Heidelberg)
AKAP4, YU138-D01*-hFc with $(G_4S)_3$ linker, monoclonal	human (recombinant)	human		Yumab GmbH, Lisa Noll (NCT Heidelberg)
CCR7, monoclonal	mouse	human	PE/Cy7	BioLegend (353225)
CD3, monoclonal	mouse	human	FITC	BioLegend (300406)
CD3, monoclonal	mouse	human	PE	BioLegend (300408)
CD4, monoclonal	mouse	human	BV785	BioLegend (300554)
CD8, monoclonal	mouse	human	PerCP/ Cy5.5	BioLegend (344710)
CD19, monoclonal	mouse	human	BV785	BioLegend (302240)

CD45RO, monoclonal	mouse	human	BV605	BioLegend (304237)
CD69, monoclonal	mouse	human	BV785	BioLegend (310932)
CD95 (Fas), monoclonal	mouse	human	PE	BioLegend (305608)
c-myc, monoclonal	mouse		HRP	Roche (11814150001)
gB HSV (HDIT101), monoclonal (isotype control)	human (recombinant)	viral		HDIT, NCT Heidelberg
Hen egg lysozyme, monoclonal (isotype control)	human (recombinant)	chicken		CrownBio (C0001)
IgG1, monoclonal	rat	mouse	PE	BioLegend (406607)
IgG, monoclonal	goat	rabbit	FITC	Life Technologies (A16125)
IgG Fc gamma, monoclonal	rabbit	human	HRP	Jackson ImmunoResearch (309-035-008)
IgG Fc gamma, monoclonal	mouse	human	HRP	Abcam (ab7499)
Isotype control IgG1κ	mouse		BV605	BioLegend (400162)
Isotype control IgG1κ	mouse		BV785	BioLegend (400170)
Isotype control IgG1κ	mouse		PE	BioLegend (400112)
Isotype control IgG1κ	mouse		PE/Cy7	Invitrogen (25471480)
Isotype control IgG2a	mouse		BV605	BioLegend (400270)
Isotype control IgG2a	mouse		PE/Cy7	BioLegend (400231)
LAG-3, monoclonal	mouse	human	PE/Cy7	Invitrogen (25223942)
M13 phage, monoclonal	mouse	phage	HRP	GE Healthcare (27-9421-01)
PD-1, monoclonal	mouse	human	BV605	BioLegend (329924)
SP17, polyclonal	rabbit	human		Proteintech (13367-1-AP)
SP17, YU106-A03-hFc with Yol linker,	human (recombinant)	human		Yumab GmbH, Valentino De Leo

monoclonal				(NCT Heidelberg)
SP17, YU106-C02-hFc with Yol linker, monoclonal	human (recombinant)	human		Yumab GmbH, Valentino De Leo (NCT Heidelberg)
SP17, YU106-D01-hFc with Yol linker, monoclonal	human (recombinant)	human		Yumab GmbH, Valentino De Leo (NCT Heidelberg)
SP17, YU106-G01-hFc with Yol linker, monoclonal	human (recombinant)	human		Yumab GmbH, Valentino De Leo (NCT Heidelberg)
SP17, YU106-F02-hFc with Yol linker, monoclonal	human (recombinant)	human		Yumab GmbH, Valentino De Leo (NCT Heidelberg)
SP17, YU106-F02*-hFc with $(G_4S)_3$ linker, monoclonal	human (recombinant)	human		Yumab GmbH, Lisa Noll (NCT Heidelberg)
SPAG9, polyclonal	rabbit	human		Proteintech (24423-1-AP)
SPAG9, YU107-A01-hFc with Yol linker, monoclonal	human (recombinant)	human		Yumab GmbH, Valentino De Leo (NCT Heidelberg)
SPAG9, YU107-B01-hFc with Yol linker, monoclonal	human (recombinant)	human		Yumab GmbH, Valentino De Leo (NCT Heidelberg)
SPAG9, YU107-D03-hFc with Yol linker, monoclonal	human (recombinant)	human		Yumab GmbH, Valentino De Leo (NCT Heidelberg)
SPAG9, YU107-E01-hFc with Yol linker, monoclonal	human (recombinant)	human		Yumab GmbH, Valentino De Leo (NCT Heidelberg)
SPAG9, YU107-F03-hFc with Yol linker, monoclonal	human (recombinant)	human		Yumab GmbH, Valentino De Leo (NCT Heidelberg)
SPAG9, YU107-G01-hFc with Yol linker, monoclonal	human (recombinant)	human		Yumab GmbH, Valentino De Leo (NCT Heidelberg)
SPAG9, VD1.E6-hFc with Yol linker, monoclonal	human (recombinant)	human		Yumab GmbH, Valentino De Leo (NCT Heidelberg)
SPAG9, VD1.E6*-hFc with $(G_4S)_3$ linker, monoclonal	human (recombinant)	human		Yumab GmbH, Lisa Noll (NCT Heidelberg)
TIM-3, monoclonal	mouse	human	BV785	BioLegend (345032)

2.1.13 Enzymes and proteins

Table 12. List of used enzymes and proteins

Enzymes / Proteins	Supplier (Cat. No.)
AKAP4-His	Cusabio (CSB-YP702494HU)
Alkaline phosphatase from calf intestine	New England Biolabs (M0290S)
BSA, biotinylated	Thermo Fisher Scientific (29130)
BmtI	New England Biolabs (R0658S)
DpnI	New England Biolabs (R0176S)
Gateway LR Clonase II	Invitrogen (11791-100)
Human Fc (hFc), protein A chromatography purified	Dr. Katharina Aichelin, NCT Heidelberg
Interleukin-7	Miltenyi (130-095-363)
Interleukin-15	Miltenyi (130-095-765)
KAPA2G Fast Ready Mix with Dye	Roche (KK5103)
Lysozyme	Roche (10837059001)
Murine Fc (mFc), protein A chromatography purified	Valentino De Leo, NCT Heidelberg
NarI	New England Biolabs (R0191S)
NcoI-HF	New England Biolabs (R3193S)
NotI-HF	New England Biolabs (R3189S)
PfuTurbo DNA Polymerase	Agilent Technologies (600250)
Protein A	Thermo Scientific (21181)
Protein L, biotinylated	GenScript (M00097)
SP17-His	Novus Biologicals (NBP2-22818)
SP17-mFc, protein A chromatography purified	Valentino De Leo, NCT Heidelberg
SPAG9A1A2 peptide, biotinylated	AG Mier, Dept. of Pharmaceutical Chemistry, University Hospital Heidelberg
Streptavidin	Thermo Scientific (21125)
Streptavidin-APC	BioLegend (405207)
T4 DNA Ligase	Thermo Scientific (EL0016)
XbaI	New England Biolabs (R0145S)

2.1.14 Software and online tools

Table 13. List of applied software and online tools

Software / Online tool	Description	Supplier/Homepage
BD FACS Diva	Acquisition and analysis of flow cytometric data	BD Biosciences
BD FACS Suite	Acquisition and analysis of flow cytometric data	BD Biosciences
BIACORE Control/ BIAevaluation	BIACORE controlling and sensorgram evaluation	GE Healthcare
Chemo Star Imager 3.14	Fluorescence and ECL visualization	Intas Science Imaging
Epson Scan	Image scan and digitalization	Epson
ExPASy ProtParam	Computation of physical and chemical parameters of amino acid sequences	http://web.expasy.org/protparam/
FlowJo 10.3	Flow cytometric data evaluation	Tree Star
FlowJo 9	Flow cytometric data evaluation	Tree Star
Geneious 10.1	Cloning manager	Biomatters
GraphPad Prism 7.0	Statistical analysis and graph illustrator	GraphPad Software
IMGT/V-Quest	Database containing human antibody gene sequences	http://www.imgt.org/IMGT_vquest/vquest
Intas GDS 3.3.9	DNA visualization and documentation	Intas Science Imaging
Mendeley	Reference manager	Elsevier
Microsoft Office 2010	Data evaluation, illustration and text processing	Microsoft
NanoDrop 1000 3.8.1	Spectrophotometer control	Thermo Fisher Scientific
Photoshop Elements 10	Image editing	Adobe Systems
RTCA 2.0	RTCA instrument control	Roche Diagnostics GmbH
Tecan i-control 3.7.3	Absorbance/fluorescence reader control	Tecan Austria
Unicorn 5.10	FPLC control	GE Healthcare
Unicorn 6.3	FPLC control	GE Healthcare
VBASE2	Database containing human antibody gene sequences	http://www.vbase2.org/vbquery.php

2.2 Methods

2.2.1 Phage display

2.2.1.1 AKAP4, SP17 and SPAG9 antigens used for phage display

According to Shankar *et al*. SPAG9 contains three putative antigenic regions within the extracellular section referred to as A1, A2 and A3 [173]. We designed a peptide comprising the antigenic regions A1 and A2 as well as flanking amino acids, an N-terminal biotin and a polyethylene glycol 2 (PEG_2) spacer (*Figure 7*). The peptide was synthesized by the group headed by Prof. Dr. Walter Mier (Dept. of Pharmaceutical Chemistry, University Hospital Heidelberg). We denoted the peptide as biotinylated SPAG9A1A2 (bio-SPAG9A1A2).

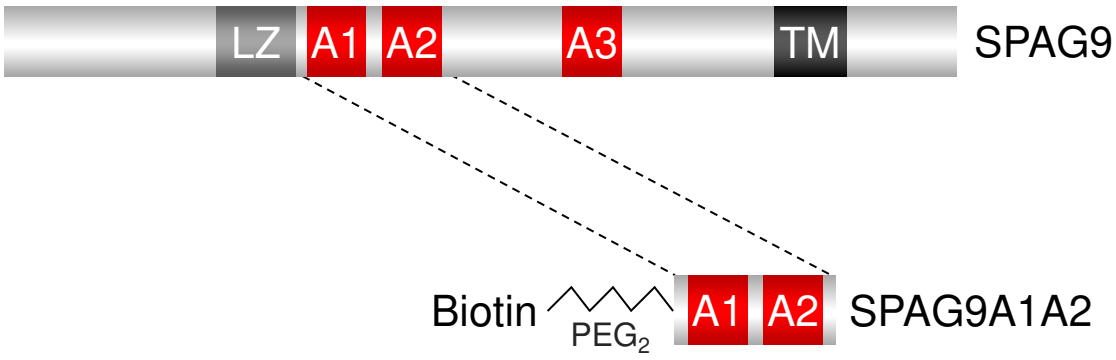

Figure 7. Biotinylated SPAG9A1A2 peptide design. Derived from the extracellular section of SPAG9, the putative antigenic regions A1 and A2, flanking amino acids, as well as the intermediate sequence between A1 and A2 were included in a peptide design. A PEG_2 spacer links the N-terminal biotin and the SPAG9A1A2 sequence to bridge the streptavidin binding pocket during the phage display selection procedure using streptavidin coupled magnetic beads.

To generate SP17-mFc fusion protein and mFc as control protein, we amplified and cloned the corresponding coding sequences separately into the mammalian expression vector pYD5, produced them in HEK293-6E and purified the proteins via protein A chromatography and preparative size exclusion chromatography as described in *2.2.4*. The AKAP4-His protein was purchased from Cusabio.

2.2.1.2 Library phage titer determination

Prior to the selection process (*2.2.1.3*) the titers of the library phage stock and the VCSM13 helper phages were determined to ensure sufficient phage presence and phage infectivity. *E. coli* TG1 were plated on minimal agar and incubated overnight at 37 °C. One single colony was added to 5 mL 2x YT medium and incubated overnight at 180 rpm, 37 °C. 100 µL of

E. coli TG1 overnight culture were transferred to 20 mL 2x YT medium and incubated at 180 rpm, 37 °C to an OD_{600} of 0.4 to 0.5. A serial dilution with library phages and helper phages was set up in 2x YT ranging from 10^{-8} to 10^{-14} and 10^{-6} to 10^{-12}, respectively. 285 µL of log phase *E. coli* TG1 were infected with 15 µl of each phage dilution and incubated at 37 °C, 30 min without shaking and another 30 min at 160 rpm. After infection, 100 µL of *E. coli* TG1 were either plated on 2x YT-GA (library phage infected) or 2x YT-K (helper phage infected) in duplicates. Agar plates were incubated overnight at 30 °C. Colony count was determined the following day and transducing units per mL (TU/mL) were calculated considering dilution factor and the mean value. Phage display procedure requires 10^{12} to 10^{14} TU/mL of library phages and a minimal titer of 10^{11} TU/mL of helper phages.

2.2.1.3 Phage display selection of bio-SPAG9A1A2 specific antibody fragments from LYNDAL

We used our in-house antibody library LYNDAL (LYmph Node Derived Antibody Libraries) initially generated by Philipp Diebolder [188] and extended internally (NCT Heidelberg) to select fully human scFvs specific for bio-SPAG9A1A2. LYNDAL contains an IgG immune repertoire from B cells of tumor draining lymph nodes isolated from 19 head and neck cancer patients. LYNDAL is stored in PBS (+ 10% glycerol) as frozen VCSM13 phage library. The library phages contain the phagemid vector pHENIS which carries the scFv coding sequence fused to the minor capsid protein (g3p) gene, thus enabling scFv surface presentation.

The applied phage display protocol was originally established by Kontermann, Duebel, Chames and Baty, and allowed a selection procedure in solution (*Figure 8*) [189]. *E. coli* TG1 overnight cultures were generated the day before use by inoculating 4 mL 2x YT medium with a colony from a minimal plate and subsequent overnight incubation at 37 °C, 180 rpm.

100 µL (200 µL in round 1) of magnetic streptavidin coupled beads (in the following referred to as beads) were transferred into a 1.5 mL tube and washed with 1 mL PBS. The tube was put into a magnetic separation device to attract the beads to the tube wall (separation time of 2 min was allowed for each separation step). PBS was aspirated and the beads were taken up in 4% MPBS. Equal volumes of library phages (10^{14} in total) and beads were preincubated for 2 h at RT on a rotating shaker to remove streptavidin binders. During preincubation fresh beads were washed as described above, taken up in 1 mL 2% MPBS and incubated for 2 h at RT on a rotating shaker.

After preincubation and magnetic bead separation, phages in the supernatant were transferred to a new tube to initiate antigen binding (*Figure 8A*). 500 nM (round 1), 250 nM

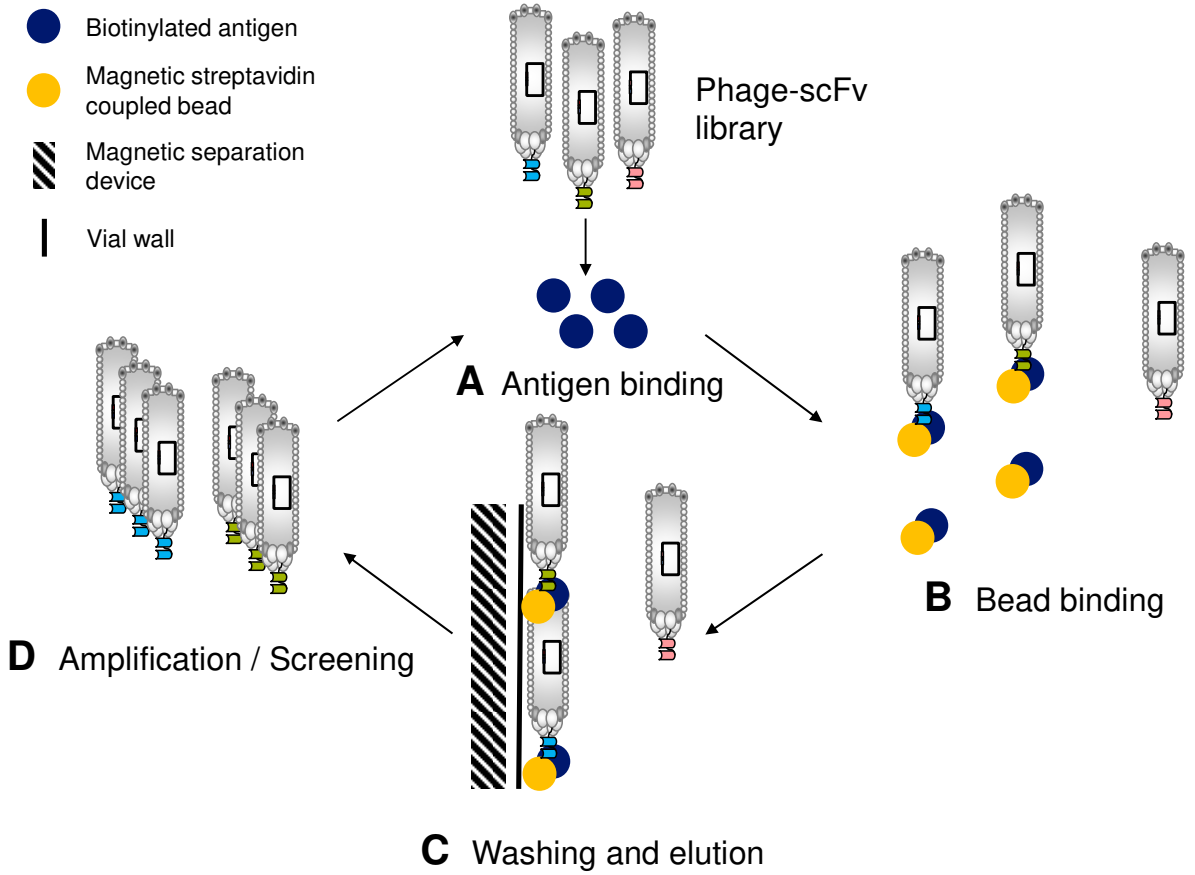

Figure 8. Phage display scFv selection using biotinylated antigens. (A) The phage-scFv library (LYNDAL) is incubated with the biotinylated antigen of interest in solution before **(B)** streptavidin coupled magnetic beads are added to capture the antigen. **(C)** The magnetic separation device attracts the beads to the vial wall. Washing steps eliminate unbound phages, binders are recovered by elution and **(D)** multiplied in bacteria. Obtained phages either pass through another selection cycle or they are tested in binding assays.

(round 2) or 50 nM (round 3) of bio-SPAG9A1A2 were diluted in 2% MPBS, added to the phages in a final volume of 1 mL and incubated for 1 h at RT on a rotating shaker. 20 mL of 2x YT medium were inoculated with 100 µL of an *E. coli* TG1 overnight culture and grown at 37 °C, 180 rpm to an OD_{600} of 0.5. Beads were recovered by magnetic separation and taken up in 250 µL MPBST. Beads were added to phage-antigen-mix and incubated for 15 min at RT on a rotating shaker (*Figure 8B*). Beads were attracted to the tube wall by the magnetic separation device. Liquid was carefully removed and the beads were washed 6x with 1 mL MPBST (magnetic attraction of 20 s was allowed between each washing step). Beads were transferred to a new tube and washed 6x with 1 mL MPBST. Beads were transferred to a new tube and washed 2x with 1 mL PBS. Phages were recovered (*Figure 8C*) by incubation with 1 mL basic elution buffer for 5 min at RT on a rotating shaker. After magnetic separation the phage containing supernatant was added to 500 µL neutralization buffer.

Remaining beads were incubated with 1 mL acetic elution buffer for 5 min at RT on a rotating shaker. After magnetic separation the phage containing supernatant was added to 500 µL neutralization buffer. Both elution fractions were pooled and 10 mL of the grown *E. coli* TG1 culture (OD_{600} = 0.5) were infected with the total phage amount by incubating at 37 °C, 30 min without shaking and another 30 min at 160 rpm. 10 µL of the infected bacteria were used for titer determination by serial dilution (10^{-2} to 10^{-6}) as described in *2.2.1.2*. Remaining bacteria were centrifuged at 500 *g* for 10 min and the supernatant was discarded. Bacterial pellet was resuspended in 1 mL 2x YT medium, streaked onto a square 2x YT-GA plate (12 cm x 12 cm) and incubated overnight at 30 °C. The following day phage titer was determined and the grown colonies on the square plate were harvested with 4 mL 2x YT medium using a triangle glass spatula.

To amplify phages (*Figure 8D*), 60 µL of the harvested bacteria were used for inoculation of 200 mL 2x YT-GA medium and glycerol was added to the remaining volume (final concentration 25%) which was stored at -80 °C. The inoculated culture was incubated at 37 °C, 180 rpm to an OD_{600} of 0.5 and then co-infected with $7.5x10^9$ VCSM13 helper phages at 37 °C, 30 min without shaking and another 30 min at 160 rpm. Helper phage infection was analyzed by plating infected bacteria on a 2x YT-K plate (incubation overnight at 37 °C). Remaining bacteria were centrifuged at 4400 *g* for 15 min and the pellet was resuspended with 200 mL of 2x YT-AK. Bacteria were incubated overnight at 30 °C, 130 rpm.

Bacteria were centrifuged at 4400 *g* for 15 min (4 °C) and five 50 mL tubes were filled with 40 mL of the phage containing supernatant. 8 mL of icecold phage precipitation buffer were added to each tube, the tubes were inverted and incubated for 1 h at 4 °C. The following steps were performed with icecold reagents. Tubes were centrifuged at 4400 *g* for 45 min (4 °C), supernatant was discarded and residual liquid was thoroughly removed. Phage pellet in each tube was resuspended with 300 µL of PBS, transferred to a 1.5 mL tube and centrifuged at maximum speed for 3 min (4 °C). Phage containing supernatant was transferred to a new 1.5 mL tube. Centrifugation and supernatant transfer were repeated until no pellet was visible anymore. Precipitated phages were stored at 4 °C and phage titer was determined by infection of an *E.coli* TG1 overnight culture and serial dilution (10^{-8} to 10^{-12}) as described before. After titer determination the phages were applied for the next selection round. In total three selection rounds were performed.

Round 3 glycerol stock was streaked onto 2x YT-GA plates and incubated overnight at 30 °C. A 96-well plate was filled with 100 µL 2x YT-GA medium per well. Each well was inoculated with a single phagemid comprising colony using sterile tips. The same tip was used for colony PCR screening (see *2.2.1.5*). The 96-well plate was covered with a breathable sealing film and incubated overnight at 37 °C, 160 rpm. 50 µL 2x YT-GA medium

with supplemented glycerol (final concentration 45%) were added to each well and the soluble scFv production process was initiated (see *2.2.1.6*). This “master plate” was stored at -80 °C.

2.2.1.4 Polyclonal phage ELISA

Enrichment of target specific scFv presenting phages throughout three consecutive phage display selection rounds was screened by polyclonal phage ELISA. The phages of each round were tested against target and negative control proteins. Proteins were diluted in PBS. The working volume was 100 µL/well and wells were blocked with 2% MPBS (350 µL/well). Each washing procedure included three PBST and three PBS washing steps (350 µL/well).

A 96-well microtiter plate was coated with 3 µg/mL biotinylated bovine serum albumin (bio-BSA), PBS, human serum albumin (HSA), lysozyme or ovalbumin and incubated overnight at 4 °C. Wells containing bio-BSA were coated with 10 µg/mL streptavidin (strep) and incubated for 1 h at RT on a plate shaker. Remaining wells were blocked with 2% MPBS. Plate was washed using an ELISA washer and 3 µg/mL bio-SPAG9A1A2 peptide were added to wells containing bio-BSA and strep except for the negative control wells. Remaining wells were blocked with 2% MPBS and the plate was incubated for 1 h at RT. Supernatants of bio-SPAG9A1A2 containing wells were aspirated and wells were blocked with 2% MPBS for 1 h at RT. Plate was washed as before. Phages of each selection round were diluted in icecold PBS to a titer of 10^{12}/well and were added to designated wells to be incubated for 1 h at RT. Plate was washed as before and anti-M13 HRP conjugated antibody (diluted 1:5000 in 2% MPBS) was added for 1 h at RT. Plate was washed as before, 100 µL/well of the TMB solution were added and incubated for 10 min in the dark at RT. Reaction was stopped with 50 µL/well of 2N sulfuric acid. Absorbance was measured at 450 nm wavelength (reference 620 nm) using a plate reader.

2.2.1.5 Single chain variable fragment integrity screening by colony PCR

To analyze full-length scFv integrity, colony polymerase chain reaction (PCR) was performed. 90 phagemid containing colonies from selection round 3 were randomly picked from agar plates (see *2.2.1.3*). Single colonies were transferred to 25 µL PCR reaction mix (*Table 14*) and subjected to PCR (*Table 15*).

Table 14. Components for colony PCR reaction mix (per reaction)

Component	Volume (µL)
Template DNA	Single colony
2x KAPA2G Fast Ready Mix with Dye	12.5
P101 LMB3long_fw (25 µM)	0.5
P102 fdseqlong_rv (25 µM)	0.5
ddH_2O	11.5
∑	**25**

Table 15. Colony PCR conditions

Step	Temperature [°C]	Time [s]	Cycles
Initial denaturation	95	300	1
Denaturation	95	15	35
Annealing	49	15	35
Elongation	72	15	35
Final elongation	72	300	1
Cooling	4	∞	1

PCR products were analyzed by agarose (1.5%) gel electrophoresis as described in *2.2.2.6*.

2.2.1.6 Production of soluble monoclonal single chain variable fragments in *E. coli*

The phagemid vector contains a lactose operon inducible by IPTG for the production of soluble scFvs decoupled from g3p. Although *E. coli* TG1 is a suppressor strain – translating the amber codon into a glutamine and not into a stop codon – it generates sufficient amounts of scFvs that are not fused to g3p.

A 96-deep-well plate filled with 125 µL/well 2x YT-A (0.1% glucose supplemented) was inoculated with 3 µL of each master plate well (see *2.2.1.3*). Plate was covered with a breathable sealing film and incubated at 37 °C for 2.5 h, 160 rpm (OD_{600} approx. 0.8 to 1.0). 25 µL/well 2x YT-A supplemented with IPTG (final concentration 1 mM) were added to start induction. Plate was covered with a breathable sealing film and incubated overnight at 30 °C, 160 rpm. Plate was centrifuged at 3200 *g* for 10 min (4 °C), the supernatant was discarded and bacterial pellets were resuspended with periplasmic preparation buffer. After a 20 min incubation on ice, 10 mM $MgSO_4$ were added and the plate was centrifuged at 3200 *g* for 10 min (4 °C). ScFv containing supernatant was transferred to a new 96-well plate and stored at 4 °C until use.

2.2.1.7 ELISA with soluble monoclonal single chain variable fragments

Clonal target specificity of round 3 selected soluble scFvs was screened by ELISA as described in *2.2.1.4*. After blocking with 2% MPBS, 50 µL/well of 4% MPBS and 50 µL/well of soluble scFvs extracted from periplasm (see *2.2.1.6*) were added to corresponding wells and incubated for 2 h at RT. Anti-c-myc HRP conjugated antibody (diluted 1:1000 in 2% MPBS) was used for detection reaction as described in *2.2.4.7*.

2.2.1.8 Monoclonal single chain variable fragment sequence analysis

ScFvs positively evaluated at the DNA (colony PCR, see *2.2.1.5*) and protein level (ELISA, see *2.2.1.7*) were shortlisted for sequence analysis. Corresponding *E. coli* TG1 clones from the master plate (see *2.2.1.3*) were grown overnight in 5 mL LB-A medium at 37 °C, 180 rpm. Plasmid DNA was extracted using a Mini preparation kit (QIAGEN) according to the manufacturer's instructions and the DNA was measured photometrically. DNA was sent in for sequencing and the results were evaluated using Geneious. Unique scFv sequences were further analyzed with the IMGT/V-Quest [190] and VBASE2 [191] databases which identify V, D and J gene segments by alignment to germline allele sequences. Nucleotide and amino acid changes compared with the closest related germline sequence were analyzed.

2.2.2 Molecular biological and microbiological methods

2.2.2.1 Single chain variable fragments from Yumab GmbH and sequence optimization

We provided our collaborator Yumab GmbH with commercial AKAP4-His (Cusabio), internally produced mFc-SP17 (mFc for negative selection) and bio-SPAG9A1A2 for phage display selection using their IgM naïve repertoires containing antibody library HAL9/10 [192].

From Yumab GmbH we received DNA encoding for two AKAP4, ten SP17 and thirteen SPAG9 specific monoclonal scFvs. Due to handling limits, we chose a manageable amount of scFvs according to the criteria highest overall binding signal and best signal-to-noise ratio in ELISA as provided by Yumab GmbH. In total, we decided for two αAKAP4, five αSP17 and six αSPAG9 scFv clones in addition to our proprietary αSPAG9 scFv as listed in *Table 16*. We fused the selected anti-cancer-testis antigen (αCTA) scFvs to a human IgG1 Fc (hFc) backbone in the eukaryotic expression vector pCMX2.5. After characterization of the αCTA scFv-hFc fusion proteins, the scFv lead candidates were chosen to be implemented in CARs. The corresponding scFv coding sequences were redesigned in terms of the V_H-V_L connecting linker ($(G_4S)_3$ instead of Yol) and the 5'/3' restriction sites were removed to eliminate artificial non-parental amino acids. Optimized scFv coding sequences were synthesized by Eurofins

and labeled with an asterisk in this thesis to indicate the modification (*Table 16*). M.Sc. Lisa Noll (NCT Heidelberg) cloned coding sequences of modified scFvs, produced scFv-hFc fusion proteins and reevaluated antigen binding characteristics [193].

Table 16. List of αAKAP4, αSP17 and αSPAG9 scFv clones chosen for hFc fusion

Target antigen	Clone name	Linker	Artificial amino acids due to restriction sites?	Identifier
AKAP4-His	YU138-C01	Yol	Yes	αAKAP4_YU138-C01
AKAP4-His	YU138-D01	Yol	Yes	αAKAP4_YU138-D01
SP17-mFc	YU106-A03	Yol	Yes	αSP17_YU106-A03
SP17-mFc	YU106-C02	Yol	Yes	αSP17_YU106-C02
SP17-mFc	YU106-D01	Yol	Yes	αSP17_YU106-D01
SP17-mFc	YU106-F02	Yol	Yes	αSP17_YU106-F02
SP17-mFc	YU106-F02*	$(G_4S)_3$	No	αSP17_YU106-F02*
SP17-mFc	YU106-G01	Yol	Yes	αSP17_YU106-G01
SPAG9A1A2	YU107-A01	Yol	Yes	αSPAG9_YU107-A01
SPAG9A1A2	YU107-B01	Yol	Yes	αSPAG9_YU107-B01
SPAG9A1A2	YU107-D03	Yol	Yes	αSPAG9_YU107-D03
SPAG9A1A2	YU107-E01	Yol	Yes	αSPAG9_YU107-E01
SPAG9A1A2	YU107-F03	Yol	Yes	αSPAG9_YU107-F03
SPAG9A1A2	YU107-G01	Yol	Yes	αSPAG9_YU107-G01
SPAG9A1A2	VD1.E6	Yol	Yes	αSPAG9_VD1.E6
SPAG9A1A2	VD1.E6*	$(G_4S)_3$	No	αSPAG9_VD1.E6*

2.2.2.2 Polymerase chain reaction

DNA sequences of αCTA scFv, CAR backbone and antigen DNA was amplified using sequence specific forward and reverse primers in a polymerase chain reaction (PCR). PCR setup is shown in *Table 17*. For each PCR experiment a negative control without template DNA was included to exclude component contamination.

PCR was performed in a thermocycler using the reaction conditions described in *Table 18*. Individual primer melting temperature was calculated according to the formula:

$Tm = 4\ °C \times (G+C) + 2\ °C \times (A+T) - 4\ °C$

Table 17. Components for PCR mix (per reaction)

Component	Final amount/ concentration	Volume (µL)
Template DNA	100 ng	X
KAPA HiFi Buffer (5x)	1x	10
KAPA HiFi Polymerase (1 U/µL)	1 U	1
dNTP Mix (10 mM)	0.2 mM	1
Forward primer (25 µM)	0.5 µM	1
Reverse primer (25 µM)	0.5 µM	1
ddH_2O		*ad* 50
∑		**50**

Table 18: PCR conditions

Step	Temperature [°C]	Time [s]	Cycles
Initial denaturation	95	300	1
Denaturation	98	20	32
Annealing	Tm	30	32
Elongation	72	60	32
Final elongation	72	600	1
Cooling	4	∞	1

2.2.2.3 Mismatch mutagenesis and overlap extension PCR

Mismatch mutagenesis PCR allows the substitution of single nucleotides. The mutagenic primers are designed to be complementary with the target sequence except for the nucleotide(s) of interest. Overlap extension PCR aligns two DNA strands at a complementary 5' and 3' site. The unaligned parts are filled up with nucleotides during the elongation phase (extension). The newly generated double strand is amplified by sequence specific primers.

Both αAKAP4_YU138 scFv clones contained the amber codon TAG which was tolerated by the bacterial suppressor strain used for phage display, but translated into a stop codon in non-suppressor strains and mammalian cells. The amber codon was substituted with a glutamine codon by mismatch mutagenesis PCR and the strands were realigned by overlap extension PCR (*Figure 9*).

PCR was performed as in *2.2.2.2* with following exceptions for the overlap extension PCR: Denaturation, annealing and elongation were run without primers for 6 cycles to allow initial single strand overlap and then primers were added for another 32 cycles.

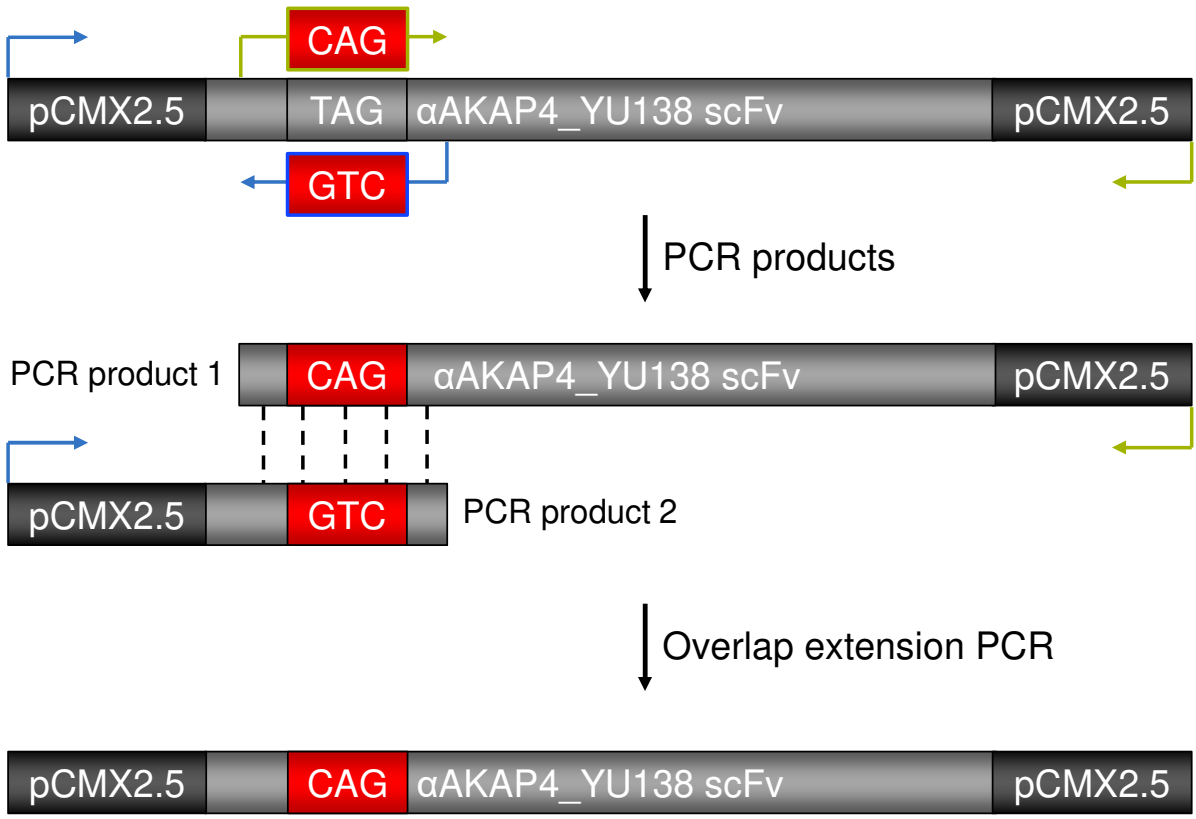

Figure 9. Substitution of the amber codon with a glutamine codon by mismatch mutagenesis and overlap extension PCR. To exchange the amber codon (TAG) within the scFv sequences from phage display, two mutagenic primers (green and blue) were designed with a nucleotide mismatch to create a glutamine codon (CAG, red) instead. A PCR with corresponding forward or reverse primer generated a PCR product each containing the mutation. Both resulting PCR products had overlapping sites which were merged, extended and amplified by overlap extension PCR. The final PCR products were cloned into the vector pCMX2.5.

2.2.2.4 Chimeric antigen receptor cloning

αSP17 and αSPAG9 scFv lead candidates were fused to various chimeric antigen receptor (CAR) backbones as binding domains. CAR backbones listed in *Table 19* were chosen for integration of each lead candidate scFv.

The hFc spacer included hinge-C_H2-C_H3 domains derived from human IgG1. The constructs annotated with CD28Δ contained a mutated CD28 signaling tail incapable to bind Lck, which was generated by replacing P560 with A560, P563 with A563 and P564 with A465 [78] using site directed mutagenesis. For this purpose, two complementary mutagenic primers were designed featuring multiple exchanged nucleotides at the site of interest on the parental sequence. The reaction was performed according to the QuikChange site directed mutagenesis kit protocol from Stratagene using the components and conditions listed in

Table 20 and *Table 21*.

Table 19. List of αSP17 and αSPAG9 specific CAR variants

Target antigen	ScFv clone	CAR backbone	Identifier
SP17	YU106-F02*	scFv-CD8α-CD28-4-1BB-CD3ζ	αSP17-CD8-28BBz
SP17	YU106-F02*	scFv-CD8 α -CD28Δ-4-1BB-CD3ζ	αSP17-CD8-28ΔBBz
SP17	YU106-F02*	scFv-CD8α-4-1BB-CD3ζ	αSP17-CD8-BBz
SP17	YU106-F02*	scFv-hFc-CD28Δ-4-1BB-CD3ζ	αSP17-hFc-28ΔBBz
SP17	YU106-F02*	scFv-hFc-4-1BB-CD3ζ	αSP17-hFc-BBz
SPAG9	VD1.E6*	scFv-CD8α-CD28-4-1BB-CD3ζ	αSPAG9-CD8-28BBz
SPAG9	VD1.E6*	scFv-CD8α-CD28Δ-4-1BB-CD3ζ	αSPAG9-CD8-28ΔBBz
SPAG9	VD1.E6*	scFv-CD8α-4-1BB-CD3ζ	αSPAG9-CD8-BBz
SPAG9	VD1.E6*	scFv-hFc-CD28Δ-4-1BB-CD3ζ	αSPAG9-hFc-28ΔBBz
SPAG9	VD1.E6*	scFv-hFc-4-1BB-CD3ζ	αSPAG9-hFc-BBz

Table 20. Components for site directed mutagenesis PCR mix (per reaction)

Component	Final amount/ concentration	Volume (µL)
Template DNA	50 ng	X
Pfu Turbo Reaction Buffer (10x)	1x	5
Pfu Turbo Polymerase (2.5 U/µL)	2.5 U	1
dNTP Mix (10 mM)	0.2 mM	1
Forward mutagenic primer (25 µM)	125 ng	1
Reverse mutagenic primer (25 µM)	125 ng	1
ddH_2O		*ad* 50
∑		**50**

Table 21: Site directed mutagenesis PCR conditions

Step	Temperature [°C]	Time [s]	Cycles
Initial denaturation	95	30	1
Denaturation	95	30	18
Annealing	55	60	18
Elongation	68	300	18
Final elongation	68	600	1
Cooling	4	∞	1

To eliminate the methylated parental plasmid (template DNA) the reaction mix was digested with DpnI (final concentration 40 U) for 2 h at 37 °C. 2.5 µL DNA were used for transformation in competent *E. coli* XL-1 Blue as described in *2.2.2.9*.

ScFvs were fused to CAR backbones by overlap extension PCR (*2.2.2.3*) to avoid the use of restriction sites which would generate artificial amino acids in the translated sequence. CAR genes were cloned into the gateway entry clone pENTR1a by restriction digest with NcoI and BamHI/XbaI (*2.2.2.7*) and subsequent ligation (*2.2.2.8*).

2.2.2.5 Gateway cloning

For the generation of lentiviral vectors the CAR coding sequences were transferred from the entry clone pENTR1a into the lentiviral destination plasmid pRRL by gateway reaction.

200 ng of the pENTR1a entry clone containing the CAR sequence flanked by attL recombination sites were mixed with 200 ng DNA of the destination vector pRRL and 1 µL LR clonase enzyme mix was added. After overnight incubation at RT the CAR gene was transferred into the destination vector by site directed recombination forming the so called expression clone (see *Figure 10*).

The reaction was stopped with 0.5 µL proteinase K (2 mg/mL) by 10 min incubation at 37 °C. Competent *E. coli* XL-1 Blue were transformed with the DNA mixture as described in *2.2.2.9* and the expression clone was rescued by ampicillin selection. Correct recombination was analyzed by control digest (see *2.2.2.7*).

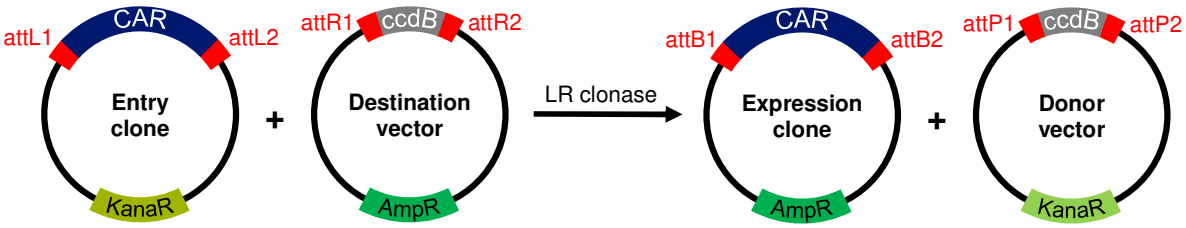

Figure 10. Gateway reaction scheme. The LR clonase exchanges the CAR sequence on the entry clone with the ccdB sequence on the destination vector as both sequences are flanked by recombination sites (attL and attR). The newly formed expression clone contains the fully integrated CAR sequence and the entry clone remains as ccdB gene carrying donor vector.

2.2.2.6 Gel electrophoresis, DNA extraction and purification

Amplified and digested PCR products were separated from template and residual DNA by preparative gel electrophoresis.

1.5% agarose was added to 1x TAE buffer, solubilized by boiling and supplemented with peqGREEN (1:20000) which intercalates with DNA and is UV excitable. Loading dye was added to the PCR mix and the sample was loaded onto the agarose gel together with a DNA size standard. Electrophoretical separation was performed at 75 volts for 1-2 h in 1x TAE as running buffer. Target DNA bands were visualized on a UV table and excised with a blade. DNA was extracted using a gel extraction kit (QIAGEN) according to the manufacturer's instructions. DNA was eluted with 30 µL ddH_2O and the concentration was determined photometrically.

If amounts of non-target DNA were negligible after PCR or restriction digest, the target DNA was purified using a PCR purification kit (QIAGEN) according to the manufacturer's instructions and without prior gel electrophoresis.

2.2.2.7 DNA digest with restriction enzymes

PCR products (insert) and vectors were digested with restriction endonucleases. Insert and vector DNA were separately incubated with the components shown in *Table 22* at the optimal enzyme working temperature (usually 37 °C) for 1-2 h.

Table 22. Components for DNA digest (per reaction)

Component	Final amount/ concentration	Volume (µL)
DNA (PCR product / vector)	up to 5000 ng	X
Cut Smart Buffer (5x)	1x	10
Enzyme I	10 U	1
Enzyme II	10 U	1
ddH_2O		*ad* 50
∑		**50**

At half time, 1 µL calf intestinal alkaline phosphatase was added to the vector to prevent religation. Digested DNA was purified as described in *2.2.2.6*.

2.2.2.8 DNA fragment ligation

Digested inserts and vectors were assembled by ligation. The ligation mix was set up as shown in *Table 23* and incubated for 1 h at RT. A religation control was included in the absence of digested insert.

Table 23. Components for DNA ligation (per reaction)

Component	Final amount/ concentration	Volume (µL)
Digested vector	10-100 ng	X
Digested insert	>3-fold molar excess	Y
T4 Ligase Buffer (10x)	1x	2
T4 Ligase (1 U/ µL)	1 U	1
ddH_2O		*ad* 20
∑		**20**

2.2.2.9 Transformation of *E. coli* with plasmids and plasmid amplification

E. coli XL-1 Blue were chemically transformed with (ligated) plasmids. Chemically competent *E. coli* XL-1 Blue (100 µL) were thawed on ice, the total ligation reaction mix was added and incubated on ice for 30 min. LB agar plates with appropriate antibiotics were prewarmed at 37 °C. Bacteria were heat shocked at 42 °C for 45 s and immediately supplemented with 1 mL SOC medium. A recovery of up to 45 min at 37 °C, 180 rpm was allowed, transformed bacteria were transferred to prewarmed plates and incubated overnight at 37 °C.

Plasmid DNA was amplified by inoculation of 5 mL LB medium (including appropriate antibiotic) with a transformed colony. After overnight incubation at 37 °C, 180 rpm, a 1 mL stock tube with 15% glycerol was prepared from the bacterial culture. The remaining culture was used for DNA extraction by a Mini preparation kit (QIAGEN) according to the manufacturer's instructions. Plasmid DNA concentration was measured photometrically and sent for sequencing together with appropriate sequencing primers. If a correct insertion was verified, the plasmids were produced in large scale for transfection of mammalian cells.

Large scale plasmid production was initiated by inoculation of 5 mL LB medium (including appropriate antibiotic) with frozen material from the bacterial glycerol stock incubating for 6 h at 37 °C, 180 rpm. 100 µL of this preculture were transferred to 200 mL LB medium (including appropriate antibiotic) and grown overnight at 37 °C, 180 rpm. DNA was isolated by an endotoxin free Maxi preparation kit (QIAGEN) according to the manufacturer's instructions and handled sterile. DNA was stored at -20 °C.

2.2.3 Cell biological methods

Cells were handled under sterile conditions at all times and incubated at 37 °C, 5% CO_2. Cells were counted visually with a microscope by 1:1 mixing with trypan blue and transferring to a Neubauer counting chamber.

2.2.3.1 Cell freezing and thawing

Cells were prepared for freezing by centrifugation for 10 min at 300 *g*, washing with adapted cell culture medium, centrifugation as before and resuspension with freezing medium (10% DMSO in FCS) to a concentration of 0.5 to 1x10^7/mL. Cryovials containing 1 mL aliquots were frozen to -80 °C at a cooling rate of 1 °C/min using a freezing container. For long-term storage, cryovials were transferred to liquid nitrogen.

Cryo-conserved vials were thawed in a water bath at 37 °C and immediately transferred to a 50 mL tube containing 10 mL of prewarmed adapted cell culture medium. The volume was split to two T25 cell culture flasks and filled up to 10 mL with prewarmed adapted medium.

Thawed HEK293-6E were transferred to a 125 mL shaking flask with filter caps containing 16 mL prewarmed adapted medium and incubated in a humidified cell culture shaker at 37 °C, 5% CO_2, 135 rpm. After overnight incubation the adapted medium was adjusted to 30 mL total volume.

2.2.3.2 Cultivation of adherent cell lines

The adherent cell lines Colo205 and SKOV-3 were cultured using RPMI-1640 medium supplemented with 10% FCS and 1% pen/strep. HEK293T were cultured using DMEM supplemented with 10% FCS and 1% pen/strep. Cells were passaged or expanded after being washed with PBS, trypsinized for 5 min at 37 °C and taken up in at least three times the amount of adapted medium compared to that of used trypsin. Cells were counted and an appropriate cell number was transferred to a new cell culture flask with fresh medium such that cells were around 90% confluent on the next day of passage. Passaging occurred every two to four days.

2.2.3.3 Cultivation of suspension cell lines

The suspension cell lines H929, MM1.S, NALM-6 and U266 were cultured using RPMI-1640 (+ GlutaMAX) medium supplemented with 10% FCS and 1% pen/strep. Granta-519 cells were cultured using DMEM supplemented with 10% FCS and 1% pen/strep. Cells were

passaged or expanded by transferring an appropriate cell number to a new cell culture flask with fresh medium such that a sufficient cell density was provided. Passaging occurred every two to four days.

The production cell line HEK293-6E was cultured using F17 medium supplemented with 2% L-glutamine, 0.1% Kolliphor and 0.05% G418. No G418 was included the day of thawing to ensure survival. Cells were seeded at $0.2x10^6$/mL (three-day-incubation) or $0.5x10^6$/mL (two-day-incubation) and were cultivated in a humidified cell culture shaker at 37 °C, 5% CO_2, 135 rpm.

2.2.3.4 Transient transfection of HEK293-6E cells to produce αCTA scFv-hFc fusion proteins

αCTA scFv-hFc fusion proteins were produced in HEK293-6E cells by transient transfection with the scFv-hFc gene encoding pCMX2.5 expression vector.

Three days prior to transfection HEK293-6E were expanded to 144 mL culture volume at a density of $0.2x10^6$/mL to yield a final density of 1.5 – $2.0x10^6$/mL at the transfection day. 1 µg per mL cell culture volume of eukaryotic expression vector and 2 µg per mL cell culture volume of PEI were each added to two separate 50 mL tubes each containing prewarmed transfection medium (1/20 of the cell culture volume). The tubes were vortexed thoroughly, the PEI solution was added to the DNA and mixed by vortexing. After incubation for 3 min at RT the transfection mix was added to the HEK293-6E culture. Cells were incubated for 24 h as described before and then fed with TN1 feeding medium (1/40 of the cell culture volume). Protein production continued for 72 h.

The cell culture volume was harvested by centrifugation for 10 min at 250 *g* followed by a second centrifugation of the supernatant for 10 min at 2250 *g*. The supernatant was dialyzed as described in *2.2.4.1*.

2.2.3.5 Flow cytometry for analysis of tumor cell lines and primary cells

Surface expression of AKAP4, SP17 and SPAG9 on tumor cell lines as well as binding of αCTA scFv-hFc fusion proteins to tumor cell lines and primary cells was analyzed by flow cytometry.

Staining volume was 50 µL/well. Washing steps were conducted by plate centrifugation at 400 *g* for 5 min (4 °C), cell resuspension with 150 µL/well of flow cytometry buffer and centrifugation as before.

Cultured cells were centrifuged at 400 *g* for 5 min and adjusted to a concentration of 10^7 cells/mL by resuspension with an appropriate volume of flow cytometry buffer. 10^6 cells per well were transferred to a 96-well U-bottom plate and washed as described above. 6-8 µg/mL of commercial polyclonal rabbit αAKAP, αSP17 or αSPAG9 antibody (diluted in flow cytometry buffer) were added to corresponding wells and incubated for 45 min at 4 °C on a shaker. Cells were washed twice and wells containing polyclonal antibodies were stained with 1.5 µg/mL secondary goat anti-rabbit FITC conjugated antibody. 0.55 µg of each αCTA scFv-hFc fusion protein and a human IgG1 isotype control were labeled with allophycocyanin (APC) using the Zenon Human IgG labeling kit according to the manufacturer's instructions. APC labeled αCTA scFv-hFc fusion proteins were added to corresponding wells in a final concentration of 11 µg/mL. The plate was incubated in the dark for 45 min at 4 °C on a plate shaker. Cells were washed twice and resuspended in 150 µL flow cytometry buffer supplemented with SYTOX Blue Dead Cell Stain (1:1000). Cell fluorescence was analyzed with a flow cytometer and the data were evaluated with FlowJo.

2.2.3.6 Lentiviral vector production in HEK293T cells

The lentiviral plasmid pRRL containing the CAR coding sequence was integrated into a lentiviral particle by co-transfection of HEK293T with two helper plasmids.

For this purpose, $2.5x10^6$ (in 1 mL) HEK293T cells were seeded per 15 cm culture plate containing 21.5 mL of adapted medium (described in *2.2.3.2*). Cells were incubated for 72 h at 37 °C and 5% CO_2. At the transfection day, the cells were 80-90% confluent. A DNA and PEI mix were separately prepared according to *Table 24*. The mixes were vortexed for 10 seconds, the PEI mix was added to the DNA mix and the final mix was again vortexed for 10 seconds before incubation for 10 min at RT.

Table 24: Lentiviral DNA transfection components

Mix	Component	Per 5 plates
DNA mix	Lentiviral plasmid (1 µg/mL)	112.5 µg
	Helper plasmid #1 (1 µg/mL)	39.5 µg
	Helper plasmid #2 (1 µg/mL)	73 µg
	NaCl (300 mM)	3950 µl
	ddH_2O	3950 µl
PEI mix	PEI (7.5 mM)	1760 µl
	NaCl (300 mM)	3950 µl
	ddH_2O	2190 µ
∑		**16025 µl**

Half of the adapted medium was exchanged with fresh medium. Then 3.1 mL/plate of the transfection mix were added dropwise to the HEK293T cells and the cells were cultivated as before for further 24 h.

The next day, the cell culture medium was removed, cells were washed with 5 mL/plate PBS and 14 mL/plate fresh DMEM without phenol red and FCS were added. Cells were cultivated as before for further 24 h to allow lentiviral release into the supernatant.

Lentiviral vector containing supernatant was transferred to 50 mL tubes and centrifuged at 300 *g* for 4 min to remove residual cells. Supernatant was sterilized with a 0.45 µM filter, transferred to a centrifugal filter unit and centrifuged at 3500 *g* for 30-60 min (4 °C). The flow-through was discarded and the concentrated lentiviral vectors were rescued from the filter by inverse centrifugation at 900 *g* for 2 min. Harvested volume was aliquoted and stored at -80 °C.

6 wells of a 24-well plate were seeded with $5x10^4$ HEK293T cells (1 mL/well) supplemented with fresh adapted medium and incubated for 24 h at 37 °C, 5% CO_2. 500 µL supernatant from each well were transferred into separate 1.5 mL tubes. Polybrene (final concentration 8 µg/mL) and concentrated lentiviral vectors (10 µL, 3 µL, 1 µL, 0.3 µL or 0.1 µL) were added, vortexed and retransferred to the corresponding wells. A mock transduction without lentiviral vectors was included as control.

After another 48 h of incubation at 37 °C and 5% CO_2, the cells were harvested, stained for CAR expression and measured by flow cytometry as described in *2.2.3.11*. Considering a cell number of 100.000 cells potentially expressing the CAR on their surface and the corresponding percentage mean value of all dilutions extrapolated to 1 µL lentiviral vector, the titer was calculated as infection units (IU) per mL according to the following formula:

$$\text{Titer [IU / mL]} = \frac{\text{Cell number } (10^5) \text{ x (mean \% positive cells x 100)}}{\text{Lentiviral plasmid volume (1 µL)}} \text{ X } 10^3$$

2.2.3.7 Isolation of human peripheral blood mononuclear cells from donor blood

Human peripheral blood mononuclear cells (PBMCs) were obtained from fresh blood or buffy coats from healthy donors by Ficoll density gradient centrifugation.

50 mL blood were transferred to a sterile T125 cell culture flask and diluted with 50 mL RPMI medium. Four 50 mL tubes were filled with 20 mL Ficoll that was overlayed with 25 mL

diluted blood and centrifuged at 400 *g* for 30 min at RT and with inactivated brakes. The supernatant was discarded, the PBMCs in the interphase were aspirated and transferred to two new 50 mL tubes. The tubes were filled up to 50 mL with RPMI and centrifuged at 300 *g* for 10 min with activated brakes. Supernatant was discarded, the pellets were resuspended in 5 mL cold PBS and pooled. The tube was filled to 50 mL with cold PBS and centrifuged at 200 *g* for 10 min. Cells were taken up in 10 mL cold PBS, counted and used for T cell activation. Remaining cells were frozen (*2.2.3.1*).

2.2.3.8 Activation of human T cells

$2x10^7$ freshly isolated or thawed PBMCs were taken up in prewarmed X-VIVO15 (+ 5% FCS) medium, centrifuged at 300 *g* for 5 min and diluted to $2x10^6$ cells/mL with the same medium containing 10 ng/mL of both, IL-7 and IL-15 (adapted medium for human T cells). 4 mL/well cells were transferred to a 12-well plate. 40 µL of T Cell TransAct (a colloidal polymeric nanomatrix conjugated to humanized CD3 and CD28 agonists) were added to each well and T cells were stimulated for 60 h. Cell types other than T cells do not survive the *ex vivo* cultivation. After activation, T cells were ready for lentiviral CAR gene transfer (see *2.2.3.9*).

2.2.3.9 Transduction of activated T cells with lentiviral vectors

Activated T cells (see *2.2.3.8*) were centrifuged at 300 *g* for 10 min and resuspended in an appropriate volume of pre-warmed X-VIVO15 medium with 5% FCS, IL-7 and IL-15 (10 ng/mL each) to yield a concentration of 10^6/mL. Per lentiviral vector 10^6 (1 mL) T cells were transferred to a 24-well plate well.

The transduction mix was prepared in 1 mL of the adapted medium mentioned above by adding polybrene (final concentration 8 µg/mL) and an appropriate amount of lentiviral plasmid to achieve a multiplicity of infection (MOI) of 5. A mock transduction without lentiviral vector was included as control. The transduction mix was transferred to the T cells and incubated for 24 h at 37 °C. The cells were centrifuged at 300 *g* for 5 min and washed twice with PBS before being supplemented with fresh adapted medium and transferred to a new 24-well plate.

2.2.3.10 CAR T cell *in vitro* cultivation and expansion

CAR and mock T cells were cultivated in X-VIVO15 medium supplemented with 5% FCS, IL-7 and IL-15 (10 ng/mL each) and were incubated at 37 °C, 5% CO_2. Expansion occurred every two to three days. At the day of expansion, cells were centrifuged at 300 *g* for 5 min,

washed with PBS, recentrifuged and resuspended with the original amount of X-VIVO15. Cells were counted and transferred to either a 12-well plate ($4x10^6$ cells/4 mL/well), 6-well plate ($5x10^6$ cells/5 mL/well), T25 culture flask ($2x10^7$ cells/10 mL/flask), T75 culture flask ($5x10^7$ cells/20 mL/flask) or T175 culture flask (10^8 cells/40 mL/flask) depending on the total cell amount. Before transfer, cells were centrifuged as before and resuspended with the corresponding amount of adapted medium.

After CAR and mock T cells were sufficiently expanded for *in vitro* assays, remaining cells were frozen as described in *2.2.3.1*.

2.2.3.11 Flow cytometry for analysis of CAR T cells

CAR expression on transduced and mock T cells (control) was measured by flow cytometry. The staining was performed in 96-well plates with a staining volume of 30 µL/well and cells were washed with 150 µL/well cold PBS. All reagents were diluted in cold PBS.

Cells were counted and 0.2 to $1x10^6$ cells per well were centrifuged at 300 *g* for 5 min (4 °C). The supernatant was removed and cells were washed with 1 mL cold PBS. Cells were centrifuged as before, resuspended in 100 µL cold PBS, transferred to wells of a 96-well plate and centrifuged as before. CAR T cells were detected using two different strategies depending on the included scFv:

a) αSP17 scFv containing CAR T cells were incubated with 2.5 µg/mL APC labeled SP17-mFc antigen and FITC conjugated anti-human CD3 antibody (diluted 1:40) for 45 min at 4 °C under shaking. SP17-mFc was directly labeled using the Zenon APC mouse IgG2a labeling kit according to the manufacturer's instructions and applied for staining without the need for secondary antibodies.

b) αSPAG9 scFv containing CAR T cells were incubated with biotinylated protein L (final concentration 1 µg/mL) for 45 min at 4 °C under shaking. Cells were centrifuged, washed as described before and incubated with APC coupled streptavidin (final concentration 0.2 µg/mL) and FITC conjugated anti-human CD3 antibody (diluted 1:40) for 30 min at 4 °C under shaking.

Cells were centrifuged and washed twice as described before. After the last centrifugation, cells were resuspended with 150 µL PBS containing SYTOX Blue Dead Cell Stain (diluted

1:1000) to label dead cells.

The expression of activation, exhaustion and T cell subset surface markers was measured by flow cytometry as well. The procedure was equal as described above. Mouse antibodies detecting the activation marker CD25 and the exhaustion markers PD-1, TIM-3 and LAG-3 were added to the strep-APC or APC labeled SP17-mFc staining mixture in an appropriate concentration. To stain T cell subsets, mouse antibodies detecting CD4, CD8, CD45RO, CCR7 and CD95 were added to the staining mixture in an appropriate concentration.

Additional stainings were performed using matching isotype control antibodies. Cell fluorescence was analyzed with a BD FACS Celesta or Verse flow cytometer and the data were evaluated using FlowJo software.

2.2.3.12 CAR T cell freeze and thaw cycle assay

Cells were frozen and thawed as described in *2.2.3.1*. CAR expression and viability were measured as described in *2.2.3.11* and compared to values before freezing.

2.2.3.13 CAR T cell stimulation assay

To stimulate CAR and mock T cells with the immobilized target antigen, 24-well non-treated cell culture plates were coated with 2 µg/mL SP17-mFc or bio-SPAG9A1A2 (500 µL/well, diluted in ddH_2O) and incubated for 4 h at 37 °C. Bio-SPAG9A1A2 was indirectly coated by bio-BSA (3 µg/mL, 1 h at 37 °C) and strep (10 µg/mL, 1 h at 37 °C) as described before (*2.2.4.7*). After incubation time, the coating liquid was discarded and plates were blocked with 1 mL/well RPMI (+ 10% FCS) for 30 min at 37 °C. $5x10^5$ CAR or mock T cells were taken up in 500 µL X-VIVO15 (+ 5% FCS) and added per well. The plates were incubated for 40 h at 37 °C, 5% CO_2. Cells were harvested and expression of CD25, CD69 and PD-1 was measured as a mean of T cell activation as described in *2.2.3.11*.

2.2.3.14 CAR T cell proliferation assay

Proliferation of T cells after stimulation was monitored by labeling of the T cells with the CFSE cell division tracker kit (BioLegend) according to the manufacturer's instructions. In short, 10^7 T cells were incubated with 1 mL of 5 µM carboxyfluorescein succinimidyl ester (CFSE) solution at 37 °C for 20 min. Staining was quenched by adding 5x the original staining volume of cell culture medium containing 10% FCS. Cells were pelleted and resuspended with 10 mL prewarmed adapted medium and were ready to use after a 10 min incubation. Labeled cells were incubated with the target antigen as described in *2.2.3.13*.

Proliferation activity was measured by flow cytometry as described in *2.2.3.11* using a PE conjugated anti-human CD3 antibody.

In order to measure T cell proliferation upon contact with antigen positive target cells, $5x10^4$ target cells/100 µL/well were seeded into a 96-well plate and 100 µL/well of CFSE labeled T cells were added at an effector-to-target ratio of 1:1. Target and effector cells were seeded in X-VIVO15 (without FCS, IL-7 and IL-15) and each condition was tested in triplicates. Cells were incubated for 72 h at 37 °C, 5% CO_2. Cells were analyzed for proliferation by flow cytometry as described in *2.2.3.11*.

2.2.3.15 Bioluminescence based CAR T cell killing assay

CAR T cell *in vitro* killing of target cell line H929 was tested using a luciferase based assay kit (LDH-Glo Cytotoxicity Assay, Promega).

H929 were seeded at 10^4 cells/50 µL/well in a 96-well plate using X-VIVO15 medium (+ 5% FCS). 50 µL/well of CAR or mock T cells were added to the H929 target cells at effector-to-target ratios of 10:1, 3:1, 1:1 and 0.3:1. The assay was performed according to the manufacturer's instructions. Each condition was tested in triplicates. In this assay, cytotoxicity of the T cells correlated to the release of lactate dehydrogenase (LDH) from killed target cells. LDH enzymatic reaction released substrates for a reductase that generated luciferin which was further converted into a measurable bioluminescent signal.

2.2.3.16 Real time monitored CAR T cell killing assay

The *in vitro* killing capacity of CAR T cells towards the adherent target cell line SKOV-3 was tested using a real-time cell analyzer optimized for monitoring the viability of adherent cells (xCELLigence RTCA SP, ACEA Biosciences).

96-well plates with gold electrodes on the bottom (E-plates) were used which measure electrical impedance correlating to the cell density. The signal is converted into a cell index and decreases when cells detach from the gold electrodes on the well bottom. Detaching corresponded to target cell killing.

The optimal assay target cell density was empirically tested by seeding cell numbers ranging from $5x10^3$ to $4x10^4$ per well and cell viability was monitored for 40 h. For the killing assay, 10^4 SKOV-3 cells/100 µL/well were seeded and incubated for 3 h at 37 °C, 5% CO_2. During incubation cells attached to the well bottom and proliferated with a doubling time of approximately 6 h, which was considered for adjustment of the effector cells.

Effector-to-target ratios of 4:1, 1:1 and 1:4 were analyzed by adding the adjusted numbers of CAR or mock T cells (100 µL/well) to the target cells and incubated for 50 h at 37 °C, 5% CO_2. Target and effector cells were each seeded in adapted medium. Each condition was tested in triplicates.

2.2.4 Protein biochemical methods

2.2.4.1 Dialysis

αCTA scFv-hFc fusion protein purification was initiated by dialysis. The production culture supernatant was filled in a 12 kDa dialysis tube and dialyzed against 5 L (> 30x volume excess) protein A binding buffer overnight at 4 °C under gentle stirring. This allowed buffer exchange and exclusion of proteins with a molecular size lower than 12 kDa until equilibrium was reached. The αCTA scFv-hFc fusion protein containing liquid from the dialysis tube was sterile filtered using a 0.22 µm low protein binding filter and stored at 4 °C until use.

2.2.4.2 Protein A affinity chromatography

αCTA scFv-hFc fusion protein purification was continued by protein A affinity chromatography using the AEKTApure fast protein liquid chromatography (FPLC) system. The flow rate was 1 mL/min for all steps.

A 1 mL protein A column was washed with water and equilibrated with protein A binding buffer for 5 min. The sterile filtered αCTA scFv-hFc fusion protein containing liquid was loaded onto the column, the column was washed with protein A binding buffer for 10 min and the αCTA scFv-hFc fusion proteins were eluted with protein A elution buffer as 1 mL fractions. The collecting tubes contained 300 µL (first two tubes 200 µL) protein A neutralization buffer. The main fraction was dialyzed against 500 mL PBS and sterile filtered as described in *2.2.4.1*. Protein concentration was measured photometrically at 280 nm considering the extinction coefficient as determined by the ExPASy ProtParam online tool.

2.2.4.3 Analytical and preparative size exclusion chromatography

An analytical size exclusion chromatography (SEC) was performed on the AEKTA FPLC system to analyze the scFv-hFc fusion protein aggregate content. A Superdex 200 Increase 10/300 GL column (20 mL column volume) was washed with 40 mL water and PBS (0.3-1 mL/min). 20-30 µg αCTA scFv-hFc were loaded onto the column by injection through a

25 µL loop and the sample passed the column at a flow rate of 0.5 mL/min. Protein elution was monitored photometrically at 280 nm. The elution time was compared to a standard run with proteins of known molecular size.

If required, a preparative SEC was performed using the HiLoad 16/60 Superdex 200 pg column (120 mL column volume) allowing the separation from multimers by fractionation. The procedure was the same as for the analytical SEC, but the total protein amount was loaded by injection through a 5 mL loop instead. Monomeric protein fractions were pooled, sterile filtered and stored at 4 °C (short term) or -80 °C (long term).

2.2.4.4 Sodium dodecyl sulfate polyacrylamide gel electrophoresis

Purified αCTA scFv-hFc fusion proteins were separated according to molecular weight by sodium dodecyl sulfate polyacrylamide gel electrophoresis (SDS PAGE). A 12% acrylamide separating gel and a 5% acrylamide stacking gel were prepared as described in *Table 25*.

The separating and the stacking gel were sequentially poured into a 1.5 mm cassette. After polymerization the gels were directly used or stored at 4 °C.

2 µg of each protein sample were added to 4 µL 5x Laemmli buffer, 5 µL 1 M DTT and complemented with ddH_2O to a final volume of 20 µL. Samples were denaturated at 90 °C for 3 min and loaded into SDS gel wells. Together with a protein standard containing proteins of known molecular weight, the gel was run at 150 V for 2 h.

Table 25. Components for 12% acrylamide separating and 5% acrylamide stacking gel

Component	Separating gel (12%)	Stacking gel (5%)
Rotiphorese A	3110 µL	490 µL
Rotiphorese B	1300 µL	200 µL
Separating gel buffer	1920 µL	-
Stacking gel buffer	-	750 µL
ddH_2O	1520 µL	1500 µL
10% SDS	80 µL	30 µL
TEMED	6.5 µL	2.2 µL
10% APS	64 µL	25 µL
∑	**8000 µL**	**3000 µL**

2.2.4.5 Coomassie Blue staining

Proteins on the SDS gel were visualized with Coomassie Blue staining solution by incubation for at least 2 h on a shaker at RT followed by overnight destaining with water under the same conditions. Stained gels were scanned for documentation.

2.2.4.6 Western blot

To visualize specific proteins separated on an SDS gel, proteins were first transferred to a nitrocellulose membrane (western blot) and then immunostained with protein specific antibodies.

After electrophoresis, the SDS gel, a nitrocellulose membrane and filter blot papers were equilibrated with semi-dry blot buffer for 5 min in a shaker. Filter blot papers, nitrocellulose membrane and SDS gel were stacked on a blot transfer chamber. The transfer was carried out at 20 volts for 30 min and the membrane was blocked with 2% MPBS at RT for 60 min on a shaker. A specific HRP coupled antibody (human IgG Fc specific in case of αCTA scFv-hFc detection) was appropriately diluted in 2% MPBS and incubated with the membrane at RT for 30 min or at 4 °C overnight under shaking. The membrane was washed three times with PBST and once with PBS for 5 min while shaking. ECL substrate reagents were mixed in equal volumes and incubated with the membrane for 1 min in the dark. Target protein bands were visualized with an ECL imager at an exposure time of 1-10 min.

2.2.4.7 Enzyme linked immunosorbent assay

Specificity of purified αCTA scFv-hFc fusion proteins was analyzed by enzyme linked immunosorbent assay (ELISA). Binding to target antigens and to control proteins was tested.

Proteins were diluted in PBS. Each well contained 50 µL working volume, blocked wells contained 150 µL 2% MPBS. Each washing procedure included three PBST and three PBS washing steps.

A 96-well half area plate was coated with 3 µg/mL AKAP4-His, SP17-His, SP17-mFc, bio-BSA (3 µg/mL each) or PBS and incubated overnight at 4 °C. The plate was washed as described above. Bio-BSA containing wells were incubated with strep (10 µg/mL) and the remaining wells were blocked for 1 h at RT on a plate shaker. The plate was washed and 3 µg/mL bio-SPAG9A1A2 were added to strep coated wells (except for control wells) and incubated for 1 h at RT on a plate shaker. The plate was washed and blocked for 1 h at RT. 10 µg/mL of αCTA scFv-hFc diluted in 2% MPBS were added to corresponding wells. The plate was incubated for 2 h at RT and then washed. Anti-human IgG Fc HRP conjugated

antibody (diluted 1:3000 in 2% MPBS) was added for 1 h at RT. Plates were washed as before, 50 µL/well of the TMB solution were added and incubated for 10 min in the dark at RT. Reaction was stopped with 25 µL/well of 2N sulfuric acid. Absorbance was measured at 450 nm wavelength (reference 620 nm) using a plate reader.

2.2.4.8 Surface plasmon resonance spectroscopy

Binding affinity of lead candidate αCTA scFv-hFc fusion proteins to their target protein was investigated by surface plasmon resonance spectroscopy. This highly sensitive method allows measuring protein-protein interactions at a very low scale. A gold surface on the sensor chip is exposed to a laser beam which is reflected. Depending on the surface density, which increases upon analyte binding to the surface captured ligand, the laser beam transfers a certain amount of energy to the surface causing a change in its reflection angle. The reflection angle change is measured and translated into so called response units (RU) describing the protein-protein dynamic on the surface. The captured protein is termed ligand, the protein in the mobile phase is termed analyte.

Protein A was covalently immobilized on all flow cells of a sensor chip with a dextran matrix by adjusting the concentration to 300 µg/mL in 10 mM sodium acetate (pH 4.5) using an amine coupling kit. At a flow rate of 5 µg/mL, the surface was activated, the protein immobilized and the surface deactivated for 7 min per step.

Ligand concentration was predetermined by a test capture run with scFv-hFc proteins considering the desired outcome of maximum response units. All proteins were diluted in 1x HBS-EP buffer.

The final run included injection of scFv-hFc fusion protein at a rate of 10 µL/min for 1 min and analyte injection at rate of 30 µL/min for 2 min. Dissociation was allowed for 300 s and regeneration occurred at 30 µL/min for 1 min with a subsequent stabilization step (180 s). Flow cell 1 was used as reference (no analyte) and substracted from flow cell 2 (containing the analyte). Cancer-testis antigens were analyzed in a concentration series with 1:2 dilutions ranging from 0 nM to 2000 nM (SP17-His) or to 8000 nM (bio-SPAG9A1A2).

3 Results

3.1 Selection of AKAP4, SP17 and SPAG9 specific antibody fragments by phage display

To select fully human AKAP4, SP17 and SPAG9 specific antibody fragments by phage display, we used our in-house antibody library LYNDAL derived from B cells of tumor draining lymph nodes of head and neck cancer patients, that represents an IgG immune repertoire with a diversity of $>10^9$ clones [188]. We hypothesized that we might retrieve more specific and highly affine antibody fragments recognizing CTAs from a tumor antigen experienced antibody library such as LYNDAL compared with a tumor antigen inexperienced naïve antibody library. To investigate this question, we set up a collaboration with Yumab GmbH, a service provider for customized antibody generation. We requested Yumab GmbH to select AKAP4, SP17 and SPAG9 specific antibody fragments by phage display using the naïve human IgM antibody library HAL9/10 derived from circulating B cells of healthy donors, that contains $>10^{10}$ diverse antibody sequences [192].

We used following antigens for the selection procedure: AKAP4 was purchased from a commercial distributor (Cusabio), SP17 was produced by ourselves and a SPAG9 derived peptide was synthesized by the group of our collaboration partner Prof. Dr. Walter Mier (Radiopharmaceutical Chemistry, University Hospital Heidelberg). Our initial attempts to produce full-length AKAP4 and SPAG9 were not successful (not shown).

Since no structural information is available for AKAP4 and SP17 that clearly defines extracellular, transmembrane and intracellular sections, we decided to purchase full-length AKAP4 and to produce full-length SP17 fused to a murine Fc (mFc) tag for purification purposes (*Appendix*, *Figure 34*). In contrast, for SPAG9 an extracellular section comprising three putative antigenic regions (A1, A2, A3) was described by Shankar and colleagues [173]. We designed a SPAG9 peptide antigen containing the putative antigenic regions A1 and A2, and included an N-terminal biotin linked to the peptide by PEG_2. The PEG_2 linker allows to bridge the streptavidin binding pocket, has a low immunogenicity and excellent solubility [194]. This design enabled a selection procedure in solution using streptavidin coupled magnetic beads.

3.1.1 Enrichment of SPAG9 specific antibody fragments upon phage display selection using LYNDAL

To obtain fully human scFvs specific for SPAG9, we performed three rounds of phage display selection against the bio-SPAG9A1A2 peptide antigen using our in-house antibody library LYNDAL and magnetic streptavidin conjugated beads.

We analyzed scFv presenting polyclonal phages from each selection round by ELISA and detected binders specific for bio-SPAG9A1A2, bio-BSA and streptavidin, but not for other control proteins (*Figure 11A*). This indicates that streptavidin binders were still enriched, although we preincubated the phages with the streptavidin coupled beads and continued with the unbound phages in the supernatant for the actual selection procedure. We expected this outcome as we already observed for previous phage display experiments, that a negative selection does not fully exclude binders specific for tags fused to the antigen or for proteins coupled to beads used for the procedure (not shown). Importantly, we measured an approximately twofold higher absorbance signal for detected bio-SPAG9A1A2 specific binders than for streptavidin specific binders. This indicates an at least equal enrichment of bio-SPAG9A1A2 binders when considering the false positive streptavidin binders due to indirect coating of bio-SPAG9A1A2 via bio-BSA and streptavidin. The enrichment of biotin binders indicated by bio-BSA was negligible.

Since we found maximum enrichment of bio-SPAG9A1A2 specific binders after selection round 3, we randomly picked 90 *E. coli* TG1 colonies infected with phages from selection round 3. Then we amplified and induced these colonies with IPTG for the periplasmic production of soluble scFvs. We isolated the scFvs from the bacterial periplasm and analyzed the specificity by ELISA (*Figure 11B*). Out of 90 tested scFv clones, 35 were specific for bio-SPAG9A1A2 (39%) and only 3 specific for streptavidin (3%) as determined by an absorbance signal threshold of ≥0.5. Bio-SPAG9A1A2 specific scFvs yielding absorbance signal intensities above 1.0 upon detection reaction were considered for further analyses, 28 clones in total.

However, by colony PCR analysis we found that only 19 out of 28 bio-SPAG9A1A2 specific clones displayed full-length scFv integrity (*Appendix*, *Figure 35*). Sequence analysis of these 19 clones revealed 4 double clones, 1 clone with an out-of-frame mutation and 8 clones with multiple stop codons that affected the open reading frame. Surprisingly, the remaining 6 clones showed identical sequences as determined by sequence alignment. We termed this SPAG9 specific scFv candidate αSPAG9_VD1.E6.

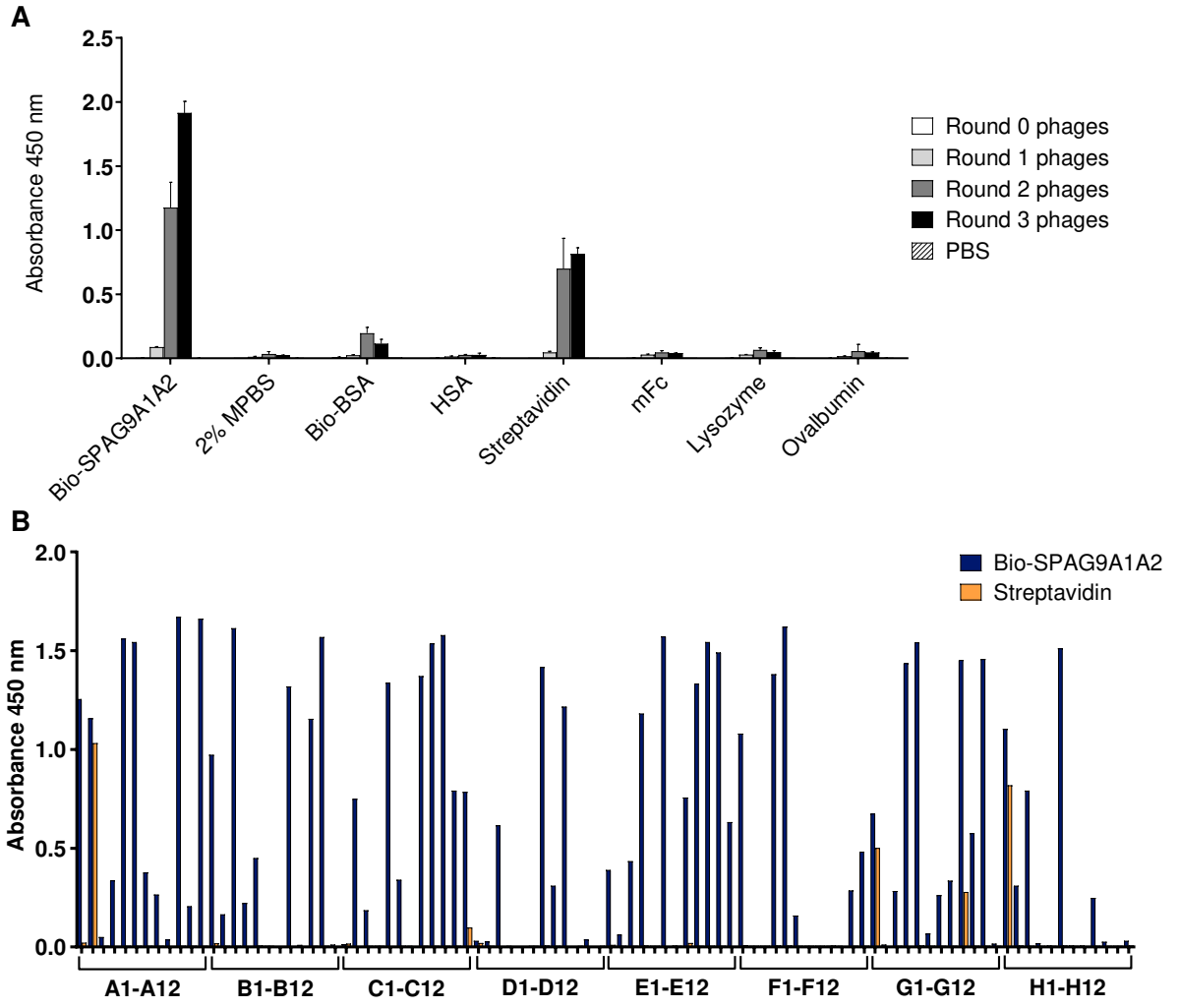

Figure 11. ELISA applying polyclonal scFv displaying phages or soluble monoclonal scFvs produced in bacteria to screen for bio-SPAG9A1A2 specificity. 3 µg/mL of each protein were immobilized in a 96-well microtiter plate. Bio-SPAG9A1A2 was indirectly coated via bio-BSA (3 µg/mL) and streptavidin (10 µg/mL), streptavidin was indirectly coated via bio-BSA. **(A)** 10^{12}/well scFv presenting polyclonal phages from phage display selection round 0 (before antigen encounter), 1, 2 and 3 were incubated with immobilized bio-SPAG9A1A2 target antigen and control proteins. Bound phages were detected with an anti-M13 HRP conjugated antibody and TMB reaction solution. Error bars represent the standard deviation of duplicates. **(B)** 90 individual *E. coli* TG1 clones infected with phages from selection round 3 were grown in a 96-deep-well plate and induced with IPTG overnight for periplasmic production of soluble scFvs. Monoclonal scFvs were extracted from the periplasm and incubated with bio-SPAG9A1A2 target antigen or streptavidin. Bound scFvs were detected with anti-c-myc HRP conjugated antibody and TMB reaction solution. D4-D6 and F7-F9 were negative control wells.

3.1.2 ScFv sequences derived from immune repertoires are more distant to the germline sequences than those derived from naïve repertoires

Our attempts to select AKAP4 and SP17 specific scFvs from LYNDAL were unsuccessful due to the enrichment of unspecific clones that did not contain full-length scFv integrity [193]. However, our collaboration partner Yumab GmbH successfully generated AKAP4, SP17 and SPAG9 specific scFvs by phage display applying the naïve antibody library HAL9/10 and subsequent high throughput screening [192]. Based on a signal-to-noise ratio of >20 in monoclonal scFv binding ELISA and sequence uniqueness as determined by CDR comparison (not shown), Yumab GmbH identified the following binders:

a) 2 out of 768 screened AKAP4 specific scFv clones
b) 10 out of 192 screened SP17 specific scFv clones
c) 13 out of 192 screened SPAG9 specific scFv clones

We continued with both AKAP4, five SP17 and six SPAG9 specific scFv clones according to best overall signal and signal-to-noise ratio.

We analyzed LYNDAL (IgG immune repertoire) and HAL9/10 (IgM naïve repertoire) selected scFv sequences using the databases IMGT/V-Quest and VBASE2, which compare the manually entered V_H and V_L sequences with the closest germline sequence, and summarized the results in *Table 28* (*Appendix*). Regarding the V_H region, we found 35 mutated nucleotides for our LYNDAL selected clone αSPAG9_VD1.E6, but only 1-18 within the sequences of HAL9/10 selected clones. These nucleotide mutations led to 19 amino acid (aa) changes within the αSPAG9_VD1.E6 scFv out of which 7 were in the CDRs and 12 in the framework regions. In contrast, HAL9/10 selected scFvs only had up to 8 aa changes in their V_H region out of which 0-4 were localized in the CDRs. As the heavy chain CDR3 (CDR-H3) loop is the most variable in length with 2-26 aa and therefore highly contributes to antigen specificity, we analyzed CDR-H3 lengths as well (not shown in *Table 28*) [195]. CDR-H3 lengths were long for both αAKAP4 scFvs (20 and 23 aa), short to medium for αSP17 scFvs (7-14 aa) and medium to long for αSPAG9 scFvs (12-20 aa, αSPAG9_VD1.E6 scFv: 20 aa). A broader length diversity as observed for αSP17 and αSPAG9 scFvs might indicate specificity against different antigen epitopes as some tertiary structures within the CDR-H3 loop are formed preferentially for certain CDR-H3 lengths [196]. Vice versa, similar CDR-H3 lengths as found for αAKAP4 scFvs might form similar tertiary structures specific for similar epitope structures.

Interestingly, among all analyzed scFv sequences the heavy chain V gene segment (IGHV) distribution was overrepresented with the IGHV1 family which is the second most frequently

used IGHV family (approx. 25%) after IGHV3 (approx. 50%) according to Matsuda *et al.* [197]. This implies that the inclusion of IGHV1 within antibodies specific for AKAP4, SP17 and SPAG9 might be advantageous for antigen binding, which needs to be further validated by analyzing a higher number of specific antibodies. Surprisingly, all αSP17 scFvs contained λ light chains, while the αSPAG9 scFvs were balanced (3 κ and 3 λ light chains, αSPAG9_VD1.E6 scFv: κ) and both αAKAP4 scFvs contained κ light chains. As the ratio of κ-to-λ light chains is approximately 2:1 in humans, preferential usage of λ could indicate structural benefits for antigen binding [1].

We observed higher accumulation of mutations and amino acid changes also for other LYNDAL selected scFv sequences compared to those selected from HAL9/10 (not shown). A study that analyzed 594 unique antibody clones specific for a tetanus toxin, defined a mean value of 20.5 aa changes (somatic hypermutations) combined for the V_H and V_L region to indicate affinity maturation [198]. This value was only achieved for the αSPAG9_VD1.E6 clone (33 aa changes), but not for any of the HAL9/10 selected scFv clones (1-16 aa changes). Therefore we assume that, in general, scFv sequences derived from immune repertoires are more distant from the germline sequences than those derived from naïve repertoires due to somatic hypermutations. We need to confirm these results by analyzing a higher number of V_H and V_L regions derived from both repertoires.

3.2 Characterization of AKAP4, SP17 and SPAG9 specific scFv-hFc fusion proteins

The coding sequences of AKAP4, SP17 and SPAG9 (abbreviated αCTA) specific candidate scFv clones were fused to a human IgG1 Fc backbone including the hinge region, C_H2 and C_H3 domains, and ligated into the mammalian expression vector pCMX2.5. To generate these IgG like scFv-hFc fusion proteins, HEK293-6E cells were transfected with the engineered pCMX2.5 vectors.

3.2.1 Purification of αCTA scFv-hFc fusion proteins by protein A chromatography

After transfection of HEK293-6E cells with the respective pCMX2.5 plasmids, we harvested the cell culture supernatant and purified the αCTA scFv-hFc fusion proteins by protein A chromatography. The yields ranged from 0.26 to 1.96 mg per 30 mL culture volume and were sufficient for characterization. We analyzed the αCTA scFv-hFc proteins by Coomassie Blue

staining and western blot after separation in SDS-PAGE (*Figure 12*). We observed Coomassie Blue stained proteins on the SDS gel with a corresponding molecular weight of approximately 60 kDa. In western blot, IgG hFc specific antibodies recognized bands with the same molecular weight, thus confirming the stained proteins as the purified scFv-hFc proteins. The apparent molecular weight of 60 kDa further corresponds to a “halfmer” of the scFv-hFc protein as expected under reducing conditions due to the split disulfide bonds. Almost all scFv-hFc proteins were visible as double bands indicating differences in posttranslational modifications such as glycosylation. Unexpectedly, for 3 out of 5 αSP17 scFv-hFc proteins additional bands were detected at >140 kDa which might be non-covalently linked aggregates (*Figure 12B*).

However, when we analyzed purity by SEC, the main elution volumes of all αCTA scFv-hFc proteins ranged between 12.0 and 12.6 mL corresponding to a molecular size of approximately 158 kDa as determined by a standard run with proteins of known molecular size (*Figure 13*). We expected this molecular size for natively folded bivalent scFv-hFc molecules. We did not observe any peaks with elution volumes <12.0 mL for αSP17 scFv-hFc proteins (*Figure 13B*), indicating the absence of aggregates. As we consider the observations in SEC more reliable due to the maintained native conformation compared to SDS-PAGE, we assume that heat denaturation might have caused aggregation. Similarly, Vermeer and Norde found partially unfolded IgG antibodies to be locked in aggregates during the denaturation process and hence could not achieve complete unfolding [199].

Low aggregate fractions observed in SEC analyses of αAKAP4 and αSPAG9 scFv-hFc proteins (*Figure 13A* and *13C*) were not visible on the Coomassie Blue stained gel or on the western blot (*Figure 12A* and *12C*). These might be covalently linked aggregates that were separated under reducing conditions. As the aggregate content was below 10% for all αCTA scFv-hFc fusion proteins, we decided not to perform preparative SEC for aggregate separation due to considerable concomitant protein loss.

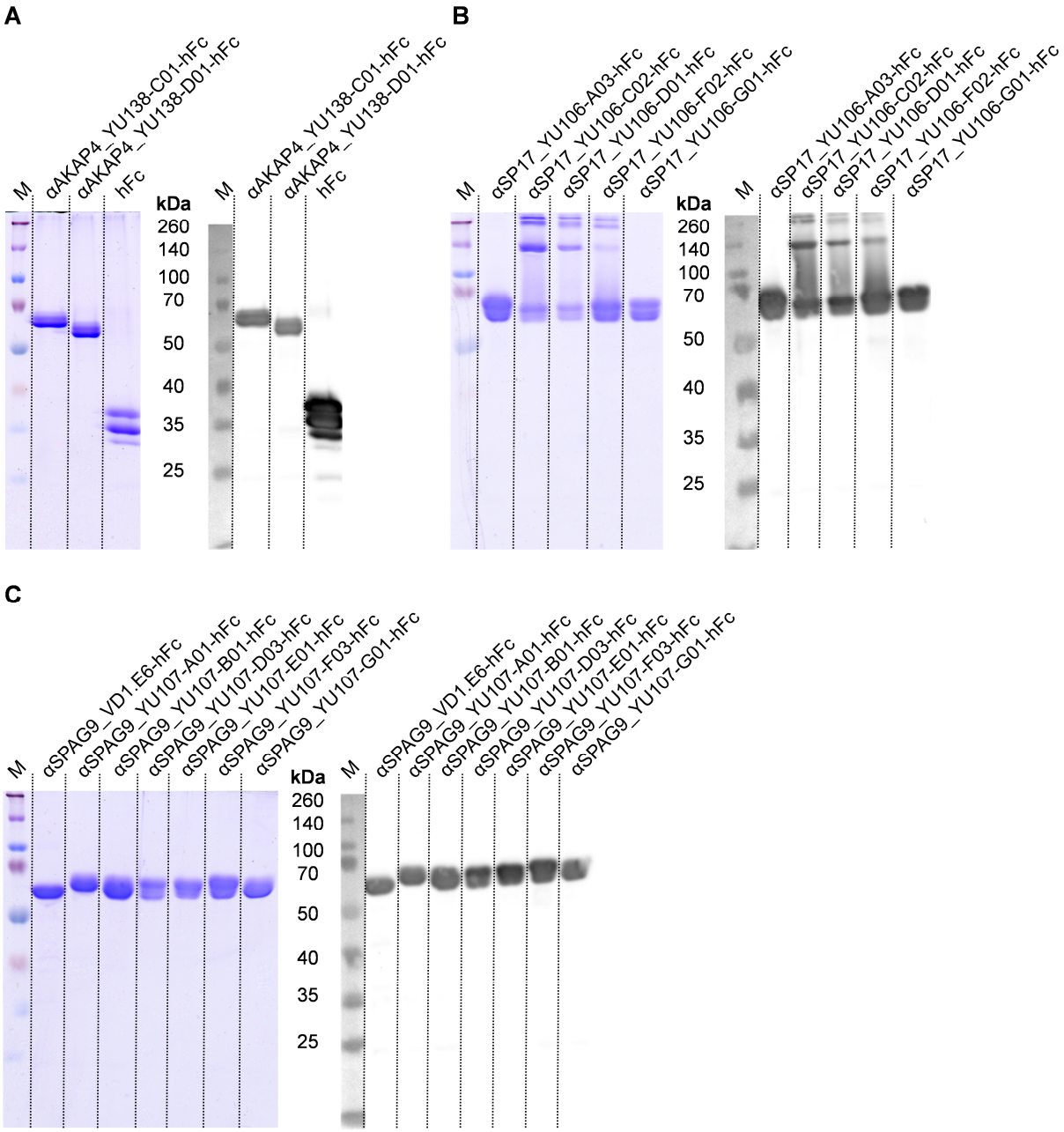

Figure 12. Coomassie Blue and western blot staining of αCTA scFv-hFc fusion proteins after electrophoretic separation. 2 µg/lane of protein A purified **(A)** AKAP4, **(B)** SP17 and **(C)** SPAG9 specific scFv-hFc fusion proteins were separated by SDS gel electrophoresis and visualized by Coomassie Blue staining as well as by western blot using a HRP coupled anti-human IgG Fc antibody. IgG1 human Fc (hFc) was included as positive control. M = marker.

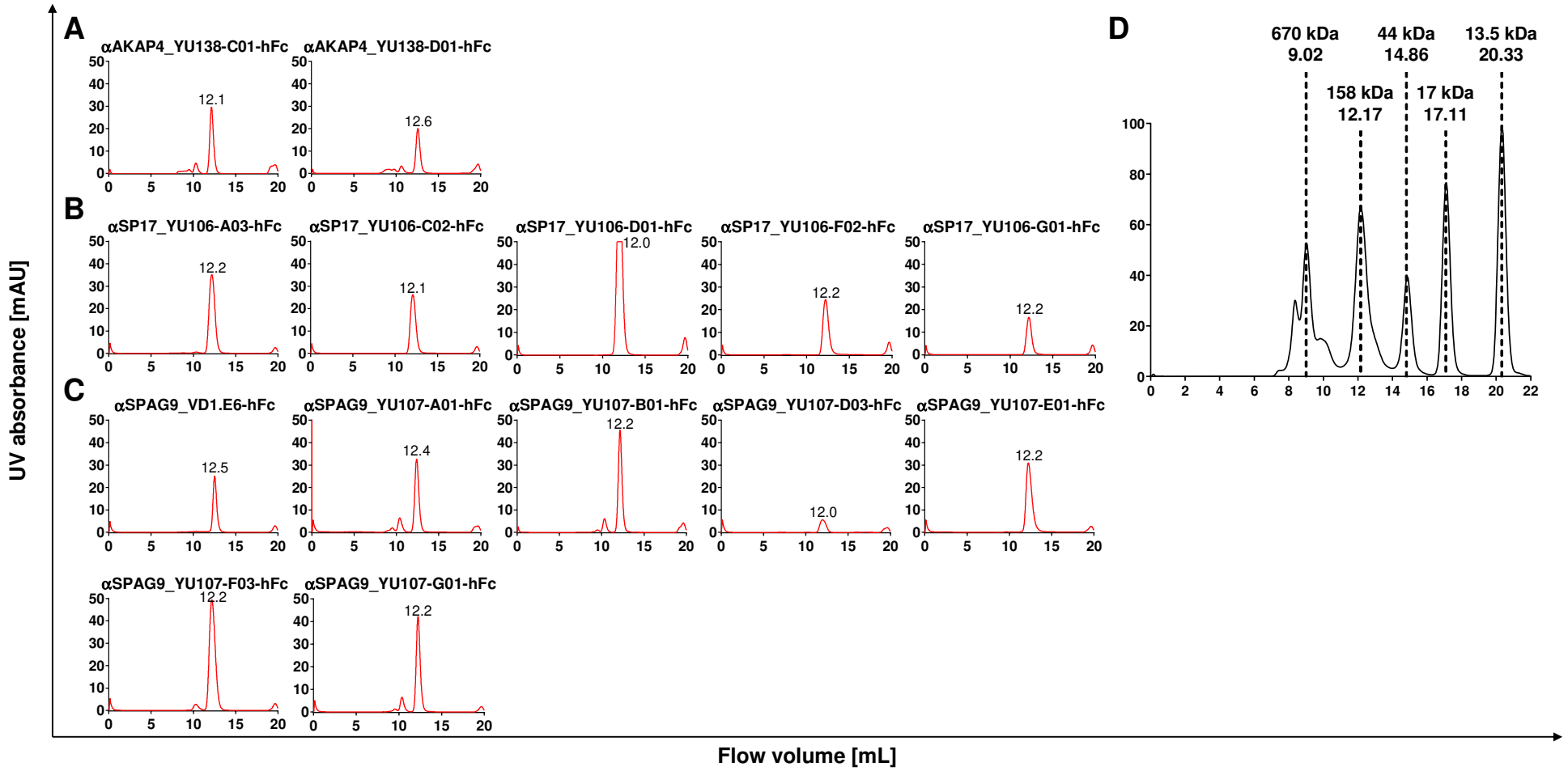

Figure 13. Size exclusion UV chromatograms of individual runs using αCTA scFv-hFc fusion proteins. 20-30 µg of **(A)** AKAP4, **(B)** SP17 and **(C)** SPAG9 specific scFv-hFc fusion proteins were loaded onto a 20 mL SEC column, carried by a mobile phase (PBS) and eluted according to descending hydrodynamic volume. **(D)** Standard proteins with known molecular size were analyzed in a separate run to determine corresponding flow volumes.

3.2.2 αCTA scFv-hFc fusion proteins specifically bind target antigens in ELISA

We analyzed the capability of soluble αCTA scFv-hFc fusion proteins to bind their cognate antigen by ELISA (*Figure 14*). To this end, we coated the purified target antigens on 96-well plates and co-incubated the wells with αCTA scFv-hFc proteins. By using an HRP coupled IgG hFc specific antibody, we detected highly specific binding of all αCTA scFv-hFc proteins to their cognate antigen except for αAKAP4_YU138-C01-hFc, which also bound to SP17-His indicating cross-reactivity with SP17 or His tag (*Figure 14A*). Thus, the αAKAP4_YU138-C01-hFc protein was excluded from further analyses. All other αCTA scFv-hFc proteins did not show unspecific binding to other tested control proteins.

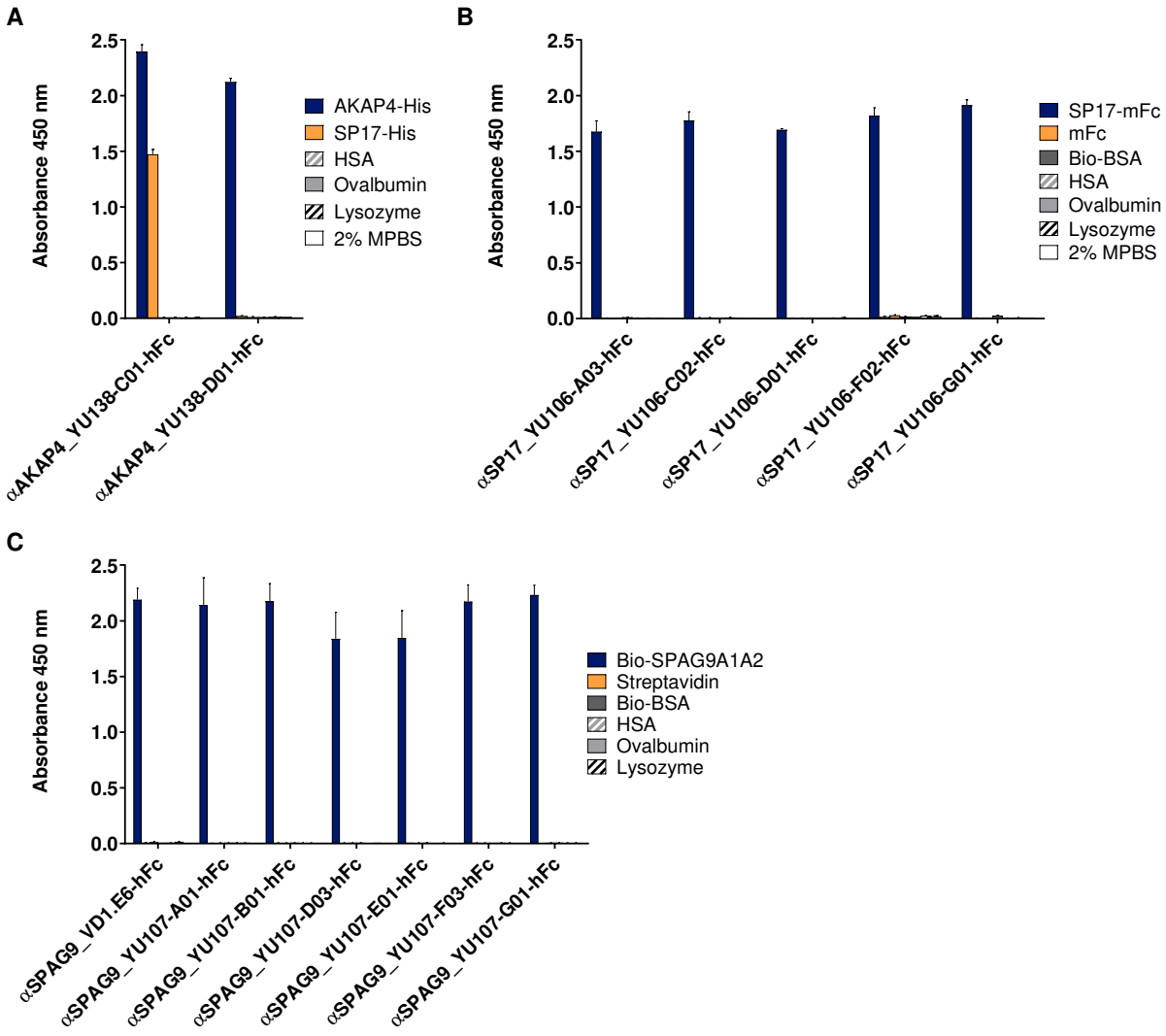

Figure 14. Antigen binding capability of αCTA scFv-hFc fusion proteins tested by ELISA. 96-well plates were coated with 3 µg/mL of indicated target and control proteins. Bio-SPAG9A1A2 was indirectly coated via bio-BSA (3 µg/mL) and streptavidin (10 µg/mL). Coated wells were co-incubated with 10 µg/mL of **(A)** αAKAP4, **(B)** αSP17 and **(C)** αSPAG9 scFv-hFc fusion proteins. Bound scFv-hFc proteins were detected by an HRP coupled IgG human Fc specific antibody. Error bars represent standard deviation of duplicates.

3.2.3 Lead candidate αSP17 and αSPAG9 scFv-hFc fusion proteins bind to the surface of solid and B cell lineage tumor cell lines

In order to identify antigen positive tumor cell lines for subsequent analyses, we first assessed the CTA surface expression profile on the solid tumor cell lines Colo205 (colorectal cancer) and SKOV-3 (ovarian cancer), as well as the B cell lineage tumor cell lines H929 (multiple myeloma), MM1.S (multiple myeloma) and NALM-6 (pre-B cell acute lymphoblastic leukemia) by flow cytometry using commercially available AKAP4, SP17 and SPAG9 specific polyclonal antibodies. We chose either identical cell lines or cell lines of the same tumor that were found to be AKAP4, SP17 and SPAG9 positive in other previous studies [153,162,163,184].

We classified CTA surface expression as highly positive (>50% positive cells), moderately positive (between 5% and 50% positive cells) or negative (<5% positive cells) compared to the isotype control antibody stainings. Bound polyclonal antibodies were detected using a secondary FITC conjugated anti-rabbit IgG Fc antibody. We found at least moderately positive AKAP4, SP17 and SPAG9 surface expression for all tested cell lines, except for Colo205 which was SP17 negative (*Figure 15*).

We then labeled our αCTA scFv-hFc fusion proteins with the fluorescent dye allophycocyanin (APC) and tested their surface binding capacity to the CTA expressing tumor cell lines. The findings are summarized in *Table 26*.

Table 26. Binding capacity of αCTA scFc-hFc fusion proteins to CTA positive tumor cell lines.

Clone	Colo205	H929	MM1.S	NALM-6	SKOV-3
αAKAP4_YU138-D01-hFc	–	–	–	+	+
αSP17_YU106-A03-hFc	–	–	–	–	–
αSP17_YU106-C02-hFc	–	–	–	–	–
αSP17_YU106-D01-hFc	–	–	–	++	–
αSP17_YU106-F02-hFc	+	++	++	++	++
αSP17_YU106-G01-hFc	–	–	–	–	–
αSPAG9_YU107-A01-hFc	–	–	–	–	–
αSPAG9_YU107-B01-hFc	–	–	–	–	–
αSPAG9_YU107-D03-hFc	–	–	–	–	–
αSPAG9_YU107-E01-hFc	–	–	–	–	–
αSPAG9_YU107-F03-hFc	–	–	–	–	–
αSPAG9_YU107-G01-hFc	–	–	–	–	–
αSPAG9_VD1.E6-hFc	++	++	++	++	++

++ = >50% positive cells, + = between 5-50% positive cells, – = <5% positive cells (negative)

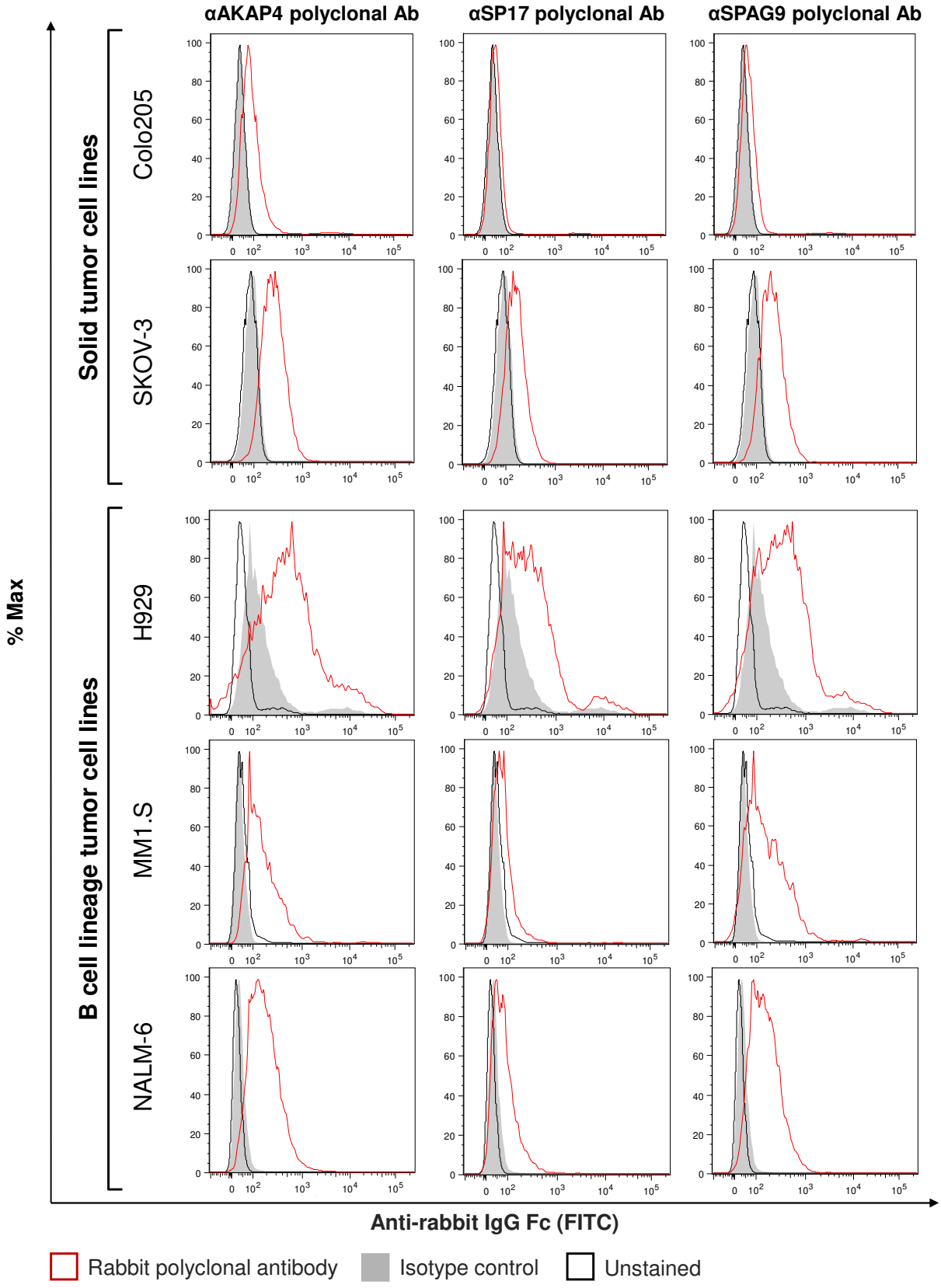

Figure 15. CTA expression on the surface of distinct tumor cell lines. Expression of AKAP4, SP17 and SPAG9 on the surface of various solid and B cell lineage tumor cell lines was analyzed by flow cytometry using specific commercially available polyclonal rabbit antibodies (red) that were detected with a secondary FITC conjugated anti-rabbit IgG Fc antibody. Unstained cells (black) and a matched isotype antibody (grey) were used as controls.

We defined the staining of tumor cell lines by scFv-hFc proteins as bright (>50% positive cells), moderate (between 5% and 50% positive cells) or negative (<5% positive cells) compared to the isotype control antibody stainings. Binding profiles of the AKAP4, SP17 and SPAG9 specific scFv-hFc clone effecting the brightest staining of all analyzed tumor cell lines are shown in *Figure 16*. Interestingly, staining with αAKAP4_YU138-D01-hFc was mostly negative except for SKOV-3 (moderate), although it specifically bound purified AKAP4 in ELISA previously (*Figure 14*). As we used full-length AKAP4 for the selection procedure, this clone might recognize an epitope that is not exposed on the cell surface and thus inaccessible for binding. We did not consider αAKAP4_YU138-D01-hFc for further studies. Similarly, none of the αSP17 scFv-hFc proteins stained any of the tested cell lines except for αSP17_YU106-D01-hFc and αSP17_YU106_F02-hFc. While the non-binding clones might recognize inaccessible epitopes as well, αSP17_YU106-F02-hFc moderately stained Colo205 cells and brightly stained all other analyzed cell lines. Surprisingly, αSP17_YU106-D01-hFc brightly stained NALM-6 cells, but none of the other tested cell lines. This might indicate that NALM-6 express an alternative form of SP17 exposing an epitope accessible for αSP17_YU106-D01-hFc, which needs further investigation.

The LYNDAL derived clone αSPAG9_VD1.E6-hFc brightly stained all of the tested cell lines, showing brightest staining for SKOV-3 and H929 cells. All other αSPAG9 scFv-hFc proteins derived from HAL9/10 did not stain any of the analyzed tumor cell lines, although they specifically bound bio-SPAG9A1A2 in ELISA previously. We assume that HAL9/10 selected αSPAG9 scFvs might possess low antigen affinity as they derive from an IgM naïve repertoire [192]. In contrast, αSPAG9_VD1.E6 scFv derives from the IgG immune repertoire of LYNDAL and was the only affinity maturated scFv among all screened ones (*3.1.2*), a prerequisite for high affinity [188].

Considering the best binding capacity to the surface of tumor cell lines in the scFv-hFc format, we chose the scFv clones αSP17_YU106-F02 and αSPAG9_VD1.E6 as lead candidates for further studies. In regard to clinical application, we designed an optimized amino acid sequence for both scFv clones that contained a $(G_4S)_3$ linker instead of a Yol linker and eliminated non-parental amino acids that were initially introduced by restriction sites for cloning purposes. Corresponding DNA sequences were synthesized by Eurofins and cloned into the mammalian expression vector pCMX2.5 containing the IgG1 hFc tag. M.Sc. Lisa Noll (NCT Heidelberg) produced the optimized scFv-hFc proteins (indicated by an asterisk after the clone name in the following) in HEK293-6E cells and purified them by protein A chromatography. In western blot analysis and SEC, we observed that optimized scFv-hFc proteins were equally pure as their unmodified counterparts and showed identical specificities in ELISA and binding capacities to tumor cell lines in flow cytometry analysis [193].

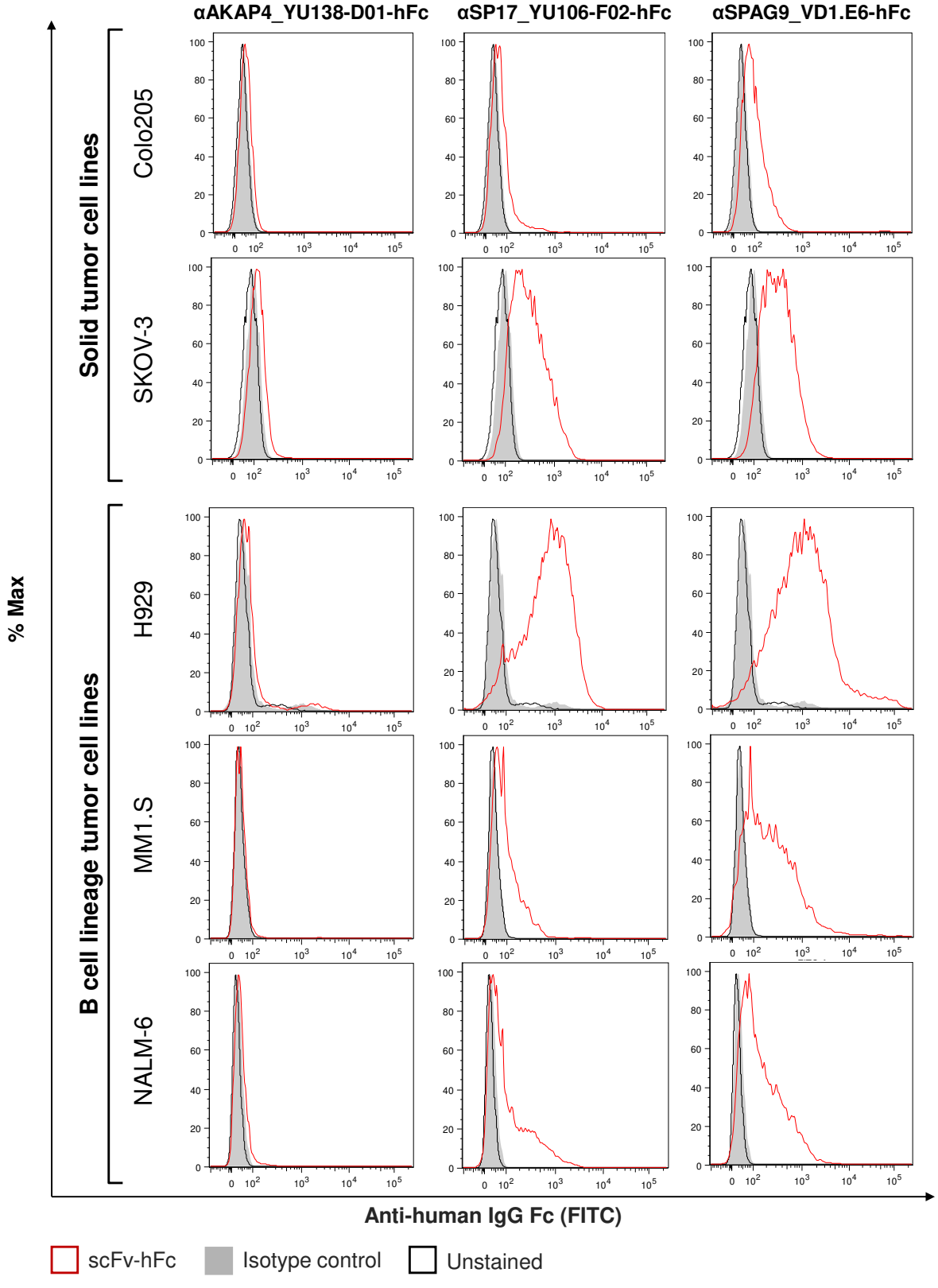

Figure 16. Binding capacity of αCTA scFv-hFc fusion proteins to tumor cell lines. Binding of αCTA scFv-hFc proteins (red) to the surface of various solid and B cell lineage tumor cell lines was tested by flow cytometry. αCTA scFv-hFc fusion proteins were labeled with a secondary FITC conjugated anti-human Fc antibody. An IgG1 antibody with irrelevant specificity was used as isotype control (grey). ScFv-hFc proteins specific for AKAP4, SP17 and SPAG9 showing the best overall binding capacity are represented.

3.2.4 Lead candidate αSP17 and αSPAG9 scFv-hFc fusion proteins bind to primary plasma cells derived from multiple myeloma patients

As we observed highest surface binding capacity for αSP17_YU106-F02*-hFc and αSPAG9_VD1.E6*-hFc to the multiple myeloma cell line H929, we collaborated with the group headed by PD Dr. Michael Hundemer (Diagnostic Laboratory for Hematological Malignancies, University Hospital Heidelberg) to include our scFv-hFc lead candidates in their diagnostic routine analyses. In these routine analyses malignant cells derived from bone marrow aspirates of patients are identified by flow cytometric immunophenotyping using a standardized eight color staining [200,201]. We labeled our scFv-hFc proteins and a human IgG1 isotype control with irrelevant specificity with APC that were used along with CD19, CD38, CD45, CD56, CD138 and κ/λ light chain specific antibodies to stain the patient samples. Plasma cell and B cell populations were identified according to distinct surface marker expression profiles defined in Flores-Montero *et al.* [201]. An overview is given in *Table 27*.

Table 27. CD marker expression on plasma cell and B cell populations compliant with Flores-Montero *et al.* [201].

Marker	Plasma cells (malignant)	Plasma cells (healthy)	B cells
CD19	–	nc	+
CD38	++	+	nc
CD45	–	+	+
CD56	++	–	–
CD138	+	+	–

++ = highly positive, + = positive, – = negative, nc = not considered (– and + possible)

In total, we analyzed plasma and B cells from bone marrow aspirates of six multiple myeloma (MM) patients and of three patients showing unremarkable bone marrow morphology (PUBM). PUBM showed no aberrant bone marrow morphology upon medical investigation and thus their bone marrows were considered as “healthy” (not shown). Cells derived from bone marrow aspirates of PUBM were used as healthy controls along with PBMCs derived from three healthy donors (HD). As for the staining of tumor cell lines, we defined staining of primary cells by scFv-hFc proteins as bright (>50% positive cells), moderate (between 5% and 50% positive cells) or negative (<5% positive cells) compared to the isotype control antibody stainings.

In the analysis that included αSP17_YU106-F02*-hFc (*Figure 17*), we observed moderate staining of plasma cells derived from patients MM.1 and MM.4 (2 out of 6), but no staining of B cells derived from MM patients. Most importantly, we found neither staining of plasma cells and B cells derived from PUBM, nor of B ($CD19^+/CD3^-$), T ($CD3^+/CD19^-$) or non-B/T cells ($CD19^-/CD3^-$) derived from HD. An exception were B cells derived from patient PUBM.2, for which we observed a brightly stained subpopulation.

Similarly, in the analysis that included αSPAG9_VD1.E6*-hFc (*Figure 18*), we found brightly stained subpopulations within plasma and B cells derived from patient PUBM.2, but no staining of those derived from other PUBM. Strikingly, we observed bright staining of distinct plasma cell subpopulations derived from patients MM.1, MM.2, MM.4 and MM.6 (4 out of 6), but no staining of B cells derived from MM patients. Also B ($CD19^+/CD3^-$), T ($CD3^+/CD19^-$) or non-B/T cells ($CD19^-/CD3^-$) derived from HD were not stained.

In summary, these findings indicate that not all primary tumor cell samples derived from MM patients were stained by our lead candidate αSP17 and αSPAG9 scFv-hFc proteins, but approximately 50% of the screened MM patients seemed to be positive. We assume that the brightly stained plasma cell subpopulations are malignant plasma cells and that the unstained plasma cells are non-malignant. We need to further investigate this hypothesis as one of the diagnostic criteria for MM is the proven presence of ≥60% of clonal plasma cells in the patient bone marrow sample, meaning that conversely ≤40% might be healthy plasma cells [202,203]. A highly important indicator which supports our hypothesis is the fact, that we found no staining of cells derived from healthy controls (PUBM and HD), except for patient PBUM.2. According to the diagnosis report, patient PBUM.2 did not show any signs of a hematological malignancy. As cells derived from all other healthy controls were negative, we recommend a second medical investigation of patient PUBM.2 to fully exclude the presence of premalignant clones and an approaching hematological malignancy. We need to confirm these results for a larger number of patients and healthy donors.

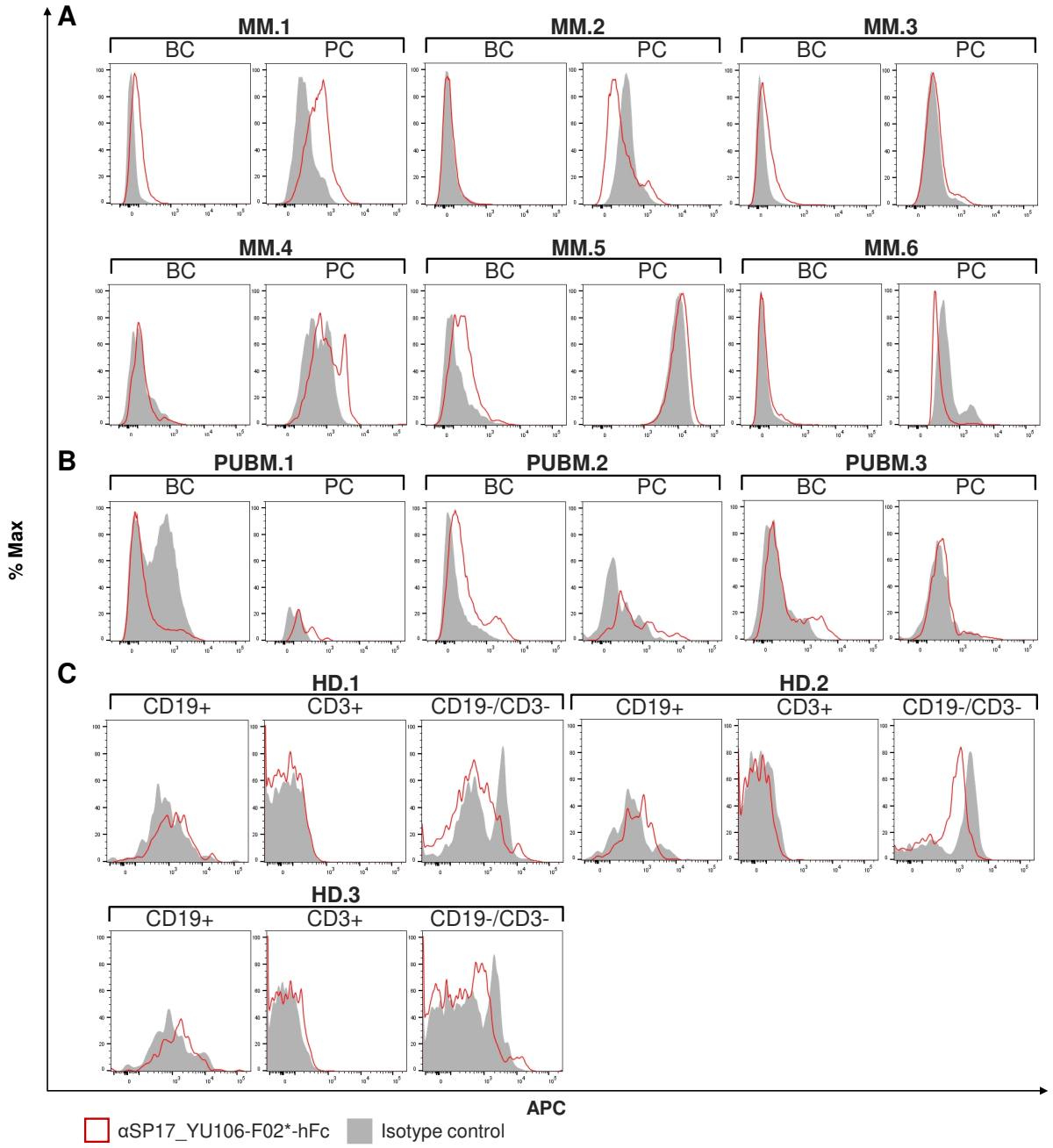

Figure 17. Binding capacity of αSP17_YU106-F02*-hFc to primary malignant and non-malignant blood cells. αSP17_YU106-F02*-hFc (red) and an IgG1 isotype control with irrelevant specificity (grey) were labeled with APC using the Zenon human labeling kit. Surface binding to B cells (BC) and plasma cells (PC) derived from bone marrow aspirates of **(A)** multiple myeloma patients (MM) and of **(B)** patients showing unremarkable bone marrow morphology (PUBM) was analyzed by flow cytometry. Surface binding to $CD19^+$, $CD3^+$ and $CD19^-/CD3^-$ blood cells of PBMCs derived from **(C)** healthy donors (HD) was tested as well. Flow cytometric analyses of healthy donor PBMCs were performed by M.Sc. Lisa Noll [193].

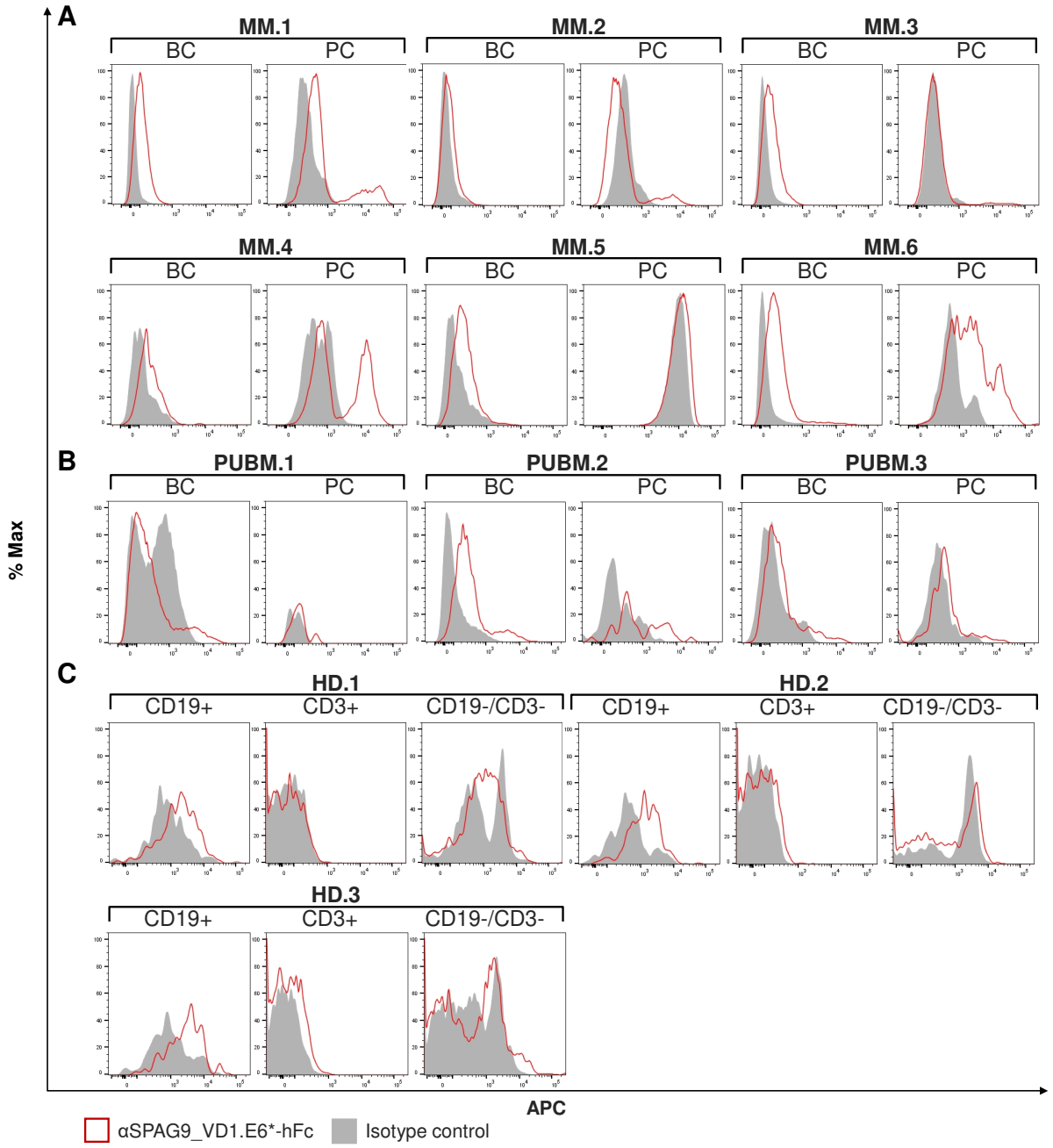

Figure 18. Binding capacity of αSPAG9_VD1.E6*-hFc to primary malignant and non-malignant blood cells. αSPAG9_VD1.E6*-hFc (red) and an IgG1 isotype control with irrelevant specificity (grey) were labeled with APC using the Zenon human labeling kit. Surface binding to B cells (BC) and plasma cells (PC) derived from bone marrow aspirates of **(A)** multiple myeloma patients (MM) and of **(B)** patients showing unremarkable bone marrow morphology (PUBM) was analyzed by flow cytometry. Surface binding to $CD19^+$, $CD3^+$ and $CD19^-/CD3^-$ blood cells of PBMCs derived from **(C)** healthy donors (HD) was tested as well. Flow cytometric analyses of healthy donor PBMCs were performed by M.Sc. Lisa Noll [193].

3.2.5 Surface plasmon resonance analysis of lead candidate αSP17 and αSPAG9 scFv-hFc fusion proteins

We evaluated the affinity of our lead candidate αSP17 and αSPAG9 scFv-hFc fusion proteins toward their cognate antigen by surface plasmon resonance (SPR) spectroscopy. To this end, we immobilized the αSP17 and αSPAG9 scFv-hFc proteins on the surface of a protein A coated sensorchip, followed by injections of increasing concentrations of the purified target antigen. Resulting sensorgrams are shown in *Figure 19*.

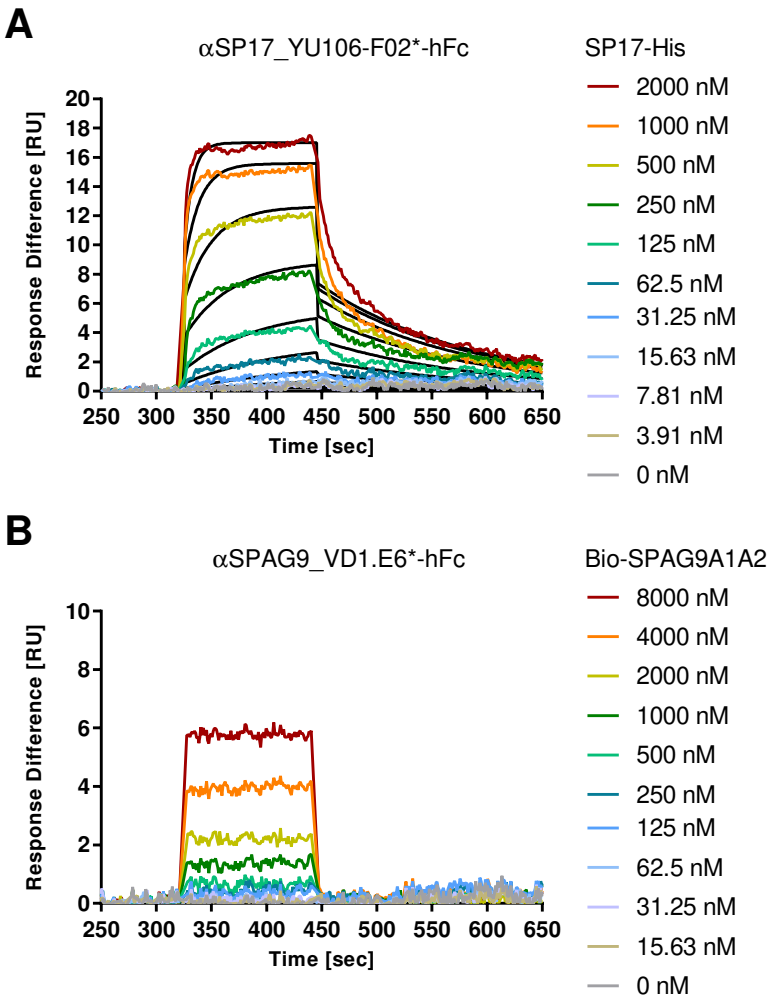

Figure 19. SPR sensorgram showing the binding interaction between the αCTA scFv-hFc fusion protein and the cognate antigen. SPR spectroscopy was conducted on the Biacore 2000. **(A)** αSP17_YU106-F02*-hFc and **(B)** αSPAG9_VD1.E6*-hFc were immobilized on a protein A coated CM5 sensorchip. A concentration series of soluble analyte ranging from 0 nM to 2000 nM (SP17-His) or to 8000 nM (bio-SPAG9A1A2) was tested. Black curves in **(A)** represent the 1:1 Langmuir binding fit model while measurement in **(B)** was fitted with the steady state affinity model (not shown). Curves represent mean values of duplicates.

We found that SP17-His rapidly associated to αSP17_YU106-F02*-hFc, but only slowly dissociated, indicating a stable binding complex. The curves were fitted with the standard 1:1 Langmuir binding model (χ^2 = 0.364), which revealed a k_D value of 107 nM (*Figure 19A*).

In contrast, bio-SPAG9A1A2 association to αSPAG9_VD1.E6*-hFc was very fast as well as the subsequent dissociation as indicated by sharp increase and decrease of the response difference (*Figure 19B*). Peptide-antibody interactions are known to commonly form less stable complexes, which is also the case in our SPR measurement using the bio-SPAG9A1A2 peptide [204,205]. As the 1:1 Langmuir model includes the association and dissociation phases for the calculation of the k_D value, this model was inappropriate. Instead, we fitted the sensorgram with the steady state affinity model that only included the equilibrium phase (χ^2 = 0.014), revealing a k_D value of >7960 nM. However, this value can only be regarded as estimation, because no full saturation was reached using the highest tested analyte concentration of 8000 nM. To determine a reliable k_D value, a full-length SPAG9 protein is needed to be used as analyte.

3.3 Characterization of SP17 and SPAG9 specific CAR T cells *in vitro*

In order to generate CTA specific chimeric antigen receptors (CARs), we fused the lead candidate scFvs αSP17_YU106-F02* and αSPAG9_VD1.E6* (shortened to αSP17 and αSPAG9 in the following) as antigen binding domains to three second (2^{nd}) generation and two third (3^{rd}) generation CAR backbones by molecular cloning. A schematic representation of the resulting CAR constructs is shown in *Figure 20*.

The CAR coding sequences were cloned into the entry clone pENTR, which was used to transfer the CAR gene into the destination vector pRRL by gateway cloning. The CAR containing pRRL plasmid was then used to co-transfect HEK293T cells together with two lentiviral helper plasmids to generate lentiviral vectors for T cell transduction.

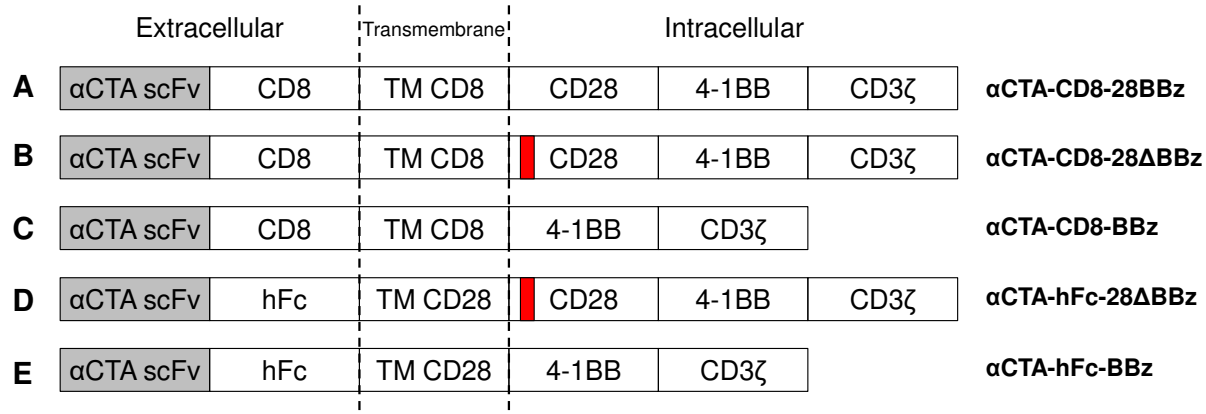

Figure 20. Schematic representation of αCTA CAR constructs. αSP17_YU106-F02* and αSPAG9_VD1.E6* scFvs were fused to the CAR backbones **(A)** CD8-28BBz, **(B)** CD8-28ΔBBz, **(C)** CD8-BBz, **(D)** hFc-28ΔBBz and **(E)** hFc-BBz by overlap extension PCR. 3rd generation CAR backbones **(A, B, D)** contained CD28 and 4-1BB (CD137) costimulatory domains, while 2nd generation CAR backbones **(C, E)** contained only 4-1BB as costimulatory domain. Two 3rd generation CAR backbones **(B, D)** contained a mutated CD28 signaling tail (represented as red line) incapable to bind to Lck and thereby abrogating IL-2 secretion. The mutations included within this 28Δ domain were P560A, P563A, P564A [78]. TM = transmembrane section.

3.3.1 Expression of αSP17 and αSPAG9 CARs in primary human T cells

To obtain primary human T cells for lentiviral transduction, we isolated human PBMCs from fresh blood or buffy coats derived from healthy donors by Ficoll density gradient centrifugation. T cells among $2x10^7$ freshly isolated or thawed PBMCs were specifically activated in adapted medium for 60 h using a colloidal polymeric nanomatrix conjugated to CD3 and CD28 agonists (T Cell TransAct), while cell types other than T cells do not survive the *ex vivo* cultivation.

We transduced activated T cells with lentiviral vectors in order to express the CAR constructs and included a mock transduction control without lentiviral vector. We monitored T cell expansion and CAR expression over a period of up to 19 days after initial T cell activation (*Figure 21*).

Throughout *ex vivo* cultivation, all CAR T cells efficiently expanded up to 80-fold, which is comparable to the expansion of other CAR T cells that were described previously [206,207]. T cells expressing 3rd generation CARs tended to expand more efficiently than the 2nd generation counterparts. Similarly, da Silva *et al*. found that T cells expressing a 3rd generation CAR, which included CD28 and 4-1BB, showed 23-fold higher expansion *in vivo* compared to those expressing a 2nd generation CAR, which only included CD28, most probably due to additional costimulation [208]. The expansion of non-transduced mock T

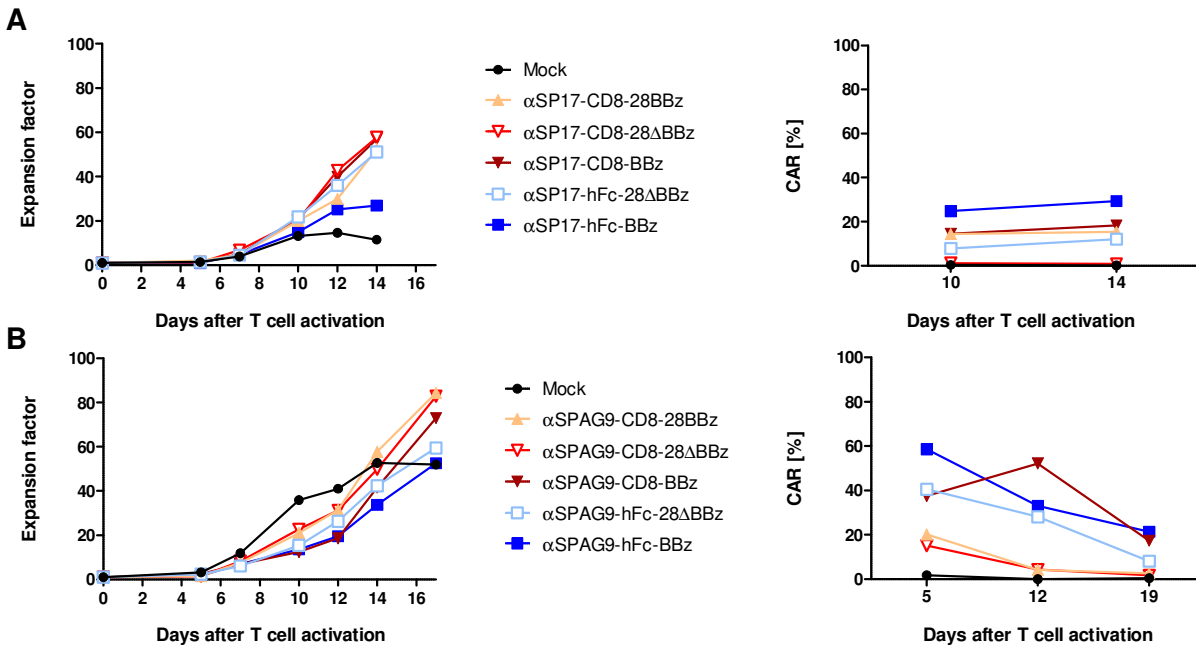

Figure 21. αSP17 and αSPAG9 CAR T cell expansion and CAR expression *ex vivo*. T cells expressing αSP17 CARs were derived from a different donor than those expressing αSPAG9 CARs. After activation and lentiviral transduction, T cells were cultured in X-VIVO15 (+ 5% FCS, 10 ng/mL IL-7 and IL-15). Expansion and CAR expression were monitored **(A)** up to 14 days for αSP17 and **(B)** up to 19 days for αSPAG9 CAR T cells. Mock and CAR T cell expansion was calculated as expansion factor relative to the initial amount of T cells. CAR expression was measured by flow cytometry using mFc-SP17 labeled with APC (αSP17 CARs) or biotinylated protein L combined with APC coupled streptavidin (αSPAG9 CARs).

cells stagnated after approximately day 10-12 post T cell activation, similar to a previous report, in which expansion was monitored [206].

We found successful surface expression of all CAR constructs except for αSP17-CD8-28ΔBBz. However, we observed considerable differences concerning transduction efficiencies and CAR expression stability over time. Transduction efficiencies tended to be higher for T cells expressing 2nd generation CARs compared to those expression 3rd generation CARs (34% vs. 20%, mean values) and expression of 2nd generation CARs seemed to be more stable over time. Higher transduction efficiencies for 2nd generation CARs compared to 3rd generation CARs were also observed in other studies [209]. As increased CAR expression was found to induce antigen independent T cell exhaustion, we next investigated if our CAR T cells were indeed affected by exhaustion [80].

3.3.2 T cells expressing 2nd generation αSP17 and αSPAG9 CARs show no signs of exhaustion during *ex vivo* expansion

T cell exhaustion results from antigen independent constitutive signaling upon CAR clustering and limits the efficacy of CAR T cells. Increased surface expression of CARs drives constitutive signaling and further promotes CAR clustering [80,206]. To analyze if our CAR T cells were affected by exhaustion, we monitored surface expression of the activation marker CD25 and the exhaustion markers PD-1, TIM-3 and LAG-3 by flow cytometry. We gated CAR positive T cells according to *Figure 22*.

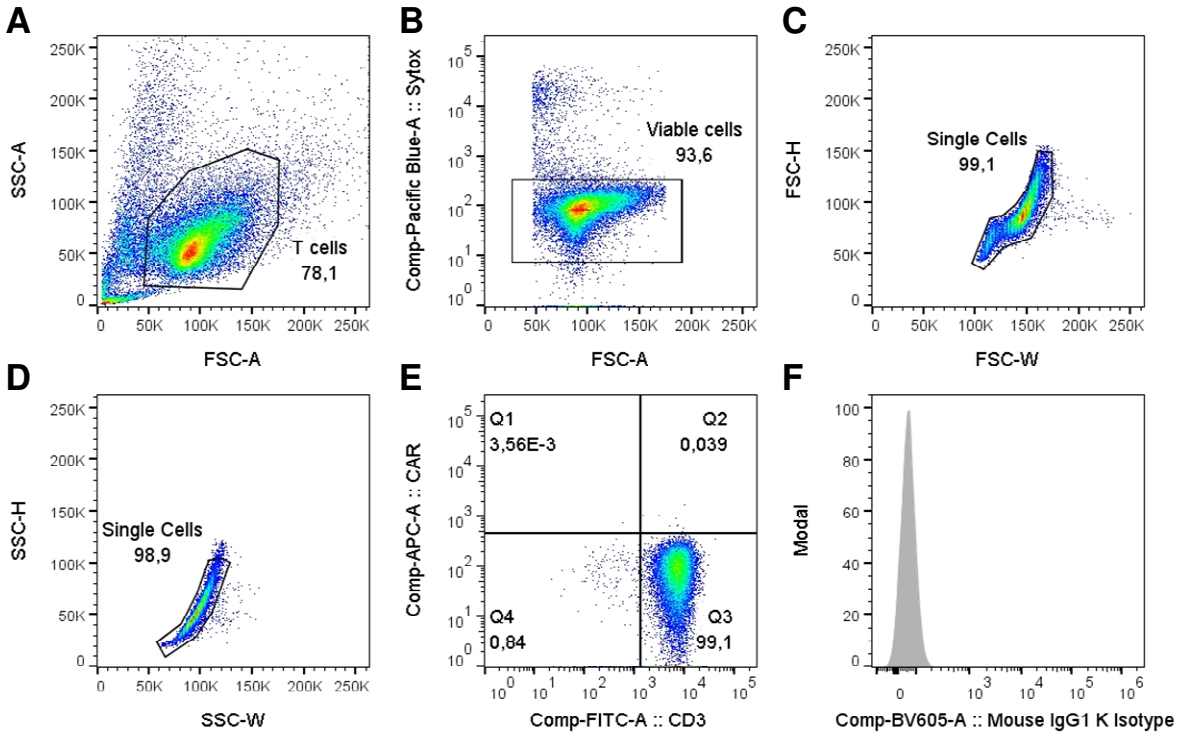

Figure 22. Gating strategy for T cell activation and exhaustion marker analysis by flow cytometry. (A) T cells were gated according to size and granularity by sideward and forward scatter. **(B)** Viable cells were negative for SYTOX Blue dead cell stain. **(C, D)** Doublets were excluded via forward and sideward scatter by plotting height against width. **(E)** Mock T cells (shown here) were used to set the threshold for CAR positivity. CAR positive T cells were found in Q2. **(F)** Histogram plots with the detected markers of interest were created.

A bar graph overview of the activation and exhaustion marker expression profile of αSP17 and αSPAG9 CAR T cells during *ex vivo* expansion is shown in *Figure 23*, for corresponding histogram plots see *Appendix* (*Figure 36 – Figure 40*). T cell activation and exhaustion levels were not well distinguishable up to day 12 after initial T cell activation, but from day 14, T cells expressing 2nd generation αSP17 CARs showed decreased CD25, TIM-3 and LAG-3

levels (*Figure 23A*). In contrast, T cells expressing 3rd generation αSP17 CARs showed increased CD25, TIM-3 and LAG-3 levels, which may indicate constitutive CAR signaling. Surprisingly, on day 19, T cells expressing 2nd generation αSPAG9 CARs showed increased CD25, but low PD-1 and TIM-3, and decreased LAG-3 levels compared with those expressing the 3rd generation CARs (*Figure 23B*). This might indicate that 2nd generation αSPAG9 CARs induce constitutive signaling, but not T cell exhaustion.

In summary, T cells expressing 2nd generation CARs not always showed lowest expression of the activation marker CD25 throughout *ex vivo* expansion, but always had the lowest combined expression of the exhaustion markers TIM-3 and LAG-3 among all tested CARs, indicating that they were not affected by exhaustion. In contrast, although T cells expressing 3rd generation CARs showed elevated levels of TIM-3 and LAG-3, no expression of PD-1 could be detected in long-term cultures, implying that T cell exhaustion is not induced by the incorporated αCTA scFv domains.

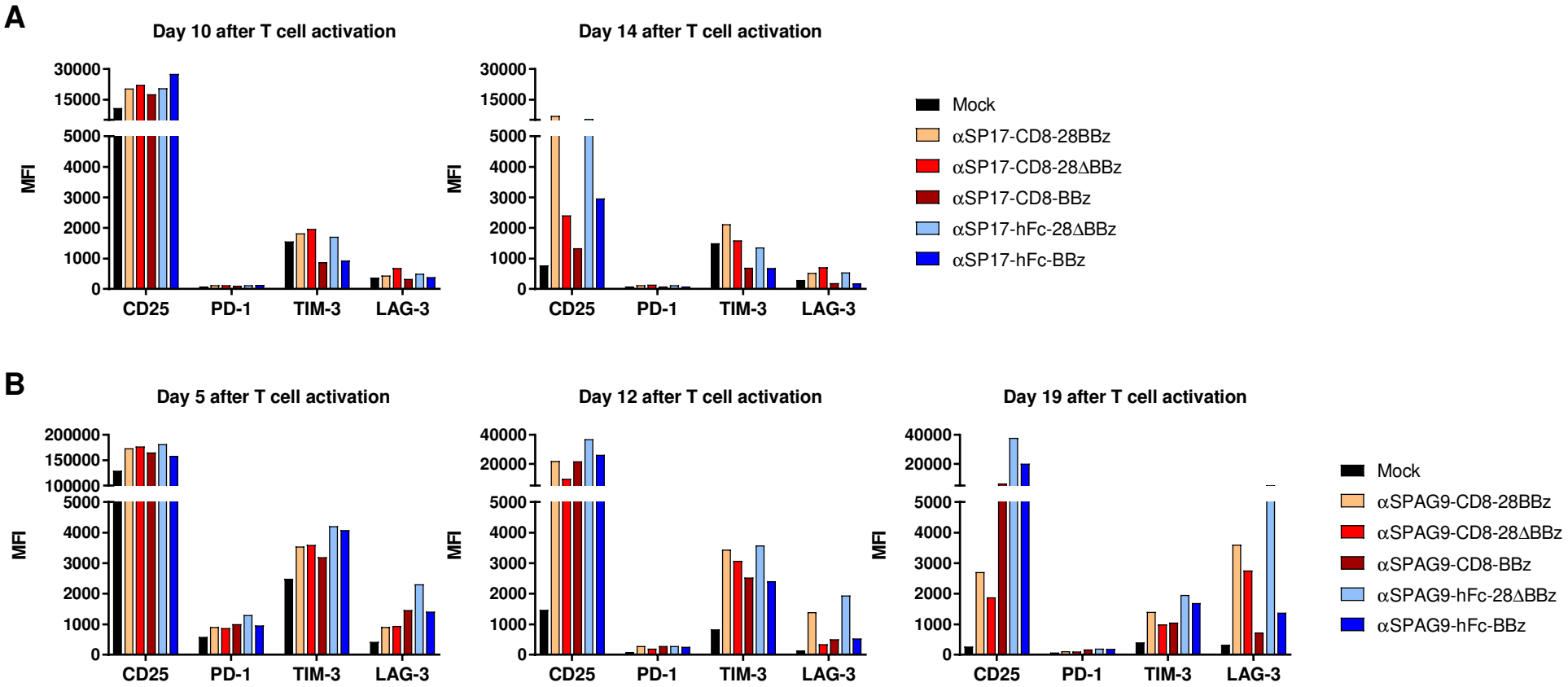

Figure 23. Activation and exhaustion marker expression profile of αSP17 and αSPAG9 CAR T cells throughout *ex vivo* cultivation. CAR T cells were analyzed by flow cytometry and gated according to *Figure 22*. Median fluorescence intensity (MFI) values representing expression of the activation marker CD25 and the exhaustion markers PD-1, TIM-3 and LAG-3 are summarized for **(A)** αSP17 and **(B)** αSPAG9 CAR T cells. αSP17 CAR T cells were monitored at day 10 and 14, αSPAG9 CAR T cells at day 5, 12 and 19 after initial T cell activation.

3.3.3 CD8$^+$ T cells expressing 2nd generation αSP17 and αSPAG9 CARs preferentially differentiate toward the central memory subset

In various studies, prolonged persistence of CAR T cells was shown to be crucial for therapeutic efficacy due to more stable and enduring antitumor responses [103]. In this regard, the less differentiated stem cell memory (Tscm) and central memory (Tcm) T cells were considered to be more beneficial for therapeutic use compared with the more differentiated effector memory (Tem) and effector (Teff) T cells. Tscm and Tcm cells possess a longer lifespan and are able to develop an immunological memory which might prevent tumor recurrence [97-99]. These individual T cell subsets have distinct expression profiles of the surface markers CCR7, CD45RO and CD95. An according gating strategy (*Figure 24*) allows the phenotypical determination of naïve T (Tn, CCR7$^+$/CD45RO$^-$/CD95$^-$), Tscm (CCR7$^+$/CD45RO$^-$/CD95$^+$), Tcm (CCR7$^+$/CD45RO$^+$/CD95$^+$), Tem (CCR7$^-$/CD45RO$^+$/ CD95$^+$) and Teff (CR7$^-$/CD45RO$^-$/CD95$^+$) cells by flow cytometry [97].

We investigated T cell subsets of our CD8$^+$ CAR T cells at day 10 after initial activation as described above (*Figure 25*). Compared to non-activated PBMCs, Tn and Tscm subsets were largely absent among CAR T cells, most probably due to progressive differentiation caused by initial activation via CD3/CD28 agonistic beads and *ex vivo* cultivation with IL-7 and IL-15 [210]. The Teff cell population was always less than 5%. As we showed in the previous section (*3.3.2*) that T cell activation levels were high up to day 12, it is possible that terminally differentiated Teff cells were lost due to activation induced cell death [211]. T cells expressing 2nd generation CARs predominantly showed the Tcm phenotype (51-66%, mean value 60%), while those expressing 3rd generation CARs tended to be mainly Tem cells (34-80%, mean value 63%). These findings are consistent with a report that showed 4-1BB costimulation to drive T cells toward the Tcm phenotype, while CD28 costimulation yielded high proportions of Tem cells [76]. Furthermore, we demonstrated above that T cells expressing 3rd generation CARs showed elevated levels of the exhaustion markers TIM-3 and LAG-3 (*3.3.2*), which was described to share phenotypic characteristics with effector T cells [212].

Considering superior CAR expression stability (*3.3.1*), no indication of exhaustion (*3.3.2*), and the preferential differentiation toward the Tcm subset, we selected the 2nd generation CAR constructs for further studies in a second T cell donor.

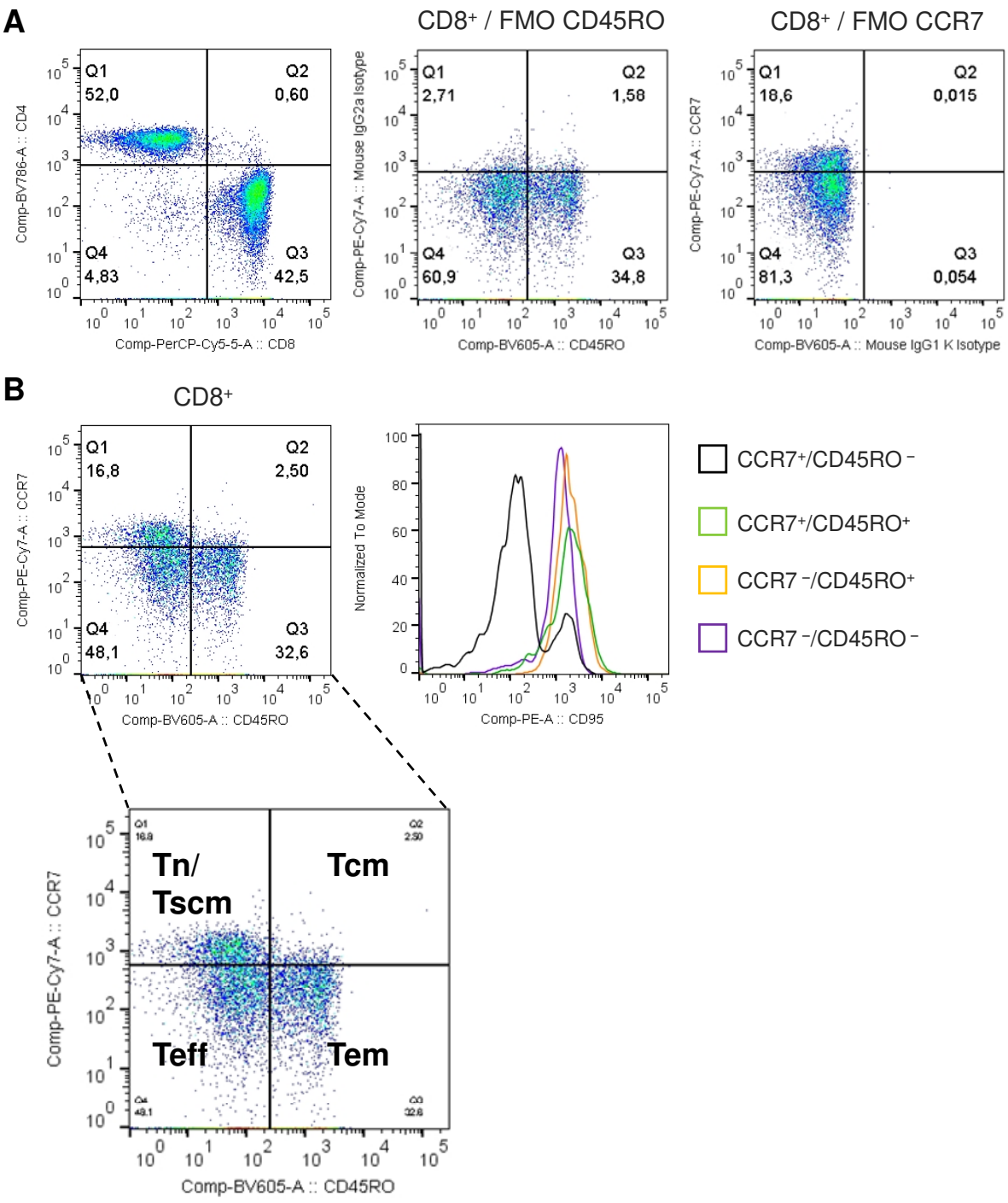

Figure 24. Gating strategy to analyze T cell subsets by flow cytometry. CAR T cells were gated according to *Figure 22*. Gating strategy for T cell subset analysis is exemplarily shown for PBMCs. **(A)** $CD4^+$ and $CD8^+$ positive T cell populations were separated and $CD8^+$ T cells were monitored for CCR7 and CD45RO expression according to CD45RO and CCR7 Fluorescence Minus One (FMO) control stainings. **(B)** T cell subsets were identified by the differential surface expression of CCR7, CD45RO and CD95. Subsets were classified as naïve (Tn, $CCR7^+/CD45RO^-/CD95^-$), stem cell memory (Tscm, $CCR7^+/CD45RO^-/CD95^+$), central memory (Tcm, $CCR7^+/CD45RO^+/CD95^+$), effector memory (Tem, $CCR7^-/CD45RO^+/CD95^+$) or effector (Teff, $CCR7^-/CD45RO^-/CD95^+$) T cells.

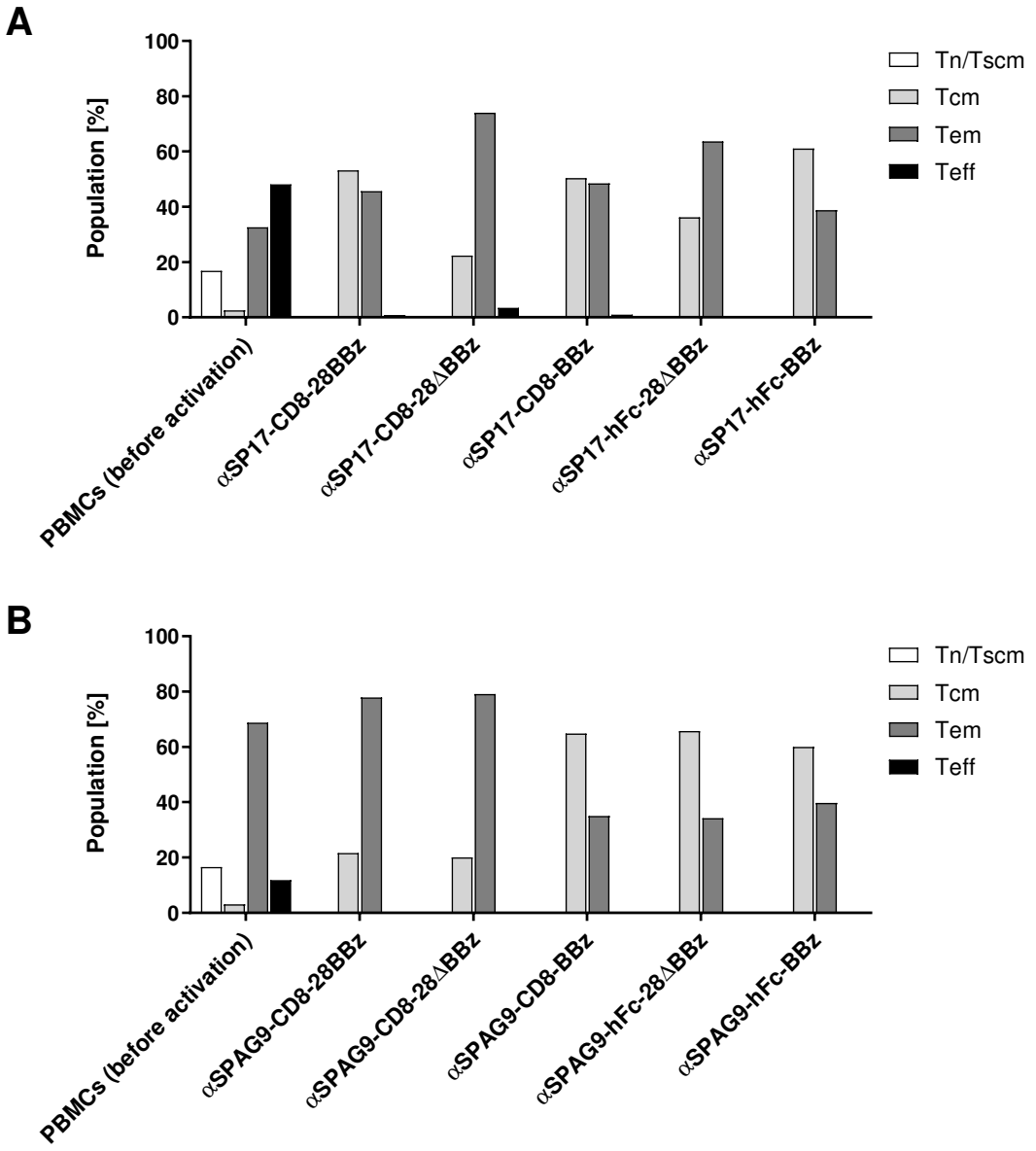

Figure 25. Subset analysis of CD8$^+$ αSP17 and αSPAG9 CAR T cells. T cell subsets were immunophenotyped for CD8$^+$ **(A)** αSP17 and **(B)** αSPAG9 CAR T cells at day 10 after initial activation and analyzed by flow cytometry. CAR T cells were gated according to *Figure 24.* Distinct subsets were naïve/stem cell memory (Tn/Tscm), central memory (Tcm), effector memory (Tem) and effector (Teff) T cells. CD8$^+$ T cells from PBMCs before activation were screened as control.

3.3.4 Characteristics of T cells expressing 2nd generation αSP17 and αSPAG9 CARs in a second donor

To confirm our data on 2nd generation CAR constructs, we transduced activated T cells from a second donor with lentiviral vectors carrying DNA that encoded for the αSP17 and αSPAG9 CARs. We monitored T cell expansion and CAR expression over a period of 17 days after initial T cell activation (*Figure 26*).

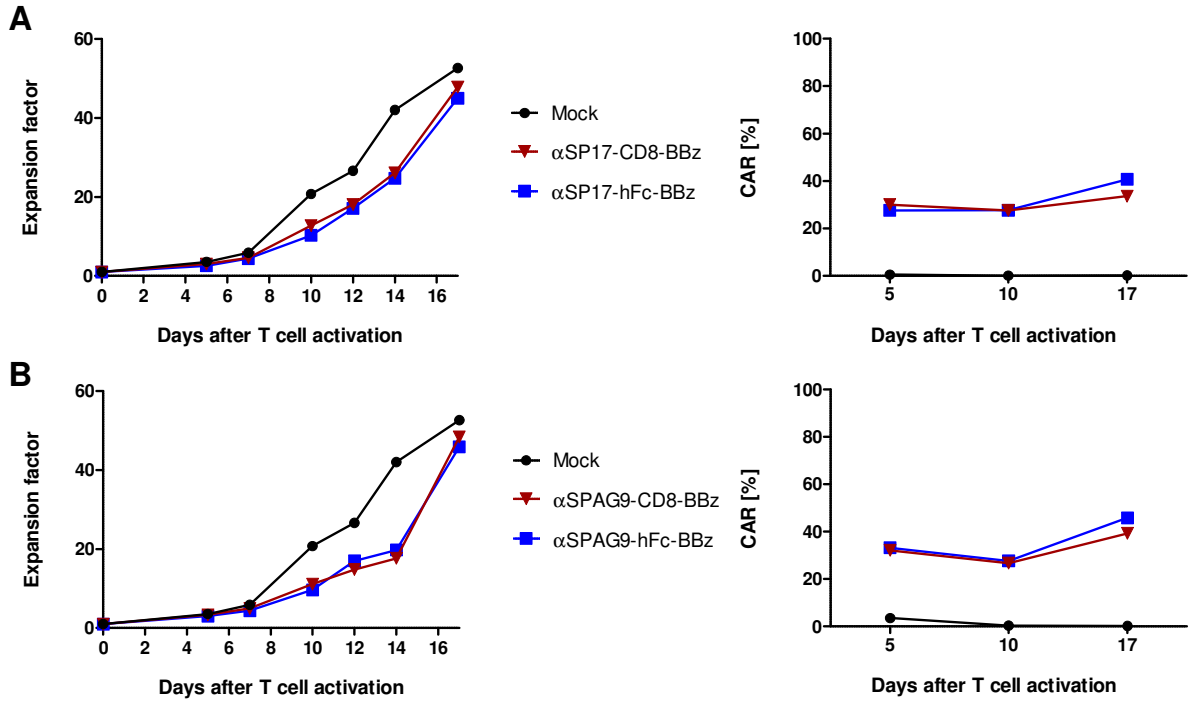

Figure 26. αSP17 and αSPAG9 CAR T cell expansion and CAR expression *ex vivo*. All T cells were derived from the same donor. After activation and lentiviral transduction, T cells were cultured in X-VIVO15 (+ 5% FCS, 10 ng/mL IL-7 and IL-15). Expansion and CAR expression were monitored up to 17 days for T cells expressing 2nd generation **(A)** αSP17 and **(B)** αSPAG9 CARs. Mock and CAR T cell expansion was calculated as expansion factor relative to the initial amount of T cells. CAR expression was measured by flow cytometry using mFc-SP17 labeled with APC (αSP17 CARs) or biotinylated protein L combined with APC coupled streptavidin (αSPAG9 CARs).

Throughout *ex vivo* cultivation, T cells expressing 2nd generation αSP17 and αSPAG9 CARs efficiently expanded up to 50-fold which is comparable with the first donor that we analyzed (*3.3.1*). In contrast to the first donor, the expansion of non-transduced mock T cells did not stagnate after day 10. CAR constructs were successfully expressed on the surface with expression rates ranging from 30-45%. CAR expression remained stable or even slightly increased during *ex vivo* culturing.

We analyzed T cell exhaustion as before (*3.3.2*) and summarized the activation and

exhaustion marker expression profile of αSP17 and αSPAG9 CAR T cells in a bar graph overview (*Figure 27*). For corresponding histogram plots see *Appendix* (*Figure 41* and *Figure 42*). T cell activation and exhaustion levels were not well distinguishable until day 10 after initial T cell activation. On day 17, αSP17 CAR T cells showed up to two-fold higher CD25 expression compared with mock T cells, but similar levels of PD-1 and TIM-3 and only slightly higher levels of LAG-3 (*Figure 27A*). Similarly, activation and exhaustion levels of αSPAG9 CAR T cells were almost equal compared with mock T cells. All T cells were PD-1 negative when older than 10 days. These findings suggest that our 2nd generation CAR constructs indeed do not induce constitutive signaling and T cell exhaustion.

We investigated T cell subset phenotypes at day 10 after activation as described in *3.3.3*. As observed previously, Tn, Tscm and Teff subsets were not present among CD8^{+} αSP17 and αSPAG9 CAR T cells (*Figure 28*). Instead, CAR T cells contained large fractions of Tcm cells (65-92%), confirming the preferential differentiation toward this phenotype also in a second donor.

As we found consistent characteristics of our 2nd generation CAR constructs for transduced T cells derived from two individual donors, we continued to study these constructs in functional assays.

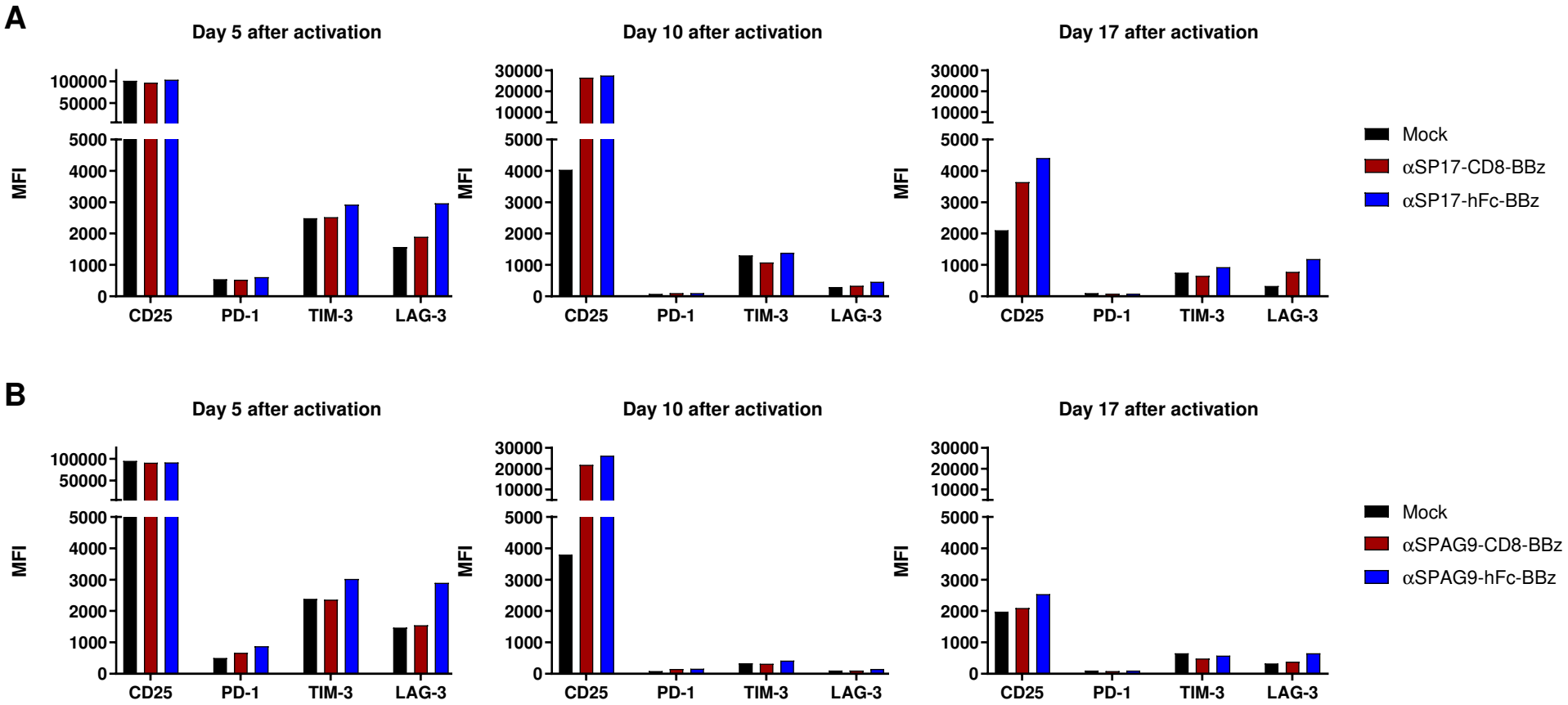

Figure 27. Activation and exhaustion marker expression profile of T cells expressing 2nd generation αSP17 and αSPAG9 CARs throughout *ex vivo* cultivation. CAR T cells were analyzed by flow cytometry and gated according to *Figure 22*. Median fluorescence intensity (MFI) values representing expression of the activation marker CD25 and the exhaustion markers PD-1, TIM-3 and LAG-3 are summarized for **(A)** αSP17 and **(B)** αSPAG9 CAR T cells. CAR T cells were monitored at day 5, 10 and 17 after initial T cell activation.

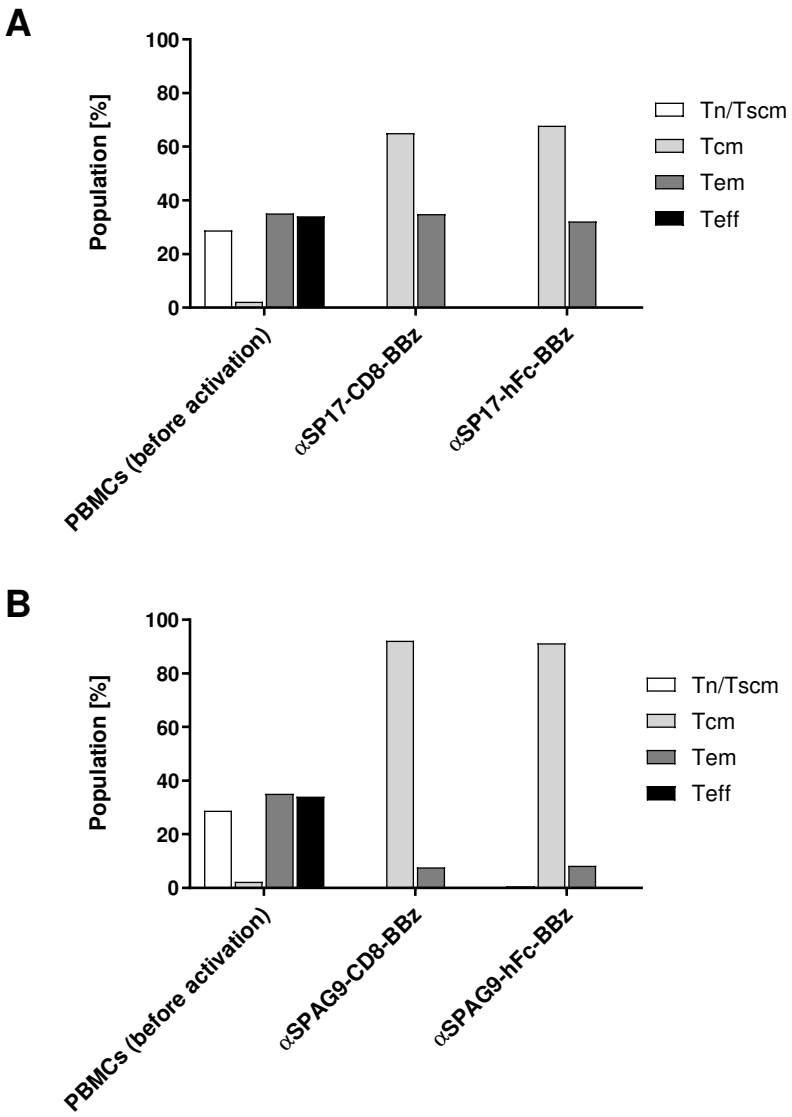

Figure 28. Subset analysis of CD8$^+$ T cells expressing 2nd generation αSP17 and αSPAG9 CARs. T cell subsets were immunophenotyped for CD8$^+$ **(A)** αSP17 and **(B)** αSPAG9 CAR T cells at day 10 after initial activation and analyzed by flow cytometry. CAR T cells were gated according to *Figure 24.* Distinct subsets were naïve/stem cell memory (Tn/Tscm), central memory (Tcm), effector memory (Tem) and effector (Teff) T cells. CD8$^+$ T cells from PBMCs before activation were screened as control.

3.3.5 αSP17 and αSPAG9 CAR T cells are specifically activated upon stimulation by target antigen and target tumor cells

To test specific functionality of our 2nd generation CAR constructs, we measured CAR T cell activation and proliferation upon stimulation with immobilized target antigen and/or co-incubation with the target antigen positive tumor cell lines SKOV-3 and H929. We chose both as target cell lines, as we previously observed that the clones αSP17_YU106-F02* and αSPAG9_VD1.E6* showed a bright staining of these cell lines in the scFv-hFc format (*3.2.3* and [193]). We analyzed activation by monitoring the surface expression of the activation markers CD25 and CD69, and of the exhaustion marker PD-1 which are upregulated on activated T cells [213,214]. To track proliferation, we labeled mock and CAR T cells with the fluorescent dye CFSE, which is diluted upon cell division. Activation and proliferation were investigated by flow cytometry.

Upon stimulation with the immobilized cognate antigen, we observed a combined increase of CD25, CD69 and PD-1 expression on αSP17 and αSPAG9 CAR T cells (*Figure 29*). Compared to unstimulated CAR T cells, CD25, CD69 and PD-1 levels were increased up to 306-fold. In contrast, mock T cells co-incubated with or without immobilized antigens did not upregulate CD25, CD69 or PD-1 expression, indicating a specific activation of the CAR T cells by their cognate antigen.

When monitoring proliferation, we observed an equal basal proliferation of mock and CAR T cells as indicated by CFSE dilution, despite neither adding FCS nor IL-7/IL-15 to the X-VIVO15 medium (*Appendix*, *Figure 43*, unstimulated). As X-VIVO15 is an optimized growth medium for lymphocytes derived from blood, it is most likely that using this medium for cultivation of T cells is sufficient to induce proliferation. Importantly, upon co-incubation with immobilized target antigen (*Appendix*, *Figure 43*) and target antigen positive SKOV-3 or H929 cells (*Figure 30*), we observed increased proliferation of the CAR T cells compared with that of mock T cells. Interestingly, we found that T cells expressing hFc spacer CARs proliferated more efficiently than those expressing CD8 spacer CARs, although previously activation levels among αSP17 or αSPAG9 CAR T cells did not show considerable differences after stimulation with immobilized target antigen (*Figure 29*). This effect became even more apparent when we quantified T cell populations according to number of cell divisions after co-incubation with SKOV-3 or H929 cells (*Figure 30B*). T cells expressing hFc spacer CARs contained approximately twice the amount of the subpopulation that showed more than three cell divisions compared with those expressing CD8 spacer CARs.

In summary, αSP17 and αSPAG9 CAR T cells were specifically activated by their cognate antigen and showed an increased proliferative capacity upon co-incubation with the target antigen and target tumor cells.

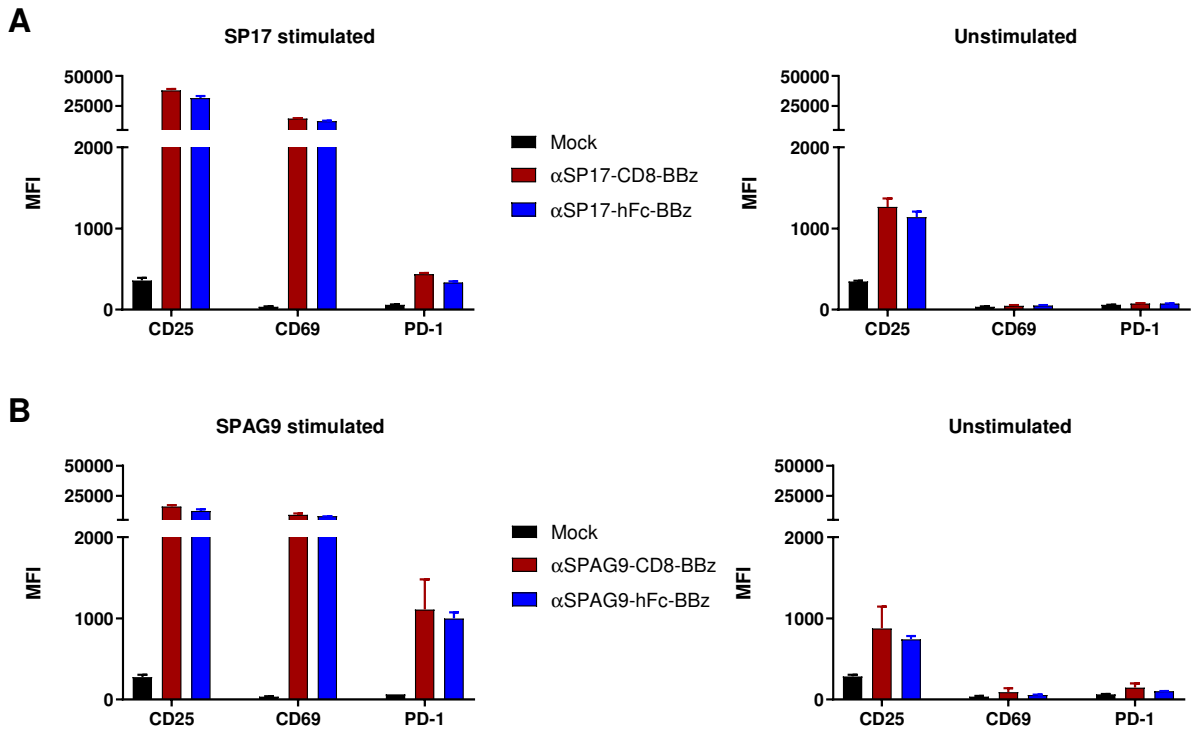

Figure 29. Activation marker expression profile of αSP17 and αSPAG9 CAR T cells upon stimulation with target antigen. 24-well non-treated cell culture plates were coated with 2 µg/mL of SP17-mFc or bio-SPAG9A1A2. Bio-SPAG9A1A2 was indirectly coated via bio-BSA (3 µg/mL) and streptavidin (10 µg/mL). Coated wells were co-incubated with $5x10^5$/well mock or CAR T cells for 40 h and compared to T cells co-incubated with control wells that did not contain immobilized target antigen. After incubation, expression of the activation markers CD25 and CD69, and of the exhaustion marker PD-1 was analyzed by flow cytometry. Expression profiles are shown for T cells expressing 2nd generation **(A)** αSP17 and **(B)** αSPAG9 CARs. Error bars represent standard deviation of triplicates. MFI = Median fluorescence intensity

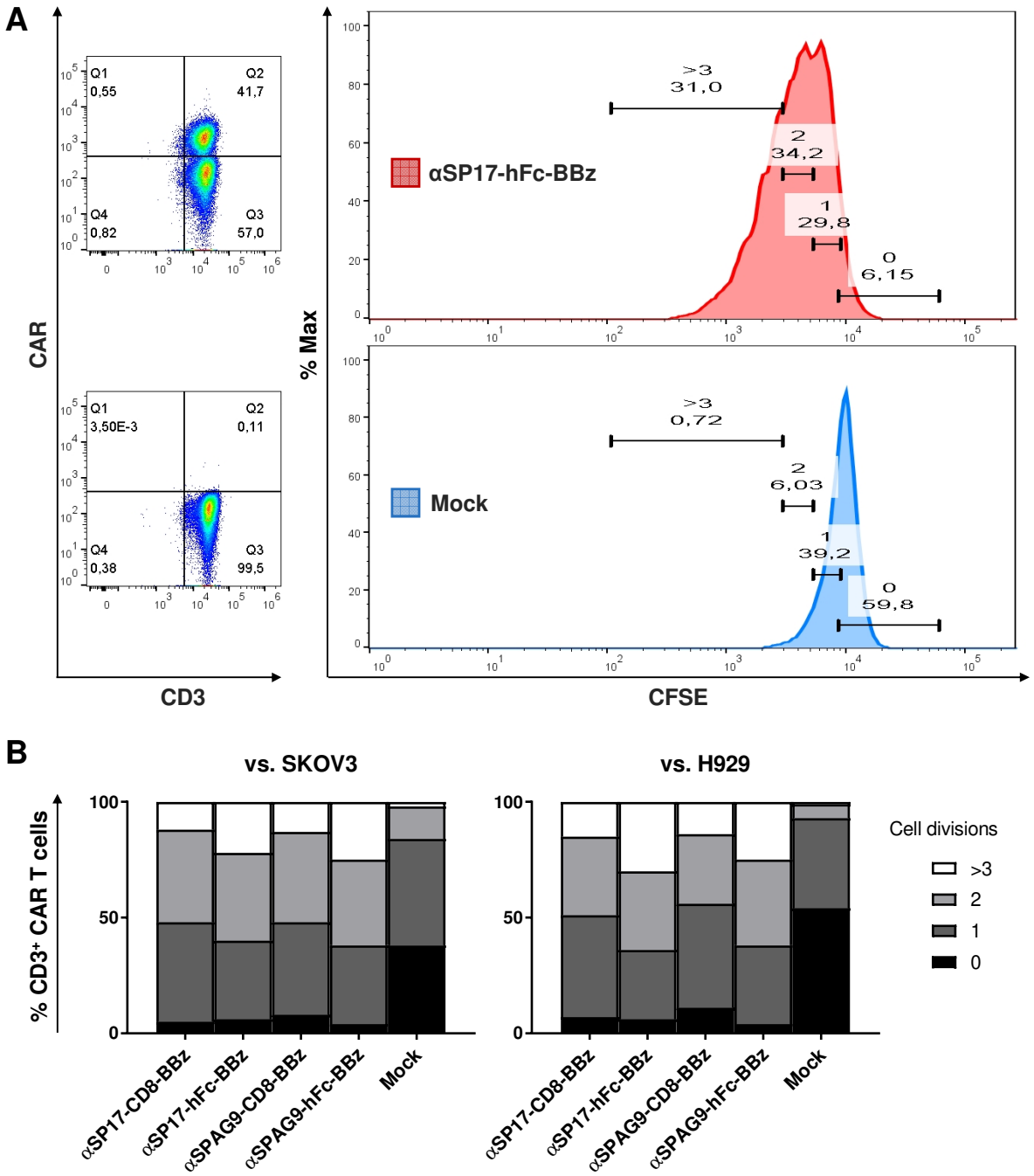

Figure 30. Proliferation monitoring of αSP17 and αSPAG9 CAR T cells upon stimulation with target antigen positive tumor cell lines. T cells were co-incubated with 5x10^4 target antigen positive SKOV-3 or H929 cells in an effector-to-target ratio of 1:1. To track proliferation, mock T cells and T cells expressing 2nd generation αSP17 and αSPAG9 CARs were labeled with fluorescent CFSE. After stimulation for 3 days, T cell proliferation was analyzed by flow cytometry according to **(A)** gating strategy exemplarily shown for αSP17-hFc-BBz CAR and mock T cells after co-incubation with H929. T cell populations were quantified according to number of cell divisions as defined by distinct peaks. **(B)** Quantification of T cell populations by number of cell divisions.

3.3.6 αSP17 and αSPAG9 CAR T cells show specific killing of target tumor cells *in vitro*

To test cytotoxicity of our αSP17 and αSPAG9 CAR T cells, target antigen expressing tumor cell lines SKOV-3 and H929 were separately co-incubated with the CAR T cells in different effector-to-target cell ratios and killing of target cancer cells was assessed by different *in vitro* cytotoxicity assays. We analyzed presence of SP17 and SPAG9 on the surface of SKOV-3 and H929 by flow cytometry on the same day we started the cytotoxicity assay and found similar staining intensities as observed previously (not shown).

By employing the xCELLigence RTCA system, a device optimized for analyzing adherent target cells such as SKOV-3, we monitored viability of the tumor cells in real time (*Figure 31*) [215,216]. The tested αSP17 and αSPAG9-hFc-BBz, but not αSPAG9-CD8-BBz CAR T cells possessed enhanced cytotoxicity toward SKOV-3 cells (*Figure 31*, red curves) compared with non-transduced mock T cells (*Figure 31*, black curves). We observed that T cells expressing hFc spacer CARs killed SKOV-3 target cells more effectively compared to those expressing CD8 spacer CARs. In this regard, αSP17-hFc-BBz CAR T cells showed the best cytotoxic capacity (*Figure 31B*).

The cytotoxicity of CAR T cells toward H929 cells was analyzed by using the LDH-Glo Cytotoxicity Assay. In this bioluminescent assay, the house keeping enzyme lactate dehydrogenase is quantified, which is released into the culture medium upon disruption of the plasma membrane caused by cytotoxic agents. Interestingly, we found that only αSP17-CD8-BBz CAR T cells induced efficient cytotoxicity (*Figure 32*).

Taken together, in first cytotoxicity assays, we identified αSP17-hFc-BBz and αSP17-CD8-BBz CARs as the most effective constructs toward SKOV-3 and H929 cells, respectively. We need to confirm these findings by analyzing T cells derived from additional donors.

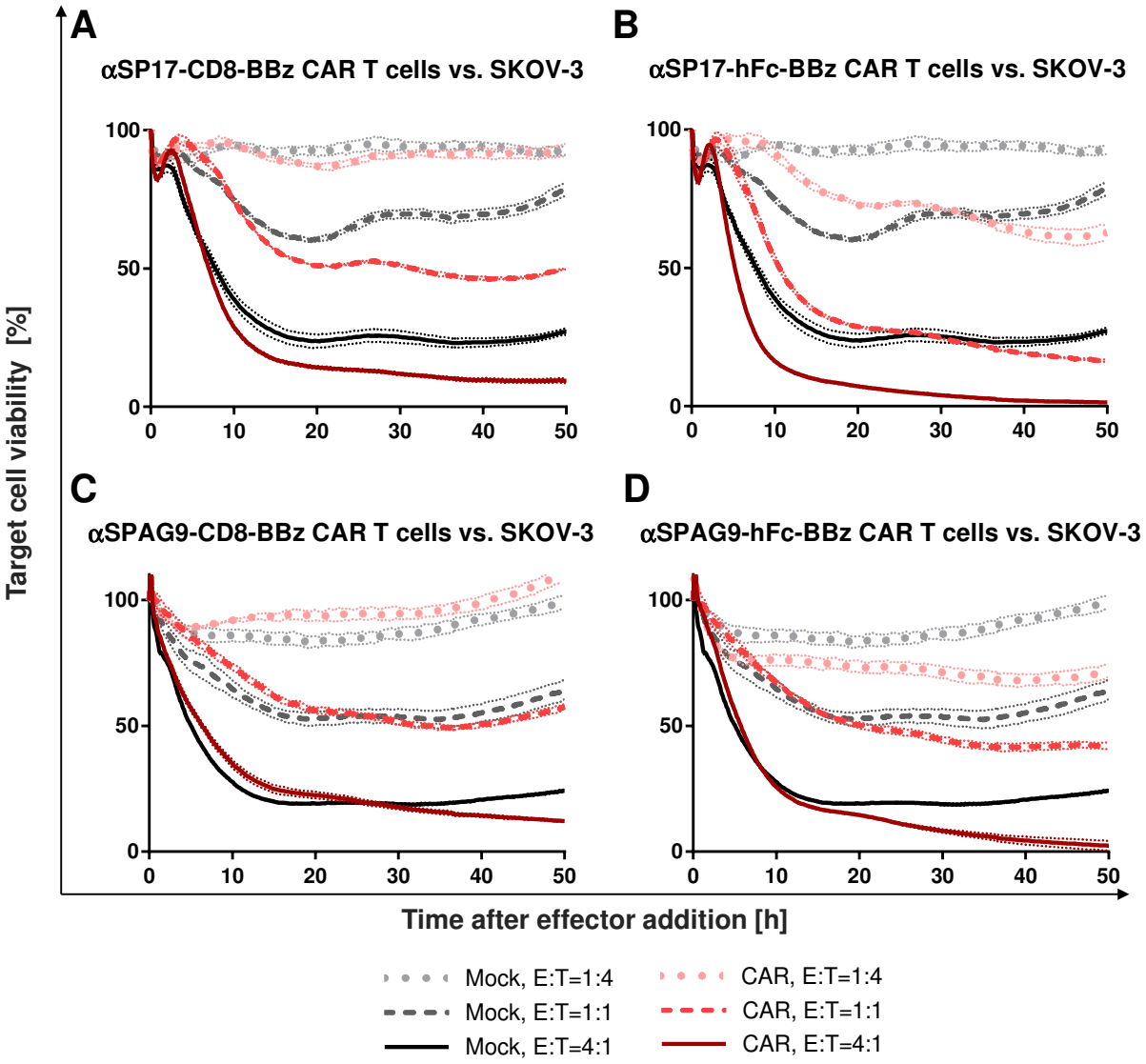

Figure 31. Real time monitoring of αSP17 and αSPAG9 CAR T cells cytotoxicity toward SKOV-3 cells. 10^4/well SKOV-3 cells were seeded in a 96-well E-plate and the adjusted amount of mock or CAR T cells was added. Mock T cells (black), **(A)** αSP17-CD8-BBz, **(B)** αSP17-hFc-BBz, **(C)** αSPAG9-CD8-BBz and **(D)** αSPAG9-hFc-BBz CAR T cells (red) were co-incubated with target antigen positive SKOV-3 cells in an effector-to-target ratio of 1:4 (light dotted line), 1:1 (dashed line) or 4:1 (dark solid line). Cells were incubated at 37 °C for 50 h. Target cell viability correlated to cell attachment on the well bottom. Data points were generated in 5 min intervals. Error dots represent the standard error of the mean of triplicates.

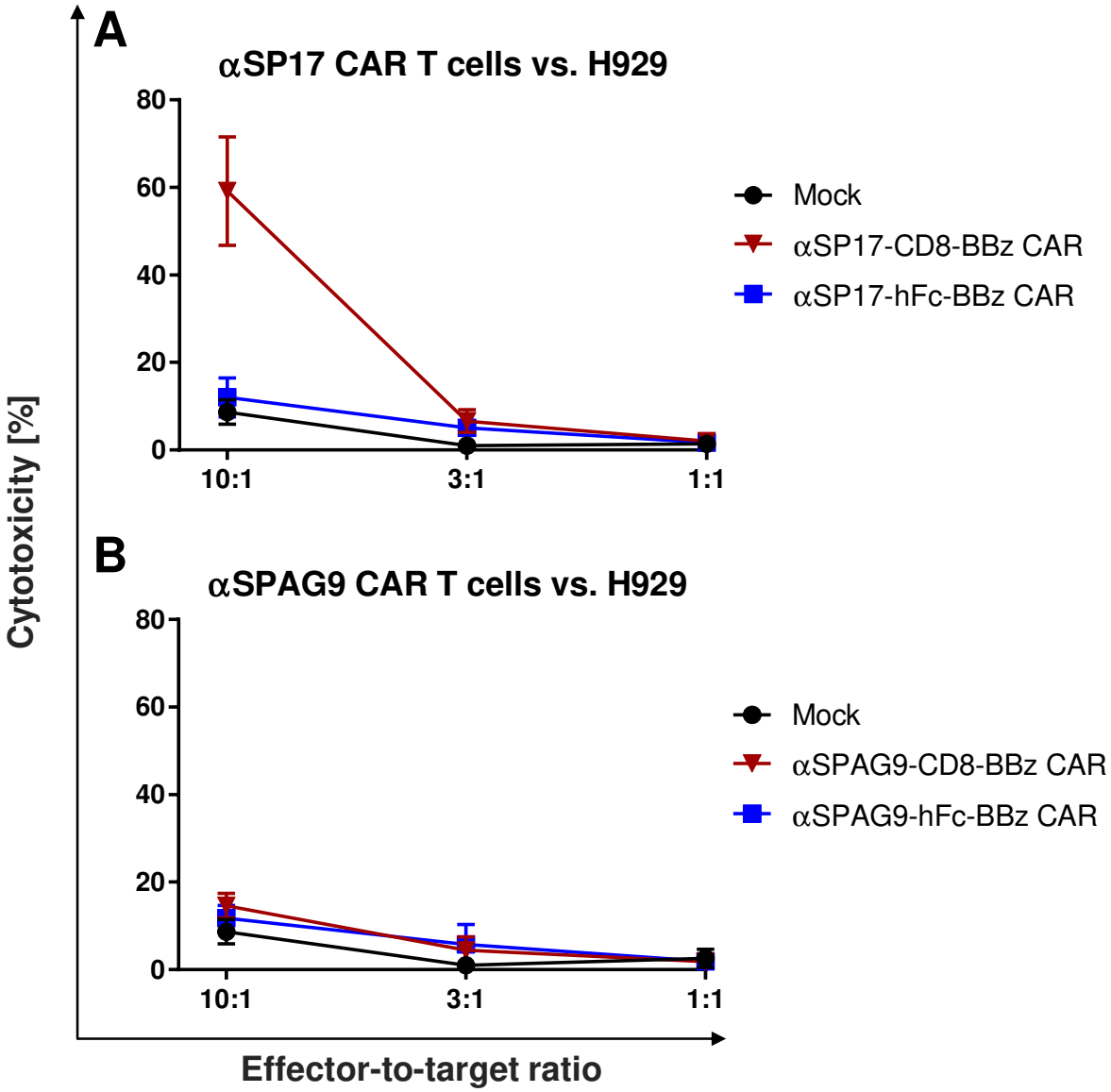

Figure 32. Cytotoxicity of αSP17 and αSPAG9 CAR T cells toward H929 cells. 10^4/well H929 cells were seeded in a 96-well plate. **(A)** αSP17 and **(B)** αSPAG9 CAR T cells were added to target antigen positive H929 cells in effector-to-target ratios of 10:1, 3:1 or 1:1. Assay was performed with the LDH-Glo Cytotoxicity Assay Kit according to the manufacturer's instructions. Cytotoxicity correlated with the amount of lactate dehydrogenase released by killed target cells. Error bars represent standard deviation of triplicates.

3.3.7 T cells stably express αSP17 and αSPAG9 CARs after a freeze and thaw cycle

For clinical translation, cryopreservation of CAR T cells is a prerequisite to allow storage until use for patient infusion [217]. At day 17 after activation, we froze $5x10^6$ CAR T cells in 1 mL freezing medium, placed the cryovial in a freezing container and stored it at -80 °C overnight, before transferring the cryovial to liquid nitrogen. After at least 24 h, CAR T cells were thawed to study cryostability.

We monitored CAR expression as well as cell viability before freezing and after thawing (*Figure 33*). T cells maintained CAR expression (35-48%) and viability (>88%) after the freeze and thaw cycle. Similar values were reported in another study using different CAR T cells, indicating that our CAR T cells were suitable for cryopreservation [218].

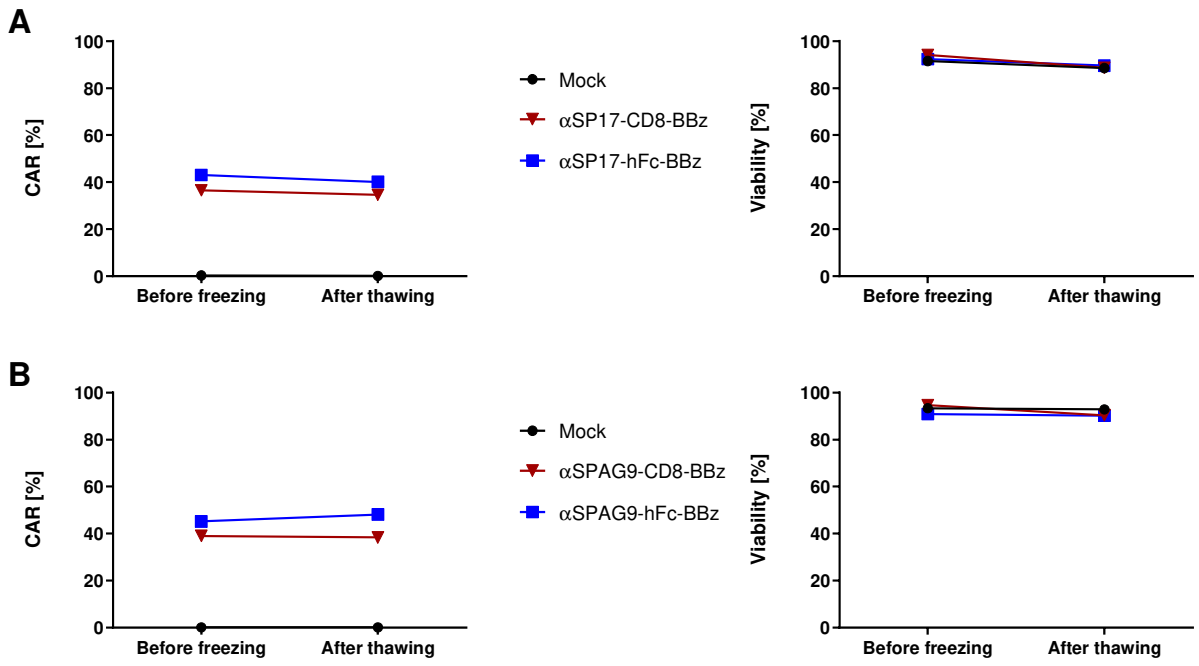

Figure 33. CAR stability and cell viability of αSP17 and αSPAG9 CAR T cells after a freeze and thaw cycle. $5x10^6$ CAR T cells expressing 2^{nd} generation **(A)** αSP17 or **(B)** αSPAG9 CARs were frozen and stored in liquid nitrogen for at least 24 h. CAR expression and cell viability were monitored by flow cytometry before and after a freeze and thaw cycle.

4 Discussion

Over the past years, the accumulated knowledge in the fields of immunology and oncology culminated into clinical strategies, in which the immune system is manipulated to combat cancer. In this field called cancer immunotherapy, several strategies evolved including the use of monoclonal antibodies or adoptive transfer of autologous immune cells. In this regard, adoptive therapy applying T cells engineered to express a chimeric antigen receptor (CAR), which actively redirects the T cells to a predefined tumor associated antigen, has attracted attention due to spectacular results when treating hematological malignancies [104,105].

However, despite its success in blood cancers, CAR T cell therapy has been less efficient for solid tumors so far. Current challenges involve insufficient tumor infiltration by CAR T cells and the immunosuppressive microenvironment within the tumor that downregulates the CAR T cell response. Furthermore, solid cancers commonly express antigens that are surface expressed on healthy tissues as well, increasing the risk of fatal on-target/off-tumor toxicities during CAR T cell therapy [109,119]. In this context, tumor associated antigens belonging to a distinct class – the so called cancer-testis antigens (CTAs) – might be highly interesting targets for novel immunotherapeutic approaches as they are exclusively expressed by germ cells in healthy individuals, but were found to be reactivated in a broad range of solid and non-solid cancer entities. Therefore, it is expected that targeting of CTAs would result in improved safety of immunotherapeutical interventions due to minimized risk of on-target/off-tumor cross-reactions with healthy tissues [128,154,219].

4.1 Selection of AKAP4, SP17 and SPAG9 specific antibody fragments to be incorporated into CARs as targeting domains

We selected the CTAs AKAP4, SP17 and SPAG9 as targets for a specific CAR T cell therapy. In their normal function, AKAP4 is mainly localized in the sperm fibrous sheath and involved in sperm motility [144], while SP17 and SPAG9 are found in the acrosomal compartment and mediate sperm-oocyte interaction during the fertilization process [159,174]. Moreover, these CTAs also function as adaptor proteins to orchestrate signal transduction pathways [158,220,221]. These characteristics might explain the benefit of reactivated CTA expression in cancers: CTAs most probably act as tumorigenic drivers for survival signaling, enhanced cell-cell contact or cell motility [129,131]. However, the underlying mechanisms are not fully understood. Interestingly, AKAP4, SP17 and SPAG9 were also described to be localized on the surface of several tumor cell lines representing colorectal [153,176,222],

ovarian [149,162,223], blood [151,163,184] and many other cancers [140,219]. Similarly, stress response proteins were shown to be aberrantly expressed on the surface of cancer cells, but not on normal cells, and were therefore suggested as targets for immunotherapy [224,225].

We evaluated AKAP4, SP17 and SPAG9 as targetable surface antigens by analyzing extracellular binding of commercially available polyclonal AKAP4, SP17 and SPAG9 specific antibodies to distinct tumor cell lines via flow cytometry. In accordance with the literature, we analyzed the cell lines Colo205 (colorectal cancer) [153], SKOV-3 (ovarian cancer) [162], H929 (multiple myeloma), MM1.S (multiple myeloma) [163] and NALM-6 (pre-B cell acute lymphoblastic leukemia) [184]. We found highest AKAP4, SP17 and SPAG9 surface expression on SKOV-3, H929 and NALM-6 cells. MM1.S cells showed high expression of AKAP4 and SPAG9, but only low expression of SP17. Colo205 cells had the lowest AKAP4 and SPAG9 expression among all tested cell lines and were negative for SP17. These results largely confirmed AKAP4, SP17 and SPAG9 surface expression patterns as indicated in the literature [153,162,163,184]. At the same time, we demonstrated simultaneous expression of multiple CTAs on the cell surface of tumor cell lines. In this regard, mRNAs coding for more than one CTA were described to be commonly expressed in a coordinated manner in cancers [128].

Next, we developed proprietary AKAP4, SP17 and SPAG9 specific antibody fragments by taking advantage of our in-house phage display antibody library LYNDAL [188]. We additionally set up a collaboration with Yumab GmbH, a service provider for customized antibody generation, that uses a naïve human antibody library (HAL9/10) for the selection of antibody fragments against theoretically any target protein by phage display [192]. For screening purposes, we generated a mammalian expression vector that contained the full-length AKAP4, SP17 or SPAG9 sequence fused to a murine Fc (mFc). We transfected HEK293-6E with this vector and purified the produced fusion proteins from cell free supernatant by protein A and size exclusion chromatography. However, only SP17-mFc was produced in amounts that were sufficient for use in phage display selection. Unfortunately, no structural information is available for AKAP4 that clearly defines intracellular, transmembrane or extracellular domains. Therefore, we decided to purchase full-length AKAP4-His. For SPAG9 we found a predictive segmentation of intracellular, transmembrane and extracellular regions. Within the extracellular section of SPAG9, three putative antigenic regions (A1, A2, A3) were described [173]. We used a biotinylated SPAG9 peptide, which was synthesized by our collaborating group headed by Prof. Dr. Walter Mier (Dept. of Pharmaceutical Chemistry, University Hospital Heidelberg), comprising the closely located putative antigenic regions A1 and A2, the intermediate sequence between A1 and A2, and flanking amino acids as spacers.

We applied the described antigens for phage display selection of fully human scFvs from our antibody library LYNDAL [188]. Previous attempts to select AKAP4 and SP17 specific scFvs from LYNDAL by phage display using microtiter plates resulted in the enrichment of unspecific clones that did not contain full-length scFv sequences, but truncated variants [193]. This issue is known among phage display experts as the “sticky” phage envelope and truncated scFvs unspecifically bind to the antigen or the coating surface, which might even repress specific binders (Prof. Dr. Stefan Duebel, personal communication) [189]. In contrast, the biotinylated SPAG9 peptide allowed a phage display procedure in solution with streptavidin coupled magnetic beads, which resulted in a predominant enrichment of full-length scFv clones in our selection experiment. When we induced 90 *E. coli* TG1 clones infected with phages from selection round 3 to produce soluble scFvs, we identified 28 SPAG9 specific clones by ELISA, out of which 19 contained full-length sequences as determined by colony PCR. Sequence analysis of these 19 scFv clones revealed 6 intact clones, while the remaining 13 mostly contained multiple stop codons within the scFv sequence that affected the open reading frame. Surprisingly, the 6 intact clones were identical in their sequence, indicating a robustly selected SPAG9 specific scFv (referred to as αSPAG9_VD1.E6).

Yumab GmbH performed phage display selections against AKAP4-His, SP17-mFc and the biotinylated SPAG9 peptide using the naïve antibody library HAL9/10 and provided us with distinct scFv clones [192]. We chose two AKAP4, five SP17 and six SPAG9 specific scFvs according to best overall binding signal and signal-to-noise ratio, as determined by ELISA, to proceed with further characterization. Sequence comparison between the αSPAG9_VD1.E6 scFv selected from LYNDAL and scFvs selected from HAL9/10 revealed the highest number of somatic hypermutations within the variable regions, including CDRs, of the αSPAG9_VD1.E6 scFv upon alignment with the closest germline sequence. When we compared scFvs with other specificities selected from LYNDAL with those selected from HAL9/10, we also found that scFv sequences derived from HAL9/10 were closer to the germline sequence than those derived from LYNDAL (not shown). In fact, this is expected as LYNDAL contains IgG V_H and V_L repertoires derived from B cells of tumor draining lymph nodes of head and neck cancer patients which potentially encountered tumor associated antigens and are thus antigen experienced [188]. In contrast, HAL9/10 was built using IgM V_H and V_L repertoires that were amplified from circulating naïve B cells of healthy donors which were predominantly antigen inexperienced [192]. Cellular and humoral immune responses induced by CTA were reported in tumor patients – including head and neck cancer patients – increasing the probability for successful selection of CTA specific antibody fragments from LYNDAL [185,226]. Thus, the B cells from tumor draining lymph nodes might have generated a specific, affinity maturated response against CTAs that could be reflected

in accumulated somatic hypermutations within variable regions and CDRs, and high affinities toward their cognate antigen. This would explain increased rates of somatic hypermutations in LYNDAL derived scFv sequences compared to the near-germline sequences in HAL9/10 derived scFvs [227].

To evaluate the selected AKAP4, SP17 and SPAG9 specific scFv candidates for use as targeting domains in CARs or other immunotherapeutical approaches, we genetically fused the scFvs to a hFc portion and produced soluble scFv-hFc fusion proteins in HEK293-6E cells. Due to structural similarity to a membrane anchored CAR, we considered these scFv-hFc fusion proteins as “soluble CARs”. After producing the scFv-hFc molecules in HEK293-6E cells, we successfully purified them by protein A chromatography and confirmed correct molecular size by Coomassie Blue staining, western blot and SEC. We observed high purities of >90% in SEC. In ELISA experiments using coated purified target proteins, all scFv-hFc molecules specifically bound to their cognate antigen and not to tested control proteins. αAKAP4_YU138-C01-hFc bound its cognate target AKAP4-His, but also to SP17-His. Since both proteins have an N-terminal His tag in common, αAKAP4_YU138-C01-hFc might recognize the His tag. Alternatively, it may bind to SP17, which we believed to be unlikely due to very low sequence homology between AKAP4 and SP17.

When testing the scFv-hFc fusion proteins for surface staining of the previously analyzed tumor cell lines, we found that both αAKAP4 scFv-hFc molecules showed only very weak or no staining of tumor cells. Since we used recombinant soluble full-length AKAP4 for the selection procedure, both αAKAP4 scFv-hFc proteins might recognize an epitope that is not exposed on the cell surface. If this epitope is localized in the transmembrane or intracellular domains instead, it would not be accessible for binding. The same explanation might apply for the αSP17 scFv-hFc fusion proteins that did not stain tumor cells. An exception was αSP17_YU106-F02-hFc that brightly stained the tested SP17 positive tumor cell lines. Furthermore, we found that only the LYNDAL selected αSPAG9_VD1.E6-hFc clone showed bright staining of analyzed SPAG9 positive tumor cells, but none of the αSPAG9 scFv-hFc fusion proteins containing scFvs derived from HAL9/10. This observation was surprising, as all αSPAG9 scFv-hFc proteins bound the biotinylated SPAG9 peptide when tested in ELISA. However, scFvs derived from the naïve repertoire of HAL9/10 might possess affinities toward SPAG9 that are too low for stable binding to the cell surface exposed antigen. Based on these results, we chose the scFvs αSP17_YU106-F02 and αSPAG9_VD1.E6 as lead candidates for incorporation into CARs and did not further consider any of the αAKAP4 scFvs.

We optimized the lead candidate scFv sequences with regard to clinical application in that we removed non-parental amino acids initially introduced by restriction sites and by exchanging the Yol linker with the clinically accepted $(G_4S)_3$ linker. We produced and purified the sequence optimized lead candidate scFvs αSP17_YU106-F02* and αSPAG9_VD1.E6* (in the following referred to as αSP17 and αSPAG9) in the scFv-hFc format as described before and reevaluated their biochemical properties. Compared with the non-optimized counterparts, αSP17 and αSPAG9 scFv-hFc showed identical properties, including specificity toward the cognate antigen and staining of target tumor cell lines (master thesis, M.Sc. Lisa Noll [193]). Additionally, we investigated αSP17 and αSPAG9 scFv-hFc binding affinity toward the cognate antigen by SPR spectroscopy. αSP17 scFv-hFc showed a moderate binding affinity in the high nanomolar range (k_D = 107 nM). However, we could not determine an exact k_D value (>7960 nM) for αSPAG9 scFv-hFc as no binding saturation was reached by our tested analyte concentrations. The SPAG9 peptide might form an unstable complex with the immobilized αSPAG9 scFv-hFc, causing immediate dissociation after SPAG9 peptide injection stops, as was previously reported for other tested peptide-antibody complexes [204,205]. Most probably the observed bright staining of tumor cells by αSPAG9 scFv-hFc resulted from a natively folded surface SPAG9 and avidity effects.

We were interested in testing binding of our αSP17 and αSPAG9 scFv-hFc proteins to primary tumor material. For both soluble CARs we found brightest staining of the multiple myeloma cell line H929. Because CTAs were suggested in the literature as promising therapeutic targets in multiple myeloma, we collaborated with PD Dr. Michael Hundemer, head of the Diagnostic Laboratory for Hematological Malignancies (University Hospital Heidelberg), to include our soluble CARs in their routine flow cytometric analysis of primary patient samples [228]. Interestingly, we observed staining of distinct plasma cell subpopulations derived from bone marrow aspirates of multiple myeloma patients by αSP17 and αSPAG9 soluble CARs. We assume that these SP17 and SPAG9 positive subpopulations might be the malignant plasma cells, which we need to further characterize, as one of the diagnostic criteria for multiple myeloma is the detection of ≥60% of clonal plasma cells in the patient bone marrow sample. Thus, healthy plasma cells might still be present among the diseased ones [202,203]. Most importantly, we did not observe staining of healthy plasma cells derived from bone marrow aspirates of 2 out of 3 patients showing unremarkable bone marrow morphology. Furthermore, B cells ($CD19^+$), T cells ($CD3^+$) and non-B/T cells ($CD19^-/CD3^-$) derived from PBMCs of healthy donors were also not stained by our αSP17 and αSPAG9 soluble CARs. To confirm specific binding of the αSP17 and αSPAG9 soluble CARs to primary malignant blood cells, we need to investigate a much larger number of patient and healthy donor blood samples in prospective studies. In this context, it is worth to mention that we also found bright staining of the B cell lymphoma cell

line Granta-519 by our soluble CARs (master thesis, M.Sc. Lisa Noll [193]). Liggins and colleagues previously reported expression of SP17 mRNA transcripts in Granta-519 and SP17 protein expression in biopsies of B cell lymphoma patients [229]. Thus, we will include B cell lymphoma patient material in future screenings.

In summary, we found distinct expression patterns of AKAP4, SP17 and SPAG9 on the surface of various tumor cell lines as determined by commercially available antibodies. Our lead candidate αSP17 and αSPAG9 soluble CARs not only stained the antigen positive tumor cell lines, but also primary plasma cell subpopulations isolated from bone marrow aspirates of multiple myeloma patients. Importantly, T cells, B cells and myeloid cells among PBMCs isolated from healthy human donors were not stained by any of our lead candidate soluble CARs, indicating tumor-restricted specificity. The lack of SP17 expression on the surface of normal leukocytes has also been reported by others [230]. Noteworthy, for a pilot study by the National Cancer Institute from 2009, experts in the field were asked to prioritize cancer antigens according to immunogenicity (elicited T cell or antibody responses in patients), specificity (tissue restriction), oncogenicity (tumorigenic function) and other criteria. AKAP4 and SP17 were ranked among the top 62 tumor targets for T cell therapy with highest weighting on the criterion specificity [231]. Ultimately, these results indicate specific expression of SP17 and SPAG9 cells on tumor cells and safe targeting of malignant cells by our lead candidate soluble CARs.

4.2 Evaluation of αSP17 and αSPAG9 CAR T cells

Careful CAR design is essential as it impacts cytolytic activity, metabolism, persistence and other properties of the CAR expressing T cell [76]. When one (2^{nd} generation) or two (3^{rd} generation) costimulatory endodomains were added to the CD3ζ domain, CAR signaling led to efficient activation and long-term persistence of T cells, resulting in successful tumor elimination in various studies. To date, the costimulatory domains CD28 and 4-1BB are the most commonly tested in clinical trials and are included in CARs along with highly different spacers – such as short CD8 and long IgG1 or IgG4 hFc spacers [60,70,103]. This diversity in applied CAR designs shows that for each individual target antigen, an appropriate modular CAR composition needs to be empirically determined and optimized accordingly to enable the CAR T cell to establish a stable immunological synapse [232].

To identify a CAR configuration that functions best in combination with our lead candidate αSP17 and αSPAG9 scFvs, we generated two 2^{nd} generation (scFv-CD8-BBz, scFv-hFc-BBz) and three 3^{rd} generation CAR backbones (scFv-CD8-28BBz,

scFv-CD8-28ΔBBz, scFv-hFc-28ΔBBz). The mutated CD28 variant (28Δ) was included in some CAR constructs to inhibit Lck induced IL-2 secretion which should abrogate Treg formation at the tumor site [78]. We separately integrated the αSP17 and αSPAG9 scFvs as targeting domains into these CAR backbones. We transduced primary human T cells with lentiviral vectors carrying the CAR sequences and monitored CAR expression, CAR T cell expansion and functionality *ex vivo*.

We found successful surface expression of all CAR constructs except for αSP17-CD8-28ΔBBz. Initial transduction efficiencies tended to be higher for T cells expressing 2nd generation CARs compared to those expression 3rd generation CARs (34% vs. 20%, mean values) and CAR density was more stable over time for the 2nd generation constructs. Higher transduction efficiencies for 2nd generation CARs compared to 3rd generation CARs were also reported by others [209]. Throughout *ex vivo* cultivation for 17 days, our CAR T cells efficiently expanded up to 80-fold, which is comparable to CAR T cell expansion rates that were described previously [206,207]. T cells expressing 3rd generation CARs tended to expand more efficiently than the 2nd generation counterparts and non-transduced mock T cells that did not express a CAR.

A study by Frigault and colleagues described antigen independent constitutive signaling for some CARs that included the CD28 costimulatory domain, but not for those that contained 4-1BB or ICOS instead. This continuous CAR signaling depended on the scFv that was used as targeting domain, the promoter that drives CAR expression and CAR surface density. Continuous CAR signaling led to ligand independent CAR T cell proliferation throughout *in vitro* cultivation and constitutive secretion of cytokines such as IL-2, IFNγ and TNFα, but dampened *in vivo* persistence and antitumor efficacy due to the terminal differentiation status of the CAR T cells. Notably, the continuously proliferating CAR T cells expressed high amounts of PD-1, indicating an exhausted state of these T cells. The authors concluded that the CAR T cells with the non-continuous growth phenotype were superior as they showed higher antitumor efficacy and longer persistence *in vivo* compared to those with the continuous growth phenotype [206]. Consistent with this report, we observed that T cells expressing 3rd generation CARs containing CD28-4-1BB-CD3ζ stimulation domains tended to continuously proliferate as well within the monitored 14-17 days after activation. In comparison, T cells expressing 2nd generation CARs containing 4-1BB-CD3ζ stimulation domains tended to expand 1.5- to 3-fold less efficient and stopped expansion at day 11-14 after initial T cell activation. In this context, it is important to mention that we used a lentiviral vector containing the EF-1α promoter to drive CAR expression, which Frigault *et al.* found to favor continuous CAR signaling [206]. However, in contrast to Frigault *et al*., we observed highest CAR expression rates among the non-continuously proliferating CAR T cells (2nd generation CARs) and not the continuously proliferating CAR T cells (3rd generation CARs).

In another study, Long *et al*. reported the limited antitumor efficacy of anti-GD2 CAR T cells and found that these CAR T cells also expressed high amounts of PD-1, indicating T cell exhaustion [80]. Beside the marker PD-1, exhaustion is characterized by the increased expression of further inhibitory receptors on the T cell surface, such as TIM-3 and LAG-3 [84,206]. In the study of Long *et al.* these exhaustion markers were reported to be highly expressed by the anti-GD2 CAR T cells, thereby confirming their exhausted phenotype. In this case, T cell exhaustion was caused by antigen independent, constitutive activation through CAR clustering, which may result from the aggregation tendency of the extracellular anti-GD2 scFv [80]. To test if our CARs induce constitutive signaling and thereby also T cell exhaustion, we monitored expression of activation and exhaustion markers on antigen naïve CAR T cells at several time points after initial activation. Compared to the non-transduced mock T cells, we observed combined increase of TIM-3 and LAG-3 levels for the T cells expressing the 3rd generation CARs, but to a much lesser extent for T cells expressing the 2nd generation CARs. This indicates that the 3rd generation CARs may have a higher propensity to induce T cell exhaustion, possibly by their CD28 costimulatory domain, whereas the 2nd generation CARs lacking CD28 costimulation do not or only weakly. Our data are consistent with the findings of Long *et al*. who reported that T cell exhaustion is promoted by the costimulatory domain CD28 while it is attenuated by 4-1BB [80].

At day 10 after initial T cell activation, we immunophenotyped CD8$^+$ CAR T cells to identify individual subsets and observed that Tscm and Teff cell populations were barely present (0-4%). Instead, the largest fractions were memory T cells belonging either to Tcm or Tscm subpopulations. Interestingly, T cells expressing 2nd generation CARs mainly differentiated toward the Tcm phenotype (51-66%, mean value 60%), whereas the 3rd generation CARs seemed to drive the T cells into the Tem phenotype (34-80%, mean value 63%). Our findings are consistent with a report that found the costimulatory domain 4-1BB to promote CAR T cell differentiation into long-lived CD8$^+$ Tcm cells, whereas CD28 containing CARs tend to give rise to CD8$^+$ Tem cells [76]. Only the 3rd generation CARs αSP17-CD8-28BBz and αSPAG9-hFc-28ΔBBz yielded higher fractions of Tcm than Tem subset, which does not align with the above mentioned pattern. We need to verify our observations by testing our CAR constructs in T cells derived from additional donors. In various clinical trials, prolonged CAR T cell persistence correlated with therapeutic efficacy [99,100]. In this regard, the less differentiated memory T cell subsets (Tscm and Tcm) were reported to be favored over effector T cell subsets (Tem and Teff) as they demonstrated superior *in vivo* expansion, persistence and antitumor responses [97,98,233].

Taken all results together, we selected the 2nd generation CARs to proceed with further analyses as they showed higher surface expression, induced no T cell exhaustion and generated the highest fraction of CD8$^+$ Tcm cells. We tested 2nd generation αSP17 and

αSPAG9 CARs using T cells derived from a second donor. We did not observe any signs of CAR induced T cell exhaustion and found a predominant CAR expressing $CD8^+$ Tcm cell population (65-92%). Furthermore, we observed high viability of the CAR T cells and highly stable CAR expression throughout *in vitro* cultivation, even after a freeze and thaw cycle, which is a prerequisite for later clinical translation.

To test for CAR functionality, we stimulated CAR T cells with the immobilized cognate antigen and detected upregulation of CD25, CD69 and PD-1 on the surface of CAR T cells, but not on mock T cells that lack CAR expression, indicating specific antigen induced CAR T cell activation [213,214]. We further analyzed the capacity of CAR T cells to proliferate upon antigen contact by labeling the T cells with the fluorescent dye CFSE and stimulating them with immobilized target antigen or by co-incubation with target antigen positive tumor cell lines. We chose H929 and SKOV-3 as target cell lines for which we previously observed efficient binding of our soluble αSP17 and αSPAG9 CARs. We found higher proliferation activity for the CAR T cells stimulated with target antigen or target tumor cell lines compared to the unstimulated counterparts or to CAR negative mock T cells. In this regard, T cells expressing hFc spacer CARs proliferated approximately twice more efficiently than those expressing CD8 spacer CARs. In prospective proliferation assays, we will include FCS in the adapted medium to achieve an improved quantification of cell divisions as was observed in previous studies [70,234].

In order to assess cytotoxicity of our αSP17 and αSPAG9 CAR T cells toward target antigen expressing tumor cell lines, we separately co-incubated SKOV-3 and H929 cells with CAR T cells in different effector-to-target ratios and monitored target cancer cell viability. Most importantly, T cells expressing the αSP17 CARs and the αSPAG9-hFc-BBz CAR possessed enhanced cytotoxicity toward SKOV-3 cells compared with CAR negative mock T cells. T cells expressing hFc spacer CARs killed SKOV-3 target cells more effectively than those expressing CD8 spacer CARs. In particular the αSP17-hFc-BBz CAR T cells showed the best cytotoxic capacity. In contrast, we observed that only αSP17-CD8-BBz CAR T cells were cytotoxic toward H929 cells, but not T cells expressing the other CAR constructs. Previous reports demonstrated that the extracellular scFv and spacer have striking influence on the intracellular CAR signaling. The distance between CAR T cell and tumor cell is defined by the CAR spacer and the location of the epitope on the target antigen. CAR spacer length was shown to be crucial for the formation of a stable immunological synapse [67,206,235]. Thus, we hypothesize that more efficient killing induced by CARs might result from an advantageous intercellular space at the immunological synapse. However, no information is available about the membrane proximity of the extracellular domains of SP17 and SPAG9. We observed a baseline killing by CAR negative mock T cells, most probably due to a MHC mismatch between donor T cells and the tumor cell lines

causing cytotoxic alloreactivity. This issue could be overcome by using MHC matched donor T cells.

We need to confirm our findings by testing the CAR constructs in T cells from additional donors. We currently establish further readouts to analyze CAR T cell activation upon contact with antigen positive tumor cells including multiplex assay to determine cytokine release (e.g. IFNγ, IL-2, TNFα), luciferase based cytotoxicity assays and long-term expansion assays.

4.3 Targeting solid cancers with αSP17 and αSPAG9 CAR T cells

Many surface expressed and tumor associated antigens were identified in solid cancers and evaluated for clinical use, however, they often lack tumor specificity due to additional expression on healthy tissues [119,236,237]. In 2010, a case of fatal toxicity was reported, in which ERBB2 specific CAR T cells were applied to treat metastatic lung and liver cancer. Within minutes after infusion, the patient experienced highly impaired respiratory function and unfortunately did not survive despite medical intervention. The cause was found to be a low level expression of ERBB2 in normal lung tissue compared with the tumor, which resulted in CAR T cell infiltration of healthy tissue followed by the rapid release of inflammatory cytokines in high amounts and eventually leading to multi-organ failure. This report demonstrated the potentially lethal risk of on-target/off-tumor toxicity even at low antigen density on healthy tissues [116]. If SP17 and SPAG9 are indeed tumor restricted CTAs, which we need to further investigate, the choice of these targets per se would contribute to therapeutic safety. Another controllable factor is the CAR affinity toward the cognate antigen. In a study using a preclinical neuroblastoma mouse model, high affinity GD2 specific CAR T cells induced fatal encephalitis [238]. Another preclinical study directly compared ICAM-1 targeting CARs with nanomolar and micromolar affinity. Not only did the T cells expressing CARs with micromolar affinity prevent systemic toxicity compared with their nanomolar affinity counterparts, but they also killed the tumor more efficiently, most probably due to reduced trapping at the bound target cells [68]. These findings indicate that CARs with moderate affinities in the high nanomolar or even micromolar range may have superior characteristics regarding antitumoral efficacy and safety as they tolerate a low antigen density commonly found on healthy tissues [239]. In this regard, our αSP17 CAR T cells might safely target SP17 positive tumor cells while sparing healthy tissues, as we measured a high nanomolar affinity for the soluble αSP17 CAR. We need to further investigate this hypothesis.

The second hurdle to overcome for an efficient cellular therapy against solid tumors is the immunosuppressive microenvironment within the tumor mass that inhibits the antitumor activity of infiltrating lymphocytes. In contrast to blood cancers, solid tumors establish these barriers against the immune system including oxidative stress, expression of immunosuppressive proteins, recruitment of immunosuppressive immune cells such as Tregs and tumor associated macrophages, and expression of inhibitory receptors such as PD-L1. These mechanisms put the CAR T cells into an unresponsive state, thereby diminishing their antitumor efficacy [65,240]. In this regard, combined therapy with a PD-1 blocking antibody as checkpoint inhibitor was shown to increase the CAR T cell function and reduced the presence of suppressive immune cells in a breast cancer mouse model [241]. To avoid systemic checkpoint inhibition which might cause immune related adverse events, another recent report described anti-PD-1 scFv secreting CAR T cells at the tumor site. This local checkpoint inhibition resulted in long-term survival of CAR T cells within the tumor microenvironment [242,243]. Decreased apoptosis of CAR T cells was achieved, when they were modified to constitutively secrete IL-12 which further enhanced CAR T cell proliferation and cytotoxicity in a tested ovarian cancer mouse model [210]. Regarding long-term CAR T cell persistence, in some patients treated with murine scFv containing CAR T cells, anti-CAR responses induced by human anti-mouse antibodies were shown to impair the therapeutic efficacy. By using fully human scFvs as targeting domains in our CARs, we minimized the potential for this CAR T cell immunogenicity [240,244].

Taken together, the discussed studies illustrate tremendous efforts to tackle the hurdles of solid cancers. We will definitely consider these findings for our ongoing development of a SP17 and SPAG9 specific CAR T cell therapy.

4.4 Conclusion and outlook

We developed CARs specific for SP17 and SPAG9 to prospectively treat antigen positive solid and hematological malignancies with adoptively transferred autologous T cells. T cells from individual donors expressing the CARs were characterized for expansion capacities, T cell subset composition and antitumor efficacy. We found that the CARs in the 2nd generation configuration did not induce T cell exhaustion and the CAR T cells preferentially differentiated toward long-lived central memory T cells. We demonstrated CAR functionality by enhanced T cell proliferation and upregulation of activation markers upon stimulation with target antigen, and showed CAR T cell cytotoxicity against multiple myeloma and ovarian cancer target cell lines. However, these findings need to be confirmed by characterizing transduced T cells from additional donors. CAR T cell properties need to be further evaluated by using additional methods such as chromium release assay, luciferase based cytotoxicity assays, cytokine release measurements, and monitoring of long-term expansion capacities upon antigen contact and rechallenge. Finally, antitumor activity of αSP17 and αSPAG9 CAR T cells will be tested in mouse models xenografted with human antigen positive tumor cells. Most importantly, as we did not find truly SP17 or SPAG9 negative tumor cells among the screened cell lines, we initiated the generation of SP17 and SPAG9 deficient cell lines employing the CRISPR/Cas9 technology. SP17 and SPAG9 deficient cells will be used as target negative control to further demonstrate antigen specificity of our CAR targeting domains.

Furthermore, we will set out to determine SP17 and SPAG9 expression patterns in primary tumor samples derived from ovarian cancer, multiple myeloma and lymphoma patients at different stages of the disease to evaluate the suitability of our targeting domains for use in a novel CAR T cell therapy to treat patients suffering from these cancer entities.

5 Bibliography

5.1 References

[1] K. Murphy, P. Travers, M. Walport, and C. Janeway, *Janeway's immunobiology*, 8th ed. New York: Garland Science, 2012. Pages 1, 2, 28, 29, 34, 127-129, 130, 134, 135, 140, 141, 173-178.

[2] G. E. Blair and G. P. Cook, "Cancer and the immune system: an overview," *Oncogene*, vol. 27, p. 5868, Oct. 2008.

[3] L. Van Parijs and A. K. Abbas, "Homeostasis and self-tolerance in the immune system: turning lymphocytes off.," *Science*, vol. 280, no. 5361, pp. 243–248, Apr. 1998.

[4] C. A. J. Janeway, "Approaching the asymptote? Evolution and revolution in immunology.," *Cold Spring Harb. Symp. Quant. Biol.*, vol. 54 Pt 1, pp. 1–13, 1989.

[5] R. Medzhitov and C. A. J. Janeway, "Decoding the patterns of self and nonself by the innate immune system.," *Science*, vol. 296, no. 5566, pp. 298–300, Apr. 2002.

[6] C. A. J. Janeway and R. Medzhitov, "Innate immune recognition.," *Annu. Rev. Immunol.*, vol. 20, pp. 197–216, 2002.

[7] R. Clark and T. Kupper, "Old Meets New: The Interaction Between Innate and Adaptive Immunity," *J. Invest. Dermatol.*, vol. 125, no. 4, pp. 629–637, 2005.

[8] S. Tonegawa, "Somatic generation of antibody diversity," *Nature*, vol. 302, no. 5909, pp. 575–581, 1983.

[9] D. Jung and F. W. Alt, "Unraveling V(D)J Recombination: Insights into Gene Regulation," *Cell*, vol. 116, no. 2, pp. 299–311, 2004.

[10] I. C. MacLennan, "Germinal centers.," *Annu. Rev. Immunol.*, vol. 12, pp. 117–139, 1994.

[11] B. Zheng, W. Xue, and G. Kelsoe, "Locus-specific somatic hypermutation in germinal centre T cells," *Nature*, vol. 372, no. 6506, pp. 556–559, 1994.

[12] H. W. Schroeder Jr and L. Cavacini, "Structure and function of immunoglobulins," *J. Allergy Clin. Immunol.*, vol. 125, no. 2 Suppl 2, pp. S41–S52, Feb. 2010.

[13] C. A. J. Janeway, K. Bottomly, J. Horowitz, J. Kaye, B. Jones, and J. Tite, "Modes of cell:cell communication in the immune system.," *J. Immunol.*, vol. 135, no. 2 Suppl, p. 739s–742s, Aug. 1985.

[14] F. M. Burnet, "A modification of Jerne's theory of antibody production using the concept of clonal selection.," *CA. Cancer J. Clin.*, vol. 26, no. 2, pp. 119–121, 1976.

[15] I. Sela-Culang, V. Kunik, and Y. Ofran, "The structural basis of antibody-antigen recognition," *Front. Immunol.*, vol. 4, p. 302, Oct. 2013.

[16] R. Ahmed and D. Gray, "Immunological memory and protective immunity: understanding their relation.," *Science*, vol. 272, no. 5258, pp. 54–60, Apr. 1996.

[17] J. V Ravetch and J. P. Kinet, "Fc receptors.," *Annu. Rev. Immunol.*, vol. 9, pp. 457–492, 1991.

[18] R. Tisch, C. M. Roifman, and N. Hozumi, "Functional differences between immunoglobulins M and D expressed on the surface of an immature B-cell line," *Proc. Natl. Acad. Sci.*, vol. 85, no. 18, p. 6914 LP-6918, Sep. 1988.

[19] A. Frenzel, M. Hust, and T. Schirrmann, "Expression of recombinant antibodies," *Front. Immunol.*, vol. 4, p. 217, Jul. 2013.

[20] J. Maynard and G. Georgiou, "Antibody Engineering," *Annu. Rev. Biomed. Eng.*, vol. 2, no. 1, pp. 339–376, Aug. 2000.

[21] K. L. Armour, M. R. Clark, A. G. Hadley, and L. M. Williamson, “Recombinant human IgG molecules lacking Fcgamma receptor I binding and monocyte triggering activities.,” *Eur. J. Immunol.*, vol. 29, no. 8, pp. 2613–2624, Aug. 1999.

[22] G. KÖHLER and C. MILSTEIN, “Continuous cultures of fused cells secreting antibody of predefined specificity,” *Nature*, vol. 256, no. 5517, pp. 495–497, 1975.

[23] G. P. Smith, “Filamentous fusion phage: novel expression vectors that display cloned antigens on the virion surface,” *Science (80-.).*, vol. 228, no. 4705, p. 1315 LP-1317, Jun. 1985.

[24] S. Sun *et al.*, “One-pot stapling of interchain disulfides of antibodies using an isobutylene motif.,” *Org. Biomol. Chem.*, vol. 17, no. 7, pp. 2005–2012, Feb. 2019.

[25] D. C. Wraith, “The Future of Immunotherapy: A 20-Year Perspective,” *Front. Immunol.*, vol. 8, p. 1668, Nov. 2017.

[26] S. Singh *et al.*, “Monoclonal Antibodies: A Review.,” *Curr. Clin. Pharmacol.*, vol. 13, no. 2, pp. 85–99, 2018.

[27] H. Kaplon and J. M. Reichert, “Antibodies to watch in 2019,” *MAbs*, vol. 11, no. 2, pp. 219–238, Dec. 2018.

[28] M. E. Weinblatt *et al.*, “Adalimumab, a fully human anti-tumor necrosis factor alpha monoclonal antibody, for the treatment of rheumatoid arthritis in patients taking concomitant methotrexate: the ARMADA trial.,” *Arthritis Rheum.*, vol. 48, no. 1, pp. 35–45, Jan. 2003.

[29] J. Sevigny *et al.*, “The antibody aducanumab reduces Abeta plaques in Alzheimer’s disease.,” *Nature*, vol. 537, no. 7618, pp. 50–56, Sep. 2016.

[30] A. J. Grillo-Lopez *et al.*, “Rituximab: the first monoclonal antibody approved for the treatment of lymphoma.,” *Curr. Pharm. Biotechnol.*, vol. 1, no. 1, pp. 1–9, Jul. 2000.

[31] L. Dyck and K. H. G. Mills, “Immune checkpoints and their inhibition in cancer and infectious diseases.,” *Eur. J. Immunol.*, vol. 47, no. 5, pp. 765–779, May 2017.

[32] C. Paluch, A. M. Santos, C. Anzilotti, R. J. Cornall, and S. J. Davis, “Immune Checkpoints as Therapeutic Targets in Autoimmunity,” *Front. Immunol.*, vol. 9, p. 2306, Oct. 2018.

[33] F. S. Hodi *et al.*, “Biologic activity of cytotoxic T lymphocyte-associated antigen 4 antibody blockade in previously vaccinated metastatic melanoma and ovarian carcinoma patients.,” *Proc. Natl. Acad. Sci. U. S. A.*, vol. 100, no. 8, pp. 4712–4717, Apr. 2003.

[34] J. Larkin *et al.*, “Combined Nivolumab and Ipilimumab or Monotherapy in Untreated Melanoma.,” *N. Engl. J. Med.*, vol. 373, no. 1, pp. 23–34, Jul. 2015.

[35] World Health Organization, “PRESS RELEASE N° 263,” 2018. [Online]. Available: https://www.who.int/cancer/PRGlobocanFinal.pdf. [Accessed: 17-Jan-2019].

[36] M. Arruebo *et al.*, “Assessment of the evolution of cancer treatment therapies,” *Cancers (Basel).*, vol. 3, no. 3, pp. 3279–3330, 2011.

[37] P. Chames, M. Van Regenmortel, E. Weiss, and D. Baty, “Therapeutic antibodies: Successes, limitations and hopes for the future,” *Br. J. Pharmacol.*, vol. 157, no. 2, pp. 220–233, 2009.

[38] F. V Okur and M. K. Brenner, “Cellular immunotherapy of cancer.,” *Methods Mol. Biol.*, vol. 651, pp. 319–345, 2010.

[39] O. J. Finn, “Immuno-oncology: Understanding the function and dysfunction of the immune system in cancer,” *Ann. Oncol.*, vol. 23, no. SUPPL.8, pp. 8–11, 2012.

[40] N. P. Restifo, M. E. Dudley, and S. A. Rosenberg, “Adoptive immunotherapy for cancer: harnessing the T cell response.,” *Nat. Rev. Immunol.*, vol. 12, no. 4, pp. 269–281, Mar. 2012.

[41] S. A. Rosenberg, P. Spiess, and R. Lafreniere, “A new approach to the adoptive immunotherapy of cancer with tumor-infiltrating lymphocytes.,” *Science*, vol. 233, no. 4770, pp. 1318–1321, Sep. 1986.

[42] L. Mesler Muul *et al.*, “Studies of serum-free culture medium in the generation of lymphokine activated killer cells,” *J. Immunol. Methods*, vol. 105, no. 2, pp. 183–192, 1987.

[43] E. W. Nijhuis, E. vd Wiel-van Kemenade, C. G. Figdor, and R. A. van Lier, “Activation and expansion of tumour-infiltrating lymphocytes by anti-CD3 and anti-CD28 monoclonal antibodies.,” *Cancer Immunol. Immunother.*, vol. 32, no. 4, pp. 245–250, 1990.

[44] C. H. June, “Science in medicine Adoptive T cell therapy for cancer in the clinic,” *Cancer Res.*, vol. 117, no. 6, pp. 1466–76, 2007.

[45] S. A. Rosenberg *et al.*, “Durable complete responses in heavily pretreated patients with metastatic melanoma using T-cell transfer immunotherapy.,” *Clin. Cancer Res.*, vol. 17, no. 13, pp. 4550–4557, Jul. 2011.

[46] M. E. Dudley *et al.*, “Adoptive cell transfer therapy following non-myeloablative but lymphodepleting chemotherapy for the treatment of patients with refractory metastatic melanoma,” *J. Clin. Oncol.*, vol. 23, no. 10, pp. 2346–2357, Apr. 2005.

[47] L. Gattinoni *et al.*, “Removal of homeostatic cytokine sinks by lymphodepletion enhances the efficacy of adoptively transferred tumor-specific CD8+ T cells.,” *J. Exp. Med.*, vol. 202, no. 7, pp. 907–912, Oct. 2005.

[48] C. Wrzesinski *et al.*, “Increased intensity lymphodepletion enhances tumor treatment efficacy of adoptively transferred tumor-specific T cells,” *J. Immunother.*, vol. 33, no. 1, pp. 1–7, Jan. 2010.

[49] M. E. Dudley, J. R. Wunderlich, T. E. Shelton, J. Even, and S. A. Rosenberg, “Generation of tumor-infiltrating lymphocyte cultures for use in adoptive transfer therapy for melanoma patients.,” *J. Immunother.*, vol. 26, no. 4, pp. 332–342, 2003.

[50] J. L. Jorgensen, P. A. Reay, E. W. Ehrich, and M. M. Davis, “Molecular components of T-cell recognition.,” *Annu. Rev. Immunol.*, vol. 10, pp. 835–873, 1992.

[51] M. Sadelain, I. Rivière, and S. Riddell, “Therapeutic T cell engineering,” *Nature*, vol. 545, no. 7655, pp. 423–431, May 2017.

[52] A. P. Rapoport *et al.*, “NY-ESO-1-specific TCR-engineered T cells mediate sustained antigen-specific antitumor effects in myeloma.,” *Nat. Med.*, vol. 21, no. 8, pp. 914–921, Aug. 2015.

[53] G. L. Beatty and W. L. Gladney, “Immune escape mechanisms as a guide for cancer immunotherapy,” *Clin. Cancer Res.*, vol. 21, no. 4, pp. 687–692, Feb. 2015.

[54] A. D. Fesnak, C. H. June, and B. L. Levine, “Engineered T cells: the promise and challenges of cancer immunotherapy,” *Nat. Rev. Cancer*, vol. 16, no. 9, pp. 566–581, Aug. 2016.

[55] G. Gross, T. Waks, and Z. Eshhar, “Expression of immunoglobulin-T-cell receptor chimeric molecules as functional receptors with antibody-type specificity.,” *Proc. Natl. Acad. Sci.*, vol. 86, no. 24, pp. 10024–10028, Dec. 1989.

[56] Z. Eshhar, T. Waks, G. Gross, and D. G. Schindler, “Specific activation and targeting of cytotoxic lymphocytes through chimeric single chains consisting of antibody-binding domains and the gamma or zeta subunits of the immunoglobulin and T-cell receptors,” *Proc. Natl. Acad. Sci. U. S. A.*, vol. 90, no. 2, pp. 720–724, Jan. 1993.

[57] I. Stancovski, D. G. Schindler, T. Waks, Y. Yarden, M. Sela, and Z. Eshhar, “Targeting of T lymphocytes to Neu/HER2-expressing cells using chimeric single chain Fv receptors.,” *J. Immunol.*, vol. 151, no. 11, pp. 6577–6582, Dec. 1993.

[58] Z. Eshhar, T. Waks, and G. Gross, “The emergence of T-Bodies/CAR T cells,” *Cancer J. (United States)*, vol. 20, no. 2, pp. 123–126, 2014.

[59] J. Hartmann, M. Schüßler-Lenz, A. Bondanza, and C. J. Buchholz, “Clinical development of CAR T cells-challenges and opportunities in translating innovative treatment concepts,” *EMBO Mol. Med.*, vol. 9, no. 9, pp. 1183–1197, Sep. 2017.

[60] M. Sadelain, R. Brentjens, and I. Rivière, “The basic principles of chimeric antigen receptor design,” *Cancer Discov.*, vol. 3, no. 4, pp. 388–398, 2013.

[61] H. M. Finney, A. D. Lawson, C. R. Bebbington, and A. N. Weir, “Chimeric receptors providing both primary and costimulatory signaling in T cells from a single gene product.,” *J. Immunol.*, vol. 161, no. 6, pp. 2791–2797, Sep. 1998.

[62] J. Maher, R. J. Brentjens, G. Gunset, I. Riviere, and M. Sadelain, “Human T-lymphocyte cytotoxicity and proliferation directed by a single chimeric TCRzeta /CD28 receptor.,” *Nat. Biotechnol.*, vol. 20, no. 1, pp. 70–75, Jan. 2002.

[63] M. A. Pule, K. C. Straathof, G. Dotti, H. E. Heslop, C. M. Rooney, and M. K. Brenner, “A chimeric T cell antigen receptor that augments cytokine release and supports clonal expansion of primary human T cells.,” *Mol. Ther.*, vol. 12, no. 5, pp. 933–941, Nov. 2005.

[64] C. Imai *et al.*, “Chimeric receptors with 4-1BB signaling capacity provoke potent cytotoxicity against acute lymphoblastic leukemia.,” *Leukemia*, vol. 18, no. 4, pp. 676–684, Apr. 2004.

[65] H. Abken, “Driving CARs on the Highway to Solid Cancer: Some Considerations on the Adoptive Therapy with CAR T Cells,” *Hum. Gene Ther.*, vol. 28, no. 11, pp. 1047–1060, Nov. 2017.

[66] M. Chmielewski, A. A. Hombach, and H. Abken, “CD28 cosignalling does not affect the activation threshold in a chimeric antigen receptor-redirected T-cell attack.,” *Gene Ther.*, vol. 18, no. 1, pp. 62–72, Jan. 2011.

[67] M. Hudecek *et al.*, “Receptor affinity and extracellular domain modifications affect tumor recognition by ROR1-specific chimeric antigen receptor T cells,” *Clin. Cancer Res.*, vol. 19, no. 12, pp. 3153–3164, 2013.

[68] S. Park *et al.*, “Micromolar affinity CAR T cells to ICAM-1 achieves rapid tumor elimination while avoiding systemic toxicity,” *Sci. Rep.*, vol. 7, no. 1, p. 14366, 2017.

[69] A. A. Hombach, V. Schildgen, C. Heuser, R. Finnern, D. E. Gilham, and H. Abken, “T cell activation by antibody-like immunoreceptors: the position of the binding epitope within the target molecule determines the efficiency of activation of redirected T cells.,” *J. Immunol.*, vol. 178, no. 7, pp. 4650–4657, Apr. 2007.

[70] M. Hudecek *et al.*, “The Nonsignaling Extracellular Spacer Domain of Chimeric Antigen Receptors Is Decisive for In Vivo Antitumor Activity,” *Cancer Immunol. Res.*, vol. 3, no. 2, pp. 125–135, Feb. 2015.

[71] S. Minguet, M. Swamy, B. Alarcon, I. F. Luescher, and W. W. A. Schamel, “Full activation of the T cell receptor requires both clustering and conformational changes at CD3.,” *Immunity*, vol. 26, no. 1, pp. 43–54, Jan. 2007.

[72] J. Li, W. Li, K. Huang, Y. Zhang, G. Kupfer, and Q. Zhao, “Chimeric antigen receptor T cell (CAR-T) immunotherapy for solid tumors: lessons learned and strategies for moving forward,” *J. Hematol. Oncol.*, vol. 11, no. 1, p. 22, Feb. 2018.

[73] F. A. Harding, J. G. McArthur, J. A. Gross, D. H. Raulet, and J. P. Allison, “CD28-mediated signalling co-stimulates murine T cells and prevents induction of anergy in T-cell clones.,” *Nature*, vol. 356, no. 6370, pp. 607–609, Apr. 1992.

[74] T. Brocker and K. Karjalainen, “Signals through T cell receptor-zeta chain alone are insufficient to prime resting T lymphocytes.,” *J. Exp. Med.*, vol. 181, no. 5, pp. 1653–1659, May 1995.

[75] H. Abken, “Costimulation Engages the Gear in Driving CARs.,” *Immunity*, vol. 44, no. 2, pp. 214–216, Feb. 2016.

[76] O. U. Kawalekar *et al.*, “Distinct Signaling of Coreceptors Regulates Specific Metabolism Pathways and Impacts Memory Development in CAR T Cells,” *Immunity*, vol. 44, no. 2, pp. 380–390, Feb. 2016.

[77] E. Zorn *et al.*, “IL-2 regulates FOXP3 expression in human CD4+CD25+ regulatory T cells through a STAT-dependent mechanism and induces the expansion of these cells in vivo,” *Blood*, vol. 108, no. 5, pp. 1571–1579, Sep. 2006.

[78] D. M. Kofler *et al.*, “CD28 costimulation Impairs the efficacy of a redirected t-cell antitumor attack in the presence of regulatory t cells which can be overcome by preventing Lck activation,” *Mol. Ther.*, vol. 19, no. 4, pp. 760–767, Apr. 2011.

[79] M. C. Milone *et al.*, “Chimeric receptors containing CD137 signal transduction domains mediate enhanced survival of T cells and increased antileukemic efficacy in vivo,” *Mol. Ther.*, vol. 17, no. 8, pp. 1453–1464, Aug. 2009.

[80] A. H. Long *et al.*, “4-1BB costimulation ameliorates T cell exhaustion induced by tonic signaling of chimeric antigen receptors,” *Nat. Med.*, vol. 21, no. 6, pp. 581–590, 2015.

[81] B. D. Jamieson *et al.*, “Epitope escape mutation and decay of human immunodeficiency virus type 1-specific CTL responses.,” *J. Immunol.*, vol. 171, no. 10, pp. 5372–5379, Nov. 2003.

[82] E. J. Wherry and M. Kurachi, “Molecular and cellular insights into T cell exhaustion.,” *Nat. Rev. Immunol.*, vol. 15, no. 8, pp. 486–499, Aug. 2015.

[83] L. Nieba, A. Honegger, C. Krebber, and A. Pluckthun, “Disrupting the hydrophobic patches at the antibody variable/constant domain interface: improved in vivo folding and physical characterization of an engineered scFv fragment.,” *Protein Eng.*, vol. 10, no. 4, pp. 435–444, Apr. 1997.

[84] K. Catakovic, E. Klieser, D. Neureiter, and R. Geisberger, “T cell exhaustion: from pathophysiological basics to tumor immunotherapy,” *Cell Commun. Signal.*, vol. 15, no. 1, p. 1, Jan. 2017.

[85] A. A. Hombach and H. Abken, “Most Do, but Some Do Not: CD4(+)CD25(-) T Cells, but Not CD4(+)CD25(+) Treg Cells, Are Cytolytic When Redirected by a Chimeric Antigen Receptor (CAR).,” *Cancers (Basel).*, vol. 9, no. 9, Aug. 2017.

[86] M. Fransson *et al.*, “CAR/FoxP3-engineered T regulatory cells target the CNS and suppress EAE upon intranasal delivery.,” *J. Neuroinflammation*, vol. 9, p. 112, May 2012.

[87] D. Blat, E. Zigmond, Z. Alteber, T. Waks, and Z. Eshhar, “Suppression of murine colitis and its associated cancer by carcinoembryonic antigen-specific regulatory T cells.,” *Mol. Ther.*, vol. 22, no. 5, pp. 1018–1028, May 2014.

[88] T. Caza and S. Landas, “Functional and Phenotypic Plasticity of CD4(+) T Cell Subsets.,” *Biomed Res. Int.*, vol. 2015, p. 521957, 2015.

[89] C. H. June, “Principles of adoptive T cell cancer therapy.,” *J. Clin. Invest.*, vol. 117, no. 5, pp. 1204–1212, May 2007.

[90] Y. D. Mahnke, T. M. Brodie, F. Sallusto, M. Roederer, and E. Lugli, “The who’s who of T-cell differentiation: Human memory T-cell subsets,” *Eur. J. Immunol.*, vol. 43, no. 11, pp. 2797–2809, 2013.

[91] M. Merkenschlager, L. Terry, R. Edwards, and P. C. Beverley, “Limiting dilution analysis of proliferative responses in human lymphocyte populations defined by the monoclonal antibody UCHL1: implications for differential CD45 expression in T cell memory formation.,” *Eur. J. Immunol.*, vol. 18, no. 11, pp. 1653–1661, Nov. 1988.

[92] P. C. Beverley, “Functional analysis of human T cell subsets defined by CD45 isoform expression.,” *Semin. Immunol.*, vol. 4, no. 1, pp. 35–41, Feb. 1992.

[93] D. Hamann *et al.*, “Phenotypic and functional separation of memory and effector human CD8+ T cells.,” *J. Exp. Med.*, vol. 186, no. 9, pp. 1407–1418, Nov. 1997.

[94] F. Sallusto, D. Lenig, R. Forster, M. Lipp, and A. Lanzavecchia, “Two subsets of memory T lymphocytes with distinct homing potentials and effector functions.,” *Nature*, vol. 401, no. 6754, pp. 708–712, Oct. 1999.

[95] L. Gattinoni *et al.*, “A human memory T cell subset with stem cell-like properties.,” *Nat. Med.*, vol. 17, no. 10, pp. 1290–1297, Sep. 2011.

[96] E. Lugli *et al.*, “Superior T memory stem cell persistence supports long-lived T cell memory.,” *J. Clin. Invest.*, vol. 123, no. 2, pp. 594–599, Feb. 2013.

[97] G. Dotti, S. Gottschalk, B. Savoldo, and M. K. Brenner, “Design and development of therapies using chimeric antigen receptor-expressing T cells.,” *Immunol. Rev.*, vol. 257, no. 1, pp. 107–126, Jan. 2014.

[98] C. Berger, M. C. Jensen, P. M. Lansdorp, M. Gough, C. Elliott, and S. R. Riddell, “Adoptive transfer of effector CD8+ T cells derived from central memory cells establishes persistent T cell memory in primates.,” *J. Clin. Invest.*, vol. 118, no. 1, pp. 294–305, Jan. 2008.

[99] M. Kalos *et al.*, “T cells with chimeric antigen receptors have potent antitumor effects and can establish memory in patients with advanced leukemia,” *Sci. Transl. Med.*, vol. 3, no. 95, p. 95ra73-95ra73, Aug. 2011.

[100] D. L. Porter, B. L. Levine, M. Kalos, A. Bagg, and C. H. June, “Chimeric antigen receptor-modified T cells in chronic lymphoid leukemia.,” *N. Engl. J. Med.*, vol. 365, no. 8, pp. 725–733, Aug. 2011.

[101] B. G. Till *et al.*, “Adoptive immunotherapy for indolent non-Hodgkin lymphoma and mantle cell lymphoma using genetically modified autologous CD20-specific T cells,” *Blood*, vol. 112, no. 6, pp. 2261–2271, Sep. 2008.

[102] F. C. Thistlethwaite *et al.*, “The clinical efficacy of first-generation carcinoembryonic antigen (CEACAM5)-specific CAR T cells is limited by poor persistence and transient pre-conditioning-dependent respiratory toxicity,” *Cancer Immunol. Immunother.*, vol. 66, no. 11, pp. 1425–1436, 2017.

[103] C. A. Ramos, B. Savoldo, and G. Dotti, “CD19-CAR trials,” *Cancer J.*, vol. 20, no. 2, pp. 112–118, 2014.

[104] J. H. Park, M. B. Geyer, and R. J. Brentjens, “CD19-targeted CAR T-cell therapeutics for hematologic malignancies: interpreting clinical outcomes to date.,” *Blood*, vol. 127, no. 26, pp. 3312–3320, Jun. 2016.

[105] Z. Zhao, Y. Chen, N. M. Francisco, Y. Zhang, and M. Wu, “The application of CAR-T cell therapy in hematological malignancies: advantages and challenges,” *Acta Pharm. Sin. B*, vol. 8, no. 4, pp. 539–551, 2018.

[106] T. T. L. Yu, P. Gupta, V. Ronfard, A. A. Vertès, and Y. Bayon, “Recent Progress in European Advanced Therapy Medicinal Products and Beyond,” *Front. Bioeng. Biotechnol.*, vol. 6, p. 130, Sep. 2018.

[107] Novartis, “Novartis receives European Commission approval of its CAR-T cell therapy, Kymriah® (tisagenlecleucel),” *PRESS RELEASE*, 2018. [Online]. Available: https://www.novartis.com/news/media-releases/novartis-receives-european-commission-approval-its-car-t-cell-therapy-kymriah-tisagenlecleucel. [Accessed: 02-Mar-2019].

[108] Kite Pharma/Gilead, “Yescarta® (Axicabtagene Ciloleucel) Receives European Marketing Authorization for the Treatment of Relapsed or Refractory DLBCL and PMBCL, After Two or More Lines of Systemic Therapy,” *PRESS RELEASE*, 2018. [Online]. Available: https://www.gilead.com/news-and-press/press-room/press-releases/2018/8/yescarta-axicabtagene-ciloleucel-receives-european-marketing-authorization-for-the-treatment-of-relapsed-or-refractory-dlbcl-and-pmbcl-after-two-o. [Accessed: 02-Mar-2019].

[109] M. M. Boyiadzis *et al.*, “Chimeric antigen receptor (CAR) T therapies for the treatment of hematologic malignancies: clinical perspective and significance,” *J. Immunother. Cancer*, vol. 6, no. 1, p. 137, 2018.

[110] S. L. Maude *et al.*, “Chimeric antigen receptor T cells for sustained remissions in leukemia.,” *N. Engl. J. Med.*, vol. 371, no. 16, pp. 1507–1517, Oct. 2014.

[111] S. J. Schuster *et al.*, “Chimeric Antigen Receptor T Cells in Refractory B-Cell Lymphomas.,” *N. Engl. J. Med.*, vol. 377, no. 26, pp. 2545–2554, Dec. 2017.

[112] S. S. Neelapu *et al.*, “Axicabtagene Ciloleucel CAR T-Cell Therapy in Refractory Large B-Cell Lymphoma.,” *N. Engl. J. Med.*, vol. 377, no. 26, pp. 2531–2544, Dec. 2017.

[113] M. Ruella and M. V. Maus, “Catch me if you can: Leukemia Escape after CD19-Directed T Cell Immunotherapies,” *Comput. Struct. Biotechnol. J.*, vol. 14, pp. 357–362, 2016.

[114] G. Cooper, *The Cell: A Molecular Approach.*, 2nd ed. Sunderland (MA): Sinauer Associates, 2000.

[115] H. M. Knochelmann, A. S. Smith, C. J. Dwyer, M. M. Wyatt, S. Mehrotra, and C. M. Paulos, “CAR T Cells in Solid Tumors: Blueprints for Building Effective Therapies,” *Front. Immunol.*, vol. 9, p. 1740, Jul. 2018.

[116] R. A. Morgan, J. C. Yang, M. Kitano, M. E. Dudley, C. M. Laurencot, and S. A. Rosenberg, “Case report of a serious adverse event following the administration of T cells transduced with a chimeric antigen receptor recognizing ERBB2.,” *Mol. Ther.*, vol. 18, no. 4, pp. 843–851, Apr. 2010.

[117] C. Zhang *et al.*, “Phase I Escalating-Dose Trial of CAR-T Therapy Targeting CEA(+) Metastatic Colorectal Cancers.,” *Mol. Ther.*, vol. 25, no. 5, pp. 1248–1258, May 2017.

[118] C. H. Lamers *et al.*, “Treatment of metastatic renal cell carcinoma with CAIX CAR-engineered T cells: clinical evaluation and management of on-target toxicity.,” *Mol. Ther.*, vol. 21, no. 4, pp. 904–912, Apr. 2013.

[119] M. M. D’Aloia, I. G. Zizzari, B. Sacchetti, L. Pierelli, and M. Alimandi, “CAR-T cells: the long and winding road to solid tumors,” *Cell Death Dis.*, vol. 9, no. 3, p. 282, 2018.

[120] L. J. Old, “Cancer/Testis (CT) antigens - a new link between gametogenesis and cancer,” *Cancer Immun. Arch.*, vol. 1, no. 1, p. 1, Jan. 2001.

[121] L. G. Almeida *et al.*, “CTdatabase: a knowledge-base of high-throughput and curated data on cancer-testis antigens.,” *Nucleic Acids Res.*, vol. 37, no. Database issue, pp. D816-9, Jan. 2009.

[122] O. Hofmann *et al.*, “Genome-wide analysis of cancer/testis gene expression.,” *Proc. Natl. Acad. Sci. U. S. A.*, vol. 105, no. 51, pp. 20422–20427, Dec. 2008.

[123] E. Fratta *et al.*, “The biology of cancer testis antigens: putative function, regulation and therapeutic potential.,” *Mol. Oncol.*, vol. 5, no. 2, pp. 164–182, Apr. 2011.

[124] S. Liu *et al.*, “MAGE-A11 is activated through TFCP2/ZEB1 binding sites de-methylation as well as histone modification and facilitates ESCC tumor growth.,” *Oncotarget*, vol. 9, no. 3, pp. 3365–3378, Jan. 2018.

[125] J.-X. Zhou, Y. Li, S.-X. Chen, and A.-M. Deng, “Expression and prognostic significance of cancer-testis antigens (CTA) in intrahepatic cholagiocarcinoma,” *J. Exp. Clin. Cancer Res.*, vol. 30, no. 1, p. 2, Jan. 2011.

[126] Z. F. Miao *et al.*, “Overexpression of SPAG9 in human gastric cancer is correlated with poor prognosis,” *Virchows Arch.*, vol. 467, no. 5, pp. 525–533, 2015.

[127] K. Iura *et al.*, “Cancer-testis antigens PRAME and NY-ESO-1 correlate with tumour grade and poor prognosis in myxoid liposarcoma.,” *J. Pathol. Clin. Res.*, vol. 1, no. 3, pp. 144–159, Jul. 2015.

[128] O. L. Caballero and Y.-T. Chen, “Cancer/testis (CT) antigens: potential targets for immunotherapy.,” *Cancer Sci.*, vol. 100, no. 11, pp. 2014–2021, Nov. 2009.

[129] A. W. Whitehurst, “Cause and consequence of cancer/testis antigen activation in cancer.,” *Annu. Rev. Pharmacol. Toxicol.*, vol. 54, pp. 251–272, 2014.

[130] M. Fijak and A. Meinhardt, “The testis in immune privilege.,” *Immunol. Rev.*, vol. 213, pp. 66–81, Oct. 2006.

[131] M. F. Gjerstorff, M. H. Andersen, and H. J. Ditzel, “Oncogenic cancer/testis antigens: prime candidates for immunotherapy.,” *Oncotarget*, vol. 6, no. 18, pp. 15772–15787, Jun. 2015.

[132] P. van der Bruggen *et al.*, “A gene encoding an antigen recognized by cytolytic T lymphocytes on a human melanoma.,” *Science*, vol. 254, no. 5038, pp. 1643–1647, Dec. 1991.

[133] E. Jäger *et al.*, “Simultaneous humoral and cellular immune response against cancer-testis antigen NY-ESO-1: definition of human histocompatibility leukocyte antigen (HLA)-A2-binding peptide epitopes,” *J. Exp. Med.*, vol. 187, no. 2, pp. 265–270, Jan. 1998.

[134] A. Curioni-Fontecedro *et al.*, “MAGE-C1/CT7 is the dominant cancer-testis antigen targeted by humoral immune responses in patients with multiple myeloma.,” *Leukemia*, vol. 22, no. 8. England, pp. 1646–1648, Aug-2008.

[135] J. Gotter, B. Brors, M. Hergenhahn, and B. Kyewski, “Medullary epithelial cells of the human thymus express a highly diverse selection of tissue-specific genes colocalized in chromosomal clusters,” *J. Exp. Med.*, vol. 199, no. 2, pp. 155–166, Jan. 2004.

[136] R. A. Morgan *et al.*, “Cancer regression and neurological toxicity following anti-MAGE-A3 TCR gene therapy.,” *J. Immunother.*, vol. 36, no. 2, pp. 133–151, Feb. 2013.

[137] C. S. Hinrichs and N. P. Restifo, “Reassessing target antigens for adoptive T-cell therapy.,” *Nat. Biotechnol.*, vol. 31, no. 11, pp. 999–1008, Nov. 2013.

[138] J. A. Figueroa *et al.*, “Chimeric antigen receptor engineering: a right step in the evolution of adoptive cellular immunotherapy.,” *Int. Rev. Immunol.*, vol. 34, no. 2, pp. 154–187, Mar. 2015.

[139] T. Luetkens, Y. Cao, K. Bartels, S. Meyer, C. Bokemeyer, and D. Atanackovic, “Expression of the cancer-testis antigen FMR1NB on the surface of malignant cells.,” *J. Clin. Oncol.*, vol. 28, no. 15_suppl, pp. e13045–e13045, May 2010.

[140] S. Saini, N. Jagadish, A. Gupta, A. Bhatnagar, and A. Suri, “A Novel Cancer Testis Antigen, A-Kinase Anchor Protein 4 (AKAP4) Is a Potential Biomarker for Breast Cancer,” *PLoS One*, 2013.

[141] M. V Dhodapkar *et al.*, “Expression of cancer/testis (CT) antigens MAGE-A1, MAGE-A3, MAGE-A4, CT-7, and NY-ESO-1 in malignant gammopathies is heterogeneous and correlates with site, stage and risk status of disease.,” *Cancer Immun.*, vol. 3, p. 9, Jul. 2003.

[142] R. M. Turner, L. R. Johnson, L. Haig-Ladewig, G. L. Gerton, and S. B. Moss, “An X-linked gene encodes a major human sperm fibrous sheath protein, hAKAP82. Genomic organization, protein kinase A-RII binding, and distribution of the precursor in the sperm tail.,” *J. Biol. Chem.*, vol. 273, no. 48, pp. 32135–32141, Nov. 1998.

[143] Y. Hu, H. Hu, A. J. Park, D. A. O’Brien, G. Shaw, and M. B. Renfree, “A-kinase anchoring protein 4 has a conserved role in mammalian spermatogenesis,” *Reproduction*, vol. 137, no. 4, pp. 645–653, 2009.

[144] K. Miki, W. D. Willis, P. R. Brown, E. H. Goulding, K. D. Fulcher, and E. M. Eddy, “Targeted disruption of the Akap4 gene causes defects in sperm flagellum and motility.,” *Dev. Biol.*, vol. 248, no. 2, pp. 331–342, Aug. 2002.

[145] F. Jumeau *et al.*, “A-kinase anchor protein 4 precursor (pro-AKAP4) in human spermatozoa.,” *Andrology*, vol. 6, no. 6, pp. 854–859, Nov. 2018.

[146] K. Miki and E. M. Eddy, “Single amino acids determine specificity of binding of protein kinase A regulatory subunits by protein kinase A anchoring proteins.,” *J. Biol. Chem.*, vol. 274, no. 41, pp. 29057–29062, Oct. 1999.

[147] L. Rahamim Ben-Navi, T. Almog, Z. Yao, R. Seger, and Z. Naor, “A-Kinase Anchoring Protein 4 (AKAP4) is an ERK1/2 substrate and a switch molecule between cAMP/PKA and PKC/ERK1/2 in human spermatozoa.,” *Sci. Rep.*, vol. 6, no. March, p. 37922, Nov. 2016.

[148] A. Dema *et al.*, “Pharmacological targeting of AKAP-directed compartmentalized cAMP signalling.,” *Cell. Signal.*, vol. 27, no. 12, pp. 2474–2487, Dec. 2015.

[149] S. Agarwal *et al.*, “The novel cancer-testis antigen A-kinase anchor protein 4 (AKAP4) is a potential target for immunotherapy of ovarian serous carcinoma.,” *Oncoimmunology*, vol. 2, no. 5, p. e24270, May 2013.

[150] V. Kumar, N. Jagadish, and A. Suri, “Role of A-Kinase anchor protein (AKAP4) in growth and survival of ovarian cancer cells,” *Oncotarget*, vol. 8, no. 32, pp. 53124–53136, Aug. 2017.

[151] M. Chiriva-Internati *et al.*, “AKAP-4: a novel cancer testis antigen for multiple myeloma.,” *British journal of haematology*, vol. 140, no. 4. England, pp. 465–468, Feb-2008.

[152] M. Chiriva-Internati *et al.*, “Identification of AKAP-4 as a new cancer/testis antigen for detection and immunotherapy of prostate cancer,” *Prostate*, 2012.

[153] N. Jagadish *et al.*, “A-kinase anchor protein 4 (AKAP4) a promising therapeutic target of colorectal cancer.,” *J. Exp. Clin. Cancer Res.*, vol. 34, p. 142, Nov. 2015.

[154] L. Mirandola *et al.*, “Novel antigens in non-small cell lung cancer: SP17, AKAP4, and PTTG1 are potential immunotherapeutic targets,” *Oncotarget*, vol. 6, no. 5, 2015.

[155] S. Saini *et al.*, “Gene silencing of A-kinase anchor protein 4 inhibits cervical cancer growth in vitro and in vivo.,” *Cancer Gene Ther.*, vol. 20, no. 7, pp. 413–420, Jul. 2013.

[156] I. A. Lea, R. T. Richardson, E. E. Widgren, and M. G. O’Rand, “Cloning and sequencing of cDNAs encoding the human sperm protein, Sp17.,” *Biochim. Biophys. Acta*, vol. 1307, no. 3, pp. 263–266, Jul. 1996.

[157] Y. Wen, R. T. Richardson, and M. G. O’rand, “Processing of the sperm protein Sp17 during the acrosome reaction and characterization as a calmodulin binding protein.,” *Dev. Biol.*, vol. 206, no. 2, pp. 113–122, Feb. 1999.

[158] J. Frayne and L. Hall, “A re-evaluation of sperm protein 17 (Sp17) indicates a regulatory role in an A-kinase anchoring protein complex, rather than a unique role in sperm-zona pellucida binding,” *Reproduction*, vol. 124, no. 6, pp. 767–774, 2002.

[159] S. B. McLeskey, C. Dowds, R. Carballada, R. R. White, and P. M. Saling, “Molecules involved in mammalian sperm-egg interaction.,” *Int. Rev. Cytol.*, vol. 177, pp. 57–113, 1998.

[160] Y. Wen, R. T. Richardson, E. E. Widgren, and M. G. O’Rand, “Characterization of Sp17: a ubiquitous three domain protein that binds heparin.,” *Biochem. J.*, vol. 357, no. Pt 1, pp. 25–31, Jul. 2001.

[161] J. M. Straughn *et al.*, “Expression of sperm protein 17 (Sp17) in ovarian cancer,” *Int. J. Cancer*, 2004.

[162] M. Chiriva-Internati *et al.*, “A NOD/SCID tumor model for human ovarian cancer that allows tracking of tumor progression through the biomarker Sp17,” *J. Immunol. Methods*, vol. 321, no. 1–2, pp. 86–93, 2007.

[163] S. H. Lim, Z. Wang, M. Chiriva-Internati, and Y. Xue, “Sperm protein 17 is a novel cancer-testis antigen in multiple myeloma,” *Blood*, vol. 97, no. 5, pp. 1508–1510, 2001.

[164] H. Marie Lacy and R. D. Sanderson, “Sperm protein 17 is expressed on normal and malignant lymphocytes and promotes heparan sulfate-mediated cell-cell adhesion,” *Blood*, vol. 98, no. 7, pp. 2160–2165, 2001.

[165] L. Mirandola *et al.*, “Cancer testis antigen Sperm Protein 17 as a new target for triple negative breast cancer immunotherapy.,” *Oncotarget*, vol. 8, no. 43, pp. 74378–74390, Sep. 2017.

[166] C. A. Schutt *et al.*, “The cancer-testis antigen, sperm protein 17, a new biomarker and immunological target in head and neck squamous cell carcinoma.,” *Oncotarget*, vol. 8, no. 59, pp. 100280–100287, Nov. 2017.

[167] G. Gupta, R. Sharma, T. K. Chattopadhyay, S. D. Gupta, and R. Ralhan, “Clinical significance of sperm protein 17 expression and immunogenicity in esophageal cancer.,” *Int. J. cancer*, vol. 120, no. 8, pp. 1739–1747, Apr. 2007.

[168] Q. Y. Xia, S. Liu, F. Q. Li Dr., W. Bin Huang, L. N. Shi, and X. J. Zhou, “Sperm protein 17, MAGE-C1 and NY-ESO-1 in hepatocellular carcinoma: Expression frequency and their correlation with clinical parameters,” *Int. J. Clin. Exp. Pathol.*, 2013.

[169] M. F. Gjerstorff and H. J. Ditzel, “Limited SP17 expression within tumors diminishes its therapeutic potential,” *Tissue Antigens*, 2012.

[170] “Grizzi et al., 2004. Sperm Protein 17 Is Expressed in Human Somatic Ciliated Epithelia.”

[171] M. Chiriva-Internati *et al.*, “Sperm protein 17 is a suitable target for adoptive T-cell-based immunotherapy in human ovarian cancer,” *J. Immunother.*, vol. 31, no. 8, pp. 693–703, 2008.

[172] A. R. Dadabayev, Z. Wang, Y. Zhang, J. Zhang, W. R. Robinson, and S. H. Lim, “Cancer immunotherapy targeting Sp17: when should the laboratory findings be translated to the clinics?,” *Am. J. Hematol.*, vol. 80, no. 1, pp. 6–11, Sep. 2005.

[173] S. Shankar, B. Mohapatra, and A. Suri, “Cloning of a novel human testis mRNA specifically expressed in testicular haploid germ cells, having unique palindromic sequences and encoding a leucine zipper dimerization motif,” *Biochem. Biophys. Res. Commun.*, vol. 243, no. 2, pp. 561–565, 1998.

[174] N. Jagadish *et al.*, “Characterization of a novel human sperm-associated antigen 9 (SPAG9) having structural homology with c-Jun N-terminal kinase-interacting protein,” *Biochem. J.*, vol. 389, no. Pt 1, pp. 73–82, Jul. 2005.

[175] F. Chen *et al.*, “SPAG9 expression is increased in human prostate cancer and promotes cell motility, invasion and angiogenesis in vitro.,” *Oncol. Rep.*, vol. 32, no. 6, pp. 2533–2540, Dec. 2014.

[176] D. Kanojia, M. Garg, S. Gupta, A. Gupta, and A. Suri, “Sperm-associated antigen 9 is a novel biomarker for colorectal cancer and is involved in tumor growth and tumorigenicity.,” *Am. J. Pathol.*, vol. 178, no. 3, pp. 1009–1020, Mar. 2011.

[177] “Garg et al., 2007; Sperm-associated antigen 9, a novel cancer testis antigen, is a potential target for immunotherapy in epithelial ovarian cancer.”

[178] J. H. Ha *et al.*, “Aberrant expression of JNK-associated leucine-zipper protein, JLP, promotes accelerated growth of ovarian cancer.,” *Oncotarget*, vol. 7, no. 45, pp. 72845–72859, Nov. 2016.

[179] M. van Duin *et al.*, “Cancer testis antigens in newly diagnosed and relapse multiple myeloma: Prognostic markers and potential targets for immunotherapy,” *Haematologica*, vol. 96, no. 11, pp. 1662–1669, 2011.

[180] B. Ren *et al.*, “Cancer testis antigen SPAG9 is a promising marker for the diagnosis and treatment of lung cancer,” *Oncol. Rep.*, vol. 35, no. 5, pp. 2599–2605, May 2016.

[181] M. Garg *et al.*, “Sperm-associated antigen 9 is associated with tumor growth, migration, and invasion in renal cell carcinoma.,” *Cancer Res.*, vol. 68, no. 20, pp. 8240–8248, Oct. 2008.

[182] N. Jagadish *et al.*, “Sperm-associated antigen 9 (SPAG9) promotes the survival and tumor growth of triple-negative breast cancer cells.,” *Tumour Biol.*, vol. 37, no. 10, pp. 13101–13110, Oct. 2016.

[183] M. Kawamura, T. Taki, H. Kaku, K. Ohki, and Y. Hayashi, “Identification of SPAG9 as a novel JAK2 fusion partner gene in pediatric acute lymphoblastic leukemia with t(9;17)(p24;q21).,” *Genes. Chromosomes Cancer*, vol. 54, no. 7, pp. 401–408, Jul. 2015.

[184] D. Kanojia, M. Garg, S. Saini, S. Agarwal, R. Kumar, and A. Suri, “Sperm associated antigen 9 expression and humoral response in chronic myeloid leukemia,” *Leuk. Res.*, vol. 34, no. 7, pp. 858–863, Jul. 2010.

[185] S. Agarwal *et al.*, “Sperm associated antigen 9 (SPAG9) expression and humoral response in benign and malignant salivary gland tumors.,” *Oncoimmunology*, vol. 3, no. 12, p. e974382, 2014.

[186] J. Pan *et al.*, “Emerging role of sperm-associated antigen 9 in tumorigenesis.,” *Biomed. Pharmacother.*, vol. 103, pp. 1212–1216, Jul. 2018.

[187] A. Suri *et al.*, “Cancer testis antigens: A new paradigm for cancer therapy.,” *Oncoimmunology*, vol. 1, no. 7, pp. 1194–1196, Oct. 2012.

[188] P. Diebolder *et al.*, “Generation of ‘LYmph Node Derived Antibody Libraries’ (LYNDAL) for selecting fully human antibody fragments with therapeutic potential.,” *MAbs*, vol. 6, no. 1, pp. 130–142, 2014.

[189] R. Kontermann and S. Dübel, Eds., *Antibody Engineering*. Berlin, Heidelberg: Springer Berlin Heidelberg, 2010.

[190] X. Brochet, M.-P. Lefranc, and V. Giudicelli, “IMGT/V-QUEST: the highly customized and integrated system for IG and TR standardized V-J and V-D-J sequence analysis.,” *Nucleic Acids Res.*, vol. 36, no. Web Server issue, pp. W503-8, Jul. 2008.

[191] I. Retter, H. H. Althaus, R. Münch, and W. Müller, “VBASE2, an integrative V gene database,” *Nucleic Acids Res.*, vol. 33, no. suppl_1, pp. D671–D674, 2005.

[192] J. Kügler *et al.*, “Generation and analysis of the improved human HAL9/10 antibody phage display libraries,” *BMC Biotechnol.*, vol. 15, no. 1, p. 10, Feb. 2015.

[193] L. Noll, “Cancer-testis antigen specific single chain variable fragments as tumor targeting domain for chimeric antigen receptors,” *Unpubl. master’s thesis*, 2018.

[194] G. Hermanson, *Bioconjugate Techniques*, 3rd ed. Academic Press, 2013.

[195] T. T. Wu, G. Johnson, and E. A. Kabat, “Length distribution of CDRH3 in antibodies.,” *Proteins*, vol. 16, no. 1, pp. 1–7, May 1993.

[196] H. Shirai, A. Kidera, and H. Nakamura, “H3-rules: identification of CDR-H3 structures in antibodies,” *FEBS Lett.*, vol. 455, no. 1, pp. 188–197, 1999.

[197] F. Matsuda *et al.*, “The complete nucleotide sequence of the human immunoglobulin heavy chain variable region locus,” *J. Exp. Med.*, vol. 188, no. 11, pp. 2151–2162, Dec. 1998.

[198] T. R. Poulsen, A. Jensen, J. S. Haurum, and P. S. Andersen, “Limits for antibody affinity maturation and repertoire diversification in hypervaccinated humans.,” *J. Immunol.*, vol. 187, no. 8, pp. 4229–4235, Oct. 2011.

[199] A. W. Vermeer and W. Norde, “The thermal stability of immunoglobulin: unfolding and aggregation of a multi-domain protein,” *Biophys. J.*, vol. 78, no. 1, pp. 394–404, Jan. 2000.

[200] J. J. M. van Dongen *et al.*, “EuroFlow antibody panels for standardized n-dimensional flow cytometric immunophenotyping of normal, reactive and malignant leukocytes.,” *Leukemia*, vol. 26, no. 9, pp. 1908–1975, Sep. 2012.

[201] J. Flores-Montero *et al.*, “Immunophenotype of normal vs. myeloma plasma cells: Toward antibody panel specifications for MRD detection in multiple myeloma,” *Cytom. Part B - Clin. Cytom.*, vol. 90, no. 1, pp. 61–72, 2016.

[202] S. V. Rajkumar, “Updated Diagnostic Criteria and Staging System for Multiple Myeloma.,” *Am. Soc. Clin. Oncol. Educ. book. Am. Soc. Clin. Oncol. Annu. Meet.*, vol. 35, pp. e418-23, 2016.

[203] L. Torti, S. Pulini, A. M. Morelli, F. Bacci, and P. Di Bartolomeo, “New Myeloma Diagnostic Criteria: To Treat or Not to Treat? Monocentric Experience of 220 Newly Multiple Myeloma Diagnosed Patients Retrospectively Analyzed,” *Blood*, vol. 128, no. 22, p. 5629 LP-5629, Dec. 2016.

[204] D. Altschuh, M. C. Dubs, E. Weiss, G. Zeder-Lutz, and M. H. Van Regenmortel, “Determination of kinetic constants for the interaction between a monoclonal antibody and peptides using surface plasmon resonance.,” *Biochemistry*, vol. 31, no. 27, pp. 6298–6304, Jul. 1992.

[205] P. Gomes, E. Giralt, and D. Andreu, “Direct single-step surface plasmon resonance analysis of interactions between small peptides and immobilized monoclonal antibodies.,” *J. Immunol. Methods*, vol. 235, no. 1–2, pp. 101–111, Feb. 2000.

[206] M. J. Frigault *et al.*, “Identification of Chimeric Antigen Receptors That Mediate Constitutive or Inducible Proliferation of T Cells,” *Cancer Immunol. Res.*, vol. 3, no. 4, pp. 356–367, Apr. 2015.

[207] J. A. Fraietta *et al.*, “Determinants of response and resistance to CD19 chimeric antigen receptor (CAR) T cell therapy of chronic lymphocytic leukemia,” *Nat. Med.*, vol. 24, no. 5, pp. 563–571, 2018.

[208] D. Gomes da Silva *et al.*, “Direct Comparison of In Vivo Fate of Second and Third-Generation CD19-Specific Chimeric Antigen Receptor (CAR)-T Cells in Patients with B-Cell Lymphoma: Reversal of Toxicity from Tonic Signaling,” *Blood*, vol. 128, no. 22, p. 1851 LP-1851, Dec. 2016.

[209] S. Guedan *et al.*, “Enhancing CAR T cell persistence through ICOS and 4-1BB costimulation,” *JCI insight*, vol. 3, no. 1, p. e96976, Jan. 2018.

[210] O. O. Yeku, T. J. Purdon, M. Koneru, D. Spriggs, and R. J. Brentjens, “Armored CAR T cells enhance antitumor efficacy and overcome the tumor microenvironment,” *Sci. Rep.*, vol. 7, no. 1, pp. 1–14, 2017.

[211] P. Gorak-Stolinska, J. P. Truman, D. M. Kemeny, and A. Noble, “Activation-induced cell death of human T-cell subsets is mediated by Fas and granzyme B but is independent of TNF-alpha.,” *J. Leukoc. Biol.*, vol. 70, no. 5, pp. 756–766, Nov. 2001.

[212] J. S. Yi, M. A. Cox, and A. J. Zajac, “T-cell exhaustion: characteristics, causes and conversion,” *Immunology*, vol. 129, no. 4, pp. 474–481, Apr. 2010.

[213] T. Gargett *et al.*, “GD2-specific CAR T Cells Undergo Potent Activation and Deletion Following Antigen Encounter but can be Protected From Activation-induced Cell Death by PD-1 Blockade,” *Mol. Ther.*, vol. 24, no. 6, pp. 1135–1149, Jun. 2016.

[214] T. Kamiya, D. Wong, Y. T. Png, and D. Campana, “A novel method to generate T-cell receptor-deficient chimeric antigen receptor T cells.,” *Blood Adv.*, vol. 2, no. 5, pp. 517–528, Mar. 2018.

[215] N. Ke, X. Wang, X. Xu, and Y. A. Abassi, “The xCELLigence system for real-time and label-free monitoring of cell viability.,” *Methods Mol. Biol.*, vol. 740, pp. 33–43, 2011.

[216] A. J. Davenport *et al.*, “CAR-T Cells Inflict Sequential Killing of Multiple Tumor Target Cells.,” *Cancer Immunol. Res.*, vol. 3, no. 5, pp. 483–494, May 2015.

[217] B. L. Levine, J. Miskin, K. Wonnacott, and C. Keir, “Global Manufacturing of CAR T Cell Therapy,” *Mol. Ther. - Methods Clin. Dev.*, vol. 4, pp. 92–101, 2017.

[218] B. Tumaini *et al.*, “Simplified process for the production of anti-CD19-CAR-engineered T cells,” *Cytotherapy*, vol. 15, no. 11, pp. 1406–1415, Nov. 2013.

[219] A. Suri, N. Jagadish, S. Saini, and N. Gupta, “Targeting cancer testis antigens for biomarkers and immunotherapy in colorectal cancer: Current status and challenges,” *World J. Gastrointest. Oncol.*, vol. 7, no. 12, p. 492, 2015.

[220] N. Kelkar, C. L. Standen, and R. J. Davis, “Role of the JIP4 scaffold protein in the regulation of mitogen-activated protein kinase signaling pathways.,” *Mol. Cell. Biol.*, vol. 25, no. 7, pp. 2733–43, 2005.

[221] D. W. Carr, A. Fujita, C. L. Stentz, G. A. Liberty, G. E. Olson, and S. Narumiya, “Identification of Sperm-specific Proteins that Interact with A-kinase Anchoring Proteins in a Manner Similar to the Type II Regulatory Subunit of PKA,” *J. Biol. Chem.*, vol. 276, no. 20, pp. 17332–17338, 2001.

[222] Z. Wang, Y. Zhang, B. Ramsahoye, D. Bowen, and S. H. Lim, “Sp17 gene expression in myeloma cells is regulated by promoter methylation,” *Br. J. Cancer*, vol. 91, p. 1597, Sep. 2004.

[223] N. Jagadish *et al.*, “Sperm associated antigen 9 (SPAG9) a promising therapeutic target of ovarian carcinoma,” *Tumor Biol.*, vol. 40, no. 5, pp. 1–13, 2018.

[224] U. H. Weidle, D. Maisel, S. Klostermann, C. Schiller, and E. H. Weiss, “Intracellular proteins displayed on the surface of tumor cells as targets for therapeutic intervention with antibody-related agents.,” *Cancer Genomics Proteomics*, vol. 8, no. 2, pp. 49–63, 2011.

[225] Y.-L. Tsai, Y. Zhang, C.-C. Tseng, R. Stanciauskas, F. Pinaud, and A. S. Lee, “Characterization and mechanism of stress-induced translocation of 78-kilodalton glucose-regulated protein (GRP78) to the cell surface.,” *J. Biol. Chem.*, vol. 290, no. 13, pp. 8049–8064, Mar. 2015.

[226] K. Milne *et al.*, “Tumor-infiltrating T cells correlate with NY-ESO-1-specific autoantibodies in ovarian cancer.,” *PLoS One*, vol. 3, no. 10, p. e3409, 2008.

[227] M. H. Hansen, H. V Nielsen, and H. J. Ditzel, “Translocation of an intracellular antigen to the surface of medullary breast cancer cells early in apoptosis allows for an antigen-driven antibody response elicited by tumor-infiltrating B cells.,” *J. Immunol.*, vol. 169, no. 5, pp. 2701–2711, Sep. 2002.

[228] K. Shires and T. Van Wyk, “The role of Cancer/Testis Antigens in Multiple Myeloma pathogenesis and their application in disease monitoring and therapy.,” *Crit. Rev. Oncol. Hematol.*, vol. 132, pp. 17–26, Dec. 2018.

[229] A. P. Liggins, S. H. Lim, E. J. Soilleux, K. Pulford, and A. H. Banham, “A panel of cancer-testis genes exhibiting broad-spectrum expression in haematological malignancies.,” *Cancer Immun.*, vol. 10, p. 8, Aug. 2010.

[230] F. Grizzi *et al.*, “Sperm protein 17 is not expressed on normal leukocytes.,” *Blood*, vol. 99, no. 9. United States, pp. 3471–3479, May-2002.

[231] M. A. Cheever *et al.*, “The prioritization of cancer antigens: a national cancer institute pilot project for the acceleration of translational research,” *Clin. Cancer Res.*, vol. 15, no. 17, pp. 5323–5337, Sep. 2009.

[232] W. Xiong *et al.*, “Immunological Synapse Predicts Effectiveness of Chimeric Antigen Receptor Cells,” *Mol. Ther.*, vol. 26, no. 4, pp. 963–975, 2018.

[233] D. Sommermeyer *et al.*, “Chimeric antigen receptor-modified T cells derived from defined CD8+ and CD4+ subsets confer superior antitumor reactivity in vivo.,” *Leukemia*, vol. 30, no. 2, pp. 492–500, Feb. 2016.

[234] S. Terakura, T. N. Yamamoto, R. A. Gardner, C. J. Turtle, M. C. Jensen, and S. R. Riddell, “Generation of CD19-chimeric antigen receptor modified CD8+ T cells derived from virus-specific central memory T cells,” *Blood*, vol. 119, no. 1, pp. 72–82, Jan. 2012.

[235] R. D. Guest *et al.*, “The role of extracellular spacer regions in the optimal design of chimeric immune receptors: evaluation of four different scFvs and antigens.,” *J. Immunother.*, vol. 28, no. 3, pp. 203–211, 2005.

[236] H. J. Jackson, S. Rafiq, and R. J. Brentjens, “Driving CAR T-cells forward.,” *Nat. Rev. Clin. Oncol.*, vol. 13, no. 6, pp. 370–383, Jun. 2016.

[237] S. Gill, M. V Maus, and D. L. Porter, “Chimeric antigen receptor T cell therapy: 25years in the making.,” *Blood Rev.*, vol. 30, no. 3, pp. 157–167, May 2016.

[238] S. A. Richman *et al.*, “High-Affinity GD2-Specific CAR T Cells Induce Fatal Encephalitis in a Preclinical Neuroblastoma Model.,” *Cancer Immunol. Res.*, vol. 6, no. 1, pp. 36–46, Jan. 2018.

[239] K. Watanabe, S. Kuramitsu, A. D. Posey, and C. H. June, “Expanding the Therapeutic Window for CAR T Cell Therapy in Solid Tumors: The Knowns and Unknowns of CAR T Cell Biology ,” *Frontiers in Immunology* , vol. 9. p. 2486, 2018.

[240] K. Newick, E. Moon, and S. M. Albelda, “Chimeric antigen receptor T-cell therapy for solid tumors,” *Mol. Ther. - Oncolytics*, vol. 3, p. 16006, 2016.

[241] L. B. John *et al.*, “Anti-PD-1 antibody therapy potently enhances the eradication of established tumors by gene-modified T cells.,” *Clin. Cancer Res.*, vol. 19, no. 20, pp. 5636–5646, Oct. 2013.

[242] S. Rafiq *et al.*, “Targeted delivery of a PD-1-blocking scFv by CAR-T cells enhances anti-tumor efficacy in vivo.,” *Nat. Biotechnol.*, vol. 36, no. 9, pp. 847–858, Oct. 2018.

[243] J. M. Michot *et al.*, “Immune-related adverse events with immune checkpoint blockade: a comprehensive review.,” *Eur. J. Cancer*, vol. 54, pp. 139–148, Feb. 2016.

[244] M. C. Jensen *et al.*, “Antitransgene rejection responses contribute to attenuated persistence of adoptively transferred CD20/CD19-specific chimeric antigen receptor redirected T cells in humans.,” *Biol. Blood Marrow Transplant.*, vol. 16, no. 9, pp. 1245–1256, Sep. 2010.

6 Appendix

6.1 Supplementary data

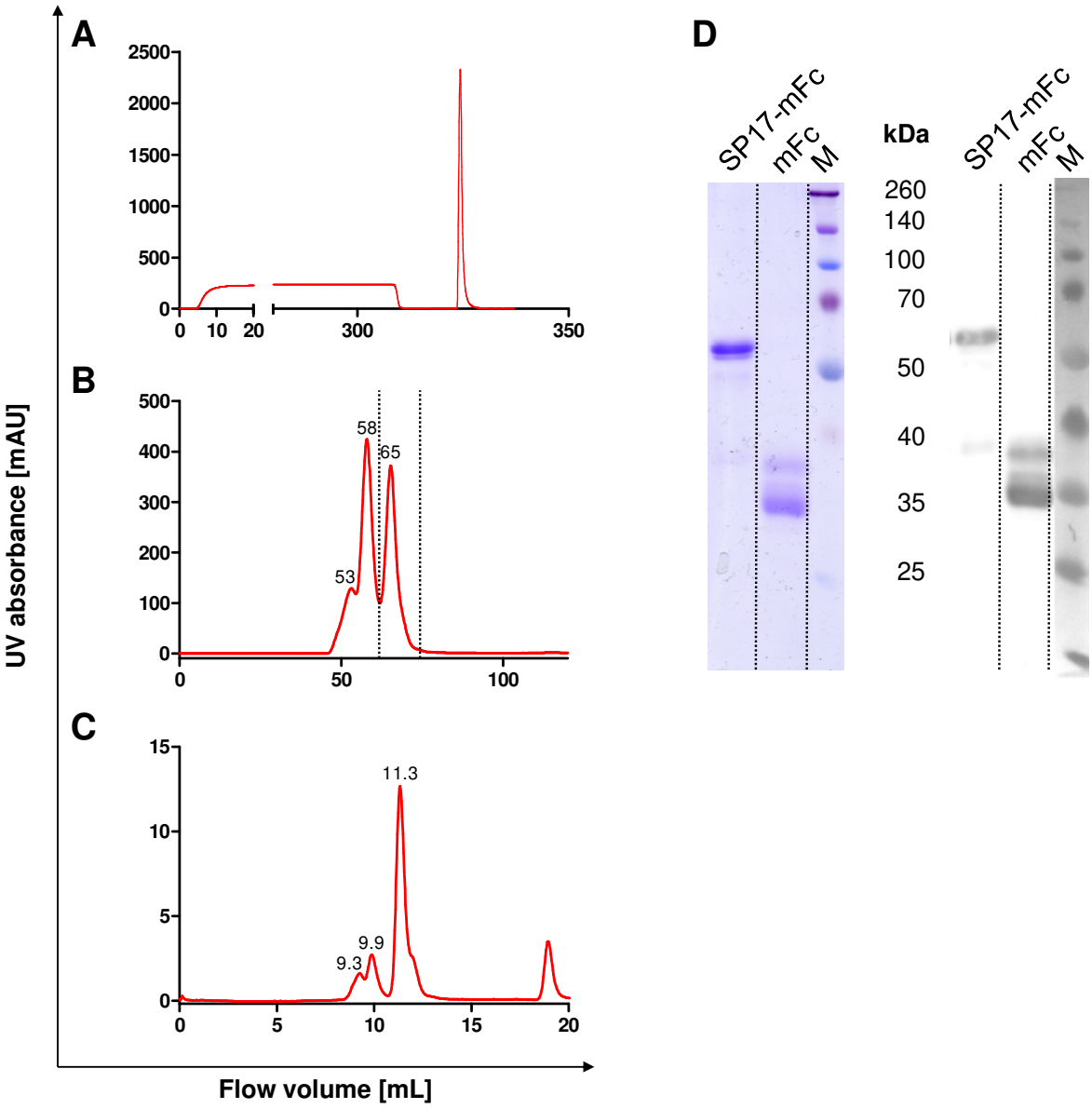

Figure 34. Monitored purification procedure of the SP17-mFc fusion antigen. We transfected HEK293-6E cells with the mammalian expression vector pYD5 that encoded the SP17-mFc antigen sequence and thereby produced the fusion protein. SP17-mFc antigen was purified by **(A)** protein A and **(B)** size exclusion chromatography. **(C)** Analytical SEC revealed only low aggregate fractions within the purified SP17-mFc antigen. **(D)** 2 µg/lane of purified SP17-mFc antigen were separated by SDS gel electrophoresis and visualized by Coomassie Blue staining as well as by western blot using a HRP coupled anti-mouse IgG Fc antibody. Murine Fc (mFc) was included as positive control. M = marker.

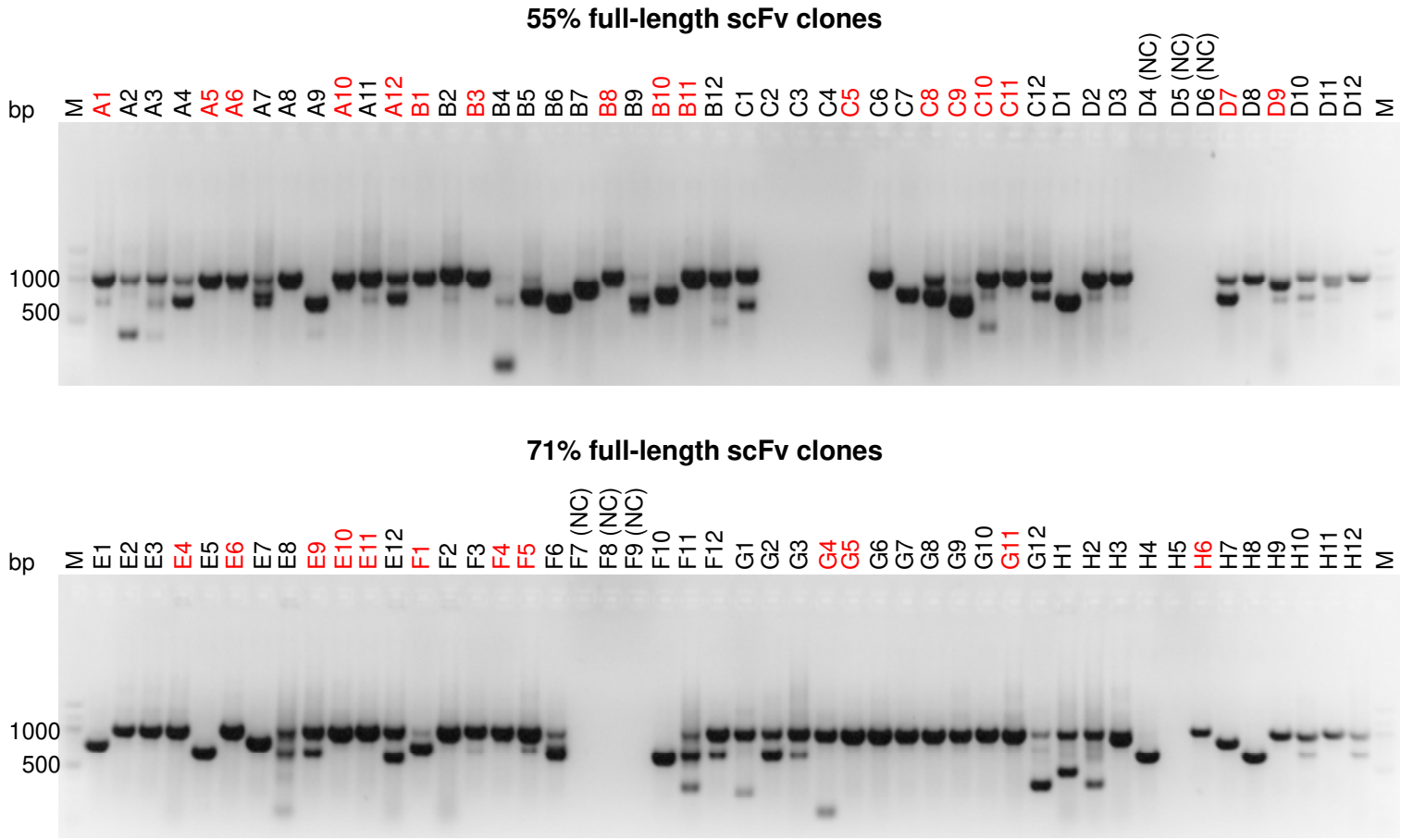

Figure 35. Analysis of αSPAG9 scFv integrity. 90 individual *E. coli* TG1 clones infected with phages from selection round 3 were screened for full-length scFv integrity. These colonies contained the phagemid vector pHENIS encoding for the selected αSPAG9 scFvs. Single colonies were transferred to 25 µL PCR mix and subjected to colony PCR. PCRs were analyzed by agarose gel electrophoresis. ScFv clones that specifically bound to target bio-SPAG9A1A2 antigen in ELISA (*Figure 11B*) are marked in red. NC = negative control (no colony), M = marker.

Table 28. Summary of scFv sequence analysis with the databases IMGT/V-Quest and VBASE2

Clone name	YU138-C01	YU138-D01	YU106-A03	YU106-C02	YU106-D01	YU106-F02	YU106-G01	VD1.E6	YU107-A01	YU107-B01	YU107-D03	YU107-E01	YU107-F03	YU107-G01
Target	AKAP4	AKAP4	SP17	SP17	SP17	SP17	SP17	SPAG9	SPAG9	SPAG9	SPAG9	SPAG9	SPAG9	SPAG9
Heavy chain														
V gene + allele (Identity in %)	IGHV1-2*02 F (99.31)	IGHV1-2*02 F (100.0)	IGHV3-33*01 F (99.65)	IGHV4-34*01 F (98.25)	IGHV4-34*02 F (98.60)	IGHV1-18*01 F (98.61)	IGHV1-18*04 F (98.26)	IGHV1-18*01 F (88.19)	IGHV1-69*14 F (99.65)	IGHV1-69*12 F (99.65)	IGHV3-30*04 F (99.65)	IGHV1-18*01 F (93.75)	IGHV3-23*04 F (97.92)	IGHV1-69*01 F (99.65)
D gene + allele	IGHD5-18*01 F	IGHD2-2*01 F	IGHD3-10*01 F	Not found	Not found	IGHD6-19*01 F	IGHD3-16*01 F	IGHD3-3*01 F	IGHD1-1*01 F	IGHD2-8*02 F	IGHD5-12*01 F	IGHD2-15*01 F	IGHD5-12*01 F	IGHD2-8*02 F
J gene + allele (Identity in %)	IGHJ6*01 F (91.94)	IGHJ6*02 F (90.32)	IGHJ4*02 F (79.17)	IGHJ6*02 F (97.83)	IGHJ6*02 F (76.60)	IGHJ4*02 F (83.33)	IGHJ4*02 F (89.58)	IGHJ6*01 F (69.84)	IGHJ6*02 F (91.94)	IGHJ6*02 F (96.77)	IGHJ4*02 F (95.83)	IGHJ6*02 F (93.55)	IGHJ4*02 F (91.67)	IGHJ6*02 F (96.77)
V region: Number of nt mutations	2	1	1	6	5	4	5	35	1	1	1	18	6	1
V region: Number of AA changes (very dissimilar)	1 (0)	0 (0)	1 (0)	4 (1)	3 (1)	1 (0)	2 (1)	19 (5)	0 (0)	1 (0)	1 (0)	8 (4)	3 (1)	0 (0)
CDR1: Number of AA changes (very dissimilar)	0 (0)	0 (0)	0 (0)	1 (0)	1 (0)	0 (0)	1 (0)	3 (1)	0 (0)	0 (0)	0 (0)	4 (2)	0 (0)	0 (0)
CDR2: Number of AA changes (very dissimilar)	0 (0)	0 (0)	0 (0)	0 (0)	0 (0)	0 (0)	0 (0)	3 (2)	0 (0)	0 (0)	0 (0)	0 (0)	0 (0)	0 (0)
CDR3: Number of AA changes (very dissimilar)	0 (0)	0 (0)	0 (0)	0 (0)	0 (0)	0 (0)	0 (0)	1 (0)	0 (0)	0 (0)	0 (0)	0 (0)	0 (0)	0 (0)
Light chain														
V gene + allele	IGKV1-39*01 F (100.0)	IGKV1-39*01 F (97.13)	IGLV2-18*02 F (95.14)	IGLV1-44*01 F (92.63)	IGLV1-44*01 F (96.84)	IGLV3-19*01 F (96.77)	IGLV3-19*01 F (100.0)	IGKV1-39*01 F (90.32)	IGKV1-27*01 F (99.28)	IGKV1-27*01 F (91.04)	IGLV6-57*01 F (91.75)	IGLV1-47*01 F (98.95)	IGLV4-60*03 F (94.90)	IGKV1-27*01 F (88.89)
J gene + allele	IGKJ 4*01 F (100.0)	IGKJ 3*01 F (97.37)	IGLJ 3*02 F (94.44)	IGLJ 2*01 F (97.14)	IGLJ 3*02 F (94.29)	IGLJ 3*02 F (100.0)	IGLJ 2*01 F (97.22)	IGKJ 4*01 F (94.74)	IGKJ 1*01 F (97.37)	IGKJ 1*01 F (94.74)	IGLJ 3*02 F (100.0)	IGLJ 2*01 F (94.44)	IGLJ 2*01 F (86.84)	IGKJ 1*01 F (94.74)
V region: Number of nt mutations	0	8	14	21	10	9	0	29	2	25	24	3	15	31
V region: Number of AA changes (very dissimilar)	0 (0)	5 (2)	7 (1)	12 (4)	8 (3)	8 (3)	0 (0)	14 (9)	2 (0)	9 (5)	12 (5)	3 (0)	9 (2)	11 (5)
CDR1: Number of AA changes (very dissimilar)	0 (0)	0 (0)	0 (0)	2 (0)	2 (1)	2 (1)	0 (0)	2 (2)	0 (0)	1 (1)	2 (0)	0 (0)	1 (0)	1 (1)
CDR2: Number of AA changes (very dissimilar)	0 (0)	0 (0)	0 (0)	2 (0)	1 (1)	1 (1)	0 (0)	2 (2)	0 (0)	1 (1)	2 (0)	1 (0)	2 (1)	1 (1)
CDR3: Number of AA changes (very dissimilar)	0 (0)	0 (0)	0 (0)	0 (0)	0 (0)	0 (0)	0 (0)	4 (3)	0 (0)	1 (0)	1 (1)	0 (0)	1 (0)	1 (0)

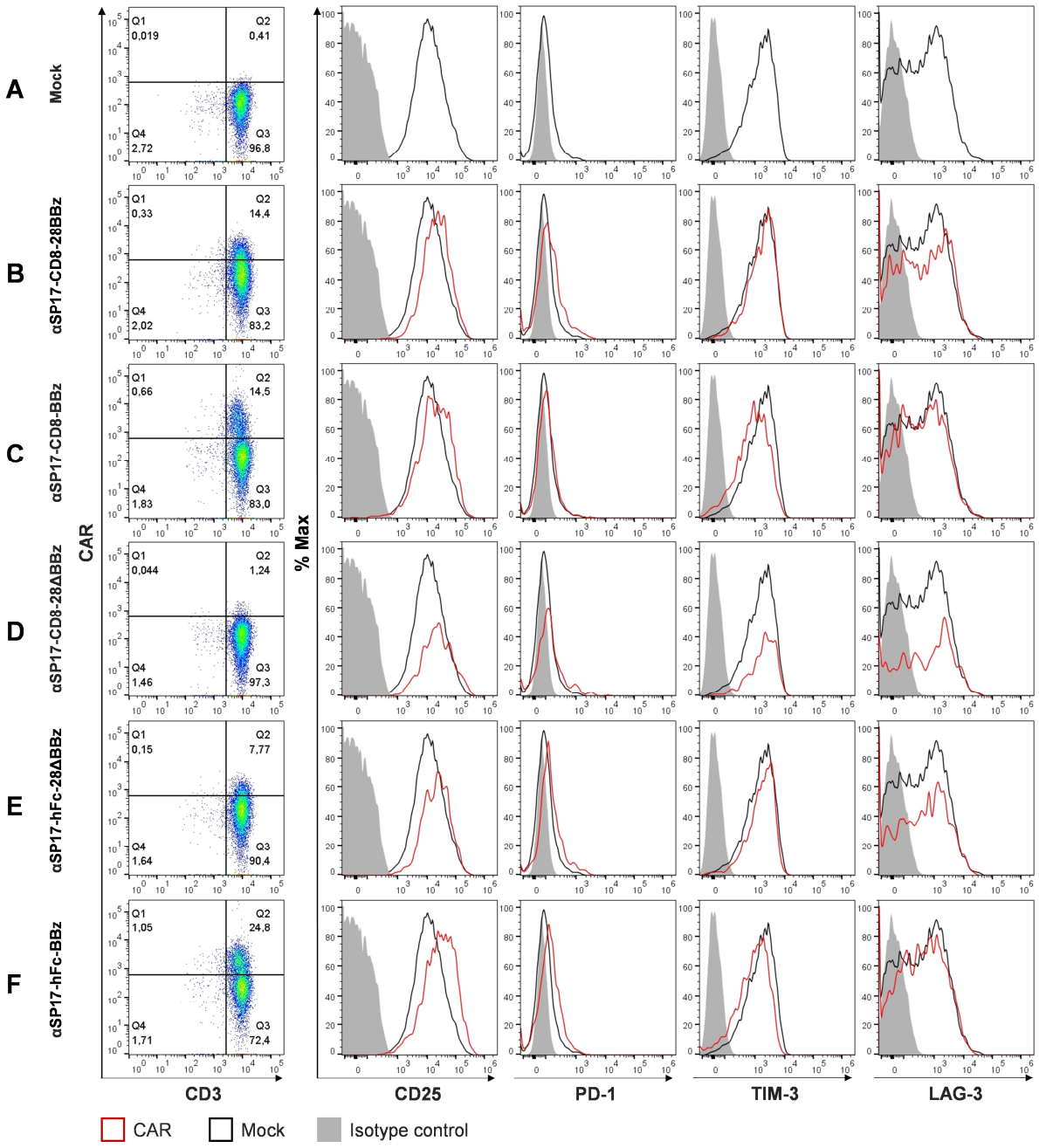

Figure 36. Expression profile of activation and exhaustion markers on αSP17 CAR T cells at day 10 after T cell activation (donor 1). αSP17 CAR positive T cells were analyzed by flow cytometry using APC labeled SP17-mFc target antigen. Activation and exhaustion markers were detected with corresponding fluorochrome coupled antibodies. Activation and exhaustion marker expression on **(A)** mock T cells (black) was compared with that on αSP17 **(B)** -CD8-28BBz, **(C)** -CD8-BBz, **(D)** -CD8-28ΔBBz, **(E)** -hFc-28ΔBBz and **(F)** -hFc-BBz CAR positive cells (red). A human IgG1 antibody with irrelevant specificity was used as isotype control (grey).

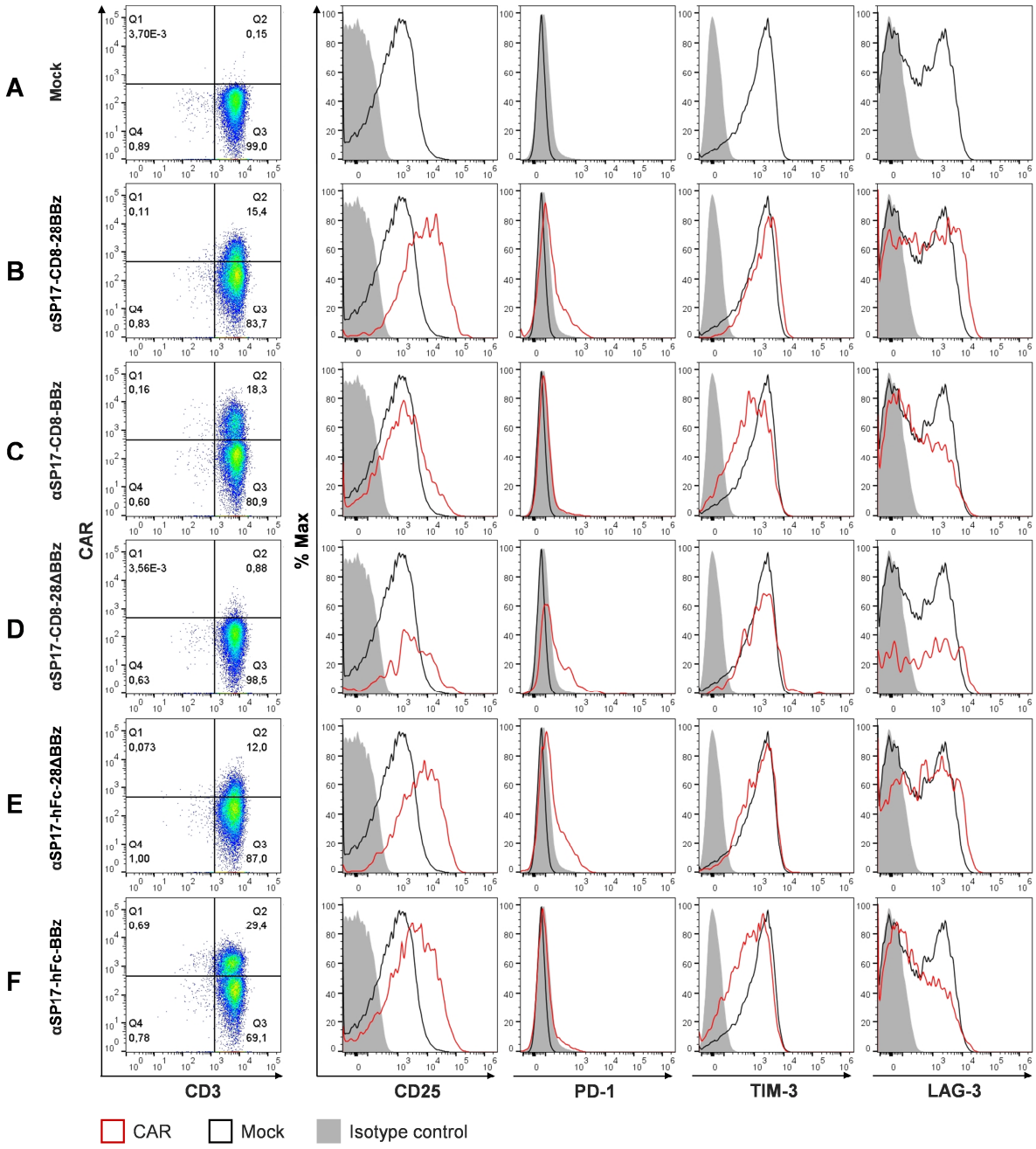

Figure 37. Expression profile of activation and exhaustion markers on αSP17 CAR T cells at day 14 after T cell activation (donor 1). αSP17 CAR positive T cells were analyzed by flow cytometry using APC labeled SP17-mFc target antigen. Activation and exhaustion markers were detected with corresponding fluorochrome coupled antibodies. Activation and exhaustion marker expression on **(A)** mock T cells (black) was compared with that on αSP17 **(B)** -CD8-28BBz, **(C)** -CD8-BBz, **(D)** -CD8-28ΔBBz, **(E)** -hFc-28ΔBBz and **(F)** -hFc-BBz CAR positive cells (red). A human IgG1 antibody with irrelevant specificity was used as isotype control (grey).

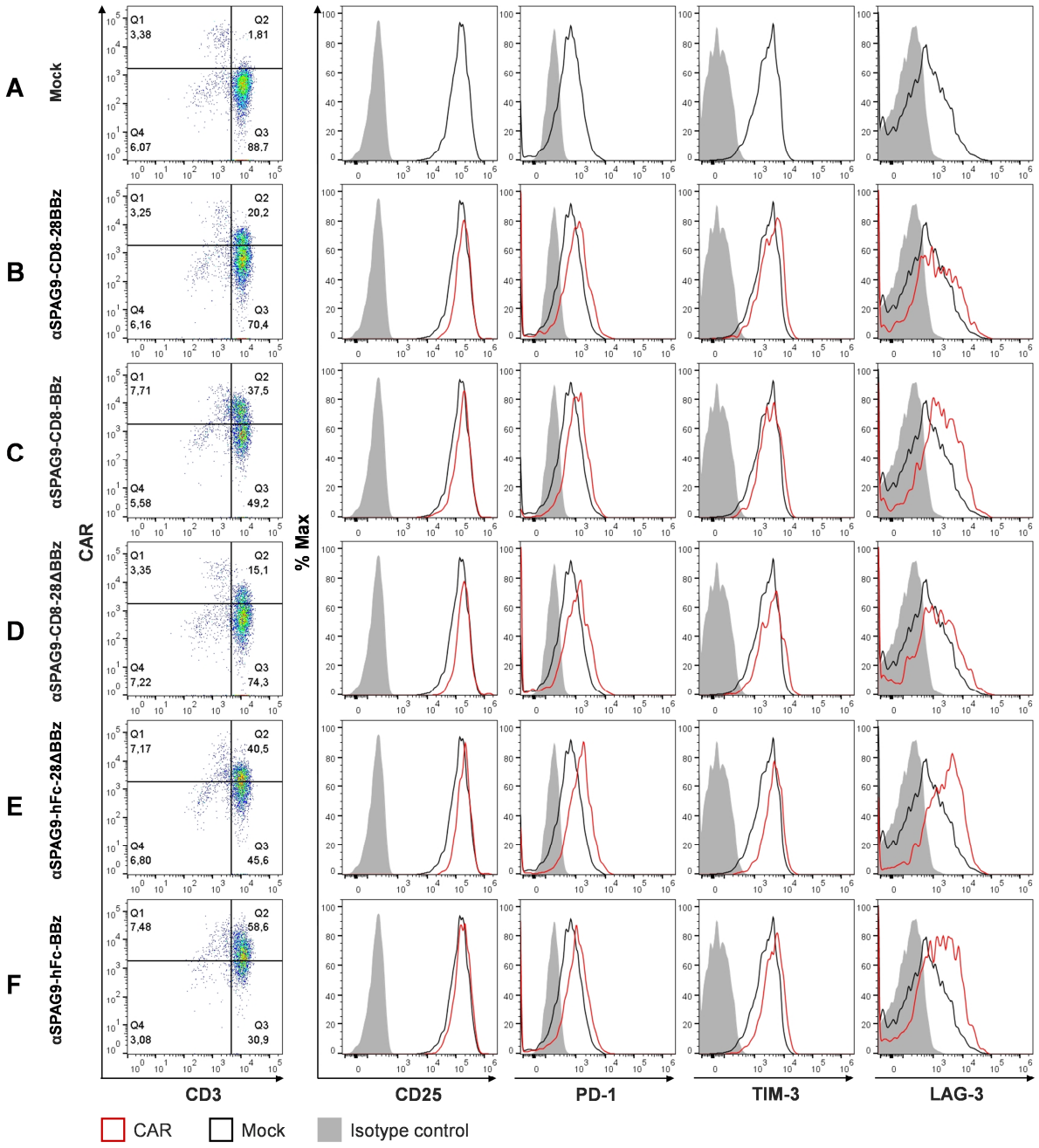

Figure 38. Expression profile of activation and exhaustion markers on αSPAG9 CAR T cells at day 5 after T cell activation (donor 2). αSPAG9 CAR positive T cells were analyzed by flow cytometry using biotinylated protein L combined with APC coupled streptavidin. Activation and exhaustion markers were detected with corresponding fluorochrome coupled antibodies. Activation and exhaustion marker expression on **(A)** mock T cells (black) was compared with that on αSPAG9 **(B)** -CD8-28BBz, **(C)** -CD8-BBz, **(D)** -CD8-28ΔBBz, **(E)** -hFc-28ΔBBz and **(F)** -hFc-BBz CAR positive cells (red). A human IgG1 antibody with irrelevant specificity was used as isotype control (grey).

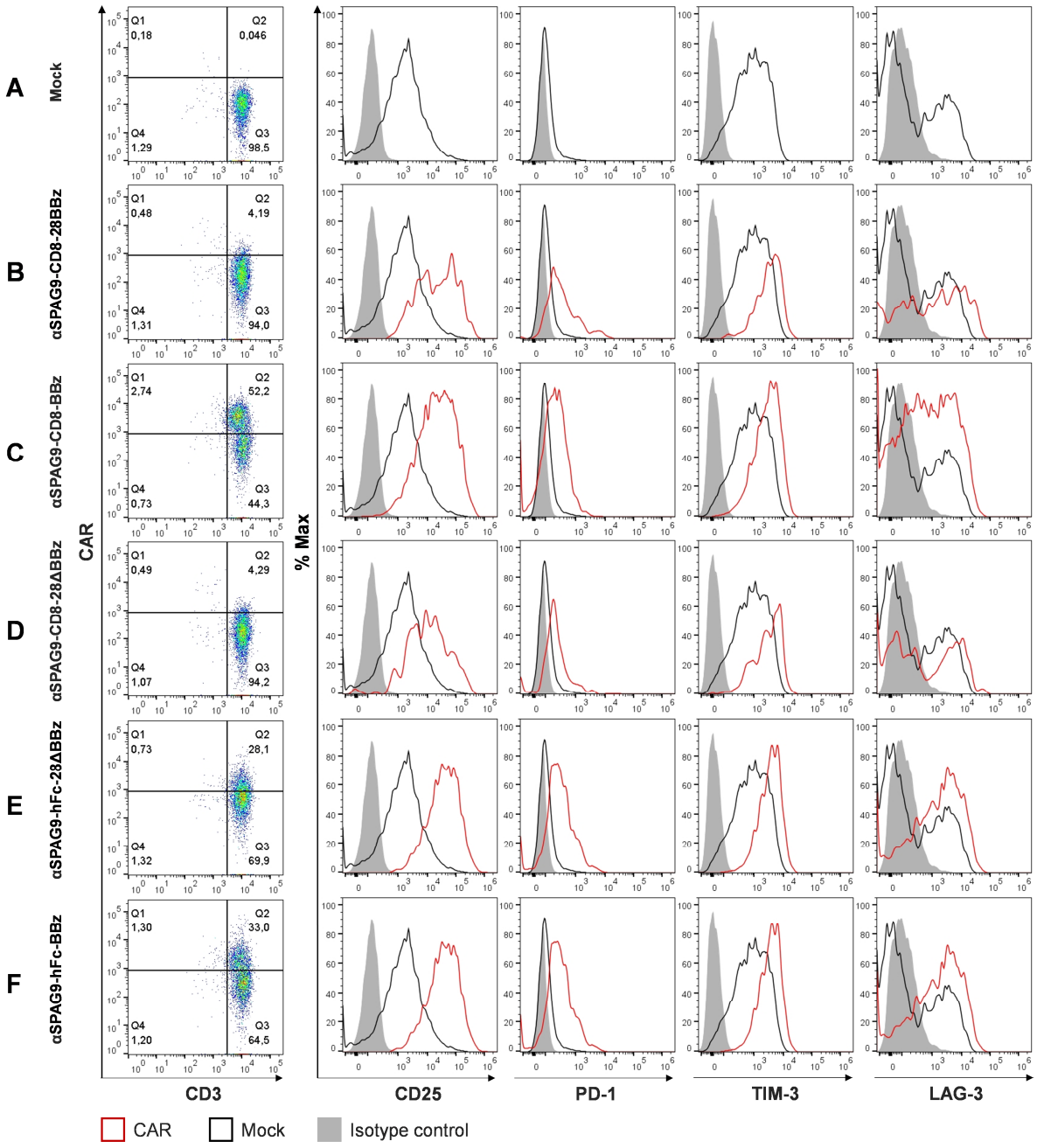

Figure 39. Expression profile of activation and exhaustion markers on αSPAG9 CAR T cells at day 12 after T cell activation (donor 2). αSPAG9 CAR positive T cells were analyzed by flow cytometry using biotinylated protein L combined with APC coupled streptavidin. Activation and exhaustion markers were detected with corresponding fluorochrome coupled antibodies. Activation and exhaustion marker expression on **(A)** mock T cells (black) was compared with that on αSPAG9 **(B)** -CD8-28BBz, **(C)** -CD8-BBz, **(D)** -CD8-28ΔBBz, **(E)** -hFc-28ΔBBz and **(F)** -hFc-BBz CAR positive cells (red). A human IgG1 antibody with irrelevant specificity was used as isotype control (grey).

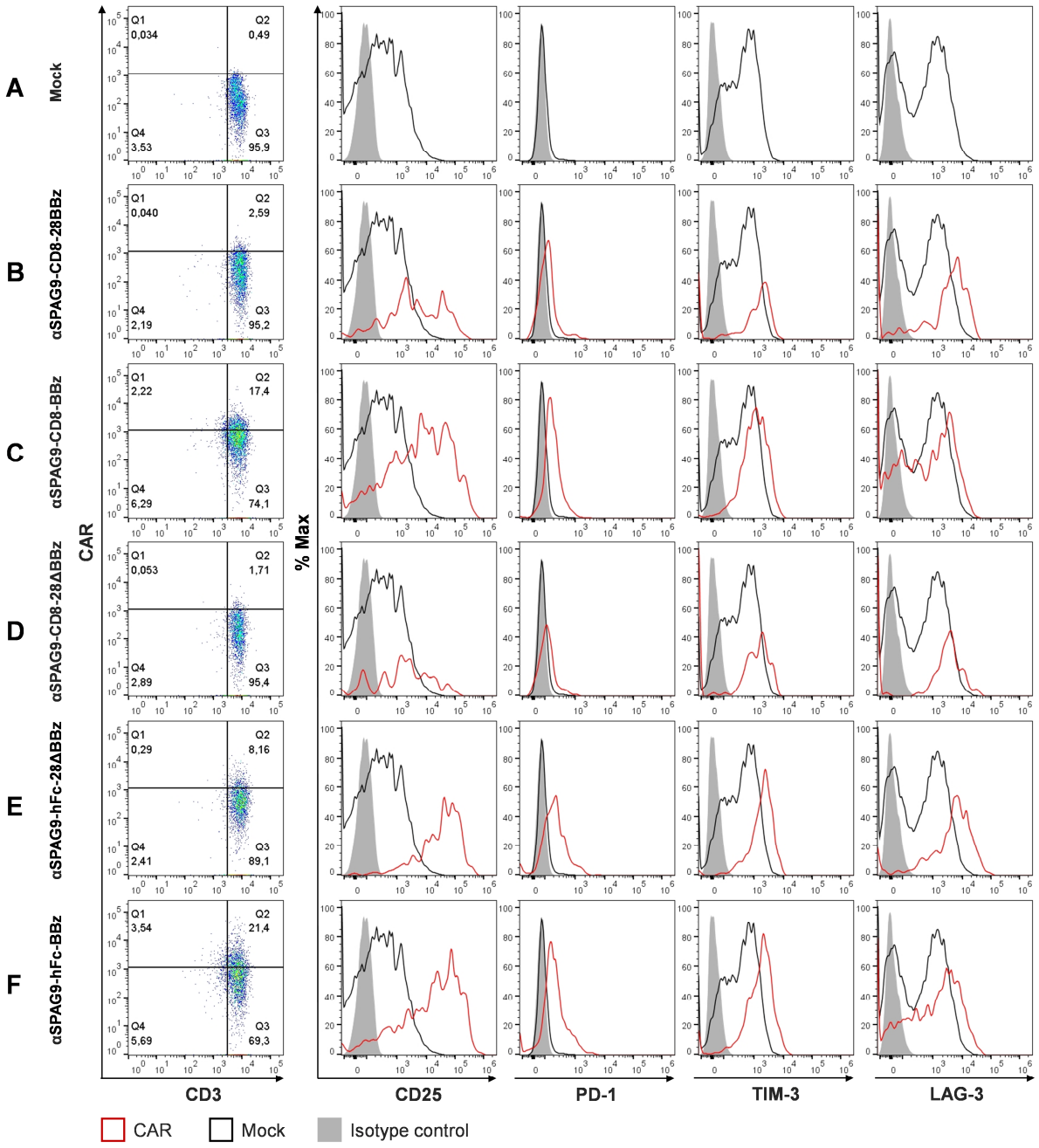

Figure 40. Expression profile of activation and exhaustion markers on αSPAG9 CAR T cells at day 19 after T cell activation (donor 2). αSPAG9 CAR positive T cells were analyzed by flow cytometry using biotinylated protein L combined with APC coupled streptavidin. Activation and exhaustion markers were detected with corresponding fluorochrome coupled antibodies. Activation and exhaustion marker expression on **(A)** mock T cells (black) was compared with that on αSPAG9 **(B)** -CD8-28BBz, **(C)** -CD8-BBz, **(D)** -CD8-28ΔBBz, **(E)** -hFc-28ΔBBz and **(F)** -hFc-BBz CAR positive cells (red). A human IgG1 antibody with irrelevant specificity was used as isotype control (grey).

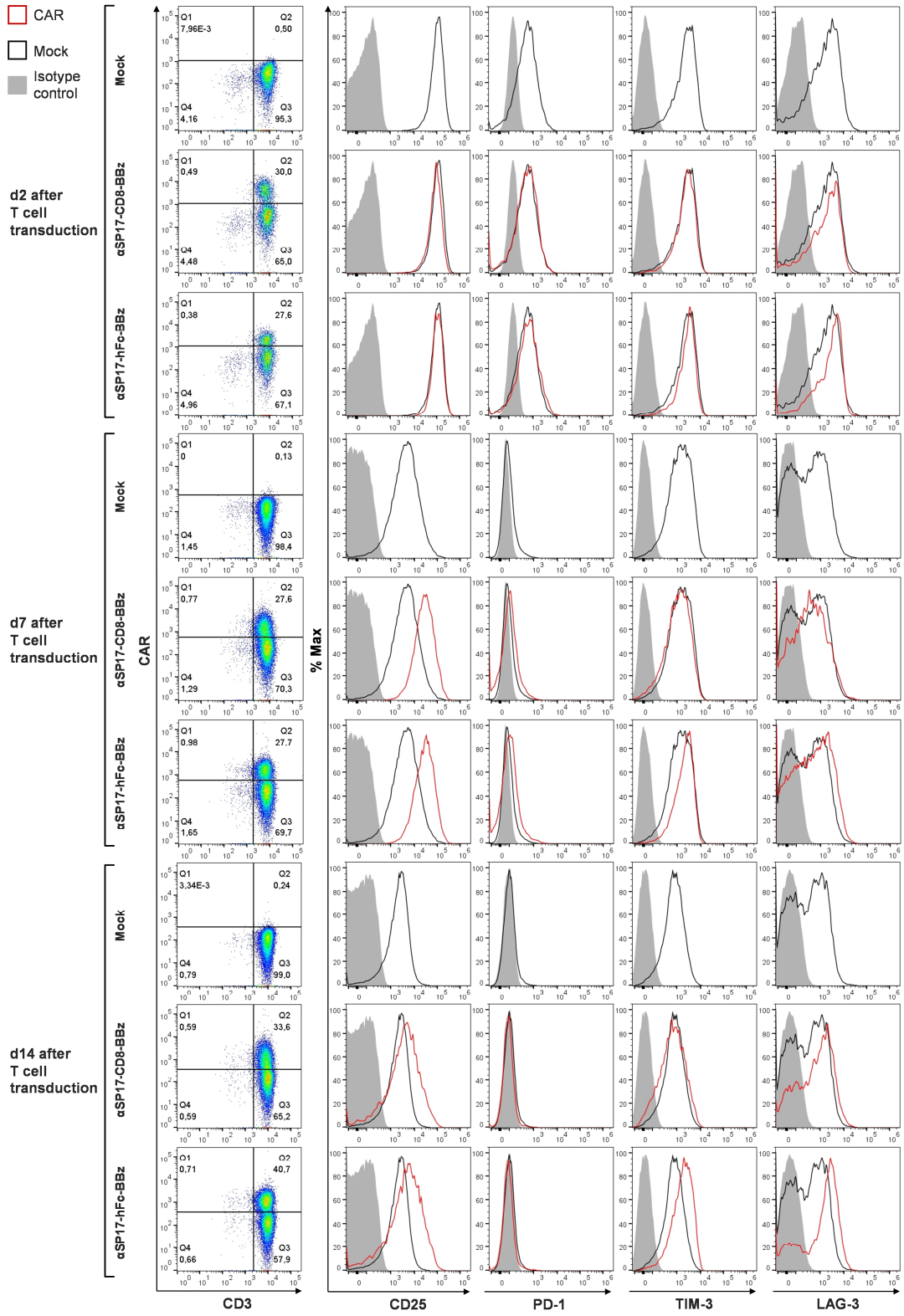

Figure 41. Expression profile of activation and exhaustion markers on T cells expressing 2nd generation αSP17 CARs at day 5, 10 and 17 after T cell activation (donor 3). αSP17 CAR positive cells were analyzed by flow cytometry using APC labeled SP17-mFc target antigen. Activation and exhaustion markers were detected with corresponding fluorochrome coupled antibodies. Activation and exhaustion marker expression on mock T cells (black) was compared with that on αSP17-CD8-BBz and -hFc-BBz CAR positive cells (red). A human IgG1 antibody with irrelevant specificity was used as isotype control (grey).

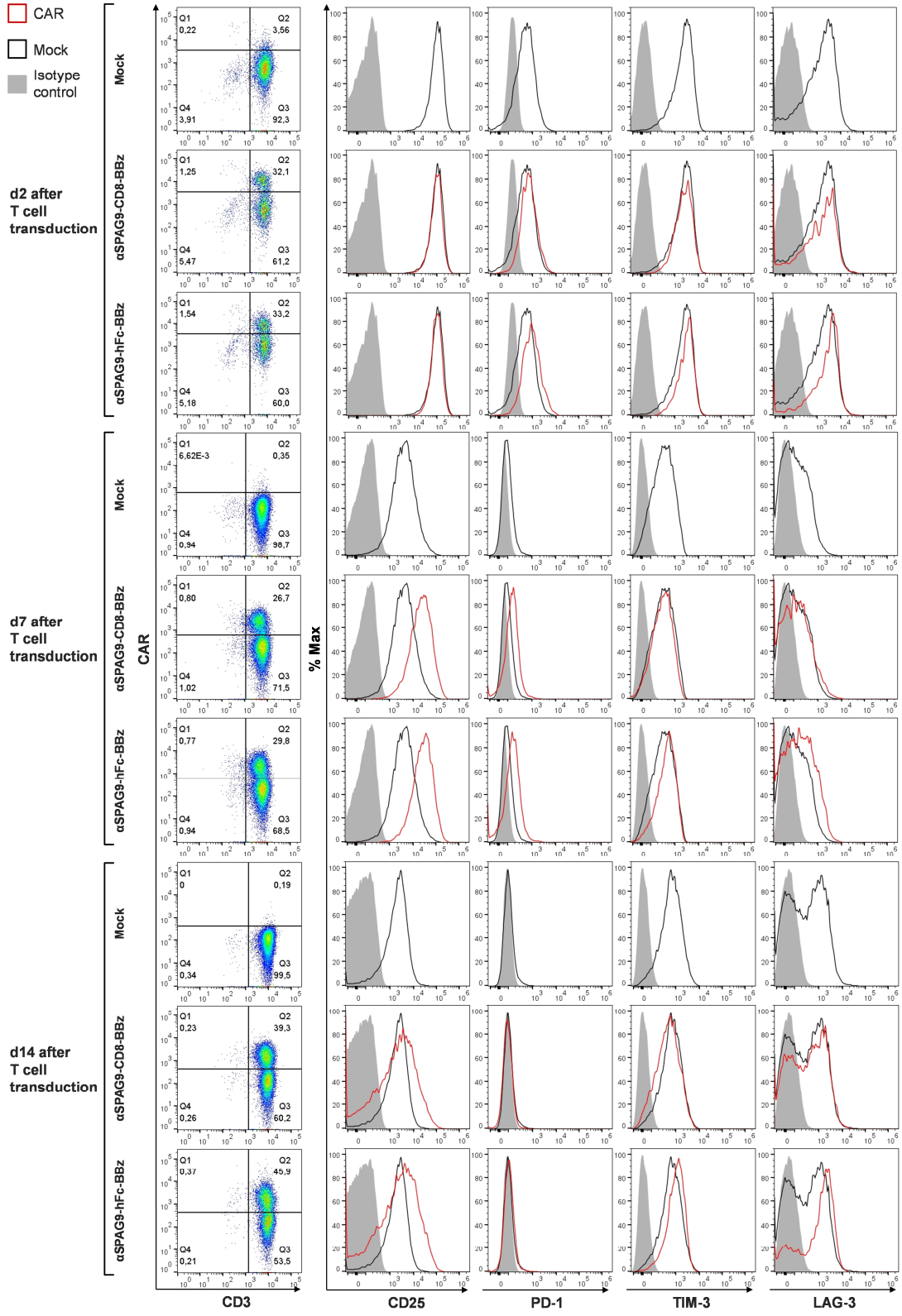

Figure 42. Expression profile of activation and exhaustion markers on T cells expressing 2nd generation αSPAG9 CARs at day 5, 10 and 17 after T cell activation (donor 3). αSPAG9 CAR positive cells were analyzed by flow cytometry using biotinylated protein L combined with APC coupled streptavidin. Activation and exhaustion markers were detected with corresponding fluorochrome coupled antibodies. Activation and exhaustion marker expression on mock T cells (black) was compared with that on αSPAG9-CD8-BBz and -hFc-BBz CAR positive cells (red). A human IgG1 antibody with irrelevant specificity was used as isotype control (grey).

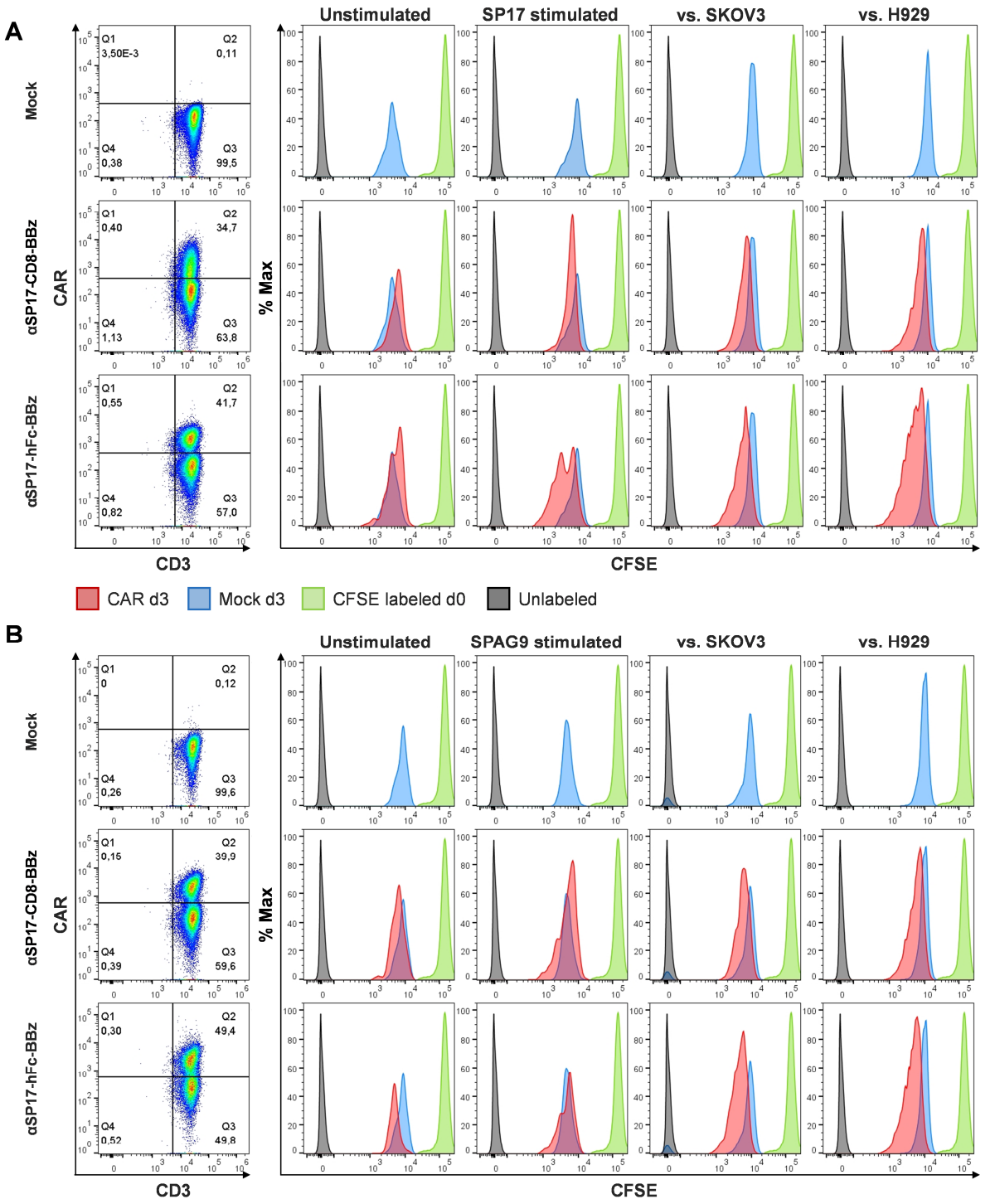

Figure 43. Proliferation monitoring of αSP17 and αSPAG9 CAR T cells upon stimulation with target antigen and target antigen positive tumor cell lines. T cells were either co-incubated with immobilized SP17-mFc or bio-SPAG9A1A2 target antigen as described in *Figure 29* or with $5x10^4$ target antigen positive SKOV-3 and H929 cells in an effector-to-target ratio of 1:1. To track proliferation, mock T cells and T cells expressing 2nd generation **(A)** αSP17 and **(B)** αSPAG9 CARs were labeled with fluorescent CFSE and analyzed by flow cytometry before co-incubation (d0, green). After stimulation for 3 days, mock (d3, blue) and CAR (d3, red) T cell proliferation was monitored by CFSE dye dilution. Unlabeled T cells represent CFSE dilution or proliferation maximum (black).

6.2 Vector maps

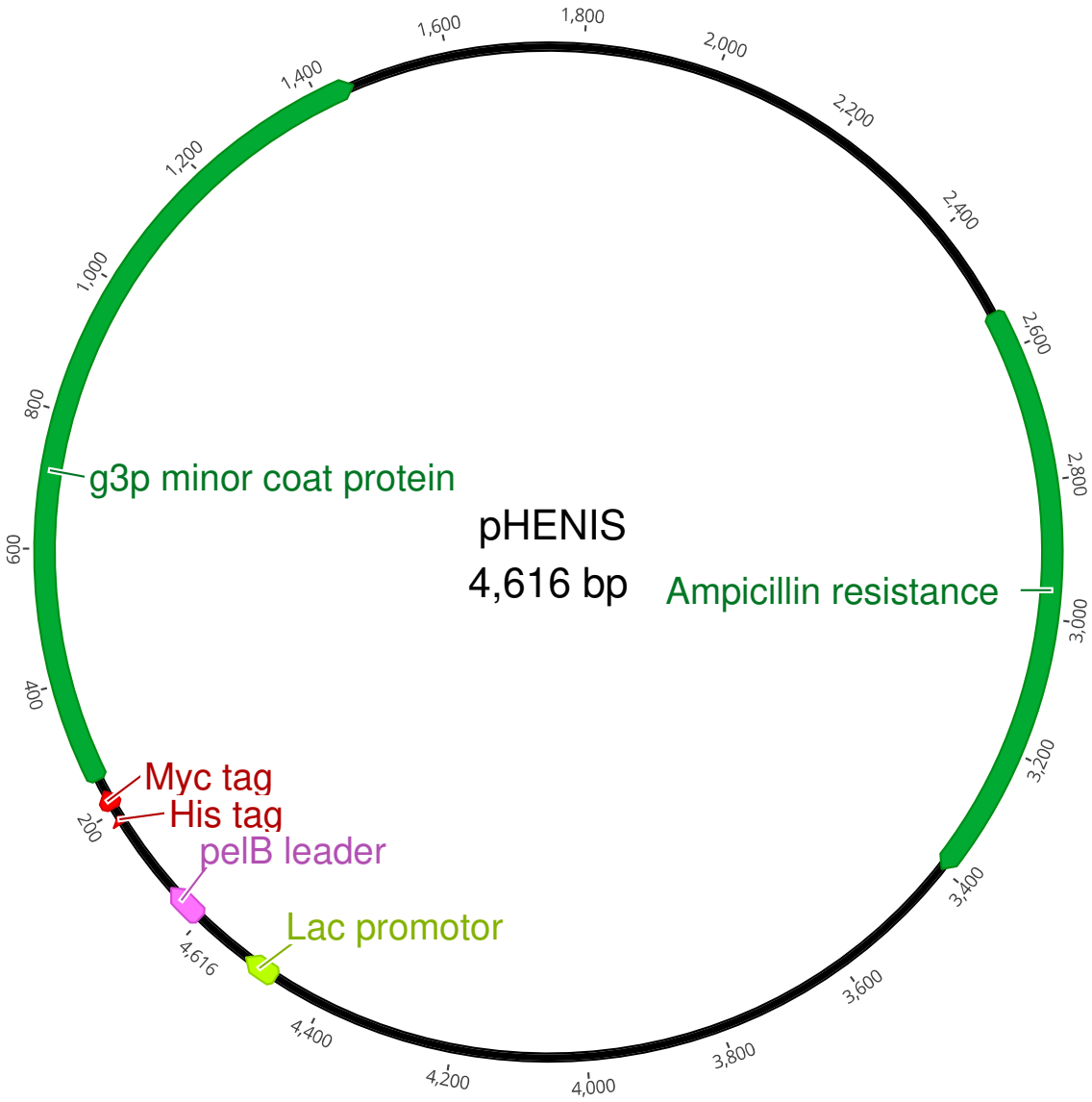

Figure 44: Map of the phagemid vector pHENIS.

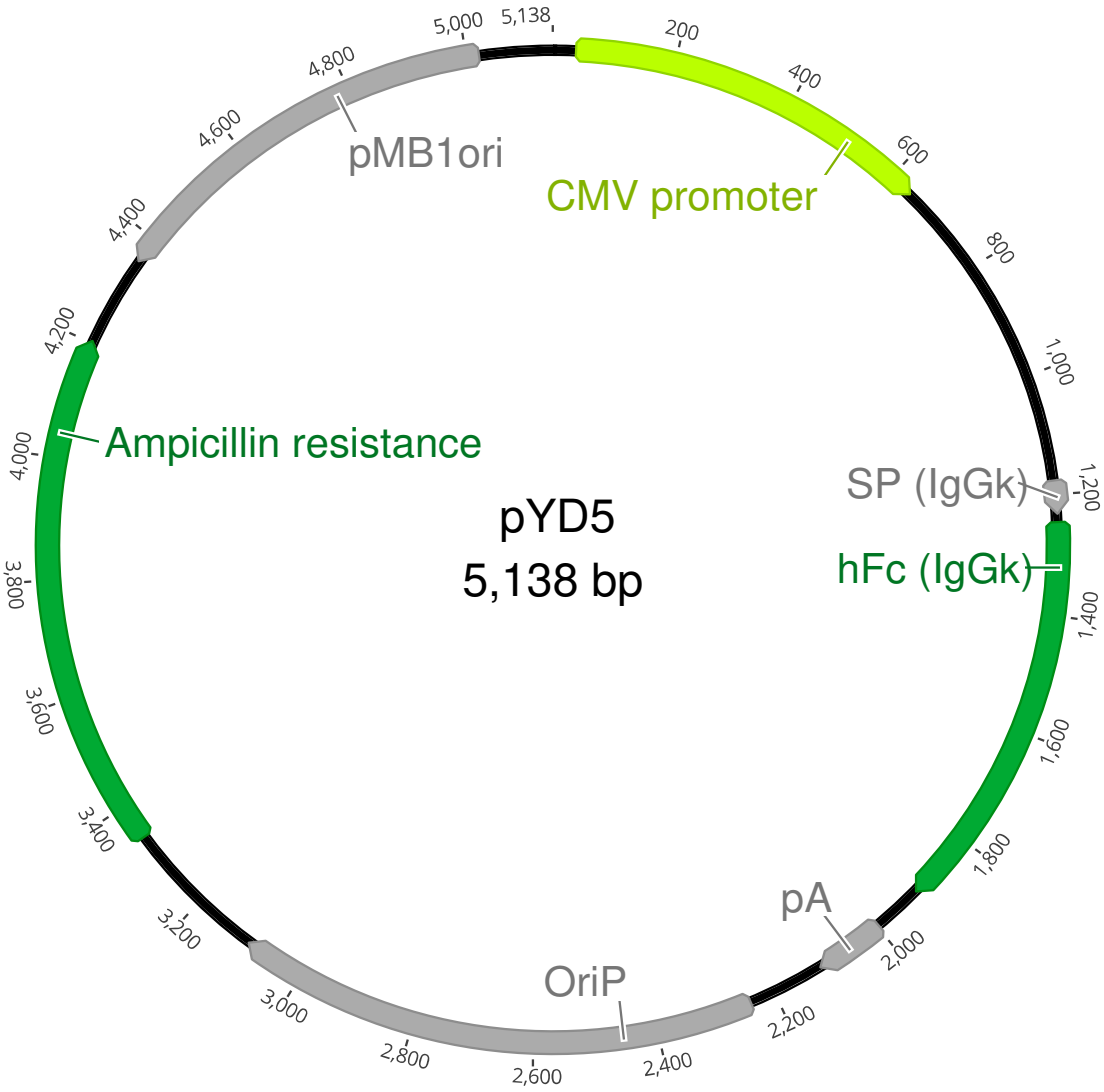

Figure 45: Map of the mammalian expression vector pYD5.

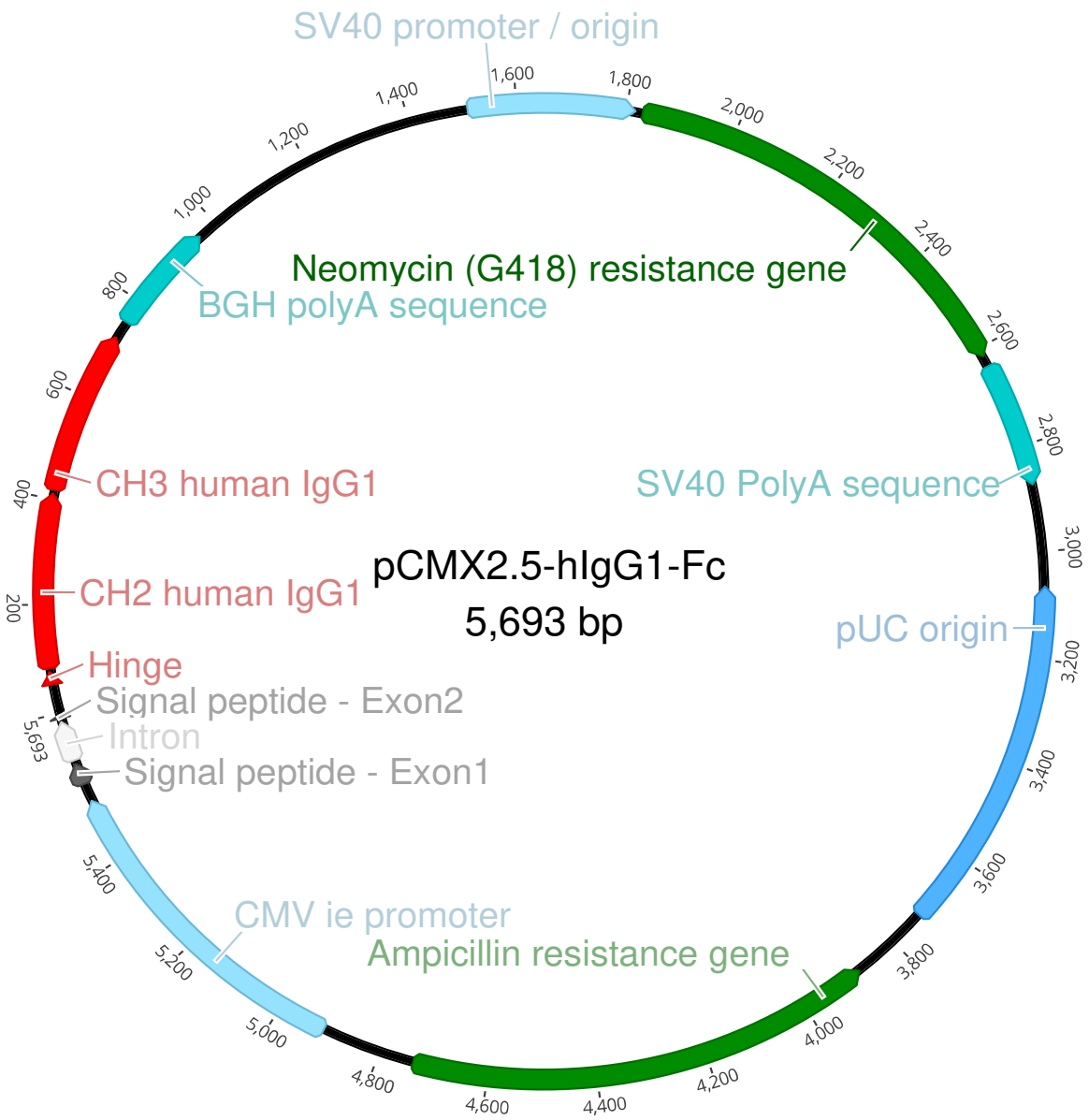

Figure 46: Map of the mammalian expression vector pCMX2.5-hIgG1-Fc.

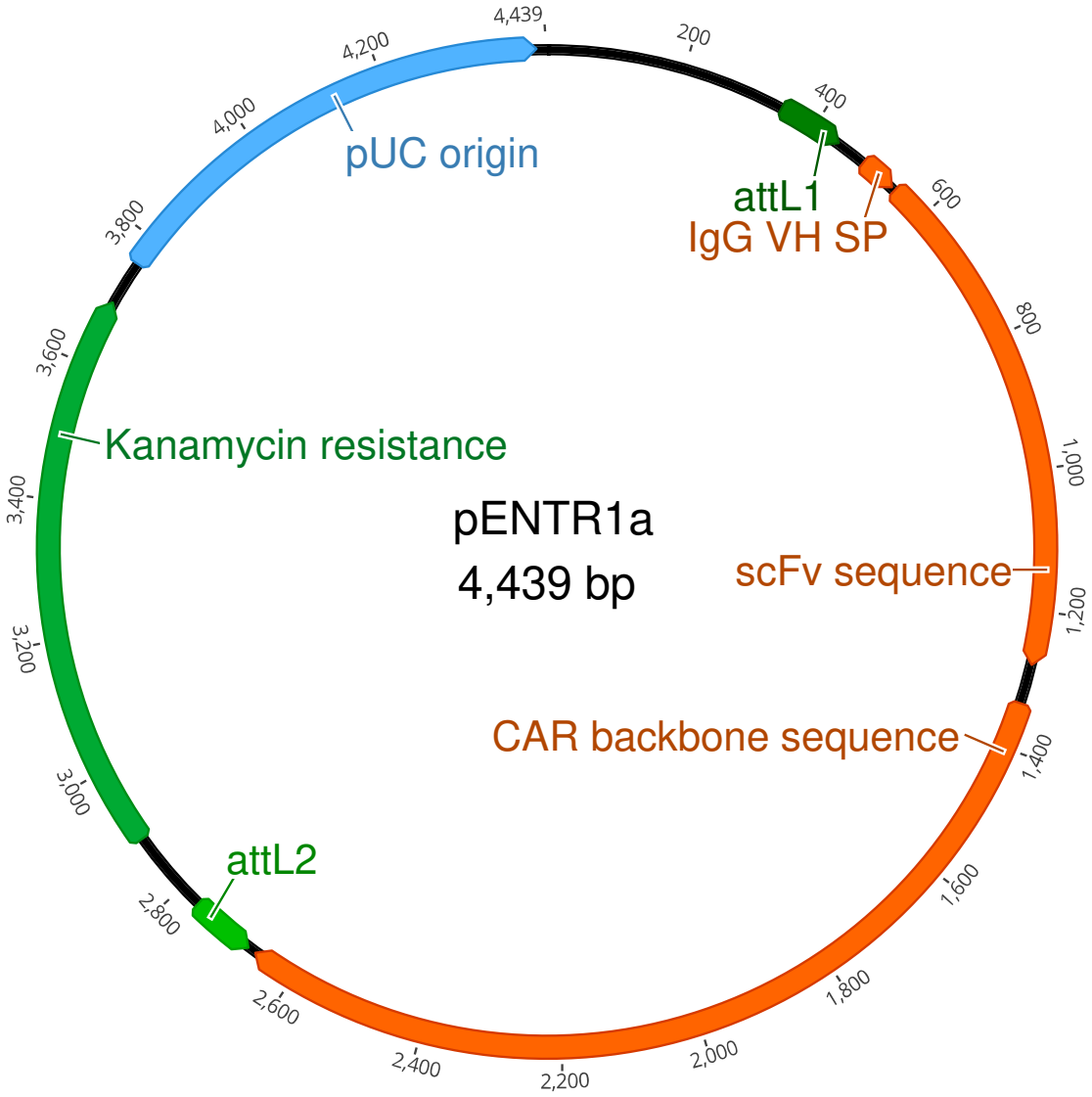

Figure 47: Map of the gateway entry vector pENTR1a.

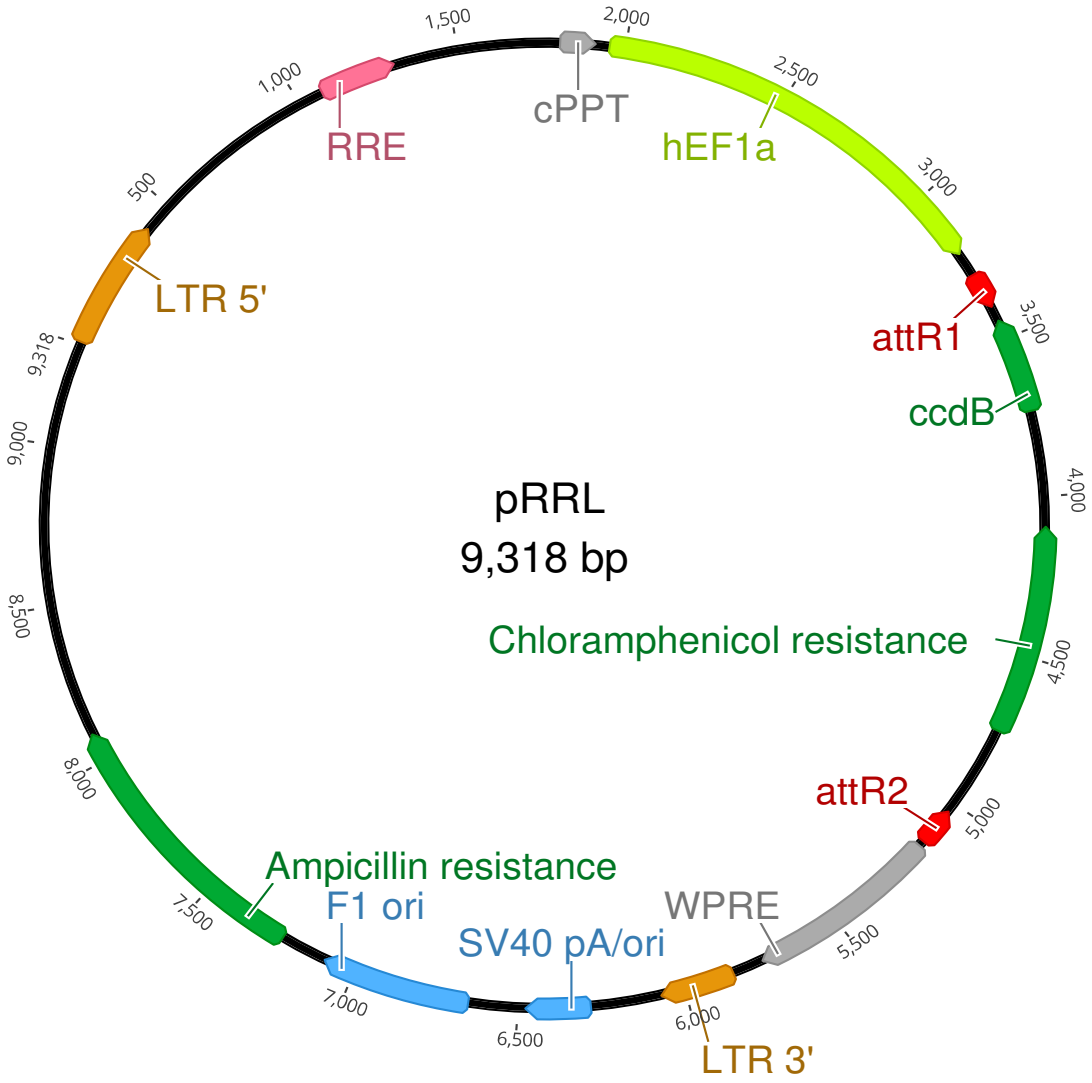

Figure 48. Map of the gateway destination vector pRRL.

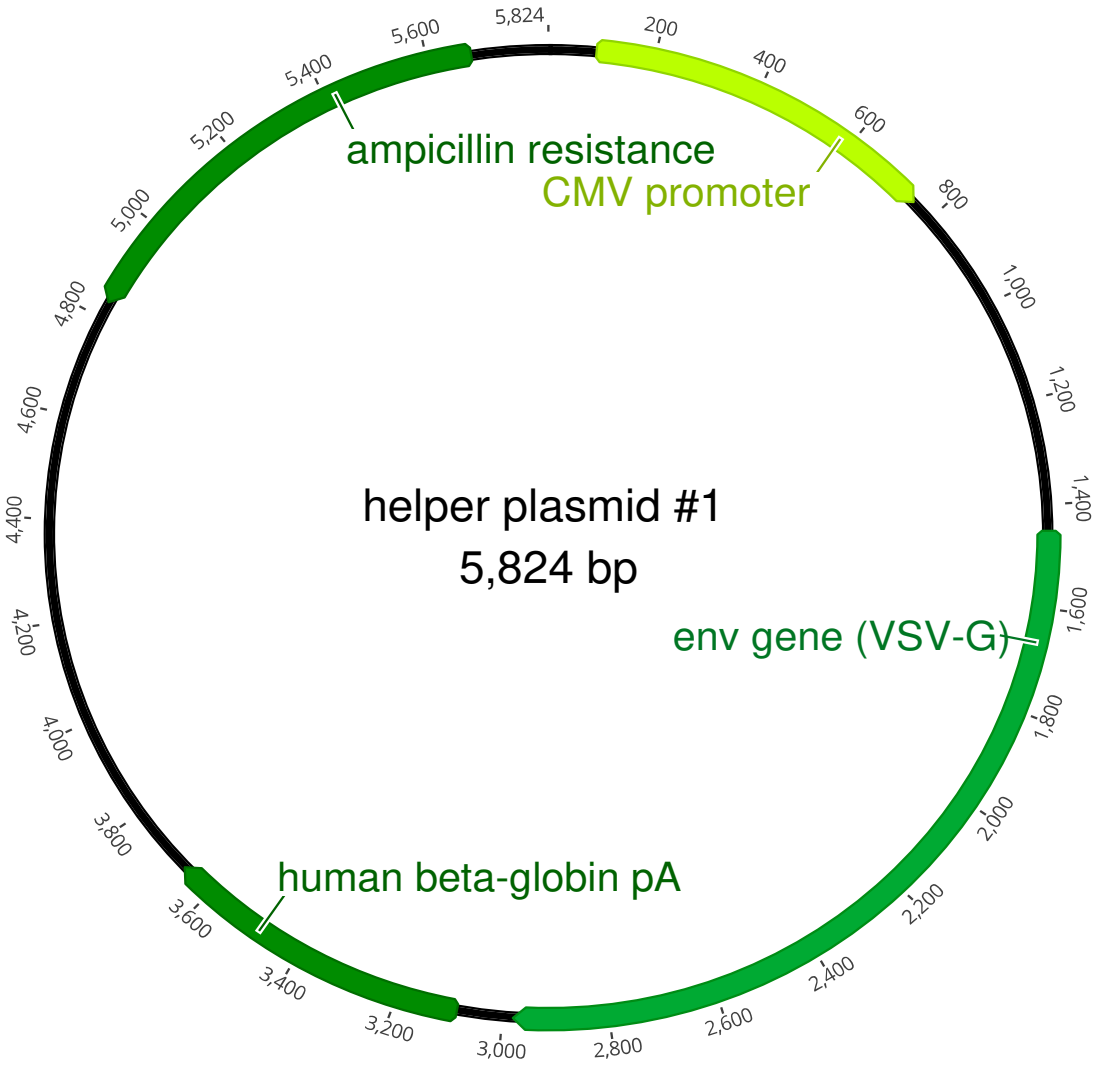

Figure 49. Map of the lentiviral helper plasmid #1.

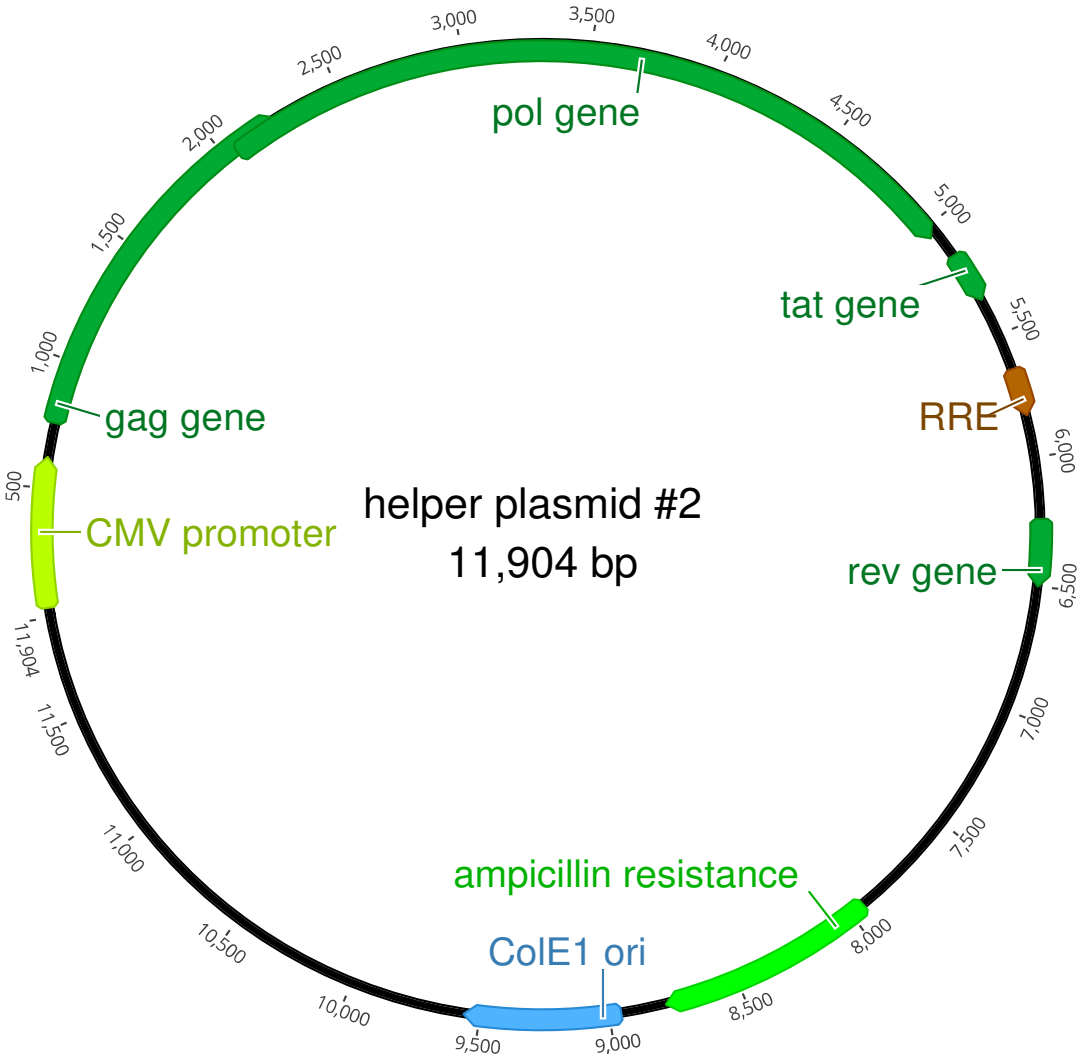

Figure 50. Map of the lentiviral helper plasmid #2.

6.3 List of figures

6.4 List of tables

7 Acknowledegments

In particular, I express my gratitude to **Dr. Michaela Arndt** and **Prof. Dr. Juergen Krauss** for their scientific guidance and support. I highly appreciate their continuous confidence in me and being given the opportunity to perform my doctoral research project in the group “Antibody-based Immunotherapeutics” at the NCT Heidelberg.

Special thanks go to **Dr. Rudolf Uebelhart** for the prime supervision of my research project. Our scientific discussions were accompanied by an intensely productive atmosphere and added precious experience values to my knowledge.

Many thanks to my first examiner **Prof. Dr. Hans-Reimer Rodewald** for the scientific guidance, the participation in my Thesis Advisory Committee and the evaluation of my doctoral thesis.

I also thank **Prof. Dr. Roland Kontermann** (University of Stuttgart) for the scientific advice as member of my Thesis Advisory Committee.

Furthermore, I thank our collaboration partners **Prof. Dr. Stefan Duebel** and **Dr. Thomas Schirrmann** (Yumab GmbH, Braunschweig), **Prof. Dr. Walter Mier** and **Prof. Dr. Hartmut Goldschmidt** as well as **PD Dr. Michael Hundemer** (University Hospital Heidelberg) for providing us with antibody fragments, peptides and for including our antibodies in patient routine analyses.

Lots of thanks to **Lisa Noll** – I guided her Master’s project – for very successfully contributing to my research project.

I am grateful to all my former and current colleagues **Dr. Katharina Aichelin**, **Christiane Christ**, **Evelyn Exner**, **Natalie Garg**, **Stephanie Haase**, **Monika Hexel**, **Dr. Torsten Schaller**, **Narges Seyfizadeh**, **Stefan Vogt** and **Dr. Tobias Weber** for the brilliant teamwork, troubleshooting and the phenomenal working atmosphere. At all times I enjoyed working together with them.

Cordial thanks to **my parents** and **my triplet siblings** for loving and supporting me throughout my stages of life.